Characterizing the proviral landscape and APOBEC3 innate immune responses within immune cells targeted by HIV-1

Submitted by Nicole Reddy

Submitted in fulfilment of the academic requirements for the degree of

Doctor of Philosophy (Medicine)

School of Laboratory Medicine and Medical Sciences
Nelson R Mandela School of Medicine
University of KwaZulu-Natal
Durban, South Africa

Supervised by Professor Thumbi Ndung'u
Co-supervised by Dr Kavidha Reddy

August 2025

Preface

The study described in this thesis was carried out at the Africa Health Research Institute (AHRI) and the HIV Pathogenesis Programme (HPP), Nelson R. Mandela School of Medicine, University of KwaZulu-Natal in Durban in South Africa between January 2020, and December 2024 under the supervision of Dr Kavidha Reddy and Prof Thumbi Ndung'u.

The study described in this thesis is original work done and reported by the author. The study has not been used in any form, by any person or submitted to any tertiary institution for award of a degree or diploma. Acknowledgments have been accorded where other people's work has been referenced in the text.

Nicole Reddy

Professor Thumbi Ndung'u

Dr Kavidha Reddy

Declarations

I, **Nicole Reddy**, declare that:

i. The research reported in this dissertation, except where otherwise indicated, is my original work.

ii. This dissertation has not been submitted for any degree or examination at any other university.

iii. This dissertation does not contain other persons' data, pictures, graphs, or other information unless specifically acknowledged as being sourced from other persons.

iv. This dissertation does not contain other persons' writing unless specifically acknowledged as being sourced from other researchers. Where other written sources have been quoted, then:

a) their words have been re-written, but the general information attributed to them has been referenced.

b) where their exact words have been used, their writing has been placed inside quotation marks and referenced.

v. This dissertation does not contain text, graphics, or tables copied and pasted from the Internet, unless specifically acknowledged, and the source is detailed in the dissertation and the References section of this thesis.

Signed: _____ Date: 27 August 2025

Nicole Reddy

Acknowledgments

I would like to express my heartfelt gratitude to the many people who have supported me on this journey:-

My supervisors, Professor Thumbi Ndung'u and Dr. Kavidha Reddy, who have been extraordinary mentors, thank you for your brilliant guidance, sacrifices, and unwavering support. Your encouragement and motivation have been the steady pulse through the highs and lows of this scientific adventure. I am incredibly grateful for the way you both have shaped my path with your insight and dedication, and the bountiful opportunities you have provided me.

My mum, thank you for your boundless love, guidance, and unshakeable belief in me. You have shown me, each day, what true strength and resilience look like, and I am forever grateful for the foundation of determination you've given me.

My dad, whose absence I feel deeply— I wish you were here to witness this moment. Your early lessons on the importance of education, along with the sacrifices you made to support my dreams, have been invaluable. I honour your memory with each step I take forward.

My family, for their steadfast support, love, and prayers over the years. You have provided a constant source of comfort and encouragement, and I am grateful for the strength you've given me.

The Ndung'u lab, Vivienne Clarence, Madupha Mukerji, and Devin Murugan thank you for the technical support throughout this project.

My friends and colleagues, specifically Chantal Molechan, Kasmira Gopee, Anisha Balgobin, Kajal Reedoy, Tatenda Chikowore, Dr. Mark Chambers, Dr. Ana Moyano de

las Muelas, and Dr. Sharon Khuzwayo—you have been my companions in both work and laughter, reminding me of the joy and camaraderie that lighten even the most challenging days.

Dr. Hylton Rodel, thank you for your bioinformatics expertise it has been much appreciated.

My thesis advisory committee members—Dr. Kamini Gounder, Dr. Guinevere Lee, and Dr. Melissa Rose Abrahams—thank you for your invaluable advice and mentorship. Your support has sharpened my work and encouraged my growth, and I am deeply grateful for your guidance.

Dr. Krista Dong and the FRESH study participants, whose dedication to science has been a source of inspiration. I thank you all for your contributions, which have made this journey not only possible but deeply meaningful.

Finally, I give thanks to God for the strength, courage, and perseverance He has granted me to reach this milestone. Through His grace, I have come this far and am ready to embrace what lies ahead.

Publications

REDDY, K., LEE, G. Q., **REDDY, N.**, CHIKOWORE, T. J. B., BAISLEY, K., DONG, K. L., WALKER, B. D., YU, X. G., LICHTERFELD, M. & NDUNG'U, T. 2024. **Differences in HIV-1 reservoir size, landscape characteristics, and decay dynamics in acute and chronic treated HIV-1 Clade C infection.** eLife, 2024.02.16.24302713.

HOSSAIN, T., LUNGU, C., DE SCHRIJVER, S., KUALI, M., CRESPO, R., **REDDY, N**., NGUBANE, A., KAN, T. W., REDDY, K., RAO, S., PALSTRA, R. J., MADLALA, P., NDUNG'U, T. & MAHMOUDI, T. 2024. **Specific quantification of inducible HIV-1 reservoir by RT-LAMP**. Commun Med (Lond), 4, 123.

Conference presentations

This work was presented at international and local conferences and internal seminar meetings

- **International Presentations**

10th International Workshop on HIV Persistence during Therapy **2022** – Miami, Florida, USA - Poster presentation

5th SANTHE Annual Consortium Meeting **2023** – Lusaka, Zambia - Oral presentation (Best Presentation Winner)

Grand Challenges **2023** – Dakar, Senegal - Poster presentation

- **Local Presentations**

1st AHRI Research Week **2024** – Durban, South Africa - Oral presentation

AHRI Indaba seminar series – Durban, South Africa – Oral presentation

List of abbreviations

Acute Tx	Acute treated
AHRI	Africa Health Research Institute
AIDS	Acquired Immunodeficiency Syndrome
APCs	Antigen-presenting cells
APOBEC3	Apolipoprotein B mRNA editing enzyme catalytic subunit 3
A3	Apolipoprotein B mRNA editing enzyme catalytic subunit 3
A3G	Apolipoprotein B mRNA editing enzyme catalytic subunit 3G
A3F	Apolipoprotein B mRNA editing enzyme catalytic subunit 3F
ART	Antiretroviral therapy
BREC	Biomedical Research Ethics Committee
BME	β mercaptoethanol
bNAbs	Broadly neutralizing antibodies
BSA	Bovine serum albumin
CART	Combination Antiretroviral Therapy
CCR5	C-C chemokine receptor type 5
cDNA	Complementary DNA
Chronic Tx	Chronic treated
CM	Central memory
CRFS	Circulating Recombinant Forms
CTLs	Cytotoxic T lymphocytes
CXCR4	C-X-C Chemokine Receptor 4
ddPCR	Droplet digital PCR
DNA	Deoxyribonucleic acid
DSI	DNA shearing index
DPOPV	Days post onset of plasma viremia
Early Tx	Early treated
EDTA	Ethylenediaminetetraacetic acid
EFV	Efavirenz
EIA	HIV enzyme immunoassay

EM	Effector memory
FACS	Fluorescent activated cell sorting
FBS	Fetal bovine serum
FLIP-seq	Full Length Individual Proviral Sequencing
FRESH	Females rising through education, support, and health
FTC	Emtricitabine
GAPDH	Glyceraldehyde-3-phosphate dehydrogenase
HIV-1	Human Immunodeficiency Virus type 1
HLA	Human leucocyte antigen
HPP	HIV pathogenesis programme
IPDA	Intact Proviral DNA Assay
Late Tx	Late treated
LRAs	Latency reversal agents
LTR-*gag*	Long terminal repeat-*gag*
M	Myeloid cells
mRNA	Messenger RNA
msRNA	Multiple spliced RNA
N	Naïve CD4+ T cell
PAMPs	Pathogen-associated molecular patterns
PBMCs	Peripheral blood mononuclear cells
PBS	Phosphate-buffered saline
PCR	Polymerase chain reaction
PEI	Polyethyleneimine
PLWH	People living with HIV
p24 Ag	plasma p24 antigen
qPCR	Quantitative PCR
QVOA	Quantitative viral outgrowth assay
RAL	Raltegravir
RNA	Ribonucleic acid
RPMI	Roswell Park Memorial Institute Medium
RT	Reverse transcription
SIV	Simian Immunodeficiency Virus

SQuHIVLa	Specific quantification of inducible HIV-1 reservoir by RT-LAMP
TDF	Tenofovir
TFV	Transmitted founder virus
TILDA	Tat/Rev Limiting Dilution Assay
TM	Transitional memory
TREC	T cell receptor excision circle
TZA	TZMbl -based quantitative assay
URFS	Unique recombinant forms
Vif	Viral Infectivity Factor
WB	Western blot
WHO	World Health Organization

Table of Contents

Table of Figures

Chapter 1

Table of Tables

Abstract

Introduction: HIV-1 persistence despite combination antiretroviral therapy (cART) is a key barrier to curing HIV, as latent reservoirs of integrated proviral DNA persist, primarily in resting CD4+ T-cells and possibly other immune cells including myeloid cells. A cure for HIV-1 can be achieved either through total eradication of the virus or a functional cure, defined as controlling HIV without ongoing ART, but both approaches remain scientifically challenging. Antiretroviral-free control of HIV by the immune system is promising but requires a better understanding of the underlying mechanisms for widespread efficacy and application. The apolipoprotein B mRNA editing catalytic polypeptide-like 3 (A3) family of cytidine deaminase proteins, particularly A3G and A3F, potently inhibit HIV-1 by inducing mutations in viral DNA, potentially rendering the virus defective. This study aimed to provide a comprehensive longitudinal analysis of the HIV-1 subtype C reservoir with immune cells from the blood of PLWH and establish the impact of A3 proteins on the viral reservoir in a cohort of young women from Durban, South Africa.

Methods: This study analysed ten women from Durban, South Africa, diagnosed with HIV during hyperacute HIV infection to evaluate the effects of ART initiation timing on HIV reservoirs. Five participants initiated ART early, within one day of plasma viremia detection (median: 1 day post-positive viral load [DPOPV]), while the other five started ART late, during chronic infection (median: 774 DPOPV, range: 399–1202 days). Peripheral blood mononuclear cells (PBMCs) were sorted into CD4+ T-cell subsets, including central memory (CM), effector memory (EM), transitional memory (TM), naïve (N), and myeloid cells (M), for analysis at multiple time points: pre-infection, and at 1, 6, and 12 months post-infection and post-ART initiation. Total HIV DNA was

quantified using ddPCR. Intact and defective HIV-1 genomes were measured using the intact proviral DNA assay (IPDA). The inducible reservoir was assessed in study participants at 3 years post-treatment using the Specific Quantification of inducible HIV-1 reservoir by LAMP (SQuHIVLa) assay. Additionally, A3G and A3F mRNA levels and proviral hypermutation were evaluated to explore the impact of host restriction factors on viral persistence.

Results: CM and EM CD4+ T cells harboured the highest total HIV DNA levels, averaging 7,695 and 5,680 DNA copies/million cells, respectively. Naïve CD4+ T cells contained detectable levels (744 copies/million cells), while myeloid cells also exhibited detectable, albeit lower than CM and EM levels of viral DNA (1,050 copies/million cells). At 12 months post-ART, proviral DNA persisted in the myeloid compartment of 4/5 late-treated participants but only 1/5 early treated participants.

Late-treated participants showed no significant decline in proviral DNA levels over 12 months, while early treated participants demonstrated significant reductions across CM ($p = 0.008$), EM ($p = 0.007$), and transitional memory, TM ($p = 0.007$) CD4+ T-cell subsets. Early treated participants had significantly lower proviral DNA across all subsets compared to late-treated participants at 12 months (CM; $p= 0.0079$, EM; $p= 0.0079$, TM; $p= 0.0070$, N; $p= 0.0476$, M; $p= 0.0400$). Intact proviral DNA was more abundant in EM cells than CM cells in late-treated participants, while ~80% of early-treated participants had undetectable intact HIV DNA in the EM subset after one year. Inducible reservoir levels were higher in late-treated participants ($p = 0.0038$).

A3G expression exceeded A3F by ~1.5-fold pre-infection. Untreated HIV-1 infections led to significant downregulation of both, with greater reductions in A3G. ART partially restored A3 expression, with robust recovery in early treated participants. Defective

proviral DNA levels were higher in late-treated participants across most subsets, except naïve CD4+ T cells. A3G expression correlated with larger defective reservoirs in TM CD4+ T cells ($p = 0.003$). Proviral DNA sequencing revealed frequent A3G-induced hypermutation ($p = 0.0006$), clustered at HIV genome regions prone to single-stranded states during reverse transcription. A3G levels positively correlated with hypermutation percentages pre-infection ($p = 0.027$, $r = 0.91$) and post-ART ($p = 0.032$, $r = 0.90$). Early ART initiation preserves A3 activity, reducing intact proviruses and enhancing immune restoration.

Conclusion: This study highlights the persistence of HIV proviral DNA across immune cell subsets, including CD4+ T cells and myeloid cells. In late-treated individuals, no significant change in reservoir size was observed, whereas early ART initiation led to substantial reductions, particularly in CD4+ T cells, underscoring the critical role of early treatment in minimizing HIV reservoirs. CM and EM CD4+ T cells were identified as key contributors to reservoir maintenance, with EM cells harbouring higher levels of intact proviral DNA, making them essential targets for intervention.

Early ART initiation not only reduces reservoir size but also preserves A3G mRNA expression, which plays a pivotal role in inducing hypermutation of proviral DNA. This preservation supports immune function and creates an environment favourable for targeting and inactivating the HIV reservoir. Enhancing A3G-mediated hypermutation may be a promising therapeutic strategy to disrupt HIV reservoirs. Overall, these findings advance the goal of a functional HIV cure by providing insights into reservoir seeding and decay in diverse immune cells following ART in acute or chronic infection and through studies of the expression and impact of a key innate immune mechanism. The results have implications for achieving an HIV-1 cure through combination mechanisms. Future research should focus on cell-specific regulation of A3 activity

through transcriptional profiling and the development of interventions to augment A3 function.

1 Chapter 1: Literature review

1.1 Human Immunodeficiency Virus Type 1 (HIV-1)

1.1.1 Global statistics

HIV-1, the virus responsible for the acquired immunodeficiency syndrome (AIDS), represents a significant global health challenge. AIDS is characterized by the immune system's inability to fend off infections, leading to increased vulnerability to life-threatening diseases and cancers, including opportunistic infections that would otherwise be easily controlled or cleared by a healthy immune system (Bijkerk H. 1981, Barré-Sinoussi et al., 1983, Jesudason, 2023). Since its identification in 1981, HIV has been recognized as a global pandemic with far-reaching implications for public health, economic stability, and societal development (Nachega et al., 2023, Jesudason, 2023, Boutayeb, 2009). Over 84.2 million people have been infected since the start of the pandemic, and while advances in treatment have been made, a definitive cure or vaccine remains elusive (Jesudason, 2023, Ndung'u et al., 2019).

Approximately 39 million people currently live with HIV, with sub-Saharan Africa being disproportionately affected and accounts for approximately 69% of all cases (Jesudason, 2023) (Figure 1.1). In 2023, there were approximately 1.3 million new infections (2023 UNAIDS Global Aids Update). In sub-Saharan Africa, young women are particularly vulnerable, with an HIV prevalence of 8.7% (De Cock et al., 2021, Nachega et al., 2023). Additionally, within sub-Saharan Africa, data from a northern district in the province of KwaZulu-Natal shows that HIV rates peak at an astonishing 62.4% among women aged 25-44 (Wong et al., 2021) (Figure 1.2).

Despite the progress made in managing the disease with the development of effective antiretroviral therapy (ART), the global response to HIV remains ongoing due to the

genetic plasticity and complexity of the virus (Vemparala et al., 2024, van Zyl et al., 2018). The persistence of viral reservoirs within sanctuary sites during treatment necessitates continued research, vaccine development, and therapeutic interventions that are essential to control and eventually eliminate the pandemic (Ndung'u et al., 2019, Churchill et al., 2016).

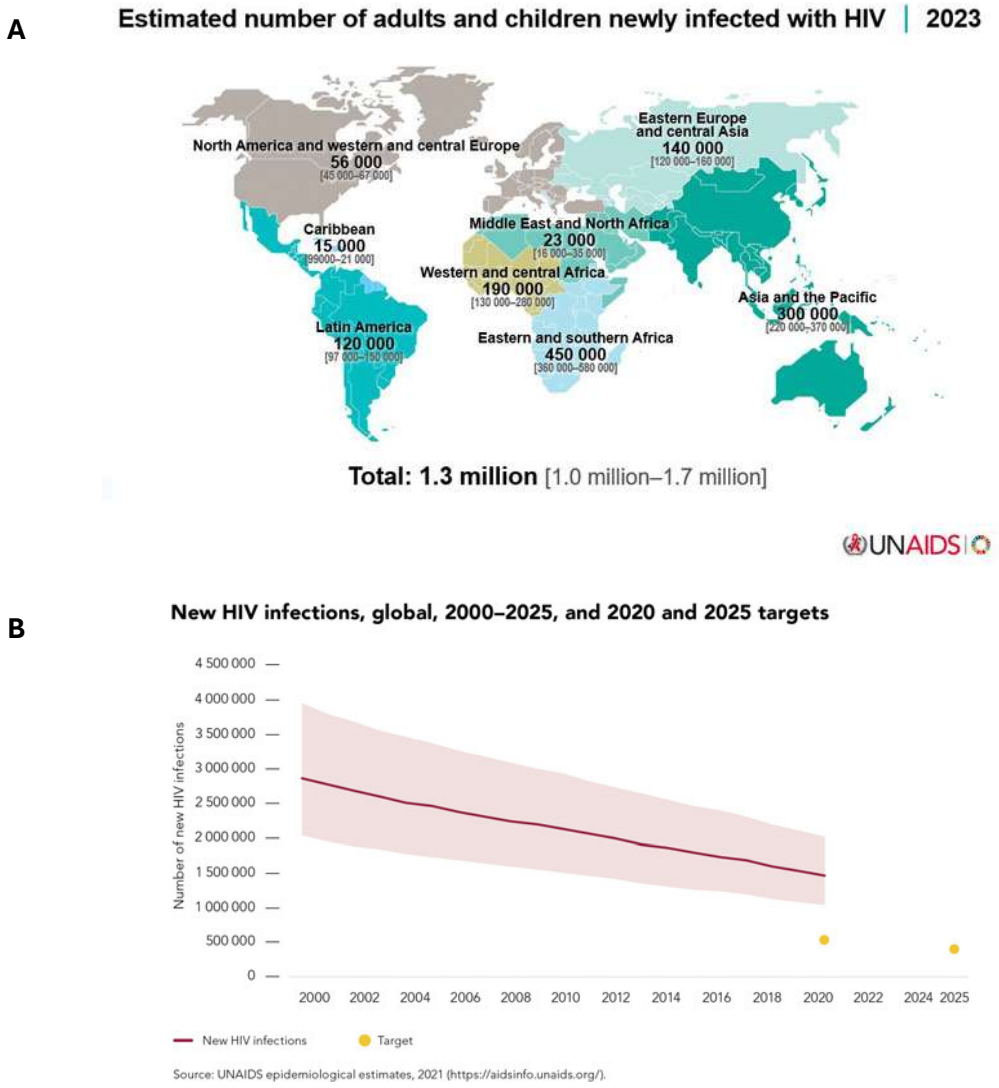

Figure 1.1 Global HIV infection statistics (A) Estimated number of new infections amongst adults and children in 2023. Sub-Saharan Africa had the highest number of

new infections in 2023 (B) New HIV infection targets indicate that globally we will miss the 2025 targets (2023 UNAIDS Global Aids Update).

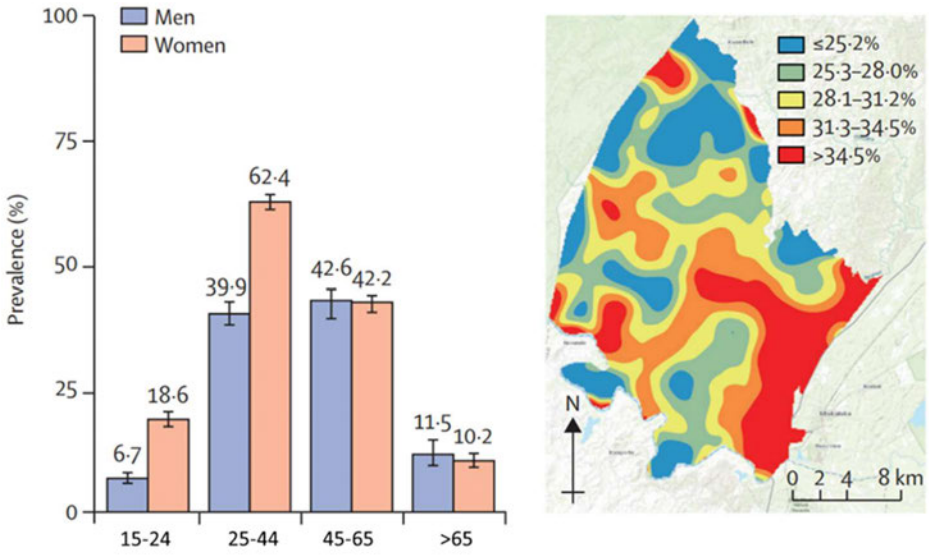

Figure 1.2 Geographical and biological HIV statistics in KwaZulu-Natal. HIV infection is highest in prevalence in women between the ages of 25-44 years of age in the uMkhanyakude district of northern KwaZulu-Natal (Wong et al., 2021).

1.1.2 Origin and evolution of HIV-1

In 1981, young homosexual men in the United States began presenting with unusual infections such as mucosal candidiasis, Kaposi's sarcoma, and Pneumocystis pneumonia (Bijkerk H. 1981, Gottlieb, 1996, Barré-Sinoussi et al., 1983). These infections were the result of severe immune system deterioration, marked by a loss of CD4+ T lymphocytes, and the condition was later named AIDS (Gottlieb et al., 1981). These were the first documented cases of AIDS (Gottlieb et al., 1981, Barré-Sinoussi et al., 1983).

In the following years, scientists identified the retrovirus HIV-1 as the causative agent of AIDS (Gallo et al., 1984, Barré-Sinoussi et al., 1983). HIV-1 originated through zoonotic transmission from primates to humans, which was due to exposure to a human immunodeficiency virus progenitor descended from simian immunodeficiency virus (SIV), possibly as a result of human exposure to primate blood during bush meat hunting in West Africa (Sharp and Hahn, 2011, Wertheim and Worobey, 2009, Gao et al., 1999). HIV-1 is classified into four lineages: M, N, O, and P, each resulting from separate cross-species transmission events (Hemelaar et al., 2019). Group M, the most diverse and prevalent group, is responsible for the global HIV-1 pandemic. Group M can be divided into various subtypes (A to K), circulating recombinant forms (CRFs), and unique recombinant forms (URFs), with the latter two arising from genetic recombination during co-infections with different subtypes (Hemelaar et al., 2019).

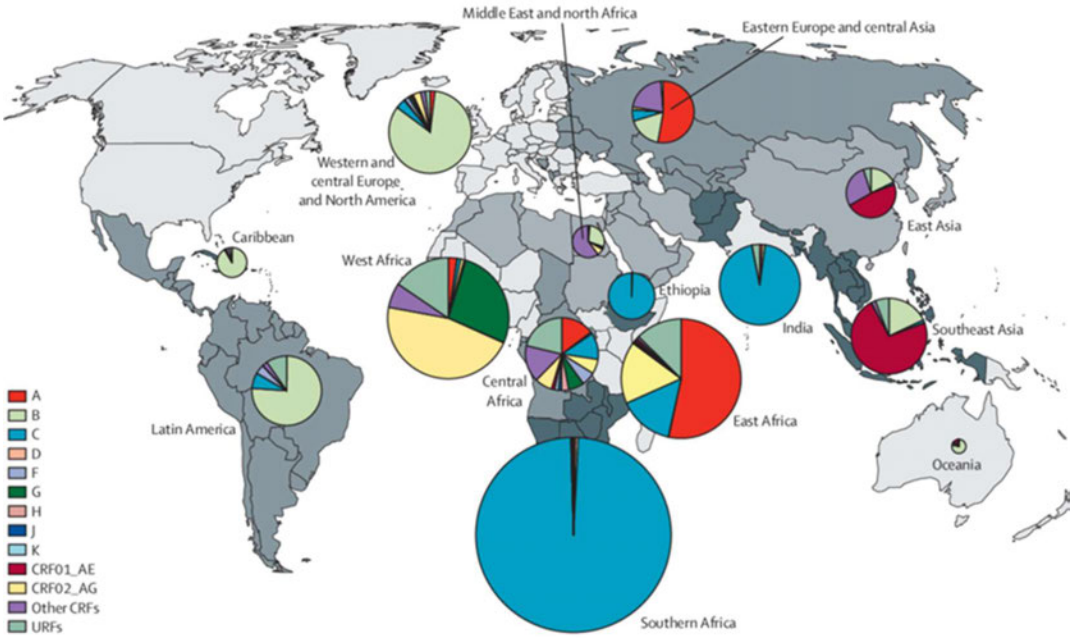

Figure 1.3 The global distribution of group M subtypes A to K, including several CRFs. Subtype C is the most prevalent globally having impacted India and southern Africa the most (Hemelaar et al., 2019).

Subtype C is the most common, accounting for 50% of global infections, while subtypes A and B account for 12% and 11%, respectively. Central Africa has the highest genetic diversity of HIV-1 (Hemelaar et al., 2019) (Figure 1.3). HIV-1 subtypes A, C, D and their recombinants drive the epidemic in sub-Saharan Africa, while subtype B infections dominate the Global North (Gartner et al., 2020). Most HIV studies and the data that is currently available on HIV-1 are based on subtype B and have focused on Caucasian males (Ogbenna et al., 2020). Africa remains understudied although it bears the brunt of the epidemic and therefore more comprehensive studies that include understanding HIV transmission and latency need to be carried out in these heavily burdened settings.

1.1.3 Biology of HIV

1.1.3.1 Morphology and Genetic structure

HIV-1 is a retrovirus from the lentivirus family, with a spherical shape and a lipid bilayer containing 72 glycoprotein spikes, composed of gp120 and gp41. These spikes facilitate the virus's entry into host cells (Arthur et al., 1992, Weiss et al., 1990, Turner and Summers, 1999).

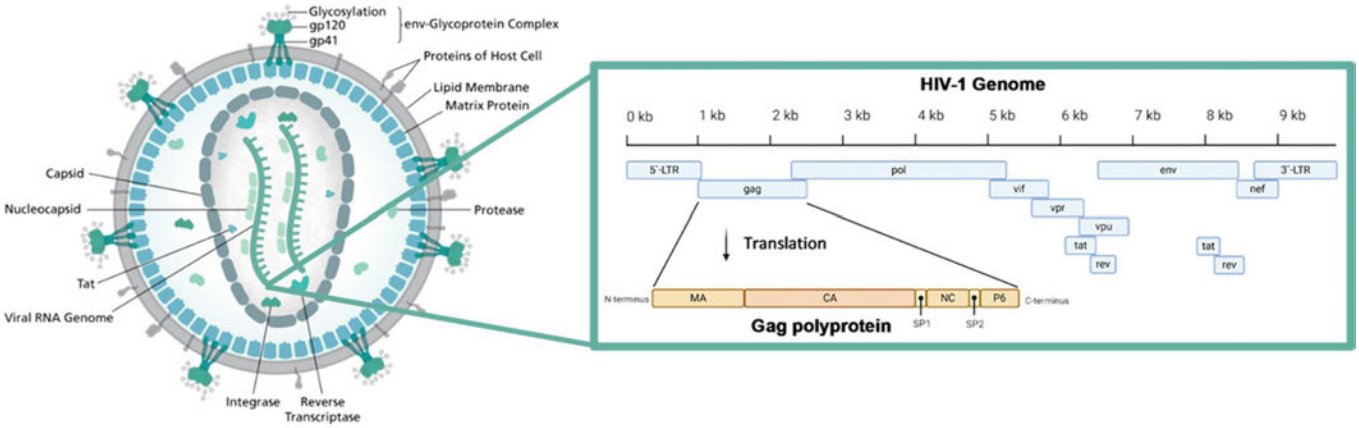

Figure 1.4 Viral and genetic structure of HIV-1. Adapted from (Rossi et al., 2021).

During viral budding, host proteins like MHC class I, II, and ICAM-1 are incorporated into the viral membrane (Burnie and Guzzo, 2019). Inside, matrix protein p17 and core antigen p24 house two RNA copies, nucleoprotein p7, reverse transcriptase, and the key enzymes integrase and protease required for viral replication (Turner and Summers, 1999) (Figure 1.4). The HIV-1 genome is composed of two identical positive-sense single-stranded RNAs, totalling 9,717 base pairs, encoding 16 protein subunits. These genes include the structural proteins (Gag, Pol, Env), regulatory proteins (Tat, Rev), and accessory proteins (Vif, Vpu, Vpr, Nef), all crucial for viral replication and infection (Li et al., 2015, Rossi et al., 2021). The genome efficiently utilizes overlapping coding sequences (Li et al., 2015) (Figure 1.4).

1.1.3.2 HIV life cycle

The HIV life cycle involves several stages, starting with attachment to CD4+ T cells and macrophages via the viral gp120 and CD4 receptor, and co-receptors CCR5 or CXCR4 (Dalgleish et al., 1984, Engelman and Cherepanov, 2012). HIV then fuses with the host cell membrane, entering the cytoplasm. Thereafter, reverse transcriptase converts viral RNA into DNA (Liu et al., 1996, Purcell and Martin, 1993, Harrich and Hooker, 2002, Zila et al., 2021) (Figure 1.5).

The viral DNA, once reverse transcribed from the viral RNA genome, is transported into the host cell nucleus, where it is integrated into the host genome by the viral enzyme integrase. This integration event establishes the provirus, a permanent copy of the viral genetic material within the host DNA (Purcell and Martin, 1993, Bushman, 2002). From this integrated state, the host's own transcriptional machinery is hijacked to produce viral RNA transcripts, which serve both as genomic RNA for new virions and as messenger RNA (mRNA) for the synthesis of viral proteins. These viral

proteins, together with the newly synthesized genomic RNA, assemble at the plasma membrane of the infected cell. Subsequently, immature viral particles bud from the host cell surface, acquiring their envelope from the host cell membrane. During or shortly after budding, the viral proteins undergo further processing, giving rise to mature, infectious virions capable of spreading the infection by entering and integrating into new target cells (Sandefur et al., 2000).

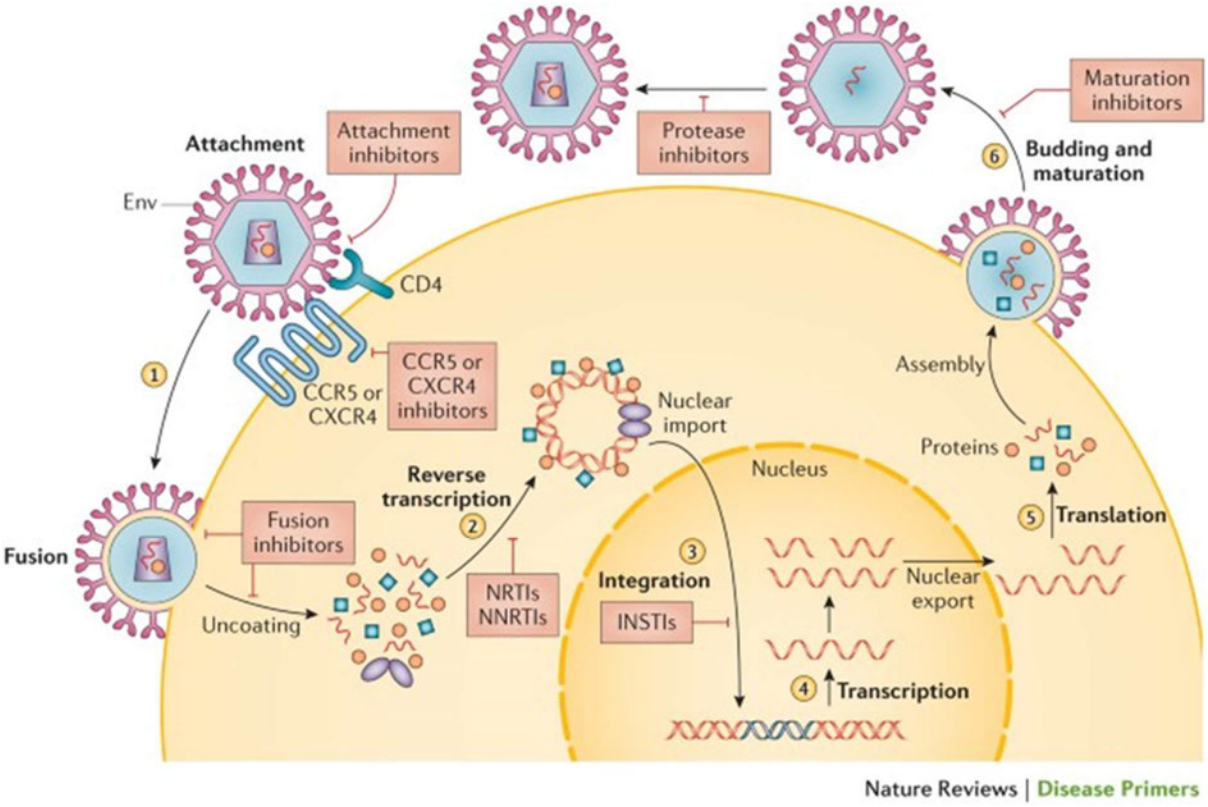

Figure 1.5 HIV replication cycle. (1) attachment of the virus to the host cell, fusion of the virus with host cell membranes, uncoating of viral components, (2) reverse transcription of the viral genome, transportation of viral genome into the nucleus of the host cell, (3) integration, (4) transcription of integrated proviral DNA, export of viral transcripts, (5) translation of viral proteins, assembly, (6) budding, release, maturation (Deeks et al., 2015).

1.1.4 Pathogenesis of HIV

1.1.4.1 Acute HIV infection

HIV transmission occurs via sexual contact, exposure to contaminated blood or needles, or from mother to child (Simon et al., 2006, Volmink and Marais, 2008, Patel et al., 2014). Following transmission, rapid viral replication occurs in mucosal surfaces, then spreads to the blood and lymphatic system (Simon et al., 2006). During the first 1-14 days (the window period), the infection is asymptomatic and undetectable by standard tests (Cohen et al., 2011). Advances in nucleic acid amplification and fourth-generation serological tests have reduced the window period and allow for earlier detection of viral RNA and HIV antigens (Cohen et al., 2010, Cohen et al., 2011).

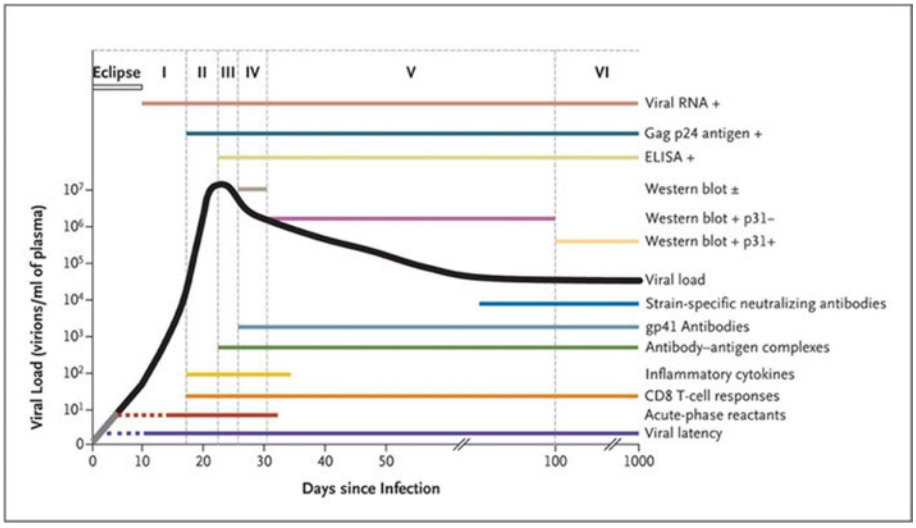

Figure 1.6 Acute HIV infection classification by the Fiebig staging system. Seven distinct stages ranging from the “eclipse phase” before detectable viremia to progressive viral RNA detection and subsequent “seroconversion” stages (Cohen et al., 2011, Fiebig et al., 2003).

Seroconversion, when HIV-specific antibodies appear, follows the asymptomatic phase. The Fiebig staging system, introduced in 2003, is widely used by researchers and public health practitioners to classify acute HIV infection (Fiebig et al., 2003). It defines six stages, beginning with the eclipse phase, where HIV RNA is first detectable, and continuing with tests detecting the Gag p24 antigen and anti-HIV antibodies, marking disease progression (Fiebig et al., 2003) (Figure 1.6).

1.1.4.2 Chronic HIV infection

HIV-1 disease progression is largely determined by events during the acute stage of infection, influenced by host and virus factors, and is thought to be generally inevitable in the absence of antiretroviral therapy because the immune system is unable to clear or permanently control the virus (Pohlmeyer et al., 2013, Naif, 2013). Chronic infection is characterized by the continued presence of infectious virus following primary infection for more than 6 months (Naif, 2013). Chronic exposure to the replicating virus, if untreated, damages the immune system, leading to a dysregulated response (Naif, 2013, Selhorst et al., 2017). This includes impaired B cell function (Hu et al., 2015), abnormal T cell activation (Williams et al., 2022), exhaustion (Fenwick et al., 2019), depletion, and chronic inflammation (Ng et al., 2013). The rapid loss of CD4+ T cells and high viral loads accelerate the progression to AIDS (Naif, 2013), increasing susceptibility to opportunistic infections like tuberculosis and meningitis. However, ART can slow disease progression and preserve immune function, significantly improving outcomes (Volberding and Deeks, 2010).

1.1.4.3 Immune responses to HIV

The immune system comprises two highly interconnected arms: the innate and the adaptive (Thompson, 2015). The innate immune system provides a rapid, non-specific response and includes physical barriers, phagocytic cells, natural killer (NK) cells, and

plasma proteins. The innate immune system also encompass host restriction factors such as DNA cytidine deaminases, TRIM5α, SAMHD1, and Tetherin (Thompson, 2015, Rashid et al., 2024, Malim and Bieniasz, 2012). Pathogens are detected through conserved structural and molecular features termed pathogen-associated molecular patterns (PAMPs), which are recognized by pattern recognition receptors (PRRs) on immune cells, initiating downstream events such as complement activation, type I interferon induction, and inflammation (Thompson, 2015). Crucially, the innate and adaptive immune responses are not sequentially exclusive. Instead, they are interdependent, with substantial cross-talk: innate immune signals guide the activation, differentiation, and magnitude of adaptive responses, while adaptive responses reinforce innate functions (Thompson, 2015).

The adaptive immune system provides antigen-specific and durable immunity through immunological memory. Adaptive immunity is mediated primarily by T and B lymphocytes, but these cells recognize antigens in distinct ways. T cells require antigen presentation in the context of major histocompatibility complex (MHC) molecules on professional antigen-presenting cells (APCs), such as dendritic cells and macrophages (Thompson, 2015). CD8+ cytotoxic T lymphocytes (CTLs) recognize peptides bound to MHC class I molecules, whereas CD4+ helper T cells recognize peptides bound to MHC class II molecules, orchestrating broader immune functions (Thompson, 2015). In contrast, B cells recognize antigen directly via the B cell receptor (BCR), a membrane-bound immunoglobulin, without the need for MHC presentation. Upon activation and differentiation into plasma cells, B cells secrete soluble antibodies that neutralize pathogens, facilitate opsonization, and promote complement-mediated lysis (Thompson, 2015).

In the context of HIV infection, the innate immune system plays an essential early role in restricting viral replication. This occurs in part through the activity of host restriction factors, notably the DNA cytidine deaminase APOBEC3, which introduces hypermutations into viral genomes (Takaori-Kondo, 2006, Sheehy et al., 2003). Cytotoxic T lymphocytes subsequently exert strong selective pressure by killing infected cells and suppressing viral replication, but they are unable to eradicate the virus due to viral escape mutations and persistence in latent reservoirs (Jones and Walker, 2016, Li et al., 2023, Yang et al., 2003). Virus escape from neutralizing antibodies is also common. HIV-specific antibodies typically arise later in infection; however, their delayed induction often diminishes their effectiveness in controlling acute viral replication (Moir and Fauci, 2017). In the absence of treatment, chronic HIV infection progressively impairs immune function, ultimately culminating in acquired immunodeficiency syndrome (AIDS). AIDS is defined by the collapse of immune surveillance, which predisposes individuals to life-threatening opportunistic infections and malignancies (Simon et al., 2006). Importantly, disease progression is heterogeneous, influenced by host immune responses, viral diversity, and host genetic factors (Kazer et al., 2020). With the advent of potent antiretroviral therapy (ART), viral replication can be durably suppressed, permitting partial reconstitution of the immune system and dramatically improving clinical outcomes (Arts and Hazuda, 2012).

1.1.5 HIV and antiretroviral therapy

The introduction of antiretroviral (ARV) drugs in the mid-1980s transformed HIV/AIDS from a fatal disease into a manageable chronic condition, although first generation drugs were toxic and often led to drug resistance especially when used singly. ART now combines multiple drugs, which improves virus suppression, reduces drug resistance, and limits treatment failure. Current innovations, such as single-tablet

regimens and long-acting injectables, enhance adherence and reduce side effects (Menéndez-Arias and Delgado, 2022, Hitchcock et al., 2024). The World Health Organization (WHO) now recommends early ART initiation regardless of CD4 count. Global ART expansion has significantly reduced AIDS-related deaths and HIV transmission (Shelton et al., 2020). However, a residual pool of latently infected long-lived immune cells prevents HIV treatment from eradicating the virus and is a significant barrier to an HIV cure (Shelton et al., 2020). Therefore, ART needs to be taken life-long and poses challenges like toxicity and financial burden, necessitating new strategies to eliminate residual viruses from sanctuary sites in the body (Feola et al., 2006).

1.2 HIV persistence and viral reservoirs.

1.2.1 Mechanisms of persistence

HIV persistence refers to the virus's ability to remain in the body despite ART (Matsuda and Maeda, 2024). The persistence is due to viral reservoirs, at specific anatomical and cellular sites where the virus can evade immune detection, even in the presence of effective treatment (Matsuda and Maeda, 2024, Chomont et al., 2009). These reservoirs are key obstacles in the development of a functional or sterilizing cure for HIV/AIDS, as these latent viruses can rebound when treatment is stopped (Ndung'u et al., 2019, Matsuda and Maeda, 2024).

Combination antiretroviral therapy (cART) effectively suppresses viral replication, reducing the viral load to undetectable levels in the blood (Gulick et al., 1997, Hammer et al., 1997, Perelson et al., 1997). However, the virus is not eliminated and enters a quiescent phase, allowing it to persist in latent forms within infected cells (Chun et al., 1997, Finzi et al., 1997), referred to as viral reservoirs (Chomont et al., 2009, Chun et al., 1997).

Studies have shown that the primary HIV reservoir resides in resting memory CD4+ T cells (Chomont et al., 2011, Finzi et al., 1999). These infected cells have a half-life of 43.9 months, and eradication of these cells could take more than 60 years (Finzi et al., 1999, Siliciano and Greene, 2011). The latent reservoir is established when activated CD4+ T cells become infected and then transition into a resting memory state (Siliciano et al., 2003). Although the frequency of these latently infected cells is low—estimated between 0.1 to 10 intact infectious units per million resting memory CD4+ T cells—they are long-lived and serve as a source for viral rebound when therapy is discontinued (Chomont et al., 2011, Chomont et al., 2009, Chun et al., 2010, Ho et al., 2013).

The persistence of the viral reservoir in resting memory CD4+ T cells can be maintained either through the survival of these cells or through their clonal expansion, which results in the proliferation of the proviral reservoir (Chomont et al., 2009, Virgilio and Collins, 2020, Eriksson et al., 2013). This process helps maintain the viral reservoir, making it difficult to eliminate the virus from the body (Siliciano and Greene, 2011) (Figure 1.7).

Another proposed mechanism for HIV persistence involves incomplete suppression of viral replication within so-called “sanctuary sites.” These include anatomical compartments such as the gut, brain, central nervous system (CNS), and lymphatic system, where antiretroviral drug penetration is often suboptimal (Lorenzo-Redondo et al., 2016, Persaud et al., 2004, Shen and Siliciano, 2008). The extent to which these sites contribute to viral persistence, however, remains controversial. Some studies have reported evidence consistent with ongoing low-level replication, suggesting that insufficient drug exposure may allow the virus to evolve and maintain reservoirs until treatment is interrupted (Zhang et al., 1999, Lorenzo-Redondo et al., 2016). According

to this view, sanctuary sites act as protected niches where replication can continue despite systemic viral suppression.

By contrast, other studies argue that residual viremia in treated individuals is not the result of ongoing replication in sanctuary sites but instead reflects the intermittent production of virus from long-lived, latently infected CD4+ T cells that stochastically reactivate (Bruner et al., 2019, Einkauf et al., 2022, Laird et al., 2016). These studies provide evidence that the majority of viral sequences detected under suppressive ART show little to no evolution over time, arguing against continuous replication (Kearney et al., 2017, Lee et al., 2024). Rather than representing new rounds of infection, the detectable viral rebound in treated people living with HIV (PLWH) is thought to result from the reemergence of archival proviruses that were integrated into host genomes prior to treatment initiation. Taken together, the role of sanctuary sites in sustaining HIV persistence is unresolved. While some data support the possibility of ongoing low-level replication under conditions of poor drug penetration, other evidence suggests that residual viremia is primarily the consequence of clonal expansion and stochastic reactivation of latently infected cells rather than incomplete suppression per se (Mohammadi et al., 2023, Lorenzo-Redondo et al., 2016). It is therefore likely that both

mechanisms may contribute to viral persistence to varying degrees depending on host, viral, and pharmacological factors (Figure 1.7)

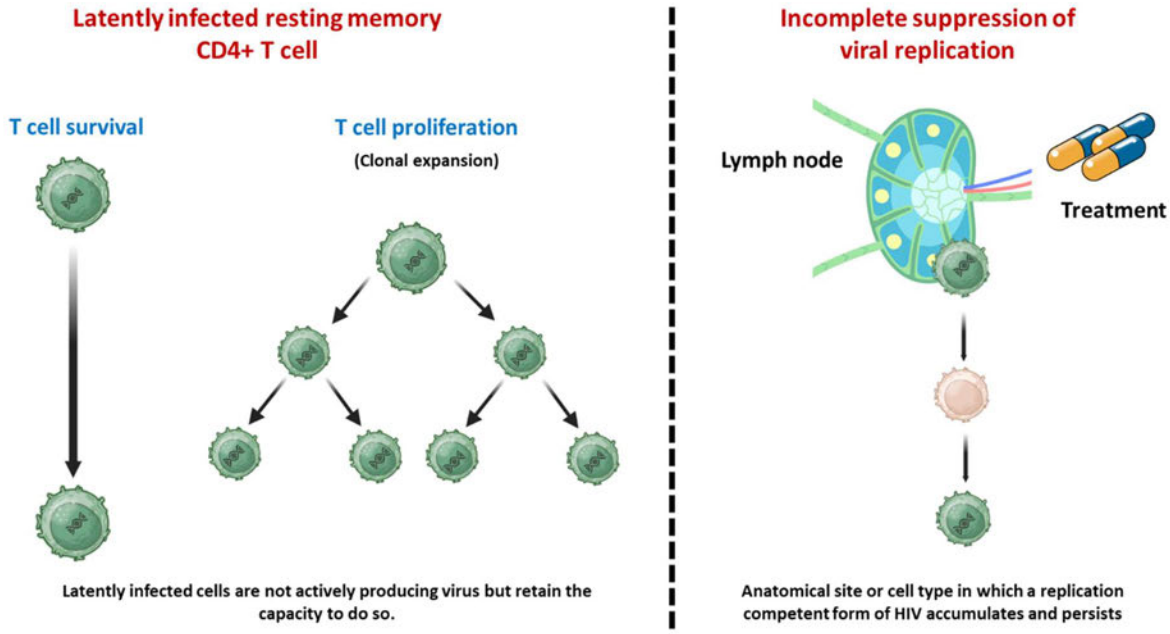

Figure 1.7 Mechanisms of persistence and maintenance of HIV within CD4+ T cells. HIV can persist through survival of long-lived memory CD4+ T cells. The reservoir can also be maintained through CD4+ T cell proliferation, referred to as clonal expansion, and can persist through incomplete suppression of viral replication in tissue sites where drug penetration is poor (Created with Biorender.com).

Within the total pool of resting memory CD4+ T cells, central memory (CM) and transitional memory (TM) subsets have been shown to harbour most of the proviral DNA reservoir (Bailey et al., 2006). Studies have shown that replication-competent viruses are more readily detected in CD4+ T cells, in particular CM, making these cells a particularly challenging target for potential cure strategies (Siliciano and Greene, 2011, Chun et al., 2010). These findings highlight the importance of developing therapies that can effectively target these latent reservoirs within memory CD4+ T cells

(Siliciano and Greene, 2011). Monocytes have also been described as a potential reservoir for HIV (Sonza et al., 2001; Honeycutt et al., 2016). Although research into the contribution of circulating monocytes to long-term viral persistence remains relatively limited, evidence suggests that a subset of CD16+ monocytes may harbour latent virus (Ellery et al., 2007).

Beyond monocytes, other myeloid cell populations have also been implicated as potential reservoirs. Tissue-resident macrophages, particularly in lymphoid tissues and the central nervous system (CNS), have been shown to sustain infection and contribute to viral rebound upon treatment interruption (Tang et al., 2023). Similarly, microglia, the resident macrophages of the CNS, are increasingly recognized as long-lived, HIV-susceptible cells that can maintain viral genomes and support low-level replication despite suppressive ART (Ganor et al., 2019). Together, these findings suggest that myeloid cells—including monocytes, macrophages, and microglia—may represent important but underexplored components of the HIV reservoir landscape (Andrade et al., 2020, Honeycutt et al., 2016).

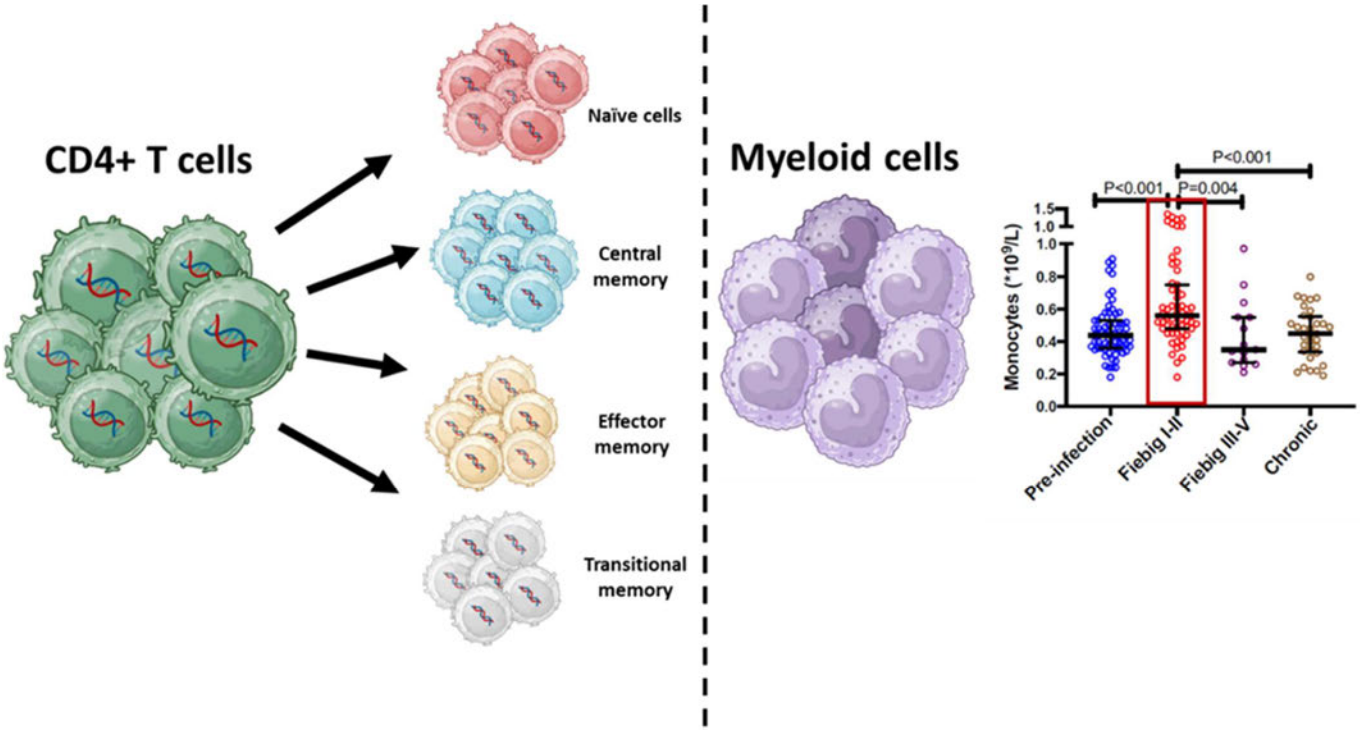

Figure 1.8 Studies have shown that CD4+ T cells particularly, central and effector memory harbor cellular reservoirs. Muema *et al.,* 2020 showed that there is monocyte expansion during the early stages of HIV infection. Myeloid cells may harbor low levels of the HIV reservoir and may contribute to viral rebound once therapy is interrupted therefore must be considered when designing targeted cellular therapies. Adapted from Muema et al., 2020 (created with Biorender.com).

The relevance of monocyte reservoirs in people receiving cART is controversial, with limited in vivo evidence suggesting that these reservoirs are relatively small (Ellery et al., 2007, Andrade et al., 2020). However, during acute HIV infection, particularly in the early Fiebig stage 1, there is an increase in monocyte activation, without an accompanying expansion or activation of CD4+ T cells (Muema et al., 2020, Naidoo et al., 2021, Dong et al., 2018) (Figure 1.8). This raises the possibility that monocytes

may be preferentially targeted for reservoir seeding during early infection and therefore may play a more significant role in viral persistence, particularly in participants initiating ART in hyperacute infection. Monocytes, along with CD4+ T cells, may therefore represent another key target in efforts to eradicate HIV reservoirs. Understanding the role of these immune cells in viral persistence is crucial for developing targeted therapies that aim to eliminate the reservoir and achieve a cure.

Additionally, most HIV reservoir and cure studies have been carried out on subtype B infection which predominates in the Global North, while non-B subtypes in Africa and other low- and middle-income settings remain understudied. This warrants the need for more comprehensive and in-depth cure studies, particularly in the sub-Saharan African region which bears the brunt of the epidemic.

1.2.2 Proviral reservoir landscape

1.2.2.1 Intact and defective proviral genomes

Understanding the intricacies of the HIV proviral reservoir is essential for developing effective strategies toward an HIV cure. The landscape of the proviral reservoir is complex and diverse (Bruner et al., 2016). Genetic characterization of HIV-1 proviruses isolated from individuals on suppressive ART has revealed that only 2%–8% of persistent HIV-1 is genetically intact and potentially replication competent with the viral reservoir being dominated by genome defective viruses (Bruner et al., 2016, Hiener et al., 2017, Horsburgh et al., 2020) (Figure 1.9).

Replication-competent proviruses are the main barrier to HIV-1 eradication, as they contribute to rebound in viral load if therapy is interrupted (Chun et al., 2010). Naïve (N) and memory CD4+ T cells are a well-defined reservoir of replication-competent HIV-1, which is differentially distributed within different CD4+ T cell subsets (Chomont et al., 2011, Chomont et al., 2009).

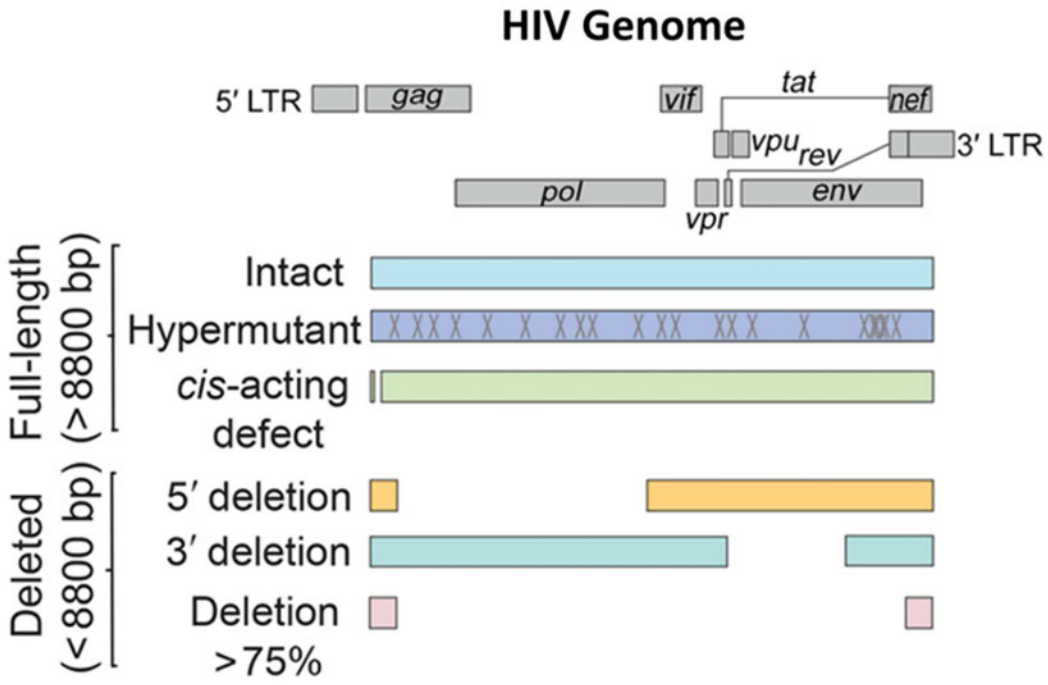

Figure 1.9 Landscape of the HIV proviral genome. The proviral genome can be intact (blue) or defective. Defective genomes exist in different forms and can be classified as having large deletions (pink), 5' deletions (orange), or 3'deletions (teal). Defective genomes can also be classified as cis-acting defects as well hypermutated genomes induced by innate immune host restriction factor APOBEC3G/-F (Duette et al., 2022).

Hiener et al., 2017 showed that genetically intact HIV-1 proviruses were unequally distributed between CD4+ T cell subsets and identified effector memory CD4+ T cells

as an important source of replication competent HIV-1 (Hiener et al., 2017). Studies have shown that cellular proliferation and death contribute to changes in the genetic composition of the persistent HIV-1 reservoir over time (Jones et al., 2020, Gandhi et al., 2021, Pollack et al., 2017). Studies have also highlighted that the reservoir is heterogeneous and diverse, and proviruses can differ between and even within an individual (Jones et al., 2020).

The scope and composition of the proviral landscape are shaped by several key factors, including the quantity of proviral DNA present within immune cells, the genetic diversity of the viral sequences, and the longevity of various CD4+ T cell subsets (Jones et al., 2020, Lee and Lichterfeld, 2016). Higher levels of proviral burden within immune cells contribute to a more complex and extensive reservoir, while increased genetic diversity among viral strains can create a more heterogeneous proviral landscape, complicating treatment and eradication efforts (Jones et al., 2020). Additionally, differences in the age and longevity of CD4+ T cell subsets, such as memory and naive cells, influence the persistence and stability of these reservoirs over time, affecting how the virus can evade immune responses and respond to therapeutic interventions (Lee and Lichterfeld, 2016). These factors collectively play a crucial role in the resilience and variability of HIV reservoirs within the body.

The majority of the HIV-1 proviral reservoir is defective (Lee et al., 2019b, Bruner et al., 2016) and harbours large deletions, sequence inversions, hypermutations, and defective splice donor and acceptor sites that prevent viral replication. These mutations and deletions can be brought about by inefficiencies of reverse transcription and host cell restriction factors such as the host restriction factor apolipoprotein B mRNA-editing enzyme, catalytic polypeptide 3G/-F (APOBEC3G/-F) (Reddy et al., 2024, Lee et al., 2019b, Hiener et al., 2018, Duette et al., 2022) (Figure 1.9).

1.2.2.2 Measuring the proviral reservoir

Quantifying the HIV-1 reservoir is crucial for understanding viral persistence, but it requires highly sensitive assays due to the low frequency of resting memory CD4+ T cells harbouring replication-competent provirus (Gupta et al., 2017). Various methods have been developed for this purpose, with polymerase chain reaction (PCR)-based assays being the most used. Techniques like quantitative PCR (qPCR) and droplet digital PCR (ddPCR) allow for the measurement of total HIV DNA, although they often overestimate the reservoir by detecting both replication-competent and defective proviruses (Gupta et al., 2017, Lee et al., 2019b, Reddy et al., 2024).

In 2019, Bruner et al. introduced the Intact Proviral DNA Assay (IPDA), which uses multiplex ddPCR to target two regions of the HIV-1 genome, allowing for a more precise identification of intact proviruses (Bruner et al., 2019, Simonetti et al., 2020). Originally designed for subtype B, the assay has since been adapted to detect both subtypes B and C (Buchholtz et al., 2024). However, a limitation of IPDA is that detectable intact genomes may not always be replication competent (Buchholtz et al., 2024, Simonetti et al., 2020).

The Full Length Individual Proviral Sequencing (FLIP-seq) assay offers more detailed insights by sequencing near full-length HIV-1 genomes, revealing the proportion of intact and potentially replication-competent viruses (Hiener et al., 2018, Hiener et al., 2017, Reddy et al., 2024). However, FLIP-seq is a long-range PCR method with lower efficiency (Gupta et al., 2017). The gold standard for measuring replication-competent reservoirs is the quantitative viral outgrowth assay (QVOA) (Siliciano and Siliciano, 2021), which detects functional viruses but is labour-intensive and may underestimate the reservoir size because not all reservoir cells are reactivated upon stimulation

(Siliciano and Siliciano, 2021). This method also requires a large amount of CD4+ T cells (Siliciano and Siliciano, 2021).

Other assays that have been developed to measure the inducible reservoir include TILDA (Tat/Rev Limiting Dilution Assay) and TZA assay (TZMbl -based quantitative assay) and offer a faster, more sensitive alternative, requiring fewer cells and less labour (Lungu and Procopio, 2022, Lungu et al., 2021, Frank et al., 2019, Sanyal et al., 2019). More recently, the novel Specific Quantification of the HIV-1 reservoir by LAMP (SQuHIVLa) assay was designed to measure multiple spliced RNA (msRNA) as an indicator of inducible latent virus (Hossain et al., 2024).

1.2.3 APOBEC3 proteins and their influence on the proviral landscape

Innate immunity serves as the first line of defence against viral infections, including HIV, and plays a crucial role during the onset of infection (Thompson, 2015). In acute HIV infection, viral PAMPS are detected by pattern recognition receptors (PRRs) on infected cells, triggering innate immune responses that attempt to restrict the virus (Cohen et al., 2011, Thompson, 2015).

A key component of this response involves APOBEC3 (A3) proteins, which function as host restriction factors with antiviral properties (Sheehy et al., 2003, Malim and Bieniasz, 2012, Farrow and Sheehy, 2008, Chiu and Greene, 2006). These proteins, characterized by Zinc clusters, are encoded on chromosome 22 (Figure 1.10) and come in seven different forms, with APOBEC3G (A3G) and APOBEC3F (A3F) being the most significant in countering HIV-1 infection (Figure 1.10) (Farrow and Sheehy, 2008) .

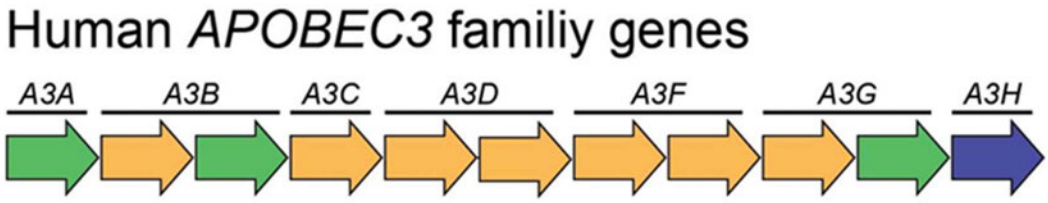

Figure 1.10 APOBEC human APOBEC3 genes are found on chromosome 22. The human A3 family genes are composed of seven members with one or two zinc-coordinating domains. These genes play an integral role in the control of HIV-1 replication (Ikeda et al., 2021).

A3 proteins are incorporated into budding virions in the absence of the viral infectivity factor (Vif) protein (Simon et al., 2005, Sheehy et al., 2003, Farrow and Sheehy, 2008, Ikeda et al., 2021). Once in a target cell, during reverse transcription, A3 proteins induce lethal G-to-A hypermutations in the viral genome, leading to the production of defective proviruses. APOBEC-induced immune footprints on the viral genome are easy to track because of the characteristic mutational patterns associated with these proteins and they can therefore serve as a useful surrogate for the impact of innate immune responses on the virus. Studies suggest that a large proportion of archived proviral genomes are defective due to A3-induced hypermutations, making these proteins critical in shaping the landscape of the HIV-1 proviral reservoir (Figure 1.11) (Ikeda et al., 2021).

Given their role in proviral hypermutation, it is essential to understand which A3 protein is most potent in inducing these mutations, as this could inform HIV cure strategies (Ikeda et al., 2021, Ikeda et al., 2023). Blocking the Vif protein could preserve A3 activity and enhance its antiviral effects (Ikeda et al., 2021). Research by Koning et al. (2009) has shown that A3G is expressed around ten times more than A3F in T cells, B cells, and monocytes, indicating its dominant role in immune responses (Koning et al., 2009). However, there remains some controversy about which A3 proteins contribute more significantly to antiviral activity in vivo (Armitage et al., 2014). Additional studies have associated higher A3G expression and hypermutation with better control of HIV-1, particularly in long-term non-progressors (LTNP) (Mussil et al., 2011, Amoêdo et al., 2011).

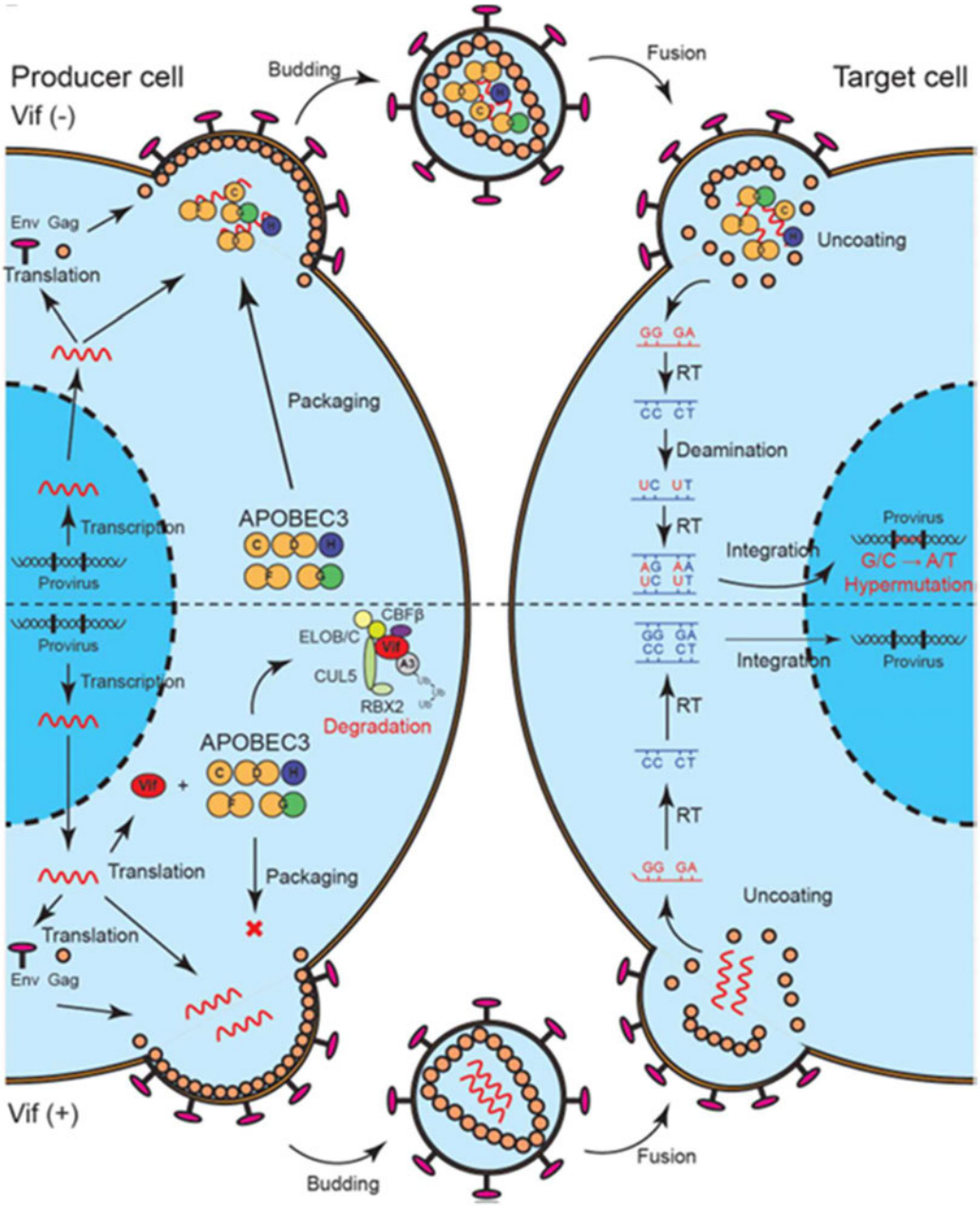

Figure 1.11 A model of HIV-1 restriction by A3 family proteins and counteraction by HIV-1 Vif. A schematic of HIV-1 restriction by five A3 family proteins and neutralization by HIV-1 Vif. A3C, A3D, A3F, A3G, and A3H are packaged into HIV-1 virions in producer cells and inactivate the virus through cytosine-to-uracil (C-to-U)/guanine-to-adenine (G-to-A) mutations (Ikeda et al., 2021).

Though A3 proteins significantly influence the viral reservoir by inducing hypermutations, data on their expression in different cellular subsets targeted by HIV and the impact of ART remain scarce. Furthermore, while Vif degrades APOBEC3 proteins to evade their antiviral activity and may also shut off APOBEC3 gene expression (Anderson and Harris, 2015) data indicates that Vif adapts during infection (Ooms et al., 2013, Reddy et al., 2016, Binka et al., 2012). However, more research is needed to fully understand the impact of A3 proteins on the HIV-1 proviral reservoir, particularly when treatment begins early in infection when innate immunity is likely most active.

1.2.4 HIV-1 cure strategies

HIV cure research explores various strategies aimed at eliminating the need for lifelong ART (Ndung'u et al., 2019, Matsuda and Maeda, 2024). These approaches are classified into two main types of cures: 1) eradication (sterilizing cure): The goal here is the total elimination of HIV from the body, 2) durable ART-free control (functional cure) and remission: HIV remains in the body but is inactive, unable to affect health or be transmitted to others and requires continuous monitoring (Cohn et al., 2020, Ndung'u et al., 2019, Deeks et al., 2021).

Several strategies are being attempted to achieve these cures. One strategy is the use of latency reversing agents (LRAs), in a method called kick and kill. Here HIV-infected resting cells in reservoirs are “kicked” into action, making them visible to the immune system (Pace and Frater, 2019, Matsuda and Maeda, 2024). Once activated, these cells are “killed” by either the immune system or therapy. Challenges include finding safe LRAs and ensuring all infected cells are activated and destroyed. Another strategy is called “Block and Lock” (Matsuda and Maeda, 2024). This approach aims to permanently silence HIV by "blocking" the virus’s ability to replicate and "locking" it

in a latent state. However, this concept is still in the early stages of development, with no approved therapies yet (Matsuda and Maeda, 2024).

Gene therapy is also another strategy that has been implemented as a cure strategy. This includes knocking out viral genes to prevent HIV from entering cells, knocking in protective genes to immune cells, or using technologies like CRISPR to cut out HIV from human DNA (Chou et al., 2024). A key example is stem cell transplants, which have led to HIV remission in several patients, including the Berlin patient and London patient (Chou et al., 2024, Hütter et al., 2009). However, stem cell therapies are risky, costly, and limited by the scarcity of suitable donors (Chou et al., 2024).

Immune-based approaches have also been considered for cure strategies (Chou et al., 2024, Beck and Blankson, 2020). These aim to enhance the immune system's ability to clear infected cells. Approaches include broadly neutralizing antibodies, natural killer cells, and CAR T-cell therapy (Ndung'u et al., 2019, Beck and Blankson, 2020, Chou et al., 2024). However, these approaches face challenges such as limited effectiveness across all HIV strains and difficulty finding the right immune cells to target HIV (Chou et al., 2024). Although each approach presents potential pathways to a cure there are also significant scientific and logistical challenges (Cohn et al., 2020, Chou et al., 2024).

1.3 Study rationale

While ART is highly effective at suppressing HIV, it cannot eliminate the virus due to persistent reservoirs in immune cells. This necessitates lifelong treatment, which poses challenges such as side effects, financial strain, and increased drug interaction risks—issues particularly acute in low- and middle-income countries (Matsuda and Maeda, 2024). Early ART can help reduce viral transmission and limit reservoir size, yet key challenges remain, including restoring life expectancy, reducing drug toxicity, and preventing organ damage (Massanella et al., 2021, Matsuda and Maeda, 2024, Chawla et al., 2018). Lifelong ART also raises the risk of age-related health complications, highlighting the need for affordable therapies that target and potentially eliminate the HIV reservoir (Matsuda and Maeda, 2024).

Finding a cure for HIV is important but challenging due to the complex nature of the HIV-1 reservoir, which is established early after infection (Deeks et al., 2021, Reddy et al., 2024). The HIV reservoir is primarily found in CD4+ T cells, but a growing body of research indicates that the virus also persists in other cell types like monocytes, macrophages, and follicular dendritic cells (Honeycutt et al., 2016, Andrade et al., 2020, Veenhuis et al., 2023), and warrants further investigation. Each of these cell types has distinct biological properties, making it difficult to target the viral reservoir (Chou et al., 2024). Therefore, this study addresses which cell type is prone to harbour more proviral DNA.

To develop curative therapies, it is essential to identify which cellular subsets harbour the highest levels of proviral DNA (Cohen et al., 2011), as these cells are crucial to HIV persistence. Understanding the characteristics of the proviral DNA landscape is necessary, as cells containing intact, replication-competent viral DNA can cause viral

rebound when ART is stopped. Identifying the cellular populations contributing to the HIV-1 reservoir and understanding how HIV persists are key steps toward finding a cure.

Additionally, it has been shown that early ART treatment has been associated with a higher likelihood of remission when ART is interrupted however the underlying mechanisms are unknown (Zhou et al., 2023). Therefore, this study sought to compare the reservoir landscape in immune cell subsets in early versus late treated individuals. This could potentially point to differences that may have clinical relevance in explaining why individuals who start ART early are more likely to go into remission following ART interruption.

Most studies on the HIV reservoir have focused on subtype B, more common in the Global North while there is limited research on subtype C, the most widespread form globally, especially in southern Africa. This knowledge gap complicates the design of HIV cure strategies that are globally effective. Additionally, little data exists on HIV reservoir characteristics in women, even though immune responses and viral loads differ between men and women, potentially influencing reservoir properties (Chang et al., 2013, Sterling et al., 2001).

The innate immune system plays an important role in controlling HIV replication. Specifically, host restriction factors, such as A3G and A3F, restrict HIV replication by introducing hypermutations into the viral genome, leading to defective viral genomes (Simon et al., 2005, Malim and Bieniasz, 2012). These proteins are suitable potential surrogates for the impact of innate responses on the reservoir because of the characteristic mutational patterns that they induce on viral DNA therefore allowing a simple readout of their effects. However, whether high levels of A3 mRNA expression

results in more defective proviruses remains unclear, and this needs further investigation. Manipulating the interaction between A3 proteins and Vif offers a promising approach for HIV cure strategies (Ikeda et al., 2021). Understanding the inducible reservoir and its relationship to immune factors like A3 mRNA expression will help guide future treatment strategies.

This study involved the longitudinal analysis of the HIV-1 subtype C reservoir and A3 proteins in immune cell subsets in a cohort of young women in Durban, South Africa, designed to detect hyperacute infection before peak viremia.

1.3.1 Aims, objectives, and hypotheses

The aims, objectives, and hypotheses of the study were as follows:

- **Aim 1**

To determine which cellular subsets are targeted for viral reservoir seeding and harbour the HIV reservoir.

- **Objective 1**

To sort total PBMC into immune cell subsets and measure total HIV proviral DNA levels using ddPCR.

- **Hypothesis 1**

We hypothesize that initiation of ART in the hyperacute phase of infection will favour the seeding of an increased proportion of the reservoir in myeloid cells due to the expansion of the myeloid cell population and lack of CD4+ T cell activation. Additionally, we hypothesized that central and transitional memory will harbour the highest levels of proviral DNA.

- **Aim 2**

To determine which cellular immune subsets, harbour the intact viral reservoir with the potential to replicate. And to establish the effects of early treatment on the inducible reservoir.

- **Objective 2**

To characterize the proviral landscape by quantifying intact and defective viral genomes in CD4+ T cell subsets and myeloid cells using the IPDA. And to measure the inducible by quantifying the levels of msRNA using SQuHIVLa.

- **Hypothesis 2**

We hypothesize that intact and defective genomes are evenly distributed amongst CD+ T cells and therefore the relative distribution of intact genomes will mirror the proportion of total DNA from different immune subsets. Furthermore, we hypothesize that participants treated during chronic infection would have higher levels of inducible reservoir compared to those individuals treated during acute infection.

- **Aim 3**

To determine APOBEC expression levels in cellular subsets and their effect on the viral reservoir genetic landscape.

- **Objective 3**

To measure A3G/-F mRNA expression in CD4+ T cells and myeloid cells using ddPCR and correlate this with the size defective reservoir determined by IPDA in aim 2. To determine the extent and distribution of A3G and A3F induced hypermutation along the viral genome by analysing previously published FRESH genome sequences (Reddy et. al., 2024).

- **Hypothesis 3**

A3G mRNA expression levels will be higher than A3F mRNA expression levels in both CD4+ T cells and myeloid cells. Additionally, A3G would have a greater effect on the proviral reservoir landscape than A3F by inducing more A3 hypermutations.

2 Chapter 2: Materials and Methods

2.1 Study cohort

For this study, we utilized the Females Rising through Education, Support, and Health (FRESH) cohort (Ndung'u et al., 2018, Dong et al., 2018), which was established in the township of Umlazi located in the province of KwaZulu-Natal, which remains at the epicentre of the HIV epidemic in South Africa. This is an observational, prospective cohort that was launched in 2012 and enrols young, HIV-1 uninfected women who are between the ages of 18 and 24 years. At the time that the cohort was established, HIV acquisition risk in young women within this age group in South Africa was known to be very high, at an estimated incidence of up to 10 per 100 person-years, resulting from poor access to education, economic opportunities, and gender inequalities (Ramjee et al., 2012).

In the FRESH cohort, approximately 75% of acute HIV-1 infections are identified during Fiebig stage I (Dong et al., 2018, Ndung'u et al., 2018, Cohen et al., 2010). Participants are screened for the presence of HIV-1 RNA PCR by fingerpick twice a week during 96 weeks of surveillance, which later changed to 48 weeks (Lee et al., 2019b, Ndung'u et al., 2018).

The FRESH study design incorporates a socioeconomic empowerment intervention component to address challenges that affect young women in this setting. In addition to blood and female genital tract mucosal fluid specimens (cervicovaginal lavage and endocervical swab), other biological specimens namely leukapheresis and excised lymph node samples are collected frequently at both pre- and post-infection time points. Peripheral blood samples were collected at 3-month intervals for HIV negative

participants in longitudinal follow-up. Following the detection of acute HIV infection, peripheral blood samples were collected at weekly intervals for a month, then every 2 weeks for 2 months, monthly for 1 year, and every 3 months thereafter (Figure 2.1). As of October 2024, 108 women have been identified with acute HIV-1 infection.

Acute HIV-1 infection is defined as a new HIV-1 RNA detection, positive on repeat testing, with an evolving HIV-1 Western blot pattern before the development of a p31-positive band. Acute infection staging according to the classification of Fiebig stages (Fiebig et al., 2003) is based on plasma HIV-1 RNA, plasma p24 antigen (p24 Ag), fourth generation HIV enzyme immunoassay (EIA) and Western blot (WB) and defined as follows: stage I (RNA+, p24 Ag−, EIA−, WB−); stage II (RNA+, p24 Ag+, EIA + or −, WB-); stage III (RNA+, p24 Ag+ or −, EIA+, WB- or indeterminate); stage IV (RNA+, p24 Ag+ or −, EIA+, WB indeterminate or +); stage V (RNA+, p24 Ag+ or −, EIA+, WB+ without p31 band) (Cohen et al., 2010, Ndung'u et al., 2018, Dong et al., 2018).

The FRESH cohort is unique and well characterized and provides us with an opportunity to understand acute HIV infection and HIV reservoir establishment, characteristics, and landscape dynamics. The longitudinal follow-up of high-risk women enrolled in this study allows for the identification of biological risk factors for HIV acquisition (Gosmann et al., 2017, Dong et al., 2018, Ndung'u et al., 2018), characterization of transmitted founder virus (TFV), and the immune responses to the transmitted founder virus (Ndhlovu et al., 2015, Kazer et al., 2020), and the assessment of virologic/immunological impact of early ART initiation (Lee et al., 2019b, Baiyegunhi et al., 2022, Muema et al., 2020, Reddy et al., 2024).

The design of the FRESH cohort allows us to address important research questions that may inform the design of future prophylactic, treatment, and cure studies relevant to a population that will benefit greatly from such interventions.

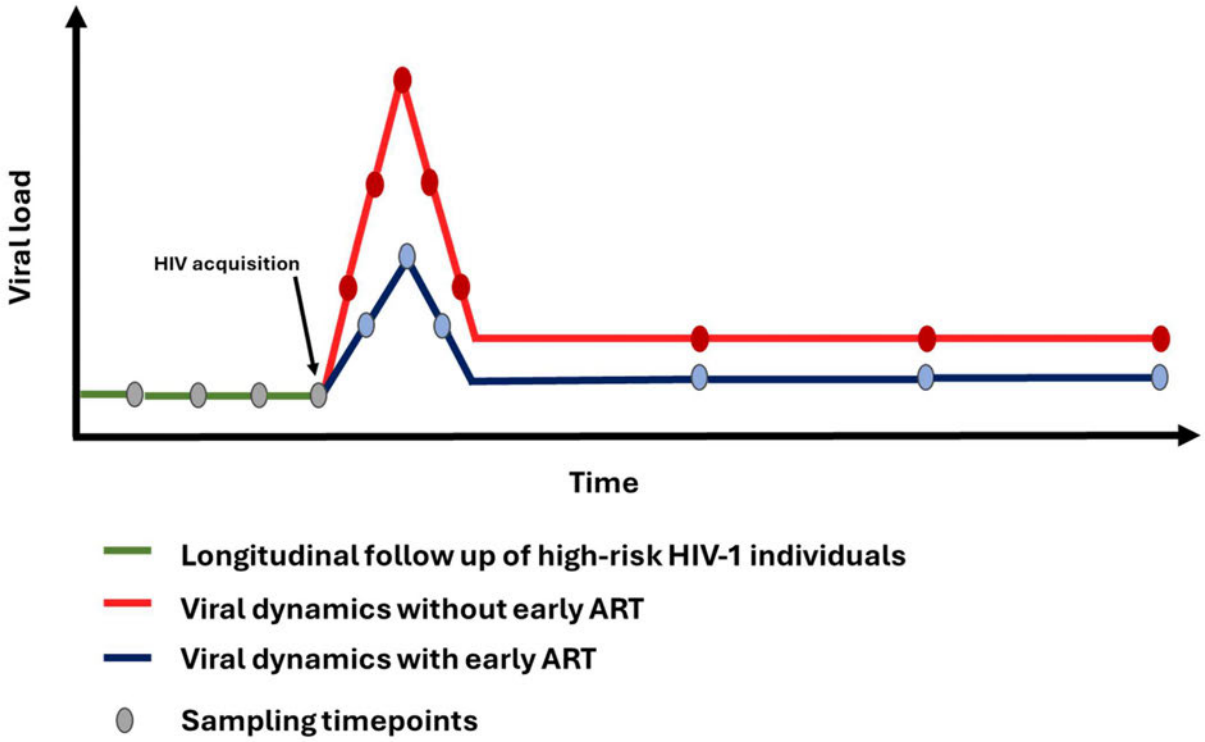

Figure 2.1 FRESH cohort study design. Women are followed up longitudinally (green) until they become HIV infected. Those who were not treated immediately after diagnosis have higher viral load trajectories (red) compared to those who were treated immediately after diagnosis (blue). Sampling timepoints are indicated by the circles and involve the collection of peripheral blood samples every 3 months for HIV negative women enrolled in the study. Following the detection of acute HIV infection, peripheral blood samples were collected at weekly intervals for a month, then every 2 weeks for 2 months, monthly thereafter for 1 year, and every 3 months thereafter.

2.2 Ethical clearance

The Biomedical Research Ethics Committee (BREC) of the University of KwaZulu-Natal (UKZN), BREC reference number BF131/11 approved the parent FRESH protocol. Ethical approval for this sub-study was also obtained from the UKZN BREC, reference number BREC/00003937/2022. All study participants provided written informed consent.

2.3 FRESH treatment regimen

During the first 19 months of the FRESH study, from December 1, 2012, to June 30, 2014, South Africa had not implemented the test and treat strategy. The first 14 study participants who were enrolled in the study did not receive treatment during acute infection. These 14 participants were only eligible for treatment once their CD4 counts dropped below 350 cells/ml, according to the South African guidelines for treatment at the time. However, once South African guidelines for treatment changed all participants offered treatment regardless of their CD4 counts (Ndung'u et al., 2018). These participants were treated with a standard 1st line 3 drug fixed-dose combination pill which includes tenofovir (TDF), emtricitabine (FTC), and efavirenz (EFV) (Dong et al., 2018).

Thereafter, all participants who were newly recruited into the cohort were treated immediately after they were diagnosed with HIV (hyperacute infection). The treatment regimen for FRESH study participants treated during hyperacute infection is a standard 1st line 3 drug regimen which is a fixed dose combination pill intensified with Raltegravir (RAL) from detection until 90 days after suppression. It was observed that participants who received RAL for the first 90 days after detection had a faster rate of

time to viral suppression compared to those individuals who did not receive RAL (Dong et al., 2018).

2.4 Study subgroups and experimental design

For this sub-study, the cohort was divided into four study subgroups based on infection and treatment status: - that is the pre-infection/uninfected arm, the untreated (or pre-therapy) group who remained without treatment during acute and into chronic infection, the chronically treated arm of participants who only initiated treatment during chronic infection and the acute treated group who initiated treatment during hyperacute infection (Figure 2.2). Representative longitudinal measurements of HIV clinical markers, HIV RNA (viral load), and CD4 T lymphocyte cell (CD4) count, for each study group are shown in Figure 2.3.

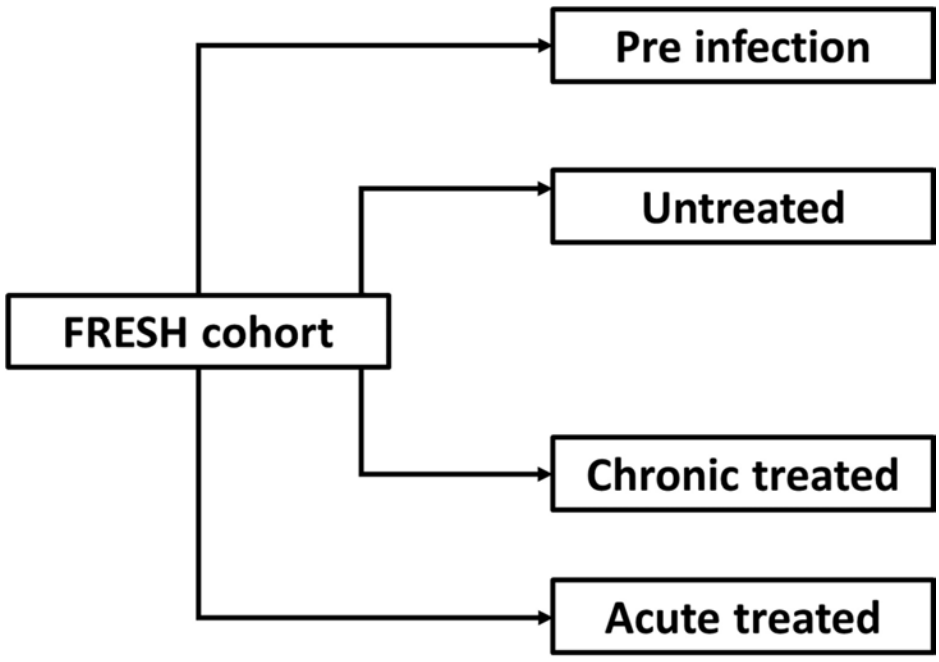

Figure 2.2 Four subgroups of the FRESH cohort included in the current sub-study.

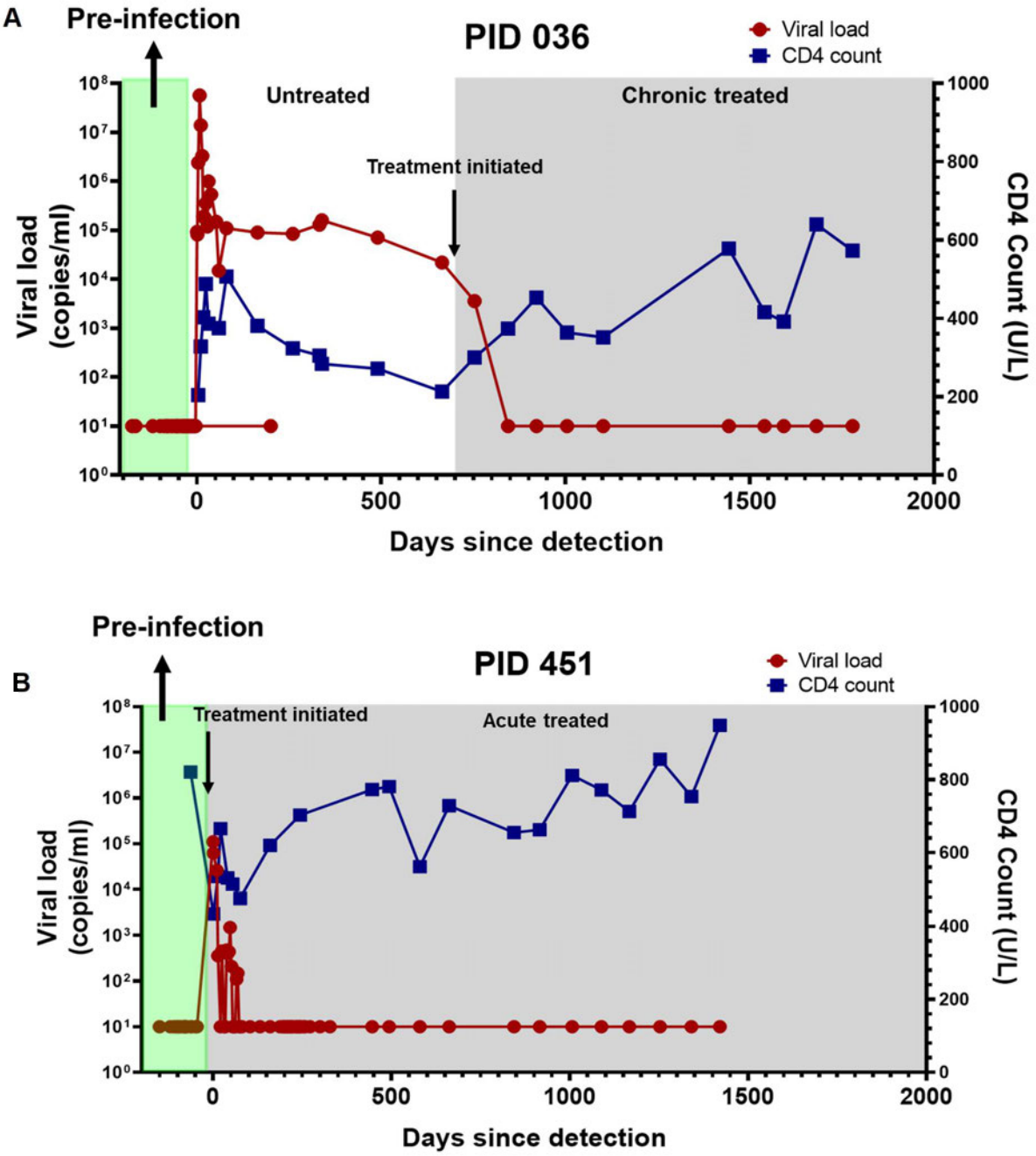

Figure 2.3 Representative viral load (red) and CD4 count trajectories (blue) for each study group. The green area shows pre-infection. The white areas on the graph represent untreated infection, and the grey areas on the graph represent treated

infection. A) shows a study participant treated during chronic infection. B) shows a study participant treated during acute infection.

This study used bio-banked, cryopreserved PBMC and leukapheresis samples. Each study arm described above included five study participants (Figure 2.4). Five participants were untreated during acute infection (untreated group) and later started ART during chronic infection (chronically treated) at a median of 774 (range= 399-1202) days post onset of plasma viremia (DPOPV), while the five acutely treated participants initiated treatment at a median of 1 DPOPV (supplementary figure 1 and 2) (Table 2.1). The median age for the chronically treated group was 23 years (range = 21-24) and the median age for participants that were acutely treated was 20 years (range = 18-23) (Table 2.1). PBMC samples were assessed at the following timepoints: - 1 month, 6 months, and 12 months post-infection as well as 1 month, 6 months, and 12 months post-treatment (Figure 2.4).

Table 2.1 Demographic and clinical characteristics of study participants

	Chronic treated (n=5)	Acute treated (n=5)
Median age at enrollment	23 years (21-24)	20 years (18-23)
Ethnicity % Black African	100%	100%
Sex % Female	100%	100%
Virological status (12 months post-treatment)	Virally suppressed	Virally suppressed
Median treatment initiation days post-detection	774 days post-detection (399-1202)	1 day post-detection*
Median viral load at 1 month post-infection	40,700 cps/ml*	<20 cps/ml
Median viral load at 1 year post-treatment	<20 cps/ml	<20 cps/ml

*All participants treated at a median of 1 day post detection

*Samples were available at 1 month post infection

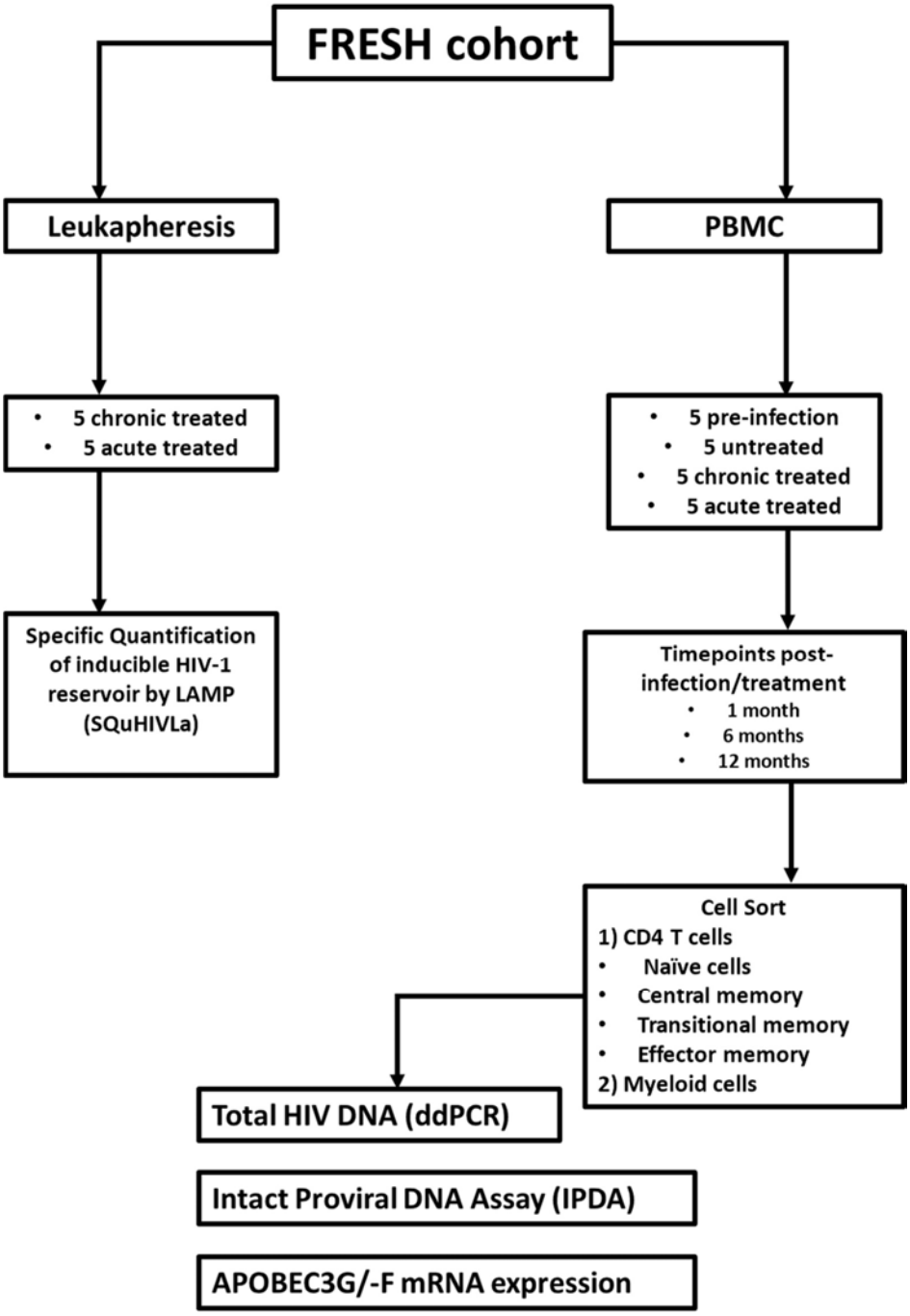

Figure 2.4 Schematic diagram of the experimental design. Sorted cell subsets from PBMC were used to measure total HIV DNA by ddPCR, viral genome intactness by IPDA, and APOBEC3G/-F mRNA expression by ddPCR. Leukapheresis samples were used to measure Tat/Rev multiply spliced RNA (msRNA) by Specific Quantification of inducible HIV-1 reservoir by LAMP SQuHIVLa.

2.5 Cell sorting using flow cytometry

To isolate the immune cell populations from the stained PBMCs according to Table 2.2 and Table 2.3, the cell suspension was subjected to acquisition on a BD FACS Aria Fusion cell sorter for flow cytometry analysis and fluorescent activated cell sorting (FACS), using the FACSDiva 6.1.1 software (BD Bioscience, New Jersey, USA). Appropriate settings were determined for all parameters and compensation to correct for spectral overlap between different fluorophores was performed using the in-house protocol in the Ndung'u lab at AHRI. Thereafter, the six immune cell populations from each PBMC sample, specifically CD4+ naïve, central memory (CM), transitional memory (TM), effector memory (EM), myeloid cells, and CD8 T cells were sorted using a BD FACS Aria Fusion cell sorter (Figure 2.5).

From total PBMCs, leukocytes which comprised both lymphocytes and myeloid cells were gated, followed by a doublet discrimination gating, from which viable cells were selected using Live/Dead Fixable dead cell stain kit (ThermoFisher Scientific). From the viable cell population, myeloid cells (CD3-CD14+) and the CD4+ cell population (CD3+CD4+) were gated for. Specifically, from the CD4+ population, CD4+ naïve (CD45RO-CCR7+CD27+) and CM (CD45RO+CCR7+CD27+) cells were gated. Lastly, based off the CD45RO+ marker, the TM (CD45RO+CD27+CCR7-) and EM (CD45RO+CD27-CCR7-) cells were gated on (Kwon et al., 2020) (BD Biosciences) (Table 2.2).

Using these cell-defining markers to identify the target cell populations, gating and sorting were performed. To ensure the collection of pure cell populations, a '4-way purity' sort option was used, and a representative post-sort analysis was done, ensuring no contamination. Cells were collected in 1.5 mL microcentrifuge Eppendorf

tubes containing 100 µL of RLT Lysis Buffer supplemented with β-mercaptoethanol (BME) (in preparation for nucleic acid extractions). These cell suspension samples were stored at -80°C until subsequent nucleic acid extractions the following day. All data were analysed using FlowJo v10.8 software (FlowJo Africa, BD Biosciences). From the total PBMCS, which was approximately 20-30 million cells, we used flow cytometry to sort the above-mentioned number of cells per population (ranges are provided). Thereafter, a portion of the cells was used for total DNA quantification, and the rest of the cells were used for IPDA (Table 8.1).

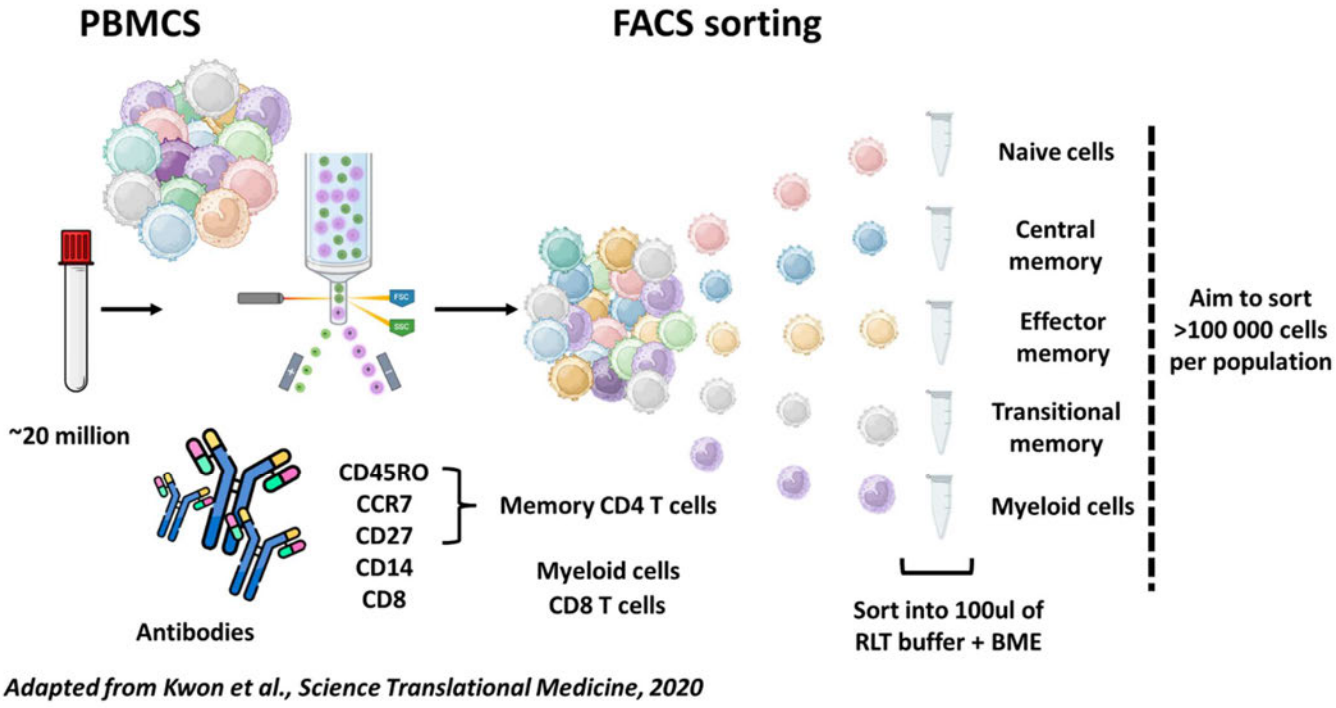

Figure 2.5 **Flow cytometry pipeline to sort memory CD4+ T cells, myeloid cells, and CD8 T cells.** PBMCs are stained with a cocktail of antibodies that target cell populations. Cells were then sorted in 100ul of RLT buffer supplemented with β mercaptoethanol (BME). A number greater than 100,000 cells per population was sorted (Adapted from (Kwon et al., 2020) (Created with Biorender.com).

Table 2.2 Antibodies and fluorochromes used to sort CD4+ T cells and myeloid cells

Antibody	Fluorochrome
CD27	BV650
CD4	BV711
CCR7	PeDazzle
CD3	PE
CD45RO	PeCy5
CD14	PeCy7
CD8	FITC

Table 2.3 Staining protocol for flow cytometry

Master mix protocol	Amount to add (µl)
CD27 BV650	3
CD4 BV711	3
CCR7 PeDazzle	3
CD3 PE	3
CD45RO PeCy5	3
CD14 PeCy7	3
CD8 FITC	3
FACS Buffer	79
Total	100

2.6 DNA/RNA extraction

RNA and DNA were extracted from each of the sorted cell populations using the Qiagen AllPrep RNA and DNA extraction kit (QIAGEN, Hilden, Germany). This kit allowed for the simultaneous purification of genomic DNA and total RNA from the same sample. The homogenized cell suspension was first passed through an AllPrep

DNA spin column containing a silica membrane, which selectively binds the DNA. The resulting filtrate was passed through an RNeasy spin column containing a silica membrane, which selectively binds the RNA.

Extractions were performed according to the manufacturer's guidelines (QIAGEN, Hilden, Germany). RNA and DNA were eluted at 30 µl and 80 µl respectively. The extracted RNA and DNA were quantified using the Nanodrop Lite spectrometer (ThermoFisher Scientific, Waltham, USA). The RNA samples were stored at -80°C and later used to assess APOBEC3G/-F mRNA gene expression levels. The DNA samples were stored at -20°C and used for the quantification and characterization of HIV proviral DNA.

2.7 Reservoir Quantification and Characterization Assays

2.7.1 Measurement of total HIV DNA by ddPCR

2.7.1.1 The 8E5/LAV cell line

The 8E5/LAV cell line was used as a positive control. This cell line contains a single copy of integrated HIV and two copies of human RPP30. Cryopreserved samples were thawed and R10 at 37˚C was added in a dropwise manner (Folks et al., 1986). R10 media consisted of 10% heat-inactivated fetal bovine serum (FBS) (Gibco, ThermoFisher Scientific, USA) and 500 mL RPMI 16140 (Gibco, ThermoFisher, USA). The starting culture was 2 x 10^6 cells per mL. After 24 hours cells were split and the new flask was seeded with 1 x 10^6 cells per mL. The cells were then passaged every 3 days thereafter. DNA was then extracted according to the manufacturer's instructions using the QIAGEN DNA blood and tissue kit (QIAGEN, Hilden, Germany) (Folks et al., 1986).

2.7.1.2 Quantification of total HIV DNA by ddPCR

Total HIV-1 DNA and host cell concentrations in the DNA extracts from sorted cell subsets were estimated using Bio-Rad ddPCR as previously described in (Lee et al., 2019b, Reddy et al., 2024) using primers and probes covering HIV-1 5′ LTR-*gag* HXB2 coordinates 684–810, listed in Table 2.3 below (Integrated DNA Technologies (IDT), Iowa, USA). PCR reaction components are listed in Tables 2.4 and 2.5. Droplets were generated using the Bio-Rad automated droplet digital PCR system (QX200 AutoDG). PCR was performed on the T100 thermocycler (Bio-Rad, California, USA) under the following cycling conditions: 95 °C for 10 min, 45 cycles of 94 °C for 30 seconds, and 60 °C for 1min, 72°C for 1min. Fluorescence of each droplet was read by the Bio-Rad QX100 droplet reader and data were analyzed using QX Manager software (Bio-Rad, California, USA) (Figure 2.6). To each reaction for the HIV LTR-*gag* PCR, 4 µL of DNA template was added to give a final volume of 22 µL (Table 2.4). To each reaction for RPP30 3 µL of DNA template was added to give a final volume of 22 µL (Table 2.5). HIV LTR-*gag* and RPP30 measurements were performed in triplicate.

Table 2.4 Primers and probes for total HIV DNA quantification

Primer/Probe	Sequence	Position HXB2
LTR- gag Forward primer	5′-TCTCGACGCAGGACTCG-3′	684–810
LTR- gag Reverse primer	5′-TACTGA CGCTCTCGCACC-3	684–810
probe/56-	FAM/CTCTCTCCT/ZEN/TCTAGCCTC/ 31ABkFQ/	781-789(RC);772-780(RC)
RPP30 gene forward primer	5′-GATTTGGACCTGC GAGCG-3′	n/a

RPP30 gene reverse primer	5′-GCGGCTGTCTCCACAAGT-3′	n/a
probe/56-	FAM/ CTGACCTGA/ZEN/AGGCTCT/31ABkFQ/	n/a

Table 2.5 Components of droplet digital PCR reaction (Total HIV LTR-*gag*)

Reagent (Total HIV LTR-*gag*)	Reagent volume (µL)
ddPCR master mix	10
H2O	5.65
Forward primer (20 µM)	1
Reverse primer (20 µM)	1
Probe (20uM)	0.35
DNA	4
Total reaction volume	22

Table 2.6 Components of droplet digital PCR reaction (RPP30)

Reagent (RPP30)	Reagent volume (µL)
ddPCR master mix	10
H2O	6.65
Forward primer (20 µM)	1
Reverse primer (20 µM)	1
Probe (20 µM)	0.35
DNA	3
Total reaction volume	22

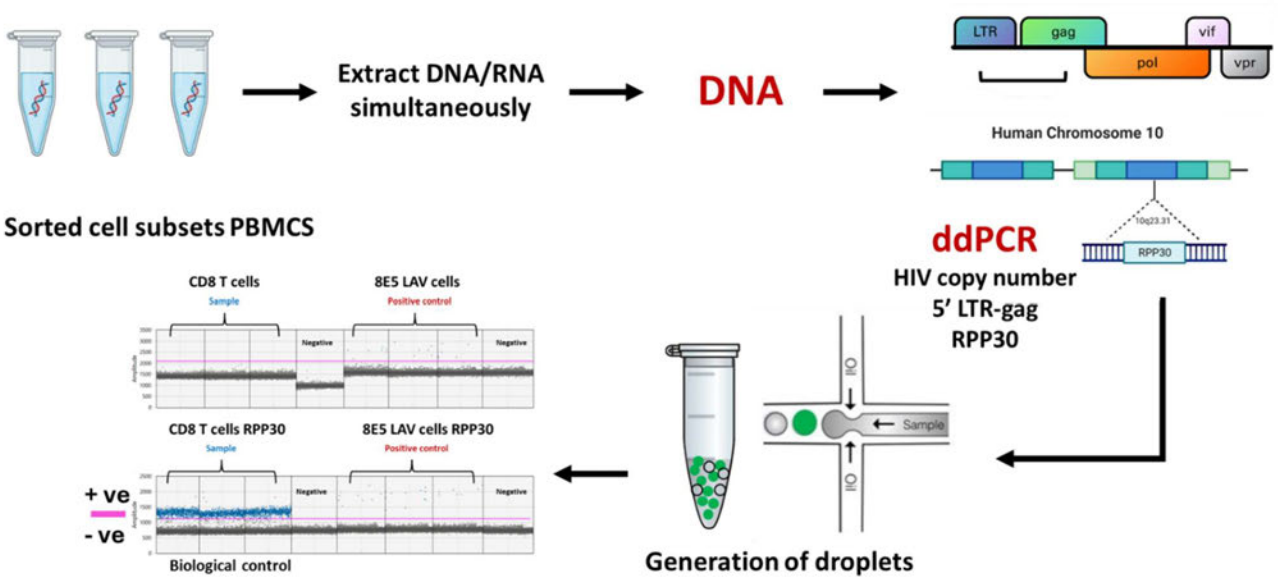

Figure 2.6 Pipeline to quantify total HIV DNA from sorted cells. ddPCR is an absolute quantification of a gene of interest. Total HIV-DNA is amplified with primers that target the 5'-LTR-Gag region. Cell input is measured by amplification of the housekeeping gene RPP30. Droplet digital PCR data can be viewed as a 1-D plot with each droplet from a sample plotted on the graph of fluorescence intensity versus droplet number. Blue dots denote positively amplified droplets while grey dots are negative. A manual threshold indicated by the pink line is set to distinguish the positive and negative droplet clouds. DNA from CD8+ T cells was included as a negative biological control. DNA from the 8E5/LAV cell line was used as a positive control.

2.7.2 Quantification of T cell Receptor Excision Circle (TREC) expression by ddPCR

To confirm the absence of T cells in the myeloid populations (Lynch and Sempowski, 2013), T cell receptor excision circle (TREC) expression was measured. Primers and probes were supplied by Integrated DNA Technologies (IDT, Iowa, USA) (Table 2.7) (Mikhael and Elsorady, 2019). TREC expression was analysed relative to the expression of the housekeeping gene GAPDH. TREC PCR reaction mix contained 5 µL of DNA template to a final volume of 22µL (Table 2.8). GAPDH PCR reaction contained 2 µL of DNA (1:50 dilution) for a final volume of 22 µL (Table 2.8). Pre-designed TaqMan assay was used to measure GAPDH mRNA expression (Hs02786624_g1) (ThermoFisher Scientific, Waltham, USA) (Table 2.9).

Relative expression levels of TREC to glyceraldehyde-3-phosphate dehydrogenase GAPDH in each sample were determined by dividing the concentration of the target gene (TREC) by the concentration of the housekeeping gene (GAPDH). The resulting target/reference ratio expressed the amount of TREC normalized to the level of GAPDH. For each cell subset, TREC and GAPDH were measured in triplicate. Droplets were then generated using the QX200 AutoDG (Bio-Rad, California, USA). The cycling conditions were as follows: 95 °C for 10 min, 45 cycles of 94 °C for 30s and 60 °C for 1 min, 72°C for 1 min.

Table 2.7 Primers and probes used for TREC ddPCR

Primer/Probe	Sequence	Position HXB2
TREC Forward primer	5’- CACATCCCTTTCAACCATGCT-3’	n/a
TREC Reverse primer	5’-GCCAGCTGCAGGGTTTAGG-3’	n/a

TaqMan probe	FAM- ACACCTCTGGTTTTTGTAAAGGTGCCCACTTAMRA	n/a

Table 2.8 Components of droplet digital PCR reaction (TREC)

Reagent (TREC)	Reagent volume (µL)
ddPCR master mix	10
H2O	4.65
Forward primer (20 µM)	1
Reverse primer (20 µM)	1
Probe (20 µM)	0.35
DNA	5
Total reaction volume	22

Table 2.9 Components of droplet digital PCR reaction (GAPDH)

Reagent (GAPDH)	Reagent volume (µL)
ddPCR master mix	10
H2O	7.65
Forward primer (20 µM)	1
Reverse primer (20 µM)	1
Probe (20 µM)	0.35
DNA	2
Total reaction volume	22

2.7.3 Quantification of intact and defective viral genomes by IPDA

Proviral DNA was quantified using a multiplex ddPCR, targeting parts of the Ψ (*psi*) and *env* region, using the primer sets described in the table below (Table 2.10). The *RPP30* cellular gene was used to measure cellular input. The DNA shearing index (DSI), was used to indicate DNA fragmentation. DNA from PBMCs of HIV-negative

donors was used as a DNA template control, J-Lat full-length clone 15.4 cells (NIH AIDS Reagent Program) as an HIV-positive control, and PCR grade water as a no template control. All cell subsets were assessed in duplicate (Buchholtz et al., 2024).

Table 2.10 Table 2.10 Overview of primers and probes used for subtype B&C IPDA (Buchholtz et al., 2024)

Primer/Probe	Sequence	Position HXB2
***psi* forward**	TCTCGACGCAGGACTCG	684–700
***psi* probe**	/56-FAM/CTCTCTCCT/ZEN/TCTAGCCTC/3IABkFQ/	772–789
***psi* reverse subtype B**	TACTGACGCTCTCGCACC	793–810
***psi* reverse subtype C**	TATTGACGCTCTCGCACC	793–810
***env* forward subtype B**	AGTGGTGCAGAGAGAAAAAAGAGC	7736–7759
***env* forward subtype C**	AGTGGTGGAGAGAGAAAAAAGAGC	7736–7759
***env* probe**	/5HEX/CCTTGGGTT/ZEN/CTTGGGAGC/3IABkFQ/	7781–7798
***env* hypermutation probe**	/5IABkFQ/CCTTAGGTTCTTAGGAGC/3IABkFQ/	7781–7798
***env* reverse**	GTCTGGCCTGTACCGTCAGC	7851–7832
***RPP30* forward 1**	GATTTGGACCTGCGAGCG	n/a
***RPP30* reverse 1**	GCGGCTGTCTCCACAAGT	n/a
***RPP30* probe 1**	/5HEX/CTGACCTGA/ZEN/AGGCTCT/3IABkFQ/	n/a
***RPP30* forward 2**	CCATTTGCTGCTCCTTGGG	n/a
***RPP30* reverse 2**	CATGCAAAGGAGGAAGCCG	n/a
***RPP30* probe 2**	/56-FAM/AAGGAGCAA/ZEN/GGTTCTATTGTAG/3IABkFQ/	n/a

First, primers and probes were titrated to give the optimal amplitude of 5,000 units in the ddPCR readout for *psi* and *env*. Additionally, the optimal amplitude for *RPP30* was 3000 units. Titration was done according to the experimental design shown in Figure 4.1 (Buchholtz et al., 2024). From the titration experiment (Figure 2.7) it was determined that the 1X concentration gave optimal amplitude at 5000 units (Supplementary Figure 3). Once this was determined primers and probes were diluted,

1X concentration stocks were made and these primer/probe stocks were frozen at -20 ˚C to be utilized in the ddPCR master mix.

Thereafter, ddPCR mastermixes were made according to Tables 2.11 and 2.12 and, for both *psi* and *env* and additionally for *RPP30*. DNA was diluted according to desired concentrations based on the nanodrop concentration we obtained after DNA extraction. DNA was diluted and was kept aside to be added to the master mix according to the protocol (Buchholtz et al., 2024). 8,7 µl DNA was added to 13,3 µl of mastermix to give a volume of 22 µl (Table 2.11). For the RPP30 reaction, DNA was diluted based on the concentration of DNA after the extraction to make a predilution mix. Thereafter 5 µl of the predilution was added to 17 µl of mastermix to give a final volume of 22 µl (Table 2.12).

Thereafter, droplets were generated using the automated droplet generator QX200 AutoDG (Bio-Rad, California, USA) (Figure 2.8). The following cycling conditions were followed: cycle conditions were performed according to the manufacturer's protocol (Bio-Rad, California, USA) 95 °C for 10 min, 45 cycles of 94 °C for 30 seconds and 58 °C for 1 min, 72°C for 1 min. QX manager software was used to analyze the results. Positive and negative droplets were discriminated by manual threshold setting (Buchholtz et al., 2024). Results were exported and analyzed using GraphPad Prism version 9.5.1.

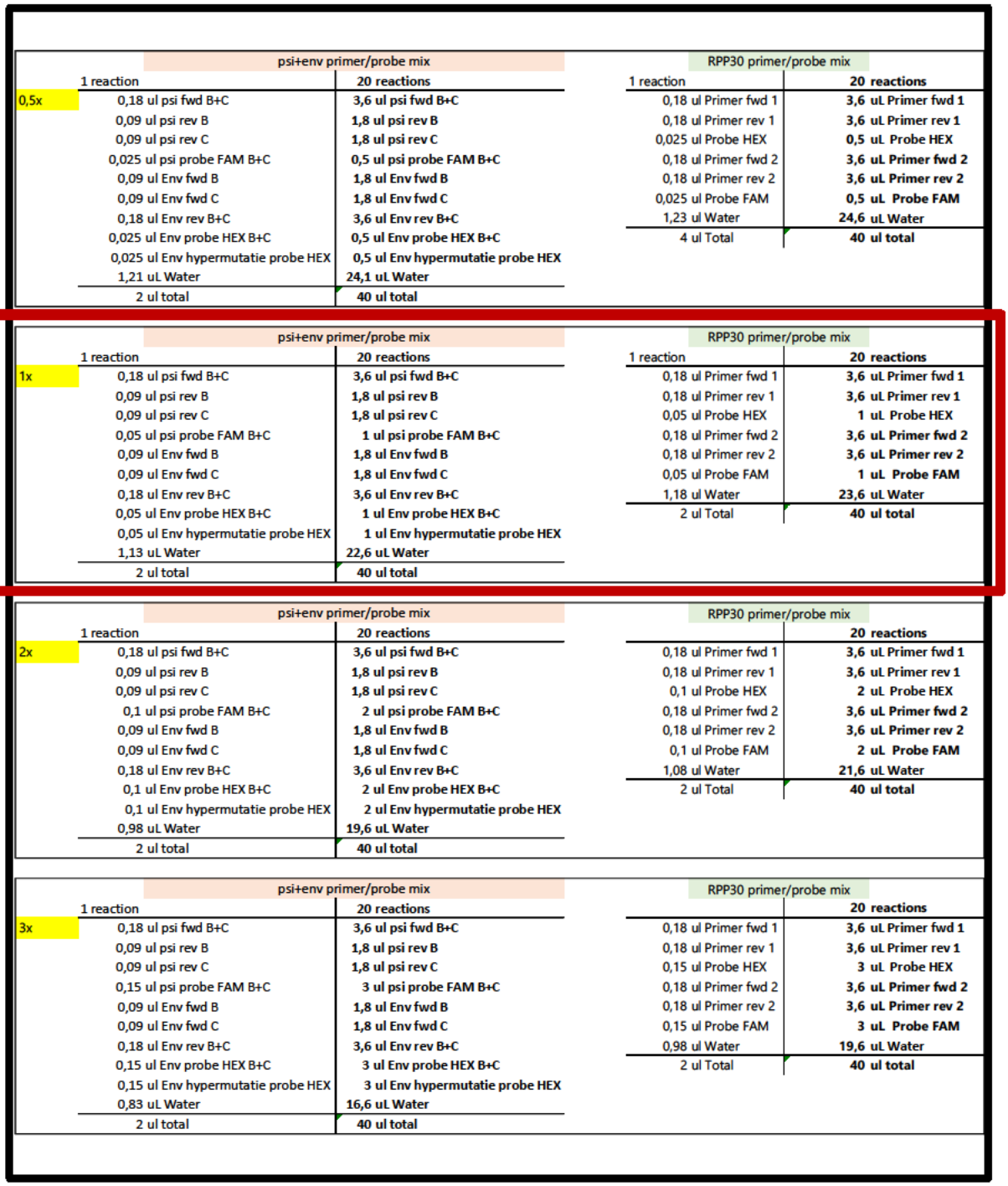

psi+env primer/probe mix			RPP30 primer/probe mix	
	1 reaction	20 reactions	1 reaction	20 reactions
0,5x	0,18 ul psi fwd B+C	3,6 ul psi fwd B+C	0,18 ul Primer fwd 1	3,6 uL Primer fwd 1
	0,09 ul psi rev B	1,8 ul psi rev B	0,18 ul Primer rev 1	3,6 uL Primer rev 1
	0,09 ul psi rev C	1,8 ul psi rev C	0,025 ul Probe HEX	0,5 uL Probe HEX
	0,025 ul psi probe FAM B+C	0,5 ul psi probe FAM B+C	0,18 ul Primer fwd 2	3,6 uL Primer fwd 2
	0,09 ul Env fwd B	1,8 ul Env fwd B	0,18 ul Primer rev 2	3,6 uL Primer rev 2
	0,09 ul Env fwd C	1,8 ul Env fwd C	0,025 ul Probe FAM	0,5 uL Probe FAM
	0,18 ul Env rev B+C	3,6 ul Env rev B+C	1,23 ul Water	24,6 uL Water
	0,025 ul Env probe HEX B+C	0,5 ul Env probe HEX B+C	4 ul Total	40 ul total
	0,025 ul Env hypermutatie probe HEX	0,5 ul Env hypermutatie probe HEX		
	1,21 uL Water	24,1 uL Water		
	2 ul total	40 ul total		

psi+env primer/probe mix			RPP30 primer/probe mix	
	1 reaction	20 reactions	1 reaction	20 reactions
1x	0,18 ul psi fwd B+C	3,6 ul psi fwd B+C	0,18 ul Primer fwd 1	3,6 uL Primer fwd 1
	0,09 ul psi rev B	1,8 ul psi rev B	0,18 ul Primer rev 1	3,6 uL Primer rev 1
	0,09 ul psi rev C	1,8 ul psi rev C	0,05 ul Probe HEX	1 uL Probe HEX
	0,05 ul psi probe FAM B+C	1 ul psi probe FAM B+C	0,18 ul Primer fwd 2	3,6 uL Primer fwd 2
	0,09 ul Env fwd B	1,8 ul Env fwd B	0,18 ul Primer rev 2	3,6 uL Primer rev 2
	0,09 ul Env fwd C	1,8 ul Env fwd C	0,05 ul Probe FAM	1 uL Probe FAM
	0,18 ul Env rev B+C	3,6 ul Env rev B+C	1,18 ul Water	23,6 uL Water
	0,05 ul Env probe HEX B+C	1 ul Env probe HEX B+C	2 ul Total	40 ul total
	0,05 ul Env hypermutatie probe HEX	1 ul Env hypermutatie probe HEX		
	1,13 uL Water	22,6 uL Water		
	2 ul total	40 ul total		

psi+env primer/probe mix			RPP30 primer/probe mix	
	1 reaction	20 reactions		20 reactions
2x	0,18 ul psi fwd B+C	3,6 ul psi fwd B+C	0,18 ul Primer fwd 1	3,6 uL Primer fwd 1
	0,09 ul psi rev B	1,8 ul psi rev B	0,18 ul Primer rev 1	3,6 uL Primer rev 1
	0,09 ul psi rev C	1,8 ul psi rev C	0,1 ul Probe HEX	2 uL Probe HEX
	0,1 ul psi probe FAM B+C	2 ul psi probe FAM B+C	0,18 ul Primer fwd 2	3,6 uL Primer fwd 2
	0,09 ul Env fwd B	1,8 ul Env fwd B	0,18 ul Primer rev 2	3,6 uL Primer rev 2
	0,09 ul Env fwd C	1,8 ul Env fwd C	0,1 ul Probe FAM	2 uL Probe FAM
	0,18 ul Env rev B+C	3,6 ul Env rev B+C	1,08 ul Water	21,6 uL Water
	0,1 ul Env probe HEX B+C	2 ul Env probe HEX B+C	2 ul Total	40 ul total
	0,1 ul Env hypermutatie probe HEX	2 ul Env hypermutatie probe HEX		
	0,98 uL Water	19,6 uL Water		
	2 ul total	40 ul total		

psi+env primer/probe mix			RPP30 primer/probe mix	
	1 reaction	20 reactions		20 reactions
3x	0,18 ul psi fwd B+C	3,6 ul psi fwd B+C	0,18 ul Primer fwd 1	3,6 uL Primer fwd 1
	0,09 ul psi rev B	1,8 ul psi rev B	0,18 ul Primer rev 1	3,6 uL Primer rev 1
	0,09 ul psi rev C	1,8 ul psi rev C	0,15 ul Probe HEX	3 uL Probe HEX
	0,15 ul psi probe FAM B+C	3 ul psi probe FAM B+C	0,18 ul Primer fwd 2	3,6 uL Primer fwd 2
	0,09 ul Env fwd B	1,8 ul Env fwd B	0,18 ul Primer rev 2	3,6 uL Primer rev 2
	0,09 ul Env fwd C	1,8 ul Env fwd C	0,15 ul Probe FAM	3 uL Probe FAM
	0,18 ul Env rev B+C	3,6 ul Env rev B+C	0,98 ul Water	19,6 uL Water
	0,15 ul Env probe HEX B+C	3 ul Env probe HEX B+C	2 ul Total	40 ul total
	0,15 ul Env hypermutatie probe HEX	3 ul Env hypermutatie probe HEX		
	0,83 uL Water	16,6 uL Water		
	2 ul total	40 ul total		

Figure 2.7 Experimental design of titration of primers and probes for IPDA. Four different volume parameters were assessed. 0,5X, 1X, 2X, and 3X to determine which probe gave an amplitude of 5,000 units. The red block highlights the volume of the probe and primers that gave optimal fluorescence (1x).

Table 2.11Components of droplet digital PCR for IPDA (*psi* and *env*)

Reagent (psi and env)	1 reaction (µL)
ddPCR master mix	11
***psi/env* B+C probe sub C**	2
XhoI (restriction enzyme)	0,28
DNA	8.73
Total reaction volume	22

Table 2.12 Components of droplet digital PCR for IPDA (*RPP30*)

Reagent (RPP30)	1 reaction (µL)
ddPCR master mix	11
H2O	3.72
RPP30 primer/probe	2
XhoI (restriction enzyme)	0.28
DNA (predilution)	5
Total reaction volume	22

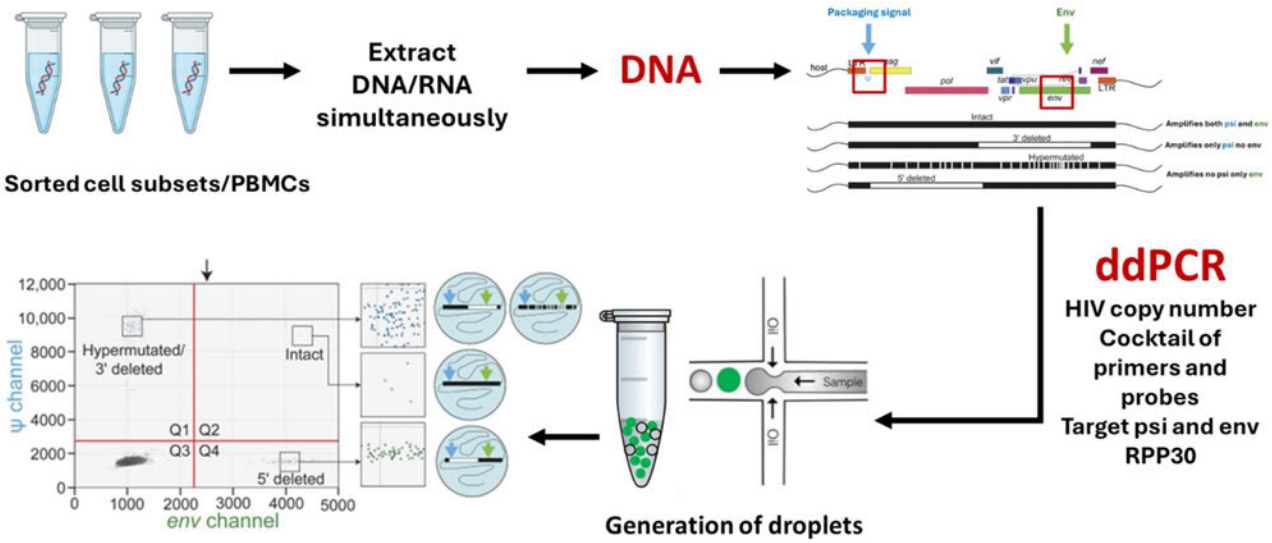

Figure 2.8 Pipeline for IPDA. Memory CD4+ T cells and myeloid cells were sorted. DNA was then extracted and then ddPCR was carried out using a cocktail of primers and probes that target the *psi* and *env* regions of the HIV genome. Droplets were generated using the automated droplet generator. Cell input was measured by amplification of the housekeeping gene RPP30. Droplet digital PCR data can be viewed as a 2-D plot with each droplet from a sample plotted on the graph of fluorescence intensity versus droplet number. Blue dots denote positively amplified droplets while grey dots are negative. A manual threshold indicated by the pink line is set to distinguish the positive and negative droplet clouds. To analyze the data 2D function was utilized on the QX Manager software (Bio-Rad, California, USA). The 3' deleted and hypermutated DNA would be in Q1, the intact DNA would be in Q2, the 5' deleted DNA would be in Q4, and the negative droplets would be in Q3 (Created with Biorender.com).

2.7.4 Measurement of the inducible reservoir by SQuHIVLa

2.7.4.1 Isolation of CD4+ T cells from leukapheresis samples

Leukapheresis samples were thawed and resuspended in culture RPMI -1640 media (Gibco, ThermoFisher Scientific, California, USA) supplemented with 10% FBS and 100ug/ul penicillin-streptomycin. This was spun at 2000 rpm for 6 minutes. The supernatant was then decanted and resuspended in 20ml of buffer, consisting of phosphate-buffered saline (PBS), bovine serum albumin (BSA), and Ethylenediaminetetraacetic acid (EDTA), supplemented with 20 µl of DNase (New England Biolabs, Massachusetts, USA). Cells were then counted and viability was determined. Thereafter, the protocol for isolating CD4+ T cells that was described by Miltenyi Biotec (Miltenyi biotech, North Rhine-Westphalia, Germany) was followed.

2.7.4.2 Specific Quantification of inducible HIV-1 reservoir by LAMP (SQuHIVLa)

Once CD4+ T cells were isolated and viability was determined. The cells were then plated out and were rested for five hours at 37˚ C in a humidified, 5% CO_2 incubator. CD4+ T cells were then stimulated with 100 ng/mL of PMA and 1 µg/mL ionomycin (Sigma) for approximately 12-14 hours (Hossain et al., 2023).

After the stimulation, the cells appeared aggregated and clumped. The activated CD4+ T cells were then counted and washed using PBS. Cells were then diluted such that, there was 4000 per µl. Primers and probes were specifically designed to analyze subtype C samples (Table 2.13) From this further dilutions were made: 20,000 cells, 5,000 cells, 1,250 cells, and 313 cells. 5 µl of each of these dilutions were added to 15µl of mastermix described in Table 2.14. For the RT-LAMP reaction the following cycling conditions were used, incubation at 45˚C for 60 minutes, continuous 65˚C with flourescence reads every 30 seconds for 180 cycles on the CFX Touch Real-Time

detection system (Bio-Rad, California, USA). After the RT-LAMP reaction, the positive wells at each dilution were scored, and the maximum likelihood method was used to determine the frequency of cells expressing *tat/rev* msRNA using the IUPMStats v1.0 online software (Rosenbloom et al., 2015) (Figure 2.9).

Table 2.13 *Tat/Rev* HIV-1 msRNA specific LAMP primers and probes sequences

Primer/Probe	Sequence
CF3	TCCTTGTAATAAGTGTTATTGTAA
CB3	CGATTCTTCCGAGCCTGTC
CFIP	CCGCTTCTTCCTGCCATAGGAATAGCTATCATTGTCTAGTTTGC
CBIP	CGACGAAGCGCTCCTCCAAGGTTTGGGGTAAGGGTTGCT
CLF Probe	TGCCTAAGCCTTTTGTC/i6-FAMK/G
CLB	CAGTGAGGATCATCAAAATC

Table 2.14 **Components of the SQuHIVLa master mix**

Reagent	1 reaction (µL)
10X Isothermal Amplification buffer	2
$MgSO_4$ (100 mM)	1.2
dNTP (10 mM)	2.8
FIP/BIP (32 µM)	1
F3/B3 (8 µM)	0.5
LF probe/LB primer (16 µM)	1
Bst 2.0 Warmstart DNA polymerase (8000 units/mL)	0.5
Warmstart RxT Reverse Transcriptase (15000 units/mL)	0.5
RNasin RNase Inhibitor (40 units/ul)	0.5
Titron X 4%	5
Template	5
Total reaction volume	20

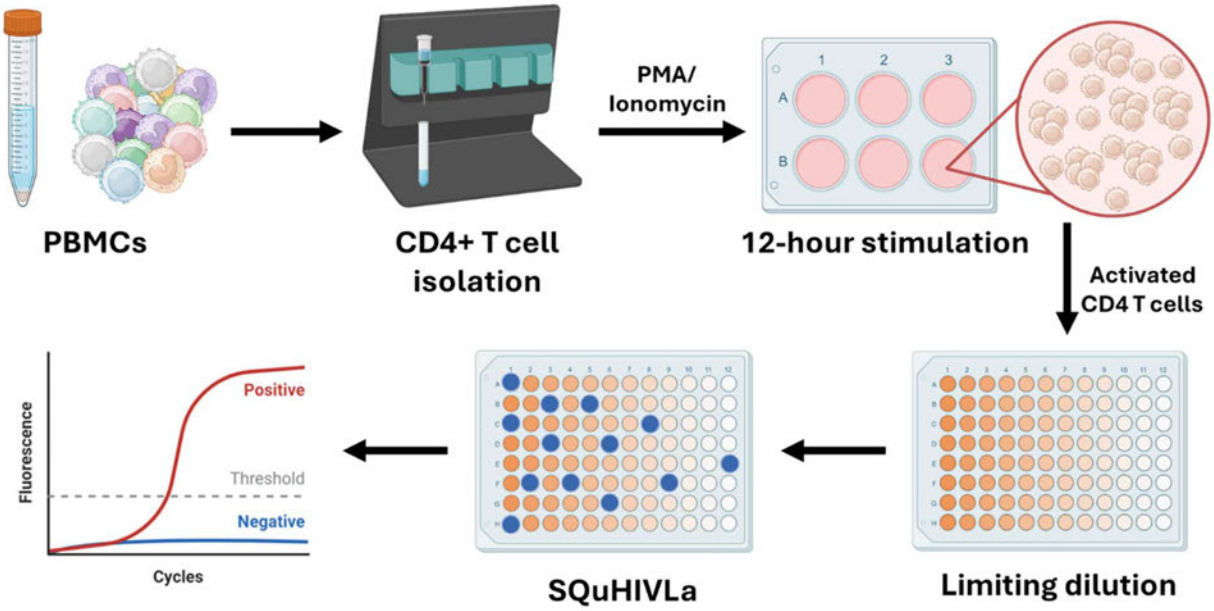

Figure 2.9 Pipeline for quantifying msRNA using SQuHIVLa. Leukapheresis samples were thawed. CD4+ T cells were isolated and thereafter stimulated with PMA and ionomycin for 12-14 hours. Activated CD4 T cells were diluted using limiting dilution and thereafter RT-LAMP PCR was performed (Created with Biorender.com).

2.8 APOBEC3G/F profiling of immune cells to establish their impact on the proviral reservoir

2.8.1 Testing in vitro expression of APOBEC3 in 293 T cells (positive control)

HEK 293 T cells were propagated up in Dulbecco's Modified Eagle Medium (DMEM) (Invitrogen, Massachusetts, USA) supplemented with 10% penicillin, L-glutamine, and fetal bovine serum (FBS). Thereafter, 3 million cells were plated out in 24-well culture plates. Cells were then co-transfected with 100ng of APOBEC3G plasmid PRT600 A3G or APOBEC3F plasmid PRT600 A3F, PRT600 GFP, and 4mg/ml transfection reagent polyethyleneimine (PEI) (Figure 2.10) (Reddy et al., 2016, Ooms et al., 2013).

Additionally, cells were incubated for 48 hours. After that, cells were lysed, and RNA was extracted. cDNA was then synthesized based on the method described below. Subsequently, ddPCR was performed, and mRNA expression was analyzed (Supplementary Figure 4). This served as a positive control when determining APOBEC3G/-F mRNA expression in participant samples.

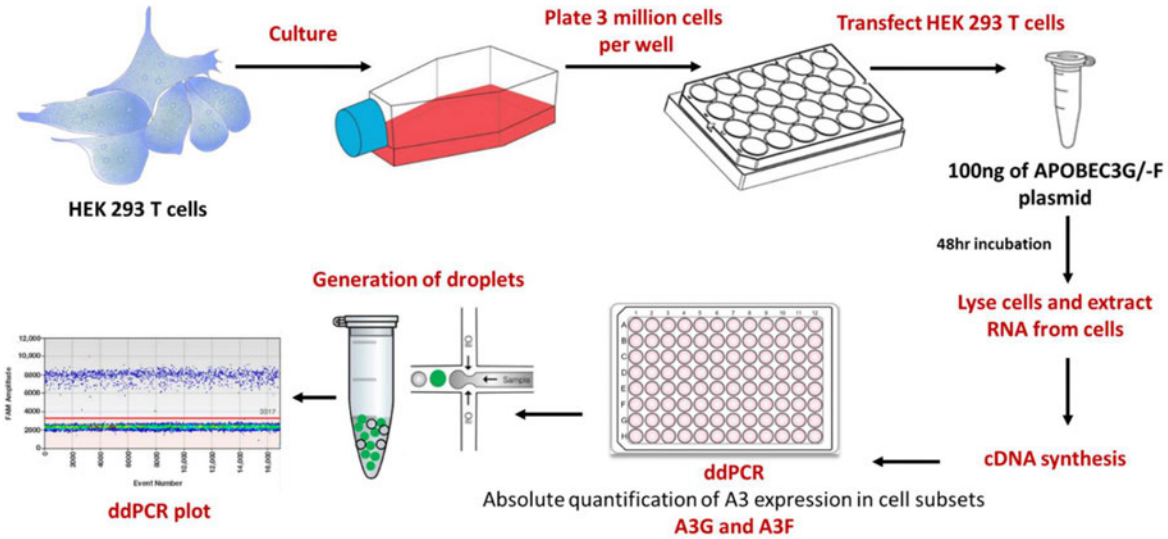

Figure 2.10 Pipeline for testing APOBEC3 expression *in vitro* (created with Biorender.com).

2.8.2 cDNA synthesis

RNA from the sorted cells was converted into cDNA using the iScriptTM cDNA synthesis kit according to manufacturer instructions (Bio-Rad, California, USA). Table 2.15 highlights the components used for the cDNA synthesis reaction.

Table 2.15 Components of the cDNA synthesis reaction

Reagent	1 reaction (µL)
Reaction Master mix	10
Reverse transcriptase	2
Nuclease free -water	10
RNA template	18
Total reaction volume	40

Cycling conditions were followed: priming for 5 minutes at 25˚C, reverse transcription (RT) at 20 minutes at 46˚C, and RT inactivation for 1 minute at 95˚C.

2.8.3 APOBEC3G/-F mRNA expression using ddPCR

APOBEC3G/F gene expression patterns in these cell subsets by digital droplet PCR (ddPCR) (Bio-Rad, California, USA) using predesigned TaqMan gene expression assays containing specific primers and probes labelled with the FAM fluorescent dye (ThermoFisher Scientific, Waltham, USA). The following kits were purchased: Predesigned TaqMan assay was used to measure glyceraldehyde-3-phosphate dehydrogenase (GAPDH) mRNA expression (Hs02786624_g1) (ThermoFisher Scientific, Waltham, USA). To measure A3G mRNA expression the following predesigned kit was used Hs00222415_m1 (ThermoFisher Scientific, Waltham, USA). Further, to measure A3F mRNA expression Hs01665324_m1 was used

(ThermoFisher, Waltham, USA). The housekeeping gene GAPDH was used as the housekeeping/reference gene (ThermoFisher Scientific, Waltham, USA). The components of each ddPCR are listed below in Tables 2.16, 2.17, and 2.187. cDNA was diluted to 1:50 and 5 µl was added to the A3G and A3F. 3 µl of the diluted cDNA was added to the reaction. ddPCR was performed using the following cycling conditions: 95 °C for 10 min, 45 cycles of 94 °C for 30 s and 60 °C for 1 min, 72 °C for 1 min (Figure 2.11). A3G and A3F mRNA expression levels were measured in cell subsets at different timepoints, including pre-infection, post-infection, and post-ART initiation. Samples and standards were run in triplicate and average values were used to compute A3G A3F and GAPDH copy number. Relative expression levels of A3G and A3F to GAPDH in each sample were determined by dividing the concentration of the target gene (A3G and A3F) by the concentration of the housekeeping gene (GAPDH). The resulting target/reference ratio expressed the amount of A3G and A3F normalized to the level of GAPDH.

Table 2.16 Components of the APOBEC3G ddPCR

Reagent (APOBEC3G)	1 reaction (µL)
ddPCR master mix	10
Nuclease free water	6
APOBEC3G gene expression kit	1
cDNA	5
Total reaction volume	22

Table 2.17 Components of the APOBEC3F ddPCR.

Reagent (APOBEC3F)	1 reaction (µL)
ddPCR master mix	10
Nuclease free water	6
APOBEC3F gene expression kit	1
cDNA	5
Total reaction volume	22

Table 2.18 Components of the GAPDH ddPCR.

Reagent (GAPDH)	1 reaction (µL)
ddPCR master mix	10
Nuclease free water	8
GAPDH gene expression kit	1
cDNA (predilution)	3
Total reaction volume	22

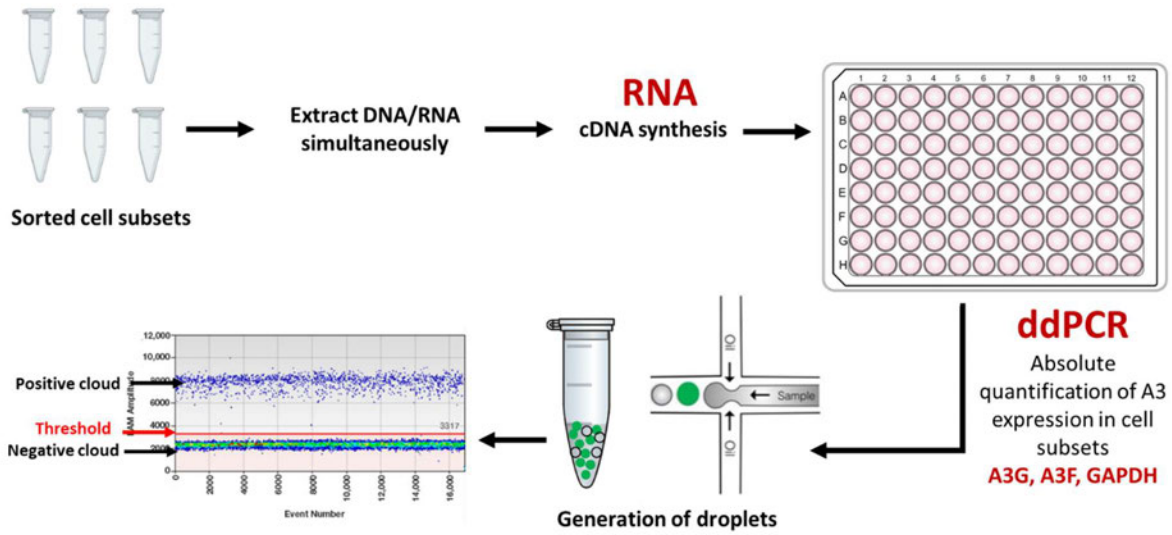

Figure 2.11 Schematic diagram showing the workflow of measuring A3 expression in sorted cell subsets. RNA was extracted and converted to cDNA. ddPCR was then performed using specific primers and probes that could detect APOBEC3 expression. Droplets were then automatically generated using a droplet generator. The PCR was performed using a T100 thermocycler (Bio-Rad, California, USA). The results were exported and analyzed.

2.9 Full-length individual proviral sequencing (FLIP-Seq) assay

Near full-length proviral sequences were generated as previously described (Reddy et al., 2024, Lee et al., 2019b). Sequences were generated and were previously published (Reddy et al., 2024). Five late treated participants were longitudinally assessed. Total HIV-DNA copy number was determined by ddPCR and was used to calculate the DNA sample dilution to achieve one PCR-positive reaction in every three reactions.

This method of limiting dilution gives a Poisson probability of 85.7% that each PCR amplicon originated from a single HIV-DNA template. A nested PCR approach was used to amplify the near-full genome using one unit of Platinum™ Taq DNA Polymerase High Fidelity (Invitrogen, Waltham, USA) with the following primers shown in Table 2.19. Reagents per reaction are highlighted in Table 2.20 and Table 2.21. The thermal cycling conditions were 2 min at 92 °C, 10 cycles [10 s at 92 °C, 30 s at 60 °C, 10 min at 68°C], 20 cycles [10 s at 92 °C, 30 s at 55 °C, 10 min at 68 °C], 10 min at 68 °C, 4 °C infinite hold.

Table 2.19 **Primers used to amplify near-full length proviral sequence**

Primer/Probe	Sequence	Position HXB2
Forward primer (First Round)	5′-AAATCTCTAGCAGTGGCGCCCGAACAG-3′	638-9632, 8994 bp
Reverse primer (First Round)	5′-TGAGGGATCTCTAGTTACCAGAGTC-3′	638-9632, 8994 bp
Forward primer (Second Round)	5′-GCGCCCGAACAGGGACYTGAAARCGAAAG-3′	638-9632, 8994 bp
Reverse primer (Second Round)	5′ GCACTCAAGGCAAGCTTTATTGAGGCTTA-3′	638-9632, 8994 bp

Table 2.20 Components used to amplify near-full length proviral sequences (Round 1)

Reagent (FLIP-SEQ)	Reagent volume (µL)
H2O	12.8
10xBuffer	2
MgSO4 (50mM)	0.8
dNTP (10mM)	0.4
Forward Primer Round 1 (20uM)	0.4
Reverse Primer Round 1 (20uM)	0.4
Taq (5U/uL)	0.2
DNA	3
Total	20

Table 2.21 Components used to amplify near-full length proviral sequences (Round 2)

Reagent (FLIP-SEQ)	Reagent volume (µL)
H_2O	10.8
10x Buffer	2
$MgSO_4$ (50 mM)	2
dNTP (10 mM)	0.8
Forward Primer Round 2 (20 µM)	0.4
Reverse Primer Round 2 (20 µM)	0.4
Taq (5U/µL)	0.4
DNA	1
Total	20

2.10 Data analysis

2.10.1 Measuring Total HIV DNA

Positive and negative droplets were distinguished using the 1-D plot function on QX Manager 1.2 Standard Edition software (Bio-Rad, California, USA). Graph Pad Prism version 9.5.0 (GraphPad, Massachusetts, USA) was used to output all data graphically. Statistical analysis used Graph Pad Prism version 9.5.0 (GraphPad, Massachusetts, USA). P values < 0.05 were considered significant.

2.10.2 Measuring intact and defective copy number

Intact and defective DNA were distinguished using the 2-D plot function on QX Manager 1.2 Standard Edition (Bio-Rad, California, USA). GraphPad Prism version 9.5.0 (GraphPad, Massachusetts, USA) was used to generate all graphs and perform statistical analysis. P values <0.05 were significant.

2.10.3 Measuring the inducible reservoir

The inducible reservoir data was analysed using the CFX Maestro Software (Bio-Rad, California, USA). Data was exported and normalized to report infectious units per million cells based on the maximum likelihood method that was used to determine the frequency of cells expressing *tat/rev* msRNA using the IUPMStats v1.0 online software (Rosenbloom et al., 2015). Statistical analysis and tests were done using GraphPad Prism (GraphPad, Massachusetts, USA). P values <0.05 were significant.

2.10.4 Measuring A3 expression and measuring hypermutation across the HIV genome

To analyse positive droplets from ddPCR to determine A3G and A3F expression levels, we used the QX Manager 1.2 Standard Edition (Bio-Rad, California, USA). A3G

and A3F mRNA expression levels were calculated relative to the housekeeping gene GAPDH. A heatmap showing expression levels in all subsets over time was generated using R Studio version 4.4.1. Correlations between A3G and A3F mRNA expression levels and the defective reservoir were done using GraphPad Prism version 9.5.0 (GraphPad, Massachusetts, USA). All graphs were generated using GraphPad Prism 9.5.0. p values < 0.05 were considered significant.

All PCR amplicons detectable by gel electrophoresis were subjected to Illumina MiSeq sequencing and thereafter the resulting small reads were de novo assembled using computational bioinformatics pipeline HIVSeqinR v2.7.1 (Lee et al., 2019b). Highlighter plots were generated using the online tool from the Los Alamos HIV Sequencing database https://www.hiv.lanl.gov/content/sequence/HIV/mainpage.html.

Calculating hypermutation levels across the HIV genome was done using the online tool from the Los Alamos HIV database https://www.hiv.lanl.gov/content/sequence/HIV/mainpage.html.

To show the distribution of hypermutation driven by A3G and A3F across the HIV genome graphs were generated using R studio 4.4.1 using the computational bioinformatic pipeline (Lee et al., 2019b).

3 Chapter 3: Distribution of total HIV DNA within immune cells before and after initiation of antiretroviral therapy in acute or chronic infection phase

3.1 Abstract

Introduction: HIV-1 persistence in infected cells, despite combined antiretroviral therapy (cART), remains a significant barrier to curing HIV. Total HIV DNA serves as a critical marker for viral reservoirs, encompassing both intact and defective proviral DNA. Early initiation of antiretroviral therapy (ART) reduces the reservoir size, limits viral diversity, and preserves immune function. This study examined HIV reservoir dynamics across immune cell subsets and assessed the effect of early treatment on reservoir size in South African female participants with subtype C infection.

Methods: The study involved ten women from Durban, South Africa, identified during hyperacute HIV infection. Five participants initiated ART during the chronic infection stage, at a median of 774 days post-infection (range: 399 – 1202 days), while five initiated ART during acute infection, within one day of onset of plasma viremia. Total HIV DNA was quantified using droplet digital PCR (ddPCR) in CD4+ T-cell subsets (central memory (CM), effector memory (EM), transitional memory (TM), and naïve (N)) and myeloid cells (M). Samples were analysed at pre-infection, 1, 6, and 12 months post-infection, and equivalent time points after ART initiation.

Results: Among immune cell subsets, CM and EM CD4+ T cells harboured the highest total HIV DNA levels, with averages of 7,695 and 5,680 DNA copies/million cells, respectively across all timepoints. Naïve cells also showed detectable HIV DNA levels (744 copies/million), while myeloid cells exhibited a 7-fold lower total HIV DNA (1,050 copies/million) overall. At 12 months post-treatment, total HIV DNA was present

in the myeloid compartment of 4/5 late-treated participants but only 1/5 early treated participants. Over a year of treatment, chronic-treated participants exhibited no significant decrease in total HIV DNA levels across cell subsets. In contrast, acutely treated participants showed a significant decline in total HIV DNA from 1 to 12 months post-treatment, particularly in CM ($p = 0.008$), EM ($p = 0.007$), and TM ($p = 0.007$) subsets. At 12 months post-treatment, acute treated participants had significantly lower total HIV DNA across all cell subsets compared to chronic-treated participants.

Conclusion: The study underscores the establishment and persistence of the HIV reservoir (total HIV DNA) across diverse immune cells, including CD4+ T-cell subsets and myeloid cells. While no significant change was observed in chronic-treated individuals, initiation of treatment in the acute phase led to a marked reduction in reservoir size across cell types, with CD4+ T cells exhibiting the greatest decrease. These findings highlight the importance of early ART initiation in reducing HIV reservoirs and emphasize the need to target diverse immune cells in therapeutic strategies.

3.2 Introduction

HIV-1 DNA persists in infected cells despite cART, resulting in the formation of viral reservoirs that are a key obstacle to curing HIV infection (Finzi et al., 1999, Siliciano et al., 2003). Evaluation of markers of the HIV reservoir is essential for understanding the complexities of HIV persistence and developing strategies aimed at achieving a cure (Richman et al., 2009, Pace and Frater, 2014). Among the various markers of HIV persistence in infected cells, total HIV DNA is currently the most widely used. Although this marker comprises all forms of HIV-DNA, without differentiating the defective from intact forms, quantification of total HIV DNA is simple, standardized, sensitive, and clinically relevant (Lewin and Rouzioux, 2011, Avettand-Fènoël et al., 2009). Studies have shown that it predicts disease progression to AIDS and death independently of HIV RNA load and CD4 cell count (Avettand-Fènoël et al., 2016). Baseline HIV DNA levels can forecast the response to cART, and while total HIV DNA decreases during treatment, it remains measurable, reflecting the history of infection and treatment efficacy (Avettand-Fènoël et al., 2009, Avettand-Fènoël et al., 2016, Ananworanich et al., 2016).

Although it cannot differentiate between replication-competent intact and defective latent viruses, total HIV DNA still offers insights into HIV pathogenesis, as all viral forms contribute to host cell activation (Siliciano et al., 2003, Simonetti et al., 2020, Duette et al., 2022). Total HIV-1 DNA incorporates all forms of intracellular HIV-1 DNA, both intact and defective, including integrated and unintegrated forms, as well as linear and circularized 2-LTR and 1-LTR forms (Avettand-Fènoël et al., 2016) (Figure 3.1). The integrated form, known as the provirus, is the most persistent and allows for the production of virions when dormant infected cells are reactivated. These virions can then infect new cells, promoting the spread of infection and maintaining the HIV

reservoir (Avettand-Fènoël et al., 2016) (Figure 3.1). Therefore, total HIV DNA serves as a key biomarker for HIV reservoirs, which encompass all infected cells and tissues that contribute to viral persistence and disease progression.

HIV-1 is primarily known to exist in latently infected memory CD4+ T cells, which can produce new viruses upon reactivation (Finzi et al., 1999, Finzi et al., 1997, Chomont et al., 2011). Moreover, studies now suggest that viral reservoirs are not limited to memory CD4+ T cells but also include other immune cells like monocytes and macrophages (myeloid cells) (Ellery et al., 2007, Honeycutt et al., 2016, Matsuda and Maeda, 2024, Veenhuis et al., 2023, Andrade et al., 2020). The heterogeneity of these reservoirs with immune cells complicates efforts to target and eradicate them (Zhao and Deng, 2020, Jones et al., 2020, Reddy et al., 2024). Although the reservoir within myeloid cells may exist at a lower frequency compared to CD4+ T cells, they are still relevant and may contribute to viral rebound upon the cessation of ART (Veenhuis et al., 2023, Ellery et al., 2007, Andrade et al., 2020). However, the contribution of the myeloid cell reservoir to HIV persistence is not fully understood, and further studies are needed to confirm the productive infection of myeloid cells.

Most studies analyzing the reservoir in immune cells have been cross-sectional and in persons who started therapy in chronic infection; therefore the dynamics of the reservoir from the time of reservoir establishment following acute infection are largely unknown. Most studies are from the Global North, where HIV-1 subtype B is most common, and they indicate that proviral DNA is readily detected in central, effector, and transitional memory CD4+ T cells (Jones et al., 2020, Duette et al., 2022). However, these findings need to be confirmed in sub-Saharan regions where HIV-1 subtype C predominates. Furthermore, it is unknown if the reservoir size within cellular subtypes targeted by HIV differs in African populations compared to Caucasian

populations. Therefore, identifying the cellular subsets where the HIV-1 reservoir is established and how the reservoir persists in these cells is a key component for developing targeted cure strategies, particularly in low- and middle-income settings.

Amongst the studies focused on a functional HIV-1 cure, some studies have shown that initiating ART early may be a crucial step in limiting the viral reservoir and achieving post-treatment viral control (Anglemyer et al., 2014, Ndung'u et al., 2018, Vemparala et al., 2024). Early initiation of ART reduces the viral reservoir size, limiting viral rebound and preserving immune function (Anglemyer et al., 2014, Ananworanich et al., 2016, Ndhlovu et al., 2015, Ndung'u et al., 2018, Naidoo et al., 2024). While early ART doesn’t prevent reservoir formation, it reduces viremia and viral diversity, potentially contributing to sustained viral remission after stopping therapy (Ndung'u et al., 2018, Reddy et al., 2024, Lee et al., 2019b, Massanella et al., 2021). Additionally, it has been shown that during early or hyperacute infection, particularly during Feibig stage I, there is monocyte expansion but not CD4+ T cell expansion or activation, suggesting that monocytes may have an important role in viral persistence in this setting (Muema et al., 2020). We therefore reasoned that reservoir seeding may be driven toward the monocyte population.

We performed a longitudinal quantification of total HIV-1 DNA within immune cells that are targeted by HIV in a well-characterized subtype C South African cohort. Total HIV DNA levels were measured in immune cells from untreated, acute treated, and chronic treated study participants. Our aims were to firstly identify the cellular subset targeted for HIV reservoir establishment and harbouring the highest levels of total HIV DNA, and secondly to determine if the timing of ART initiation impacts the size and decay of the reservoir in different immune cells.

We hypothesized that central memory and transitional memory CD4+ T cells would harbour the highest levels of total HIV DNA. Additionally, we hypothesized that initiation of ART during acute infection will direct HIV reservoir seeding and establishment towards the myeloid cell population as a result of monocyte expansion and activation in the blood. Furthermore, we hypothesized that treatment during both hyperacute and chronic infection will significantly reduce the size of the total HIV reservoir within immune cells after one year.

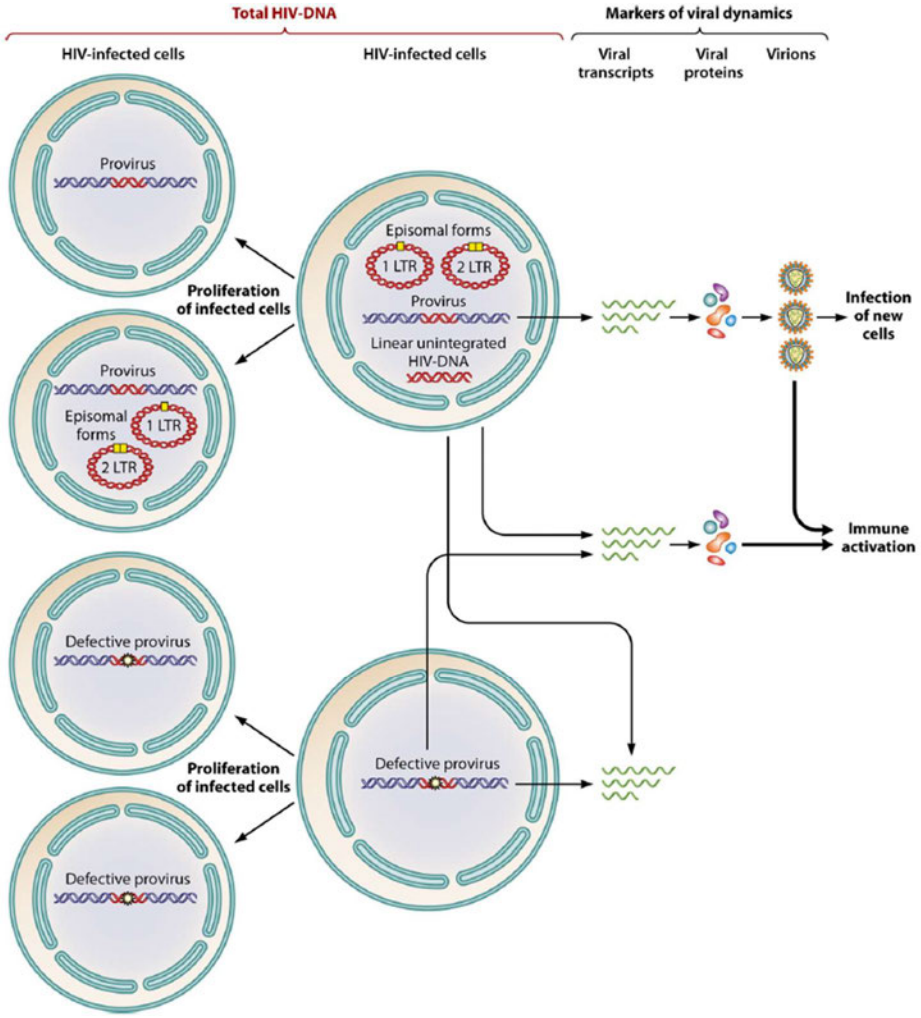

Figure 3.1 Several forms of HIV DNA contribute to total HIV DNA and play a role in HIV pathogenesis. Dynamics of HIV-infected cells and contributions to viral

persistence. The figure illustrates the various forms of HIV DNA and their potential outcomes in infected cells. Left panels: HIV-infected cells harboring either provirus, episomal forms (1-LTR and 2-LTR circles), or defective proviruses can undergo proliferation, contributing to the expansion of the infected cell pool. Central panels: Infected cells contain a combination of proviral DNA, episomal forms, and linear unintegrated HIV-DNA, representing the total HIV DNA within the cell. Right panels: Viral transcripts produced from these DNA forms are translated into viral proteins and assembled into virions, which can infect new target cells, perpetuating the infection cycle. Additionally, viral transcription can trigger immune activation, even from defective proviruses. These schematic highlights that both the proliferation of infected cells (clonal expansion) and ongoing viral transcription contribute to HIV persistence and reservoir maintenance, regardless of whether the provirus is replication-competent or defective.

3.3 Methods

3.3.1 Study participants

Cryopreserved samples from 5 pre-infection, 5 untreated, 5 late treated, and 5 early treated were assessed (Figure 3.2). Five individuals were treated during chronic infection and five during hyperacute infection in Feibig stage 1 (Figure 3.2). Table 2.1 (Chapter 2) highlights participant demographics and clinical characteristics. Viral load and CD4 counts for participants treated during chronic and acute infection are represented in Supplementary Figures 1 and 2 respectively.

3.3.2 Flow cytometry and DNA extraction

Cells were sorted into their different populations from total PBMCs according to a previously published method (Kwon et al., 2020). Leukocytes comprising of both lymphocytes and myeloid cells were gated, followed by doublet discrimination gating, from which viable cells were selected. From the viable cell population, monocytes (CD3-CD14+) and the CD4+ cell population (CD3+CD4+) were gated for. Specifically, from the CD4+ population, CD4+ naïve (CD45RO-CCR7+CD27+) and CM (CD45RO+CCR7+CD27+) cells were gated. Lastly, based on the CD45RO+ marker, the TM (CD45RO+CD27+CCR7-) and EM (CD45RO+CD27-CCR7-) cells were gated on (Kwon et al., 2020) (BD Biosciences, New Jersey, USA).

Gating and sorting was performed using the cell-defining markers to identify the target cell populations. A ‘4-way purity’ sort option was used to collect pure cell populations, and a representative post-sort analysis was done to ensure no contamination. Thereafter, DNA was extracted according to the manufacturer's instructions (Qiagen, Hilden, Germany).

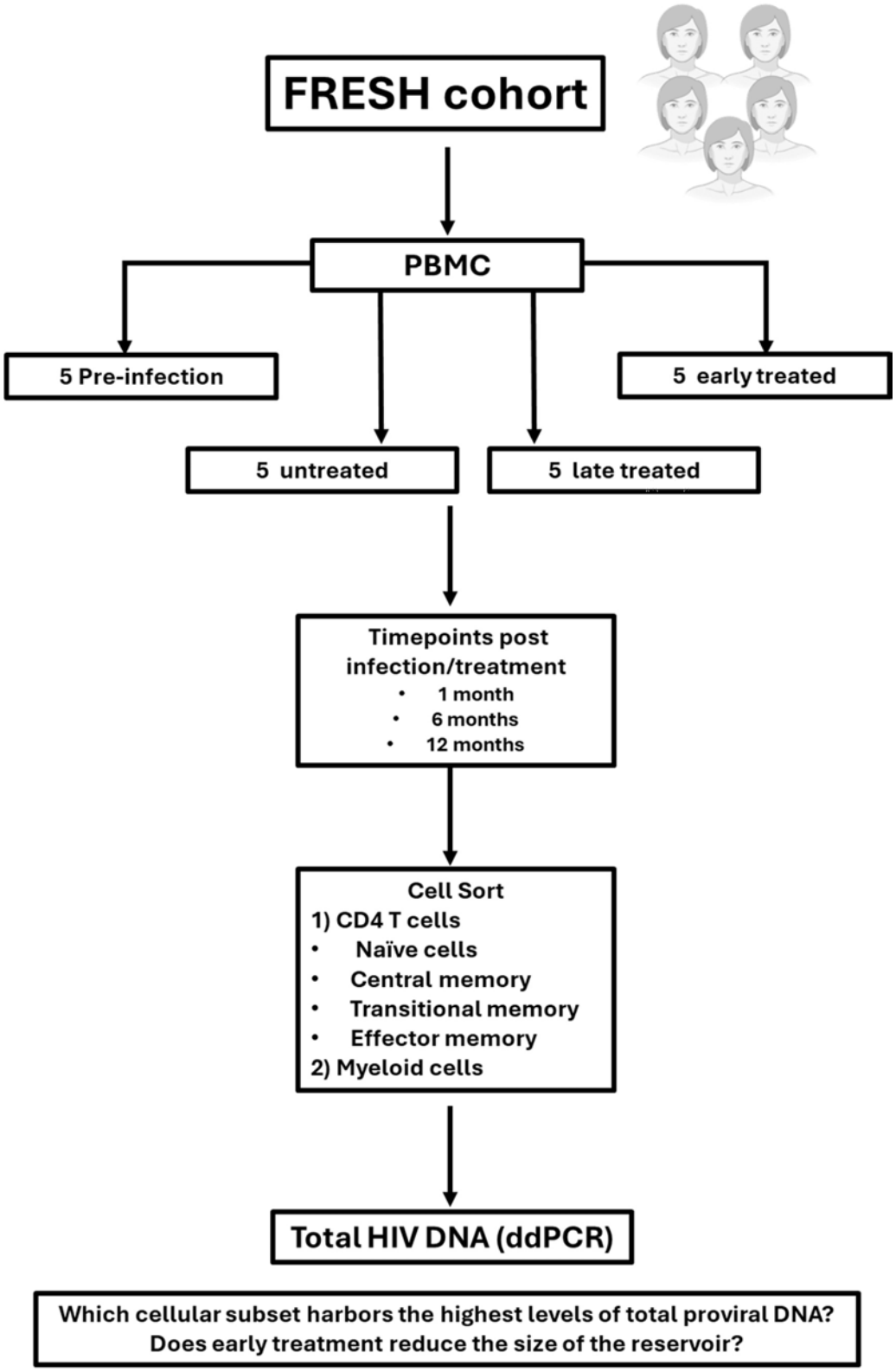

Figure 3.2 Schematic illustration of Chapter 3 outline.

3.3.3 T cell Receptor Excision Circle (TREC) expression quantification using droplet digital PCR

To confirm the purity of sorted T and myeloid cell populations, T cell receptor excision circle (TREC) expression was measured. Droplets were then generated using the QX200 AutoDG (Bio-Rad, California, USA). The following primers and probes were used: TREC forward primer 5'- CACATCCCTTTCAACCATGCT-3', TREC reverse primer5'-GCCAGCTGCAGGGTTTAGG-3', TaqMan probe FAM-ACACCTCTGGTTTTTGTAAAGGTGCCCACTTAMRA (Integrated DNA Technologies (IDT), Iowa, USA) (Mikhael and Elsorady, 2019). TREC expression was analysed relative to the expression of the housekeeping gene GAPDH. Pre-designed TaqMan assay was used to measure GAPDH mRNA expression (Hs02786624_g1) (ThermoFisher Scientific, Waltham, USA). For each cell subset, TREC and GAPDH were measured in triplicate. The cycling conditions were as follows: 95 °C for 10 min, 45 cycles of 94 °C for 30 s and 60 °C for 1 min, 72°C for 1 min.

3.3.4 Measurement of total HIV-DNA by ddPCR

3.3.4.1 ddPCR assay

Total HIV-1 DNA and host cell concentrations in the DNA extracts from sorted cell subsets were estimated using Bio-Rad ddPCR as previously described in (Lee et al., 2019b, Reddy et al., 2024) using primers and probes covering HIV-1 5′ LTR-*gag* HXB2 coordinates 684–810, (forward primer 5′-TCTCGACGCAGGACTCG-3′, reverse primer 5′-TACTGA CGCTCTCGCACC-3′ probe/56-FAM/CTCTCTCCT/ZEN/TCTAGCCTC/ 31ABkFQ/, and human RPP30 gene38 forward primer 5′-GATTTGGACCTGC GAGCG-3′, reverse primer 5′-GCGGCTGTCTCCACAAGT-3′, probe/56-FAM/

CTGACCTGA/ZEN/AGGCTCT/31ABkFQ/) (Integrated DNA Technologies (IDT), Iowa, USA). Droplets were generated using the BIORAD automated droplet digital PCR system (QX200 AutoDG).

PCR was performed on the T100 thermocycler (Bio-Rad, California, USA) under the following cycling conditions: 95 °C for 10 min, 45 cycles of 94 °C for 30 seconds, and 60 °C for 1 min, 72°C for 1 min. Fluorescence of each droplet was read by the Bio-Rad QX100 droplet reader and data were analyzed using QX Manager 1.2 Standard edition software (Bio-Rad, California, USA) (Figure 3.3). HIV 5' LTR-*gag* and RPP30 measurements were performed in triplicate. HIV copy number was normalized to RPP30 cell input.

3.4 Results

3.4.1 Sorting immune cells that are targeted by HIV-1

To elucidate the distribution of HIV-1 provirus within CD4 T cell subsets and myeloid cells we sorted cells from 10 individuals. CD4+ T resting cells were stained using the subset defining surface markers (Figure 3.3). More than 100,000 cells for each cell population were isolated. Purity for each sorted cell population ranged from 90-100%. Average purity for each cell population was CM = 91.2% (91-98%), EM = 99.4% (90-96%), TM = 93.1% (95-100%), N = 97.3% (96-100%), M = 94% (90-98%), and CD8 = 97% (91-100%) (Figure 3.4). The average number of cells sorted per population was CM = 249,621 (130,267-378,318), EM = 124,367 (106,000-189,276), TM = 132,763 (102,319-192,371), N = 287,378 (213,263-389,126), M = 214,376 (156,267-298,172) and CD8 = 218,279 (178,279-270,283).

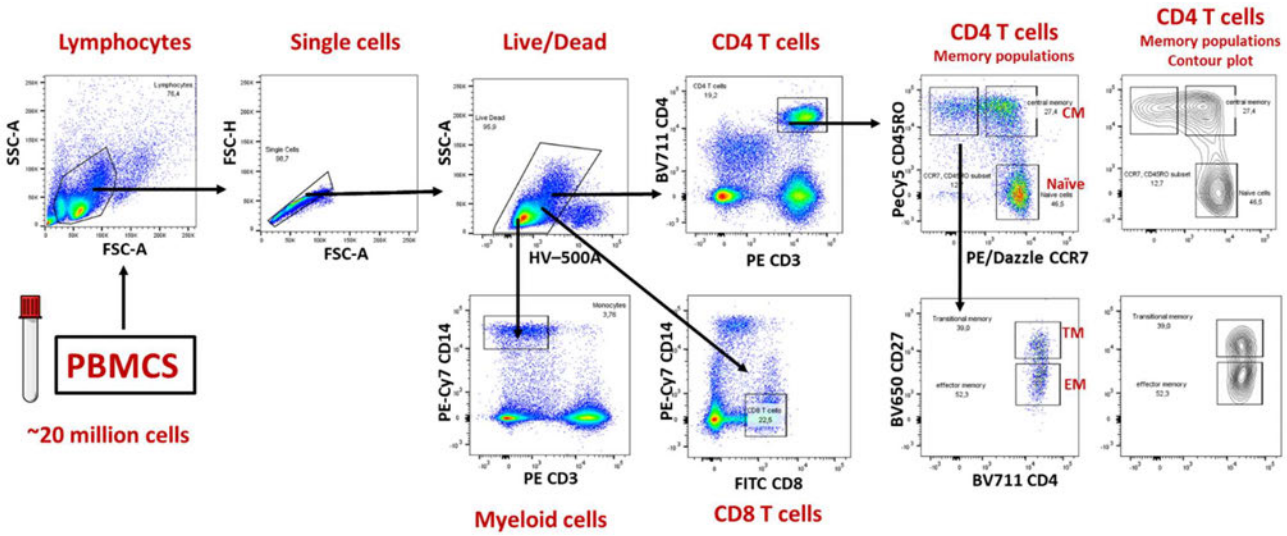

Figure 3.3 Resting CD4+ T cells and myeloid cells were isolated from 20-40 million PBMCs from 10 individuals. Purified cells were sorted into the respective subsets as shown above. Three subsets of memory CD4+ T-cells are defined by the

cell surface proteins CD45RO, CCR7, and CD27: central memory (CM: CD45RO+CCR7+CD27+), transitional memory (TM: CD45RO+CCR7−CD27+), and effector memory cells (EM: CD45RO+CCR7−CD27−) and naïve cells (N: CD45RO−CCR7+CD27+). Myeloid cells were defined as CD14+CD3- cells. CD8+ T cells were added as a biological negative control.

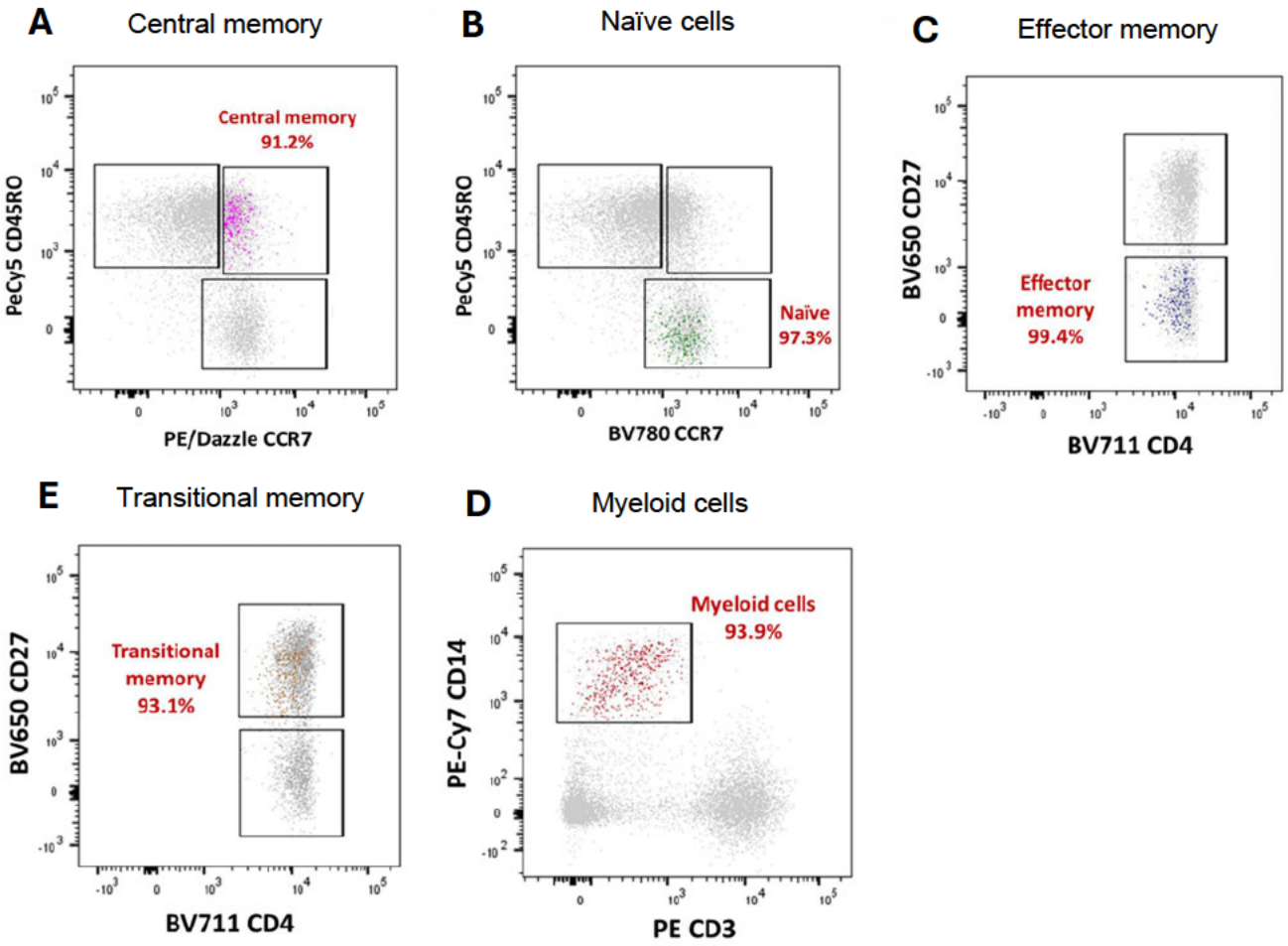

Figure 3.4 Purity of sorted CD4+ T cell memory population and myeloid cells. A) central memory B) naïve CD4+ T cells C) effector memory D) transitional memory E) myeloid cells.

3.4.2 Quantification of TREC to confirm the absence of T cell contamination in myeloid cells.

The measurement of TREC allows for the confirmation of the presence of T cells (Mikhael and Elsorady, 2019). The formation of new T cells occurs in the thymus and as a byproduct TRECs are released. Detection of TRECs by PCR is a reliable method for estimating the amount of newly formed T cells in the circulation (Mikhael and Elsorady, 2019). Measurement of TREC in 3 representative study participants (Figure 3.5). As expected, TRECs were detected at high levels within naïve CD4+ T cells (average expression = 0.430 DNA/copies per µL), followed by TM cells (average expression= 0.27 DNA/copies µL) and CM (average expression = 0.18 DNA/copies µL). We did not detect the presence of TREC within the myeloid compartment (average expression = 0 DNA/copies µL). Therefore, the myeloid compartment was free of T cell contamination as there was no expression of TREC detected (Figure 3.5).

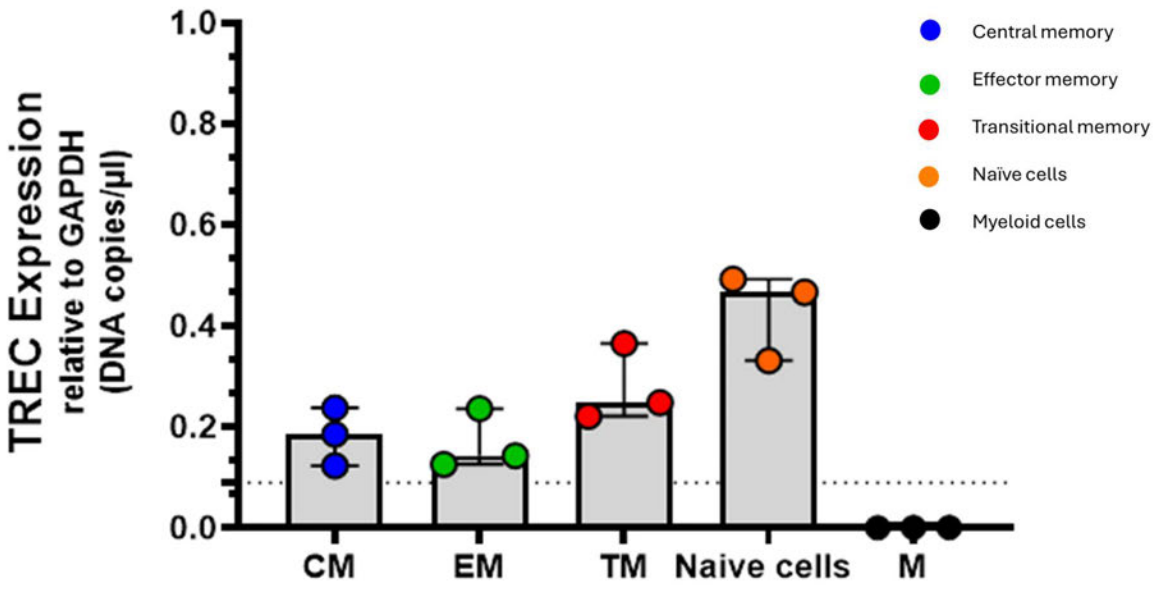

Figure 3.5 Measurement of T cell receptor excision circles (TREC) in different cell subsets. TREC expression was calculated relative to GAPDH expression. CM (central memory), EM (effector memory), TM (transitional memory), naïve cells and M (myeloid cells). The dotted line represents the limit of detection For TREC expression.

3.4.3 Distribution of immune cells in participants that were chronic and acute treated.

To investigate the distribution of the different cell subsets from different individuals we quantified the amount of CD4+ T cells and myeloid cells longitudinally for individuals who were late (Figure 3.6) and early treated (Figure 3.7). For this analysis, we included 5 untreated individuals who subsequently initiated treatment and 5 early treated individuals. Pre-infection and post-treatment timepoints were assessed for the 5 individuals who were late treated. Post-treatment timepoints were assessed for the 5 early participants (Figure 3.2).

Representative data from participant 208 is shown in Figure 3.6. Before infection CD4+ T cells contributed to 45% of the total pool of PBMCs, however, once infection occurred, this decreased to 18.2%,12.0%, and 10.3% at 1-, 6-, and 12 months post-infection respectively, and increased after 1- and 12 months of treatment from 4.0% to 12.3% respectively (Figure 3.6A). HIV infection resulted in a decrease in CD4+ T cells, however, myeloid cells fluctuated in their distribution patterns over time.

Before infection, myeloid cells contributed 6.43% to the total pool of cells, however, after infection this varied from 5%, 6%, and 5.9% at 1-, 6-, and 12 months post-infection respectively (Figure 3.6A). Naïve CD4+ T cells were abundant at all timepoints ranging from 22.5 to 38.4% over time (Figure 3.7B). CM CD4+T cells were the second most abundant population ranging from 20.9% to 27.8%. EM (7.2-15.8%) and TM (7.8-16.3%) were the least abundant CD4+ T cell populations (Figure 3.6B).

Similarly, the early treated participants exhibited a decline in CD4+ T cells however experienced an increase in CD4+ T cells 12 months post-ART initiation. Representative data from participant 920 is shown in Figure 3.6. Before infection,

CD4+ T cells represented 34% of the total pool of PBMCs. and varied from 10% to 18.2% at 1- and 12 months post-ART initiation respectively. (Figure 3.7A). Before infection myeloid cells represented 6% of the total pool of PBMCS and varied from 11% to 8% at 1- and 12 months post-ART initiation respectively Furthermore, it was observed that naïve (41.4-46.5%) and CM (18-19.8%) CD4+ T cells were also abundant in early treated individuals, while EM (6.6-9.6%) and TM (6.3-7.5%) were least abundant over time (Figure 3.7B). Other cells represented in the figures also included other minor populations of immune cells.

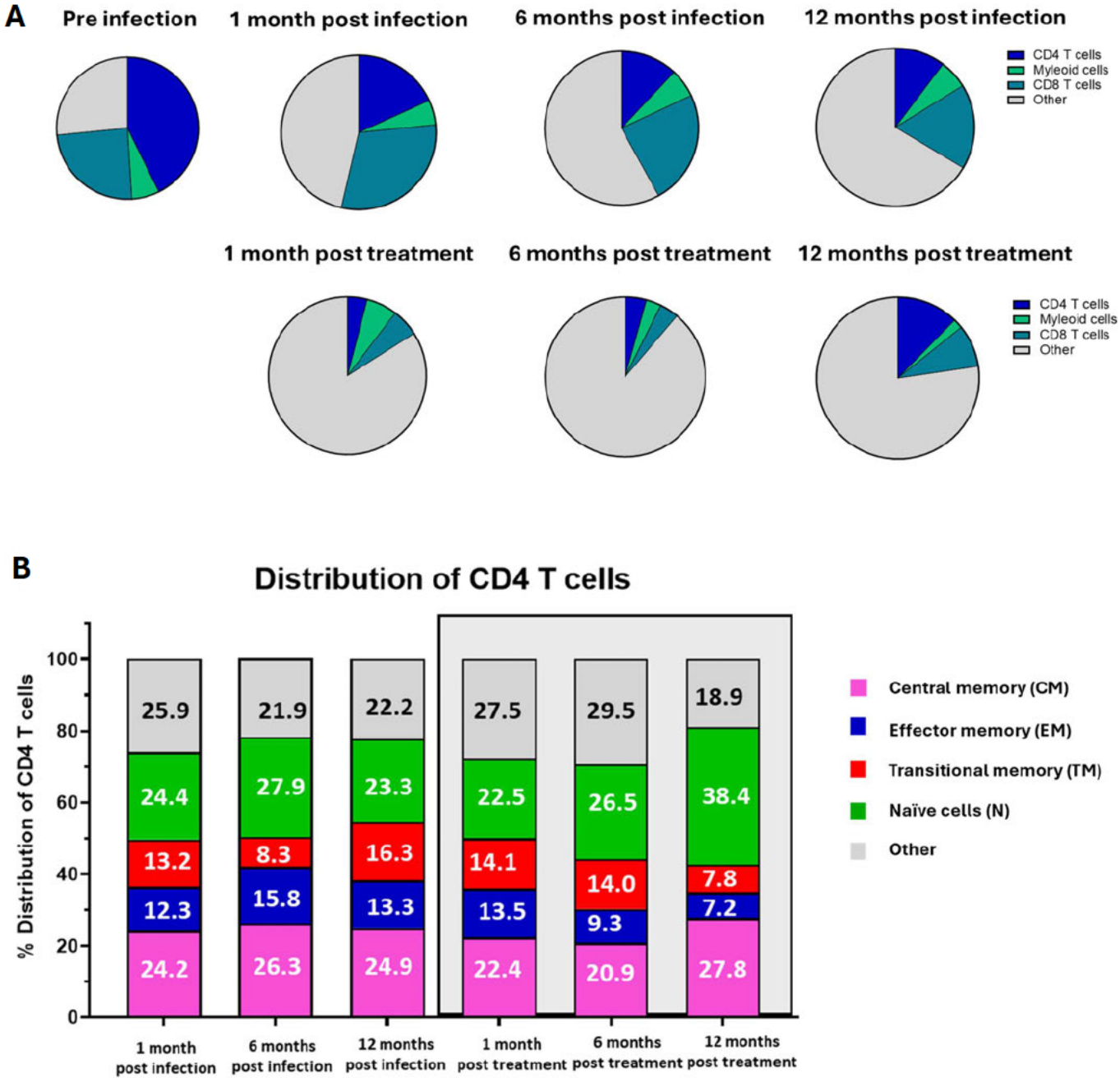

Figure 3.6 Distribution of immune cells in a representative chronically treated study participant (PID 208). A) Distribution of immune cells pre-infection, post-infection, and post-treatment for study participant PID 208. B) Distribution of CD4+ T cell subsets throughout untreated infection and following treatment.

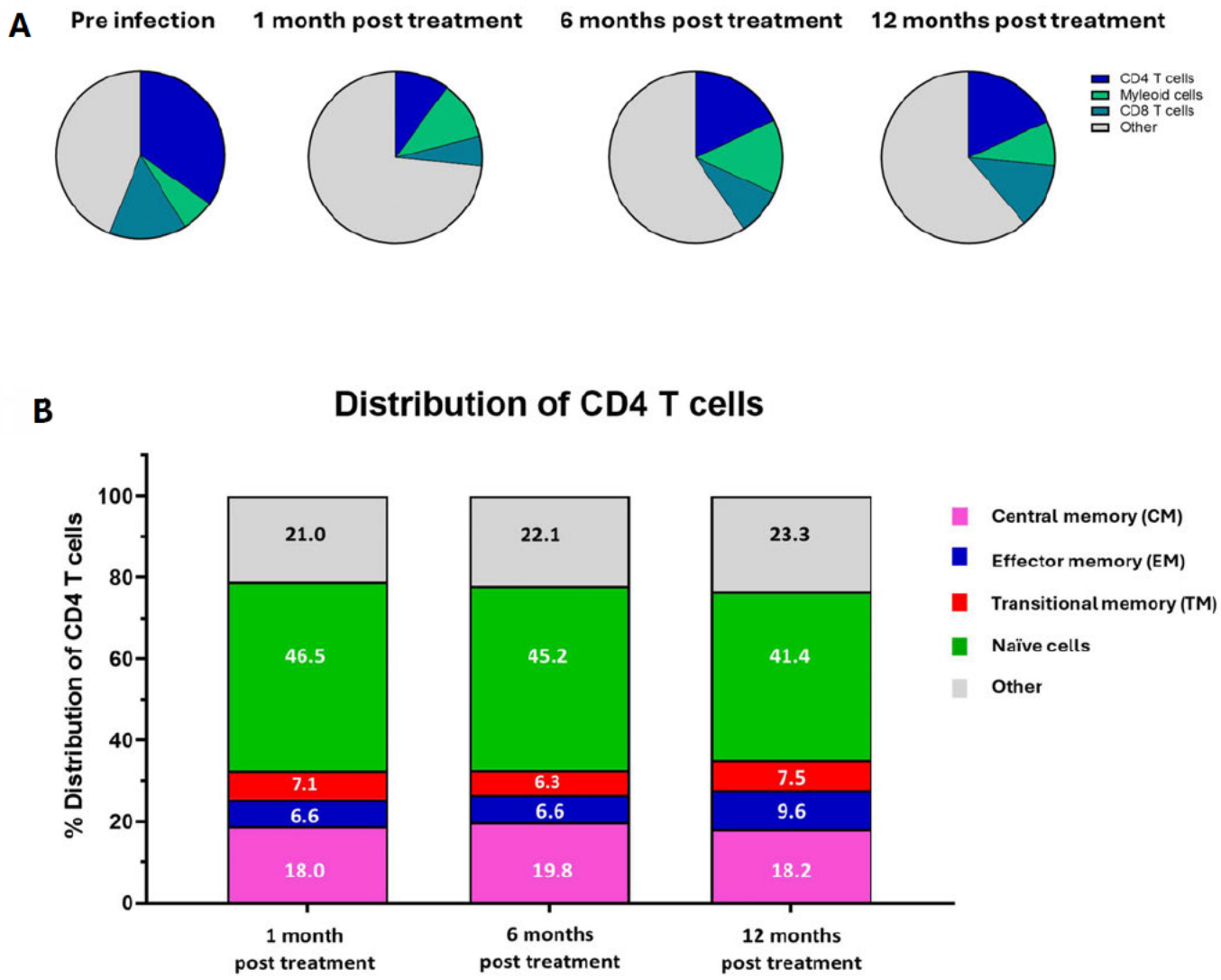

Figure 3.7 Distribution of immune cells in a representative early treated study participant (PID 920). A) Distribution of immune cells shown during the pre-infection timepoint and 1-, 6- and 12-months post-treatment in early treated participant PID 920. B) Distribution of CD4+ T cell subsets throughout untreated infection and following treatment.

3.4.4 Determining the distribution of total HIV DNA within immune cells.

Next, we aimed to investigate the levels of total HIV DNA within immune cell subsets longitudinally. Total HIV DNA was quantified in all subsets. For this analysis, we included 5 untreated individuals who subsequently went on therapy (median of 774 DPOPV) and five early treated individuals who were treated at a median of 1 DPOPV were included.

Representative clinical and total HIV DNA load data from one chronically treated study participant 102 is shown in Figure 3.8. This participant initiated therapy on day 809 post-detection (Figure 3.8A).

Total HIV DNA was unequally distributed amongst cell subsets (Figure 3.8C) with CM (pink, percentage range = 25 - 58%) and EM (blue, percentage range = 22 -36%), and TM (red, percentage range = 2.6 – 41%%) having the highest proportions of total HIV DNA. Additionally, the distribution of total HIV DNA in naïve CD4+ T cells ranged from 1.7% to 4.6% (Figure 3.8C). Interestingly, total HIV DNA in myeloid cells ranged from 2.9% to 14.2% over time. Similar patterns of total HIV DNA distribution were observed in untreated, late treated (Figure 3.8), and early treated (Figure 3.9) study groups although proportions in immune cell subsets differed from participant to participant. Interestingly, we observed total HIV DNA was present at 12 months post-treatment in the myeloid cell population in 4 out 5 study participants who initiated treatment in chronic infection (Figure 3.9). Overall, the distribution of total HIV DNA in different cellular subsets changed over time and was heterogeneous across participants (Figure 3.9).

Next, we quantified total HIV DNA levels in acutely treated participants (Figure 3.10). Representative clinical and total HIV DNA load data from one acutely treated study

participant 761 is shown in Figure 3.10. This participant initiated therapy 1 DPOPV (Figure 3.10A). CM (433 average copies/million cells) and EM (1,473 average copies/million cells) had the highest levels of total HIV DNA (Figure 3.10B), followed by TM (421 average copies/million cells) and naïve cells (135 copies/million cells). For this participant, total HIV DNA was undetectable in myeloid cells (Figure 3.10B). Total HIV DNA trajectories for all study participants are shown in Supplementary Figures 5 and 6. Total HIV DNA was undetectable in the CD8+ T cell compartment in acute treated participants (Figure 3.10B and Supplementary Figure 6).

Similar to chronically treated participants total HIV DNA was unequally distributed amongst cell subsets over time for those who initiated treatment in acute infection (Figure 3.10C). EM (blue, percentage range = 40.7-67.6%) and CM (pink, percentage range = 10-59.3%) had the highest proportion of total HIV DNA detected, followed by TM (red, percentage range = 0-25.1%) and naïve cells (green, percentage range = 0-10.6%) (Figure 3.10C). In contrast to those who initiated treatment during chronic infection, only one acute treated individual (PID 879) had total HIV DNA persisting in their myeloid compartment 12 months post-treatment initiation (Figure 3.11).

Next, to determine if the number of cells influenced total HIV DNA levels, we correlated the average distribution of CM (pink) and naïve cells (green) with the average amount of total provirus detected in CM and naïve cells (Figure 3.12). Representative data from one late treated study participant 208 is shown in Figure 3.12. Figure 3.12A shows the correlation between the average distribution of CM cells and the average total HIV DNA levels. We observed no correlation between the amount of total HIV provirus within the cells and the distribution of the cell subsets ($p = 0.26$, $r = 0.29$ (Figure 3.12A). Figure 3.12B shows the correlation between total HIV DNA levels in naïve cells and the distribution of naïve cells. We observed no correlation between the

amount of total HIV DNA levels and the distribution of naïve cells ($p = 0.67$, $r = 0.04$). This indicated that the amount of cells present didn't influence the measurement of total HIV DNA in that subset.

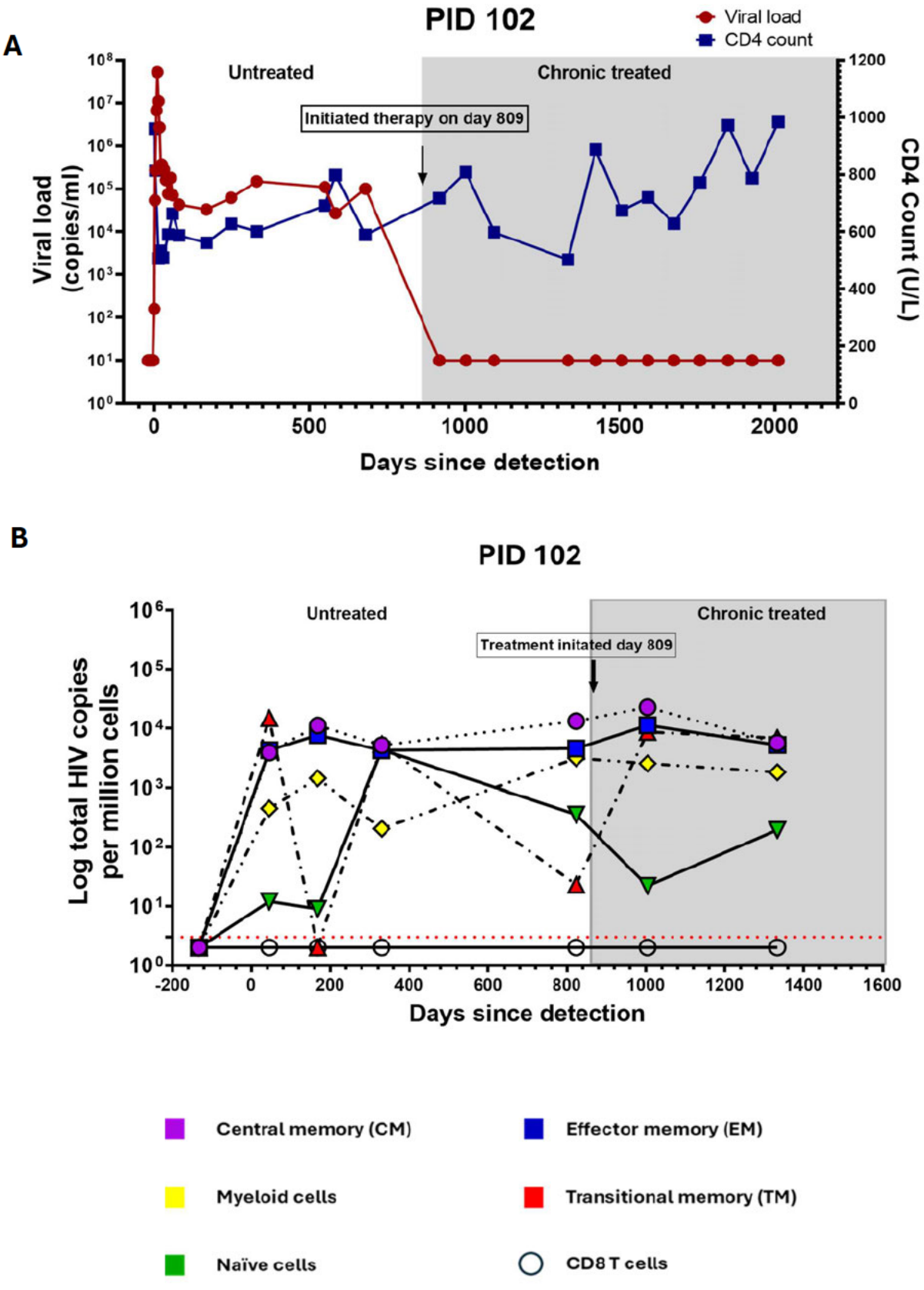
A
PID 102
Viral load
CD4 count
Untreated
Chronic treated
Initiated therapy on day 809
Viral load (copies/ml)
CD4 Count (U/L)
Days since detection
B
PID 102
Untreated
Chronic treated
Treatment initated day 809
Log total HIV copies per million cells
Days since detection
Central memory (CM)
Effector memory (EM)
Myeloid cells
Transitional memory (TM)
Naïve cells
CD8 T cells

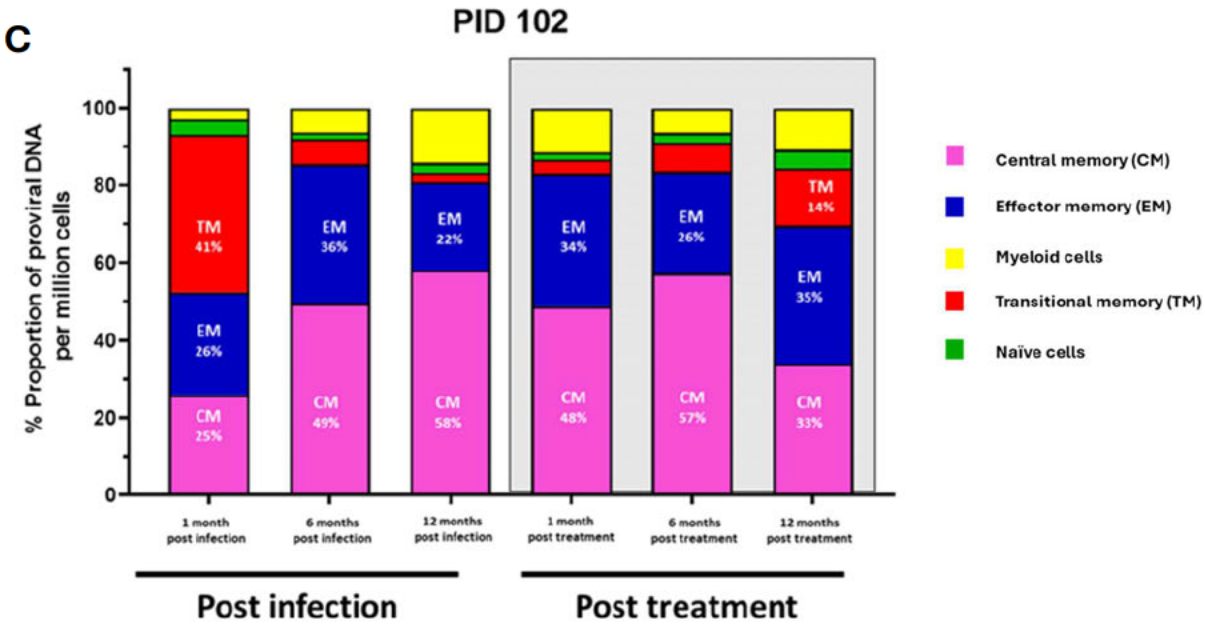

Figure 3.8 Distribution of total HIV DNA within immune cells from chronically treated participants. A) Viral load (Red) and CD4 (Blue) count for PID 102. The white area shows untreated infection the grey area shows when treatment was initiated. PID 102 initiated therapy on day 809 post-detection of viremia. **B) Log total HIV DNA copies per million cells measured in the cellular subsets.** Central memory (CM- purple), effector memory (EM– blue), transitional memory (TM– red), naïve cells (N- green), and myeloid (M– yellow) are represented by the different symbols and colours. The red dotted line represents the limit of detection. **C) Proportion of total HIV DNA per million cells.** Proportions of central memory (pink), effector memory (blue), transitional memory (red), naïve cells (green), and myeloid cells (yellow) are represented by the different colours on each bar. Each bar represents a different time point either post-infection or post-treatment.

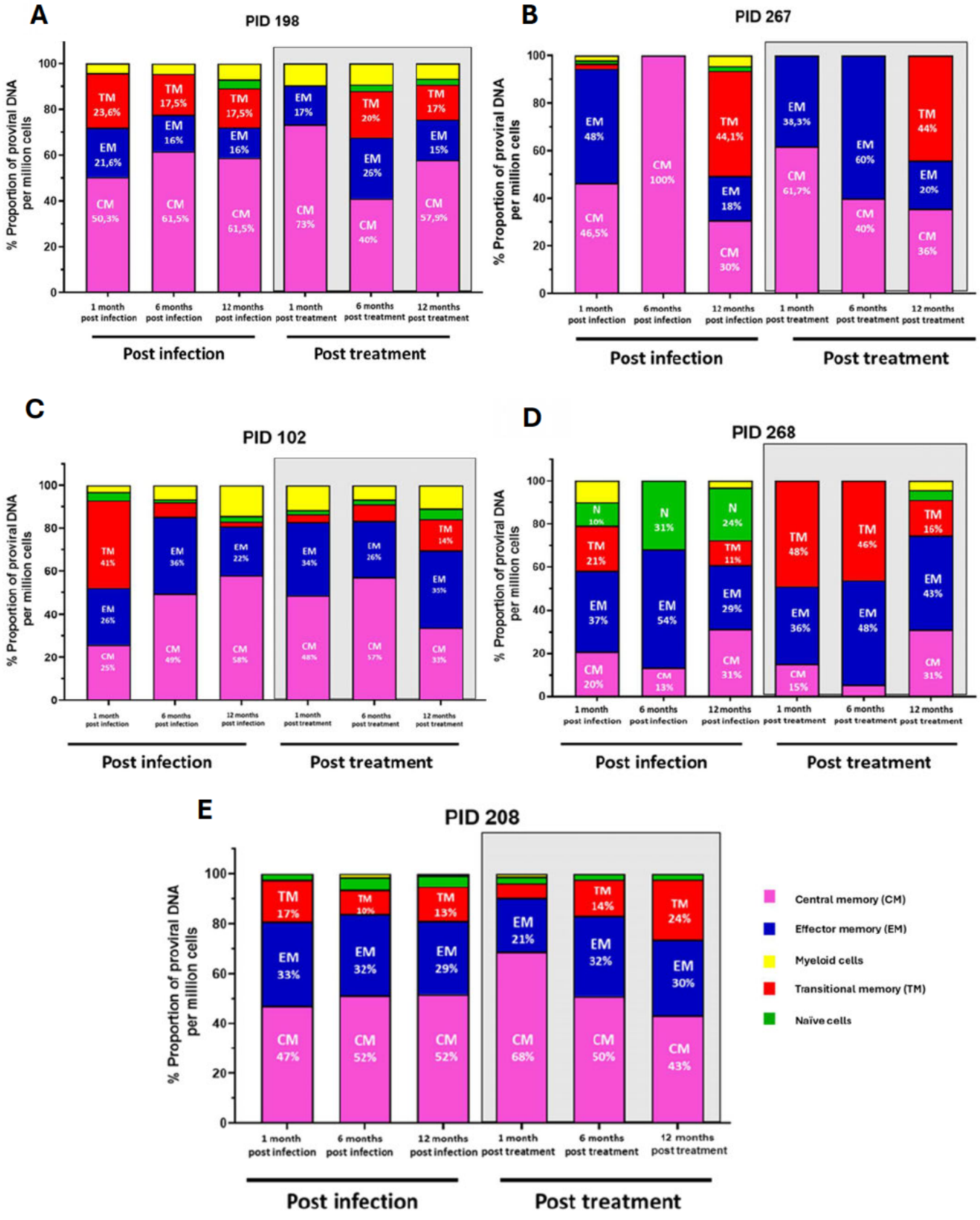
A
PID 198
% Proportion of proviral DNA per million cells
TM 23,6%
EM 21,6%
CM 50,3%
TM 17,5%
EM 16%
CM 61,5%
TM 17,5%
EM 16%
CM 61,5%
EM 17%
CM 73%
TM 20%
EM 26%
CM 40%
TM 17%
EM 15%
CM 57,9%
1 month post infection
6 months post infection
12 months post infection
1 month post treatment
6 months post treatment
12 months post treatment
Post infection
Post treatment
B
PID 267
% Proportion of proviral DNA per million cells
EM 48%
CM 46,5%
CM 100%
TM 44,1%
EM 18%
CM 30%
EM 38,3%
CM 61,7%
EM 60%
CM 40%
TM 44%
EM 20%
CM 36%
Post infection
Post treatment
C
PID 102
% Proportion of proviral DNA per million cells
TM 41%
EM 26%
CM 25%
EM 36%
CM 49%
EM 22%
CM 58%
EM 34%
CM 48%
EM 26%
CM 57%
TM 14%
EM 35%
CM 33%
Post infection
Post treatment
D
PID 268
% Proportion of proviral DNA per million cells
N 10%
TM 21%
EM 37%
CM 20%
N 31%
EM 54%
CM 13%
N 24%
TM 11%
EM 29%
CM 31%
TM 48%
EM 36%
CM 15%
TM 46%
EM 48%
TM 16%
EM 43%
CM 31%
Post infection
Post treatment
E
PID 208
% Proportion of proviral DNA per million cells
TM 17%
EM 33%
CM 47%
TM 10%
EM 32%
CM 52%
TM 13%
EM 29%
CM 52%
EM 21%
CM 68%
TM 14%
EM 32%
CM 50%
TM 24%
EM 30%
CM 43%
Post infection
Post treatment
Central memory (CM)
Effector memory (EM)
Myeloid cells
Transitional memory (TM)
Naïve cells

Figure 3.9 Total HIV DNA percentage proportion for each of the 5 study participants treated during chronic infection (A-D). The proportion of total provirus was determined for each cell subset and was reported as percentages. A different colour on the graph represents each cell subset. Each graph shows a different study participant who was chronically treated. Post-infection timepoints are shown in the white and the post-treatment timepoints are shown in the grey area.

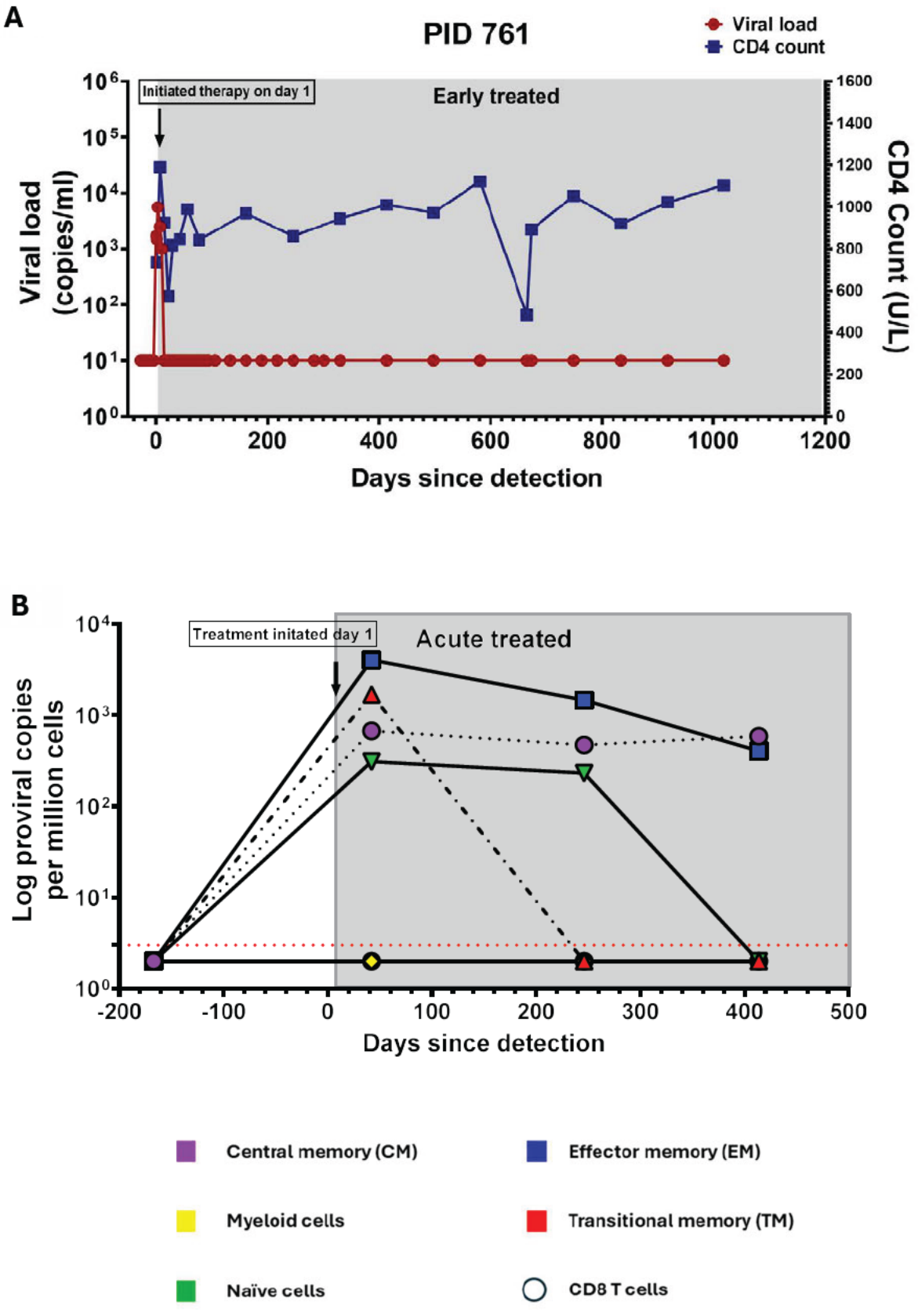
A
PID 761
Viral load
CD4 count
Initiated therapy on day 1
Early treated
Viral load (copies/ml)
CD4 Count (U/L)
Days since detection
B
Treatment initated day 1
Acute treated
Log proviral copies per million cells
Days since detection
Central memory (CM)
Effector memory (EM)
Myeloid cells
Transitional memory (TM)
Naïve cells
CD8 T cells

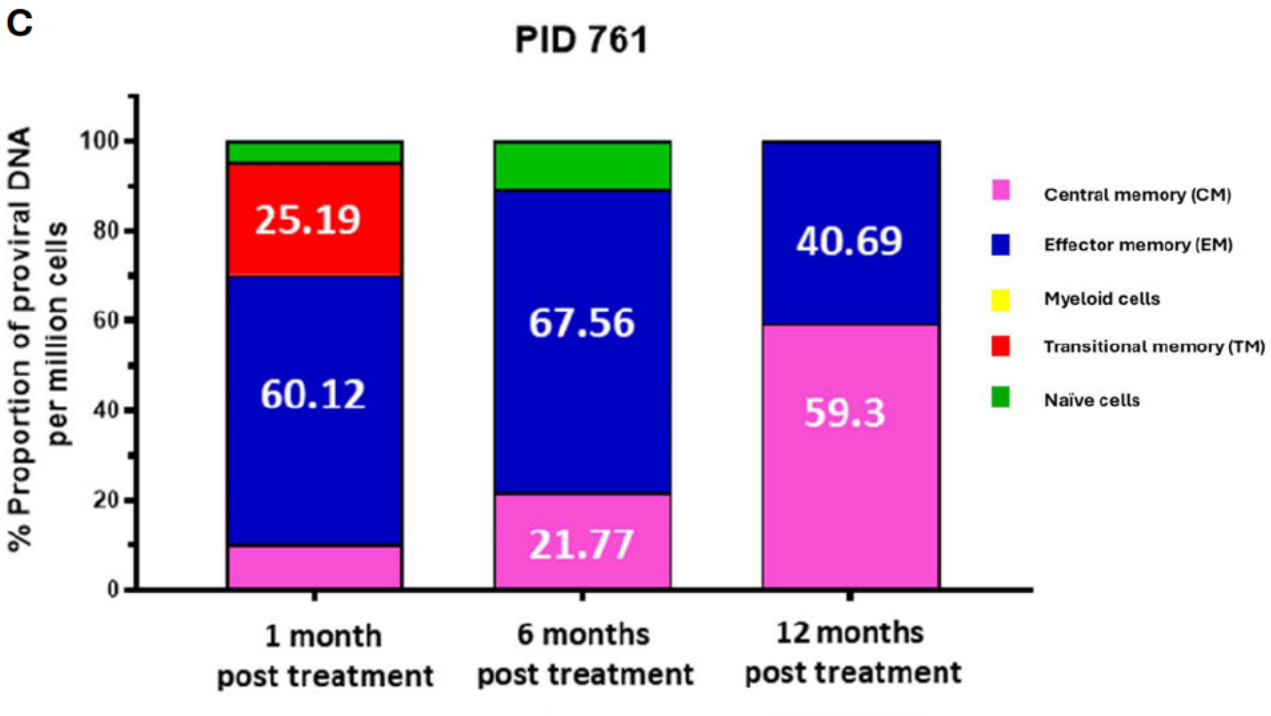

Figure 3.10 Distribution of total HIV DNA within immune cells from an early treated participant. A) Viral load and CD4 trajectories from PID 761. This participant initiated therapy 1 DPOPV. All the timepoints represented are post-treatment. The grey area on the graph denotes the post-treatment phase. This participant maintained suppressed viremia. **B) Total HIV DNA trajectory over time.** The different symbols represent different cell subsets. The red dotted line represents the limit of detection. The white area denoted untreated infection, and the grey area represents post-treatment timepoints**. C) Percentage proportion of total HIV DNA per million cells.** Each colour represents a different cell subset. 1-month, 6-month, and 12-month post-treatment timepoints are shown on the graph.

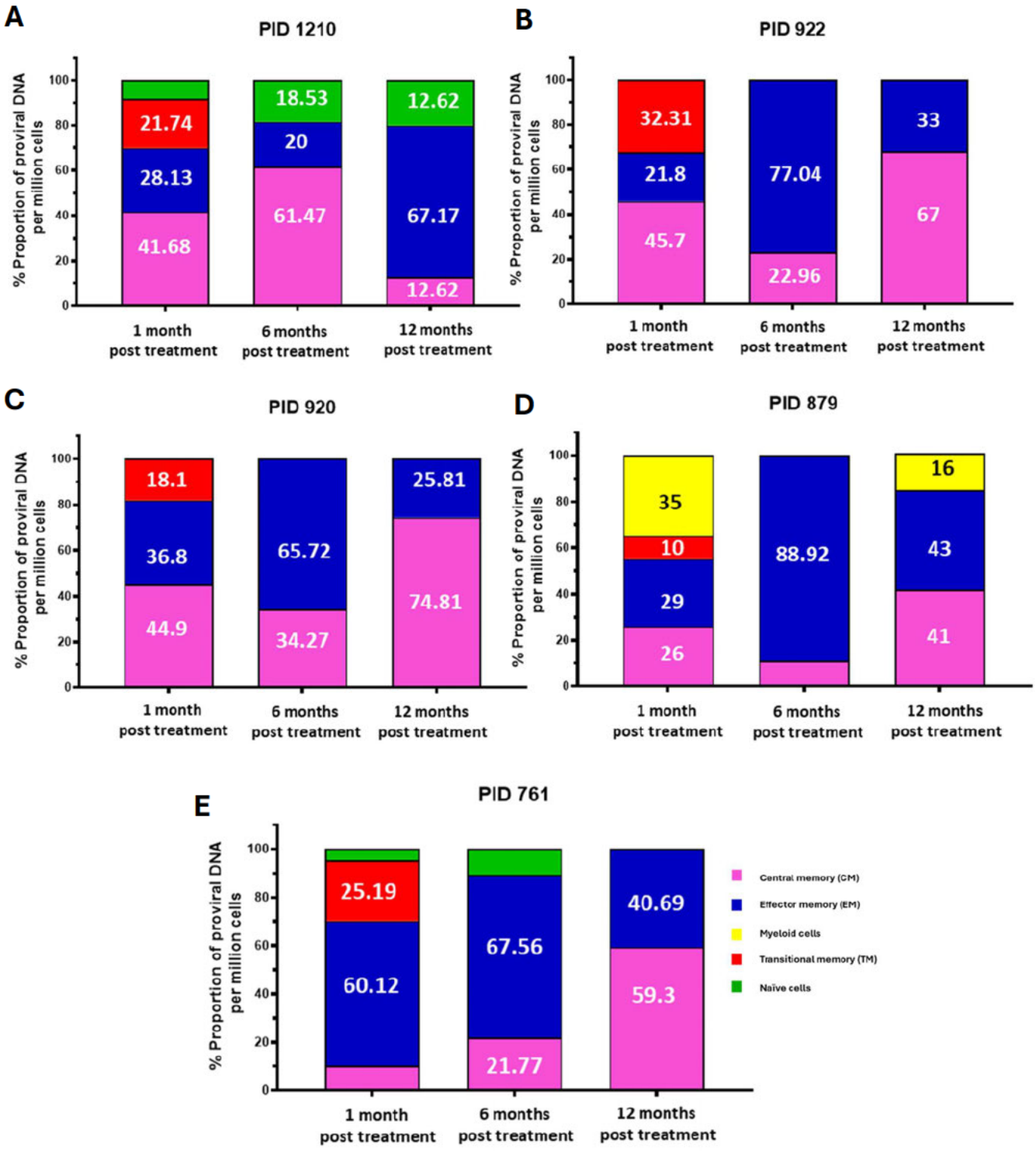

Figure 3.11 Percentage distribution of total HIV DNA within immune cells from 5 acutely treated individuals (A-D). Each cell subset is represented in a different

colour on each bar. Each graph represents a different study participant (A – D). On each graph, the percentage proportion is represented on the y-axis and the different timepoints assessed are represented on the x-axis. Interestingly only one participant (PID 879) displayed the presence of total HIV DNA after one year of treatment in their myeloid compartment highlighted in yellow.

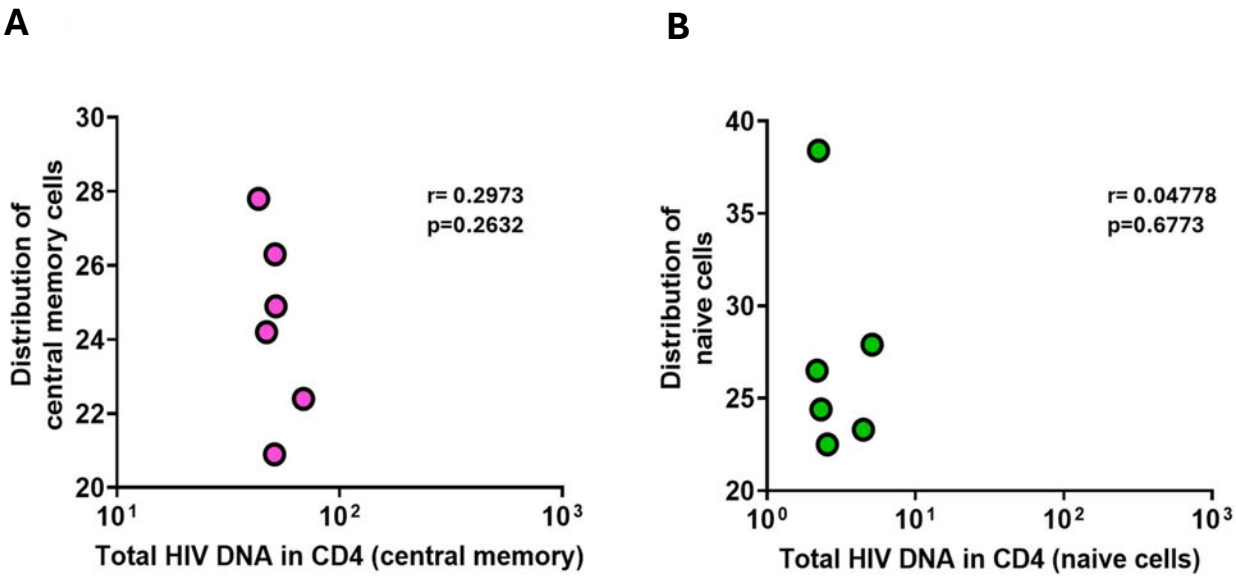

Figure 3.12 Correlation of total HIV DNA and distribution of cells (PID 208). A) Central memory (pink) shows no statistical correlation between the levels of total HIV DNA and the distribution of central memory CD4+ T cells B) Naïve CD4+ T cells (green) show no statistical correlation between the distribution of naïve cells and total HIV DNA quantified in naïve CD4+ T cells.

3.4.5 Understanding the effects of early antiretroviral therapy on the total HIV reservoir within immune cell subsets.

Antiretroviral therapy (ART) inhibits HIV replication but does not eradicate the latent reservoir (Finzi et al., 1999). Previous research suggests that earlier ART initiation provided benefits in limiting reservoir size and accelerating reservoir decay (Reddy et al., 2024). Studies suggest that the delayed response in the initiation of ART leads to the formation of a larger, more diverse reservoir (Reddy et al., 2024). However, the underlying mechanisms that influence these responses need further interrogation. Here, we wanted to determine the effects of early treatment on the total HIV DNA levels within immune cells targeted by HIV.

Total HIV DNA was measured longitudinally in all cell subsets during untreated infection (Figure 3.13). Overall, we found that in each of the cell subsets, there was no difference in the levels of total HIV DNA from 1 month post-infection to 12 months post-treatment (CM $p = 0.30$, EM $p = 0.60$, TM $p = 0.69$, naïve cells $p = 0.89$, and myeloid cells $p = 0.9$) (Figure 3.13). These results indicate that there is no significant decrease in total HIV DNA after a year of treatment when treatment is initiated during chronic infection.

Additionally, when assessing the longitudinal timepoints of those that were acutely treated (Figure 3.14) we observed a reduction in total HIV proviral DNA levels within all memory CD4+ T cell subsets from the 1 month to 12 months post-treatment (CM $p = 0.008$, EM $p = 0.007$, TM $p = 0.007$). Naïve cells and myeloid cells showed no significant decrease (naïve cell $p = 0.44$, myeloid cells $p = >0.99$) (Figure 3.14).

Next, we wanted to establish if the timing of ART initiation had an impact on viral reservoir seeding (the size of the reservoir at baseline) in each of the immune cell

subsets. At the one-month post-infection (baseline), there was no difference in total HIV DNA levels in CD4+ T cells and myeloid cells between untreated infection and early treated infection (CM p= 0.74, EM p= 0.15, TM p= 0.16, naïve cells p= 0.30, and myeloid cells p= 0.22) (Figure 3.15).

We then determined if treatment initiated in acute infection resulted in lower total HIV DNA levels in each of the cell subsets after a year of treatment compared to participants initiating treatment in chronic infection. Figure 3.16 shows the comparison between those participants who initiated treatment in the chronic phase versus those who initiated treatment in the acute phase. We observed significantly lower total HIV DNA levels in all the cell subsets (CM p= 0.0079, EM p= 0.0079, TM p= 0.0070, naïve cells p= 0.0476, myeloid cells p= 0.0400) (Figure 3.16). This indicates that early treatment resulted in significantly lower total HIV DNA burden in immune cells after a year of treatment (Figure 3.16).

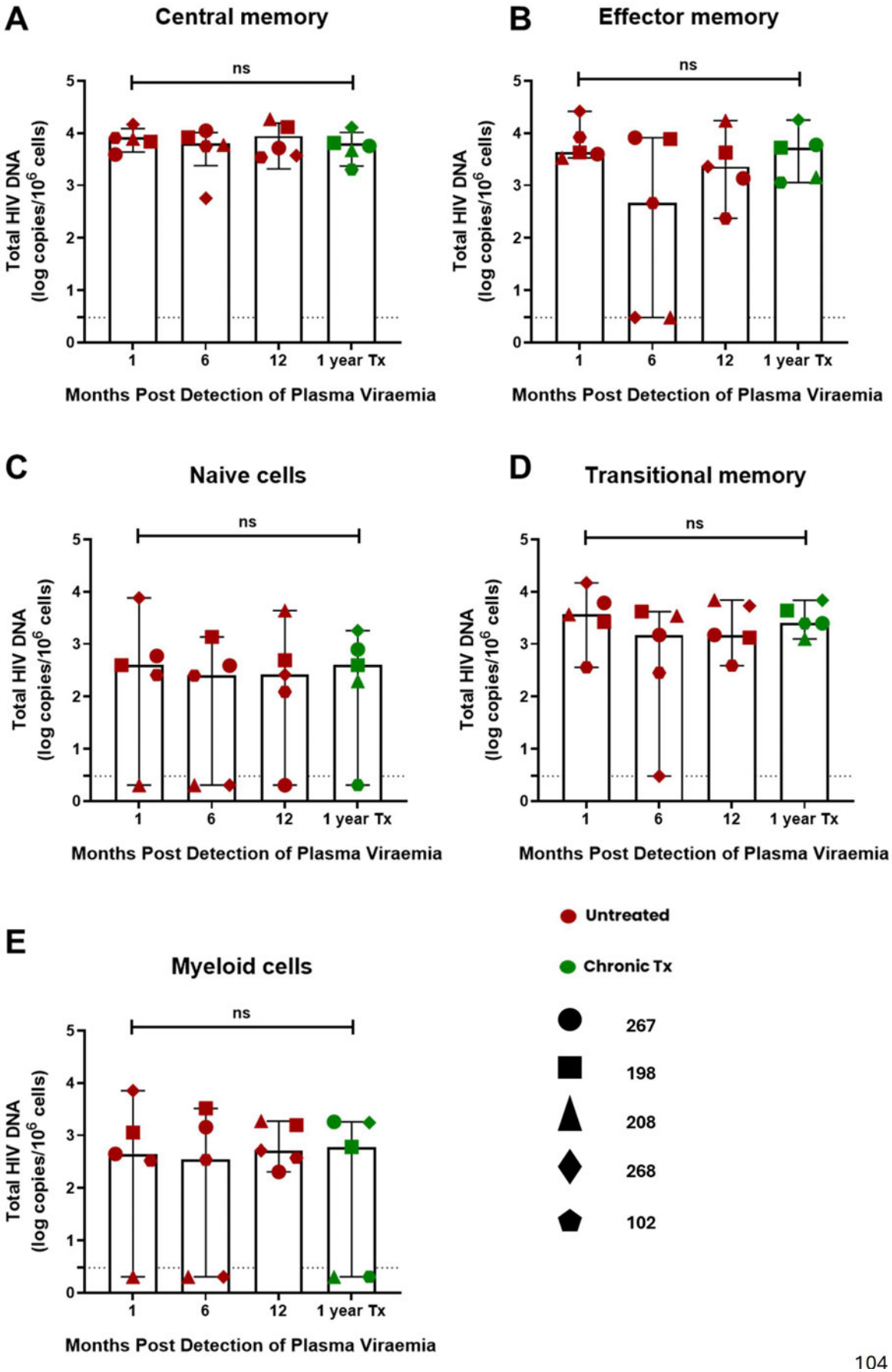
A
Central memory
B
Effector memory
C
Naive cells
D
Transitional memory
E
Myeloid cells
ns
Total HIV DNA (log copies/10^6 cells)
0
1
2
3
4
5
1
6
12
1 year Tx
Months Post Detection of Plasma Viraemia
Untreated
Chronic Tx
267
198
208
268
102

Figure 3.13 No difference in total HIV DNA levels between untreated infection and a year after treatment. Longitudinal measurement of total HIV DNA during untreated infection (red) compared to 1 year after treatment (green). Total HIV DNA (log copies/10^6 cells) is represented against months post-detection of plasma viremia (1-,6- and 12 months post-infection and 1 year post-treatment). The different panels show the different cell subsets A) CM B) EM C) TM D) naïve cells E) myeloid cells. *ns = non-significant. * p = <0.05. The different symbols indicate different study participants.

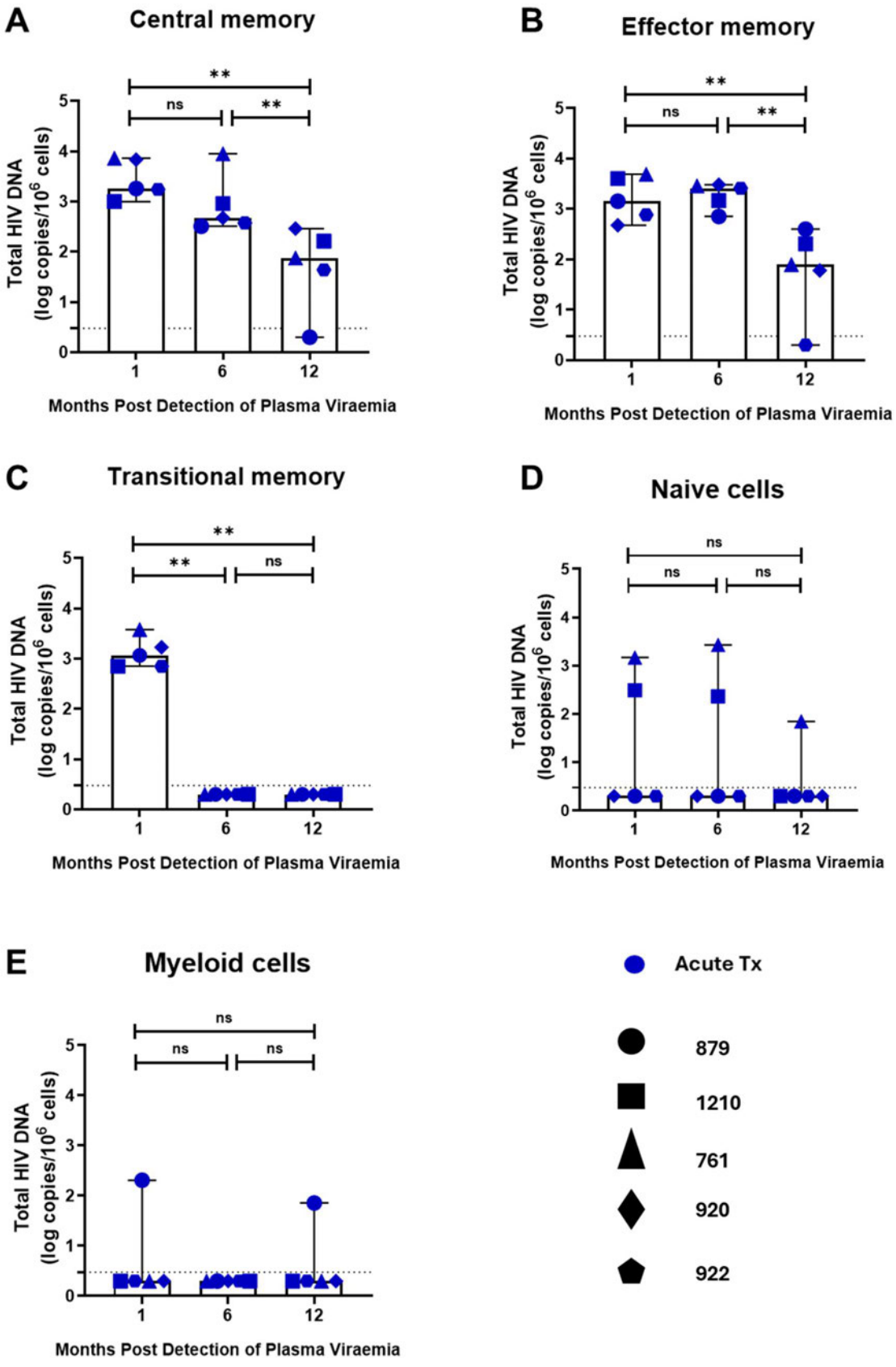
A
Central memory
B
Effector memory
C
Transitional memory
D
Naive cells
E
Myeloid cells
Total HIV DNA (log copies/10^6 cells)
Months Post Detection of Plasma Viraemia
ns
**
Acute Tx
879
1210
761
920
922

Figure 3.14 Total HIV DNA decreases steadily in early treated patients in all cell subsets. Longitudinal measurement of total HIV DNA in different cell subsets of interest from those individuals that were acutely treated over one year (1-, 6-, and 12 months shown). The different panels highlight the different cell subsets A) central memory B) effector memory C) transitional memory D) naïve cells E) myeloid cells. * p = <0.05, ns= non-significant.

A

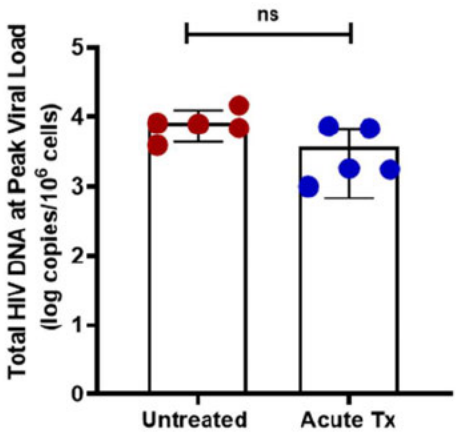
Central Memory
ns
Total HIV DNA at Peak Viral Load
(log copies/10^6 cells)
0
1
2
3
4
5
Untreated
Acute Tx

B

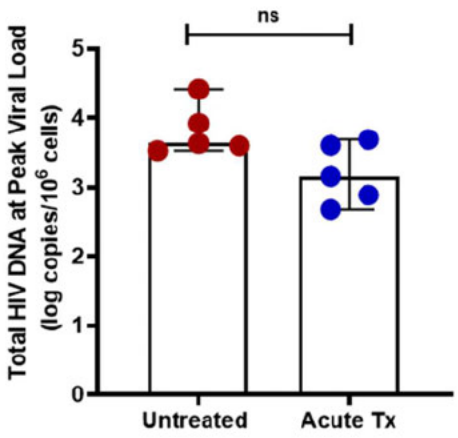
Effector Memory
ns
Total HIV DNA at Peak Viral Load
(log copies/10^6 cells)
0
1
2
3
4
5
Untreated
Acute Tx

C

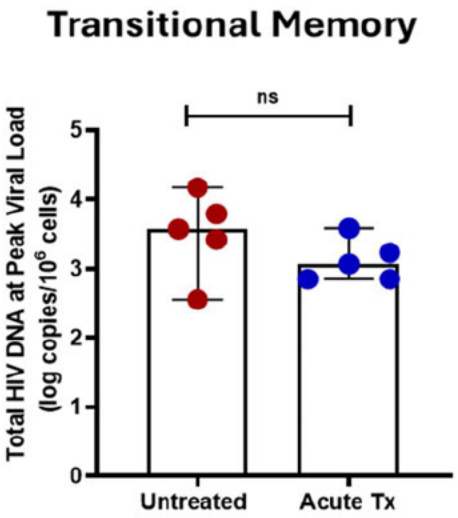
Transitional Memory
ns
Total HIV DNA at Peak Viral Load
(log copies/10^6 cells)
0
1
2
3
4
5
Untreated
Acute Tx

D

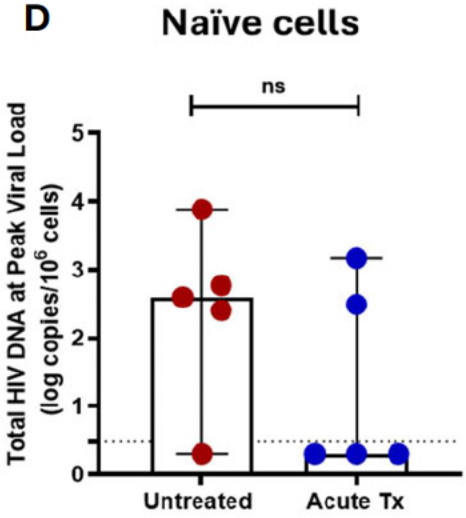
Naïve cells
ns
Total HIV DNA at Peak Viral Load
(log copies/10^6 cells)
0
1
2
3
4
5
Untreated
Acute Tx

E

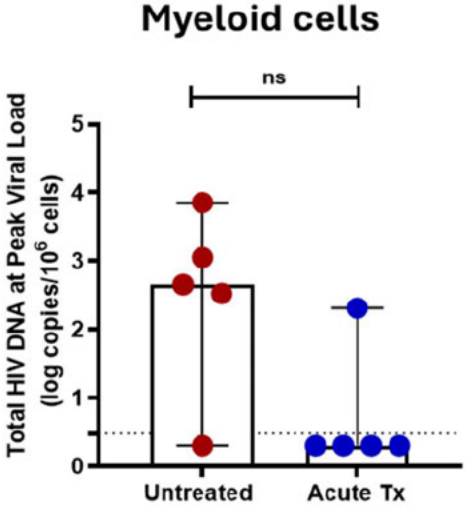
Myeloid cells
ns
Total HIV DNA at Peak Viral Load
(log copies/10^6 cells)
0
1
2
3
4
5
Untreated
Acute Tx

Figure 3.15 No difference in total HIV DNA levels from those who were untreated compared to those individuals that were early treated one month post-infection. Total HIV DNA (log copies/106 cells) versus treatment status (untreated (red) and acute treated (blue)) A) CM B) EM C) TM D) naïve cells E) myeloid cells. ns= non-significant.

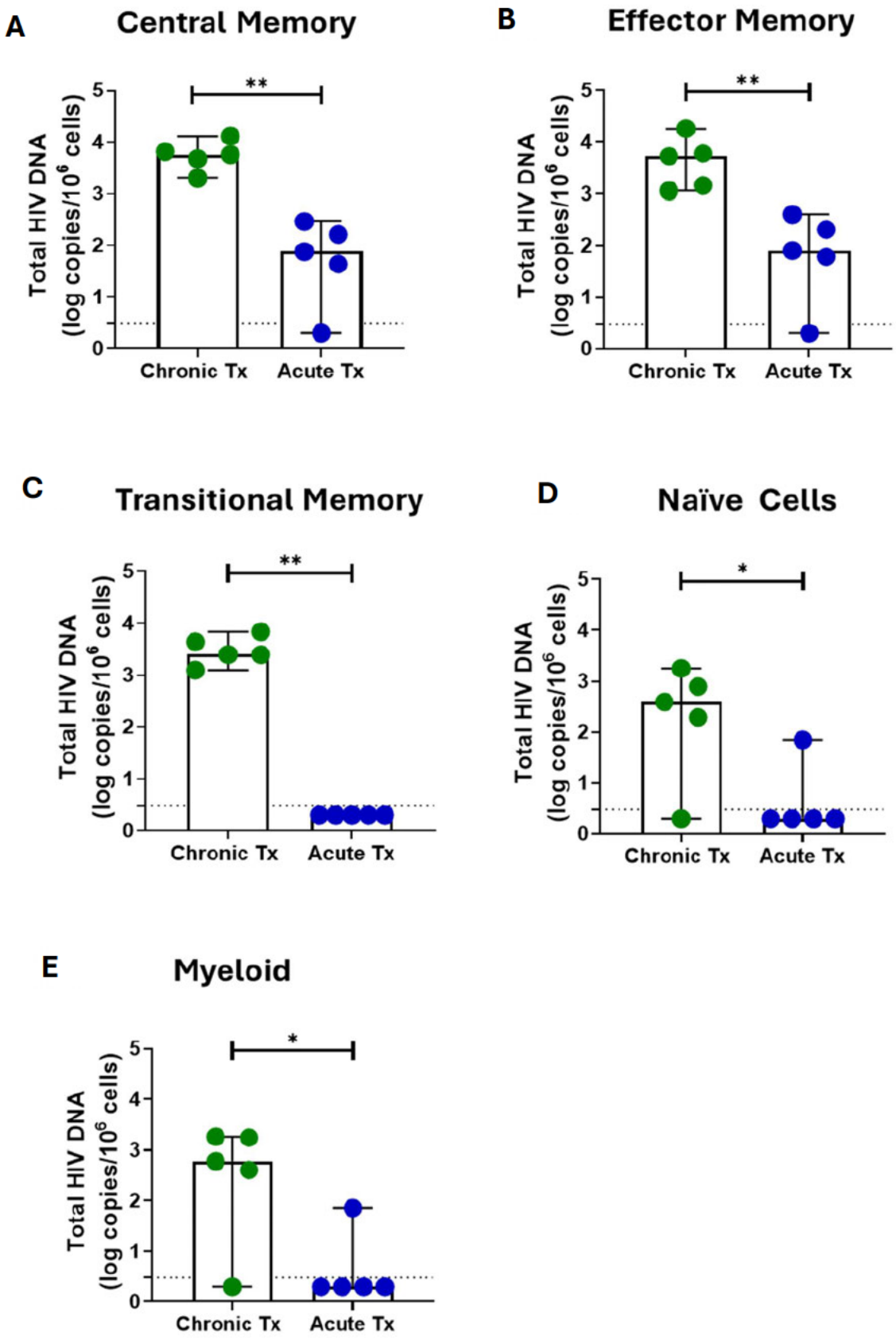
A
Central Memory
Total HIV DNA (log copies/10^6 cells)
**
Chronic Tx
Acute Tx
B
Effector Memory
Total HIV DNA (log copies/10^6 cells)
**
Chronic Tx
Acute Tx
C
Transitional Memory
Total HIV DNA (log copies/10^6 cells)
**
Chronic Tx
Acute Tx
D
Naïve Cells
Total HIV DNA (log copies/10^6 cells)
*
Chronic Tx
Acute Tx
E
Myeloid
Total HIV DNA (log copies/10^6 cells)
*
Chronic Tx
Acute Tx

Figure 3.16 Early treatment significantly reduces total HIV DNA load after one year of treatment. Comparison between those individuals that have been late treated (green) and early treated (blue) at one year of treatment. Total HIV DNA (log copies/10^6 cells) versus treatment status (chronic treated versus acute treated) is shown on each graph. The different panels highlight the different cell subsets A) CM B) EM C) TM D) naïve cells E) myeloid cells.* p= <0.05.

3.5 Discussion

Despite effective viral suppression by ART, HIV-1 persists in latent reservoirs within memory CD4+ T cells and myeloid cells, escaping immune clearance. This remains the main barrier to a cure, necessitating targeted therapies. Most research has focused on subtype B, while subtype C, the most prevalent globally, needs further study. Furthermore, research must consider Africa's key populations to develop effective cure strategies for viral persistence.

In this chapter, our primary aim was to identify which specific immune cell subsets harbours the highest levels of total HIV DNA. The persistence of HIV in reservoirs, despite antiretroviral therapy, is a key challenge in efforts to achieve a functional cure for HIV. Therefore, understanding which cells are most responsible for maintaining the viral reservoir is critical. According to existing literature, central, effector, and transitional memory, CD4+ T cells play a major role in harbouring a significant proportion of the total HIV load (Chomont et al., 2011, Duette et al., 2022, Finzi et al., 1999, Matsuda and Maeda, 2024). Based on these findings, we hypothesized that central memory CD4+ T cells would contain a substantial portion of total HIV DNA compared to other cell subsets. Furthermore, we hypothesized that early treatment would significantly shift the reservoir towards myeloid cells because of the expansion of monocytes post-infection.

To test these hypotheses, we conducted a longitudinal study to measure the levels of total HIV DNA in different immune cell subsets targeted by HIV. These measurements were taken over time in both individuals who initiated ART during the late stages of infection and those who started therapy during the early stages. Our data revealed that the reservoir in both late treated and early treated individuals was dynamic and

changed over time. More importantly, the cellular reservoir was found to be highly heterogeneous, varying from participant to participant. This heterogeneity underscores the complexity of HIV persistence and suggests that the viral reservoir cannot be fully explained by examining a single cell type or subset.

Nevertheless, our analysis revealed that central memory and effector memory CD4+ T cells consistently harboured the highest frequency of total HIV DNA. These findings align with previous research and support the hypothesis that these memory T cell subsets play a critical role in maintaining the viral reservoir (Lee and Lichterfeld, 2016, Reeves et al., 2023, Chomont et al., 2011, Duette et al., 2022). Memory CD4+ T cells have a long lifespan and can persist in a resting state, which allows them to evade immune detection and antiretroviral therapy. This persistence contributes to the stability of the HIV reservoir and its ability to reignite viral replication if therapy is stopped.

In addition to the high levels of total HIV DNA observed in CD4+ T cells, we also detected total HIV DNA within the myeloid cell compartment, although at levels approximately 10-fold lower than those found in CD4+ T cells overall across all time points. This finding is significant because it challenges the traditional view that CD4+ T cells are the exclusive or primary cellular reservoirs of HIV. While CD4+ T cells undoubtedly play a dominant role, the presence of total HIV DNA in myeloid cells suggests that these cells could also contribute to viral persistence and recrudescence. This finding highlights the need to consider all potential cellular reservoirs when designing strategies to eradicate HIV. The detection of total HIV DNA in myeloid cells reinforces the idea that multiple cell types, not just CD4+ T cells, could serve as sources of viral rebound if antiretroviral therapy is discontinued.

There has been increasing evidence that monocytes and macrophages play a significant role in contributing to the proviral burden and contribute to viral rebound once therapy is terminated (Honeycutt et al., 2016, Andrade et al., 2020). Attention has shifted toward understanding the role that the myeloid reservoir plays and studies have shown that macrophages and monocytes are not only susceptible to HIV infection but also play a role in the persistence of the HIV reservoir (Veenhuis et al., 2023, Andrade et al., 2020).

However, this topic is highly debated and confirmation of the presence of provirus within myeloid cells is needed to add to the supporting evidence. There have been controversies about the productive infection of myeloid cells versus the engulfment of latently infected CD4+ T cells by phagocytosis, as a mechanism of HIV clearance by the immune system (Baxter et al., 2014). Therefore, the elimination of CD4+ T cell contamination in the myeloid cells was necessary to show that the detection of total HIV DNA in myeloid cells was not a result of CD4+ T cell ingestion.

The measurement of TREC allowed for the detection of the presence of T cells (Mikhael and Elsorady, 2019). The formation of new T cells occurs in the thymus and as a byproduct and TRECs are released (Mikhael and Elsorady, 2019). Detection of TRECs by PCR is a reliable method for estimating the amount of newly formed T cells in the circulation (Mikhael and Elsorady, 2019). The presence of TREC within the myeloid compartment would indicate the presence of T cells. In this analysis, we used ddPCR to measure the presence of TREC within myeloid cells. Measuring TREC droplet digital PCR offers higher sensitivity, with detection limits reaching as low as 4 TREC copies/µl. This enhanced sensitivity allows for more accurate quantification of low-abundance targets, such as the presence of T cells in myeloid cell samples (Vidal-Folch et al., 2017, Kwok et al., 2020). Our results revealed that there was no TREC

measured in the myeloid, indicating that these cells were free of CD4+ T cell contamination.

Our secondary aim was to determine the impact of the timing of ART on total HIV DNA levels within the various immune cell subsets targeted by the virus. To address this, we analysed data from five participants who initiated treatment during the chronic phase of infection and five participants who started treatment during the hyperacute phase. We hypothesized that treatment would lead to a significant reduction in the size of the total HIV reservoir across all cell subsets, regardless of when therapy was initiated.

To test this hypothesis, we longitudinally assessed the impact of treatment, we observed that in participants who initiated treatment during chronic infection, there was no significant reduction in total HIV DNA levels, 12 months post-ART initiation. This lack of impact suggests that once HIV has established a reservoir, particularly in memory CD4+T cells, it becomes highly resistant to reduction through antiretroviral therapy alone, at least in the chronic phase of infection.

In contrast, participants who began treatment during the hyperacute phase of infection experienced a rapid and substantial decrease in total HIV DNA levels across all cell subsets assessed. This rapid decline indicates that early treatment initiation is crucial in limiting the size of the HIV reservoir. Additionally, we observed that comparing 1 month post-infection timepoints (baseline) for those individuals that were late and early treated we saw no statistical difference in the levels of total HIV DNA. This suggests that early treatment does not prevent seeding and establishment of reservoirs even if treatment is initiated during hyperacute infection. This was seen in all the cell subsets that we assessed. To determine if early treatment resulted in lower total HIV DNA

levels at one year post-treatment, we observed that all participants treated early had lower total HIV DNA levels compared to those treated late. This indicates that early treatment significantly reduced the proviral burden after a year of treatment.

One limitation of this study is the small number of participants, which may affect the statistical power and generalizability of the findings. Additionally, all participants were young women between the ages of 18 and 23, which limits the applicability of the results to broader populations, including men and individuals of different age groups. As a result, the findings may not fully represent the diversity of immune responses across different demographics. However, despite these constraints, this study remains the most comprehensive analysis of the reservoir in immune cells in Africa, providing valuable insights that can inform future research in this field.

These findings underscore the importance of early detection and treatment of HIV, as they suggest that early intervention can significantly alter the course of reservoir dynamics and improve long-term outcomes. In conclusion, these findings highlight that central and effector memory CD4+ T cells harbours the highest levels of total HIV DNA but also highlight the role of myeloid cells as potential contributors to the viral reservoir. Moreover, early initiation of antiretroviral therapy is essential for achieving a meaningful reduction in the HIV reservoir, emphasizing the need for prompt diagnosis and treatment in individuals with HIV.

4 Chapter 4: Characterization of the defective, intact, and inducible HIV reservoir landscape in immune cell subsets

4.1 Abstract

Introduction: Eliminating the HIV-1 reservoir remains a critical challenge in achieving a cure for HIV. The HIV reservoir is predominantly located in resting CD4+ T-cells, but the reservoir may reside in other lineages such as myeloid cells. However, the reservoir is heterogenous such that some of it is genetically defective and unable to reignite infection, some is genetically intact and potentially replication-competent, whereas a small proportion is inducible upon cellular reactivation. Here we aimed to understand the dynamics of the defective, intact, and inducible viral reservoirs in multiple immune cell subsets in participants starting ART during acute versus chronic stages of HIV infection.

Methods: Study participants included 10 women, from Durban, South Africa diagnosed with acute HIV infection. Five participants initiated ART during chronic infection (median: 774 DPOPV; range: 399 – 1202 days) and five started ART during acute infection (median: 1 DPOPV). PBMCs were sorted into central memory (CM), effector memory (EM), transitional memory (TM), and naïve (N) CD4+ T-cells, as well as myeloid cells (M), at pre-ART, and 1, 6, and 12 months post-infection and post-ART initiation time points. Intact and defective proviral DNA was quantified in each cell population by IPDA. The inducible viral reservoir was measured using the SQuHIVLa assay after 3 years of ART using PBMC samples collected by a leukapheresis procedure.

Results: After 12 months of ART, chronically treated participants exhibited the highest intact proviral DNA levels in CM (average ~18.6 DNA copies/million cells) and EM (~72.62 DNA copies/million cells) subsets, with significantly lower levels in TM (~1.6 DNA copies/million cells), myeloid (~2.4 DNA copies/million cells) and naïve T-cells (~0.78 copies/million cells). In contrast, participants treated during acute infection had significantly lower proviral DNA levels across all subsets than chronically treated participants (CM $p = 0.007$; EM $p = 0.006$; TM $p = 0.007$; N $p = 0.04$; M $p = 0.04$). Intact HIV DNA was higher in EM compared to CM cells in chronically treated participants. Notably, 4 of 5 (~80%) acutely treated participants showed undetectable levels of intact HIV DNA after one year of ART in the EM compartment. Inducible reservoir analysis revealed significantly higher levels in late-treated participants compared to early-treated participants ($p = 0.0038$).

Conclusion: Our findings underscore the importance of CM and EM CD4+ T-cells in establishing and maintaining the HIV reservoir. EM cells harbour higher levels of intact HIV DNA, making them critical targets for reservoir-focused interventions. ART initiated in acute infection significantly reduced both total and intact HIV reservoir sizes, indicating the potential of early treatment to enhance the efficacy of combination strategies aimed at eradicating the HIV reservoir.

4.2 Introduction

HIV proviral DNA is a key marker for the HIV reservoir, but it includes both intact and defective viruses (Avettand-Fènoël et al., 2016). While defective proviruses can trigger immune responses, only intact proviruses have the potential to cause viral rebound when antiretroviral therapy (ART) is stopped (Bruner et al., 2016, Kuniholm et al., 2022, Imamichi et al., 2020). Studies show that 93-98% of the latent HIV reservoir consists of defective viruses that are unable to replicate due to large genomic deletions, reverse transcription errors (Ho et al., 2013), and mutations from APOBEC3 restriction factors (Hiener et al., 2017, Harris et al., 2003, Harris and Dudley, 2015). Understanding these viral characteristics is crucial for designing effective HIV cure strategies (Matsuda and Maeda, 2024).

Various methods exist to characterize the HIV proviral reservoir (Gupta et al., 2017, Siliciano and Siliciano, 2018). The Quantitative Viral Outgrowth Assay (QVOA) is the gold standard for detecting inducible HIV reservoirs, though it is labour-intensive and may underestimate the true reservoir size (Siliciano and Siliciano, 2018, Wang et al., 2018). PCR-based and sequencing techniques, such as Full Length Individual Proviral Sequencing (FLIPS), offer a more detailed view of the proviral landscape by sequencing near-full-length HIV genomes (Hiener et al., 2018). However, FLIPS is expensive, time-consuming, and less efficient because it is a long-range PCR and also requires viral genetic sequencing (Hiener et al., 2018, Gupta et al., 2017).

To meet the demand for scalable methods, the Intact Proviral DNA Assay (IPDA) was developed (Bruner et al., 2019). IPDA uses droplet digital PCR (ddPCR) to distinguish intact from defective proviruses, originally focusing on subtype B, common in resource-rich regions such as the Global North (Bruner et al., 2019). Recent

advancements have adapted the IPDA to subtype C, which dominates in sub-Saharan Africa, ensuring more equitable HIV research (Buchholtz et al., 2024). Understanding subtype C reservoir dynamics is crucial for developing targeted cure strategies for under-resourced settings (Buchholtz et al., 2024).

However, even intact proviruses identified by IPDA are not always replication-competent (Woldemeskel et al., 2020). Recent research has found that multiply spliced RNA (msRNA) could serve as a more accurate marker of inducible reservoirs (Zerbato et al., 2021). Our group and others recently collaborated to develop a novel technique, the Specific Quantification of the Inducible HIV-1 Reservoir (SQuHIVLa), based on reverse transcription loop-mediated isothermal amplification (RT-LAMP) to rapidly and sensitively measure these reservoirs. This method is well-suited for resource-limited settings like sub-Saharan Africa, offering a promising tool for evaluating HIV cure strategies (Hossain et al., 2024).

This chapter dives into three pivotal questions listed below to address HIV-1 reservoir dynamics and understand the intact and defective HIV proviral landscape within immune cells isolated in a subtype C setting (Figure 4.1):

1. Which cellular subset harbors the highest levels of intact proviral DNA?
2. Does early treatment reduce the size of the intact reservoir in immune cells?
3. Does treatment during acute infection reduce the inducible reservoir?

To answer the first question, we implemented the IPDA that we co-developed with others to measure intact and defective DNA levels in subtype C infected samples (Buchholtz et al., 2024). Here, we hypothesized that the highest frequencies of intact genomes would be detected within central and effector memory CD4+ T cells since

we observed high levels of total HIV DNA within these two subsets in the previous chapter.

To answer the next question: how does the timing of ART initiation impact the frequency of the intact reservoir within immune cells? We compared early versus late ART initiation, the study investigated whether starting treatment earlier reduces the frequency of both intact and defective genomes. Here we hypothesized that early or late treatment diminishes the presence of both intact and defective genomes.

Lastly, to answer the question of how early ART affects the inducible HIV reservoir, we compared individuals who started ART during hyperacute infection with those treated later during chronic infection. We utilized the SQuHIVLa assay which detects Tat/Rev msRNA after stimulation with a latency reversal agent (LRA) (Hossain et al., 2024). We hypothesized that early treatment dramatically lowers the reservoir size, resulting in fewer viruses capable of being reactivated.

Together, these investigations offer crucial insights into elucidating the complexities of the HIV proviral reservoir. Understanding which cells harbour intact proviruses, how the timing of treatment influences the reservoir landscape, and how much inducible the virus remains after therapy, are all fundamental to advancing HIV cure research, particularly in an HIV-1 subtype C setting such as sub-Saharan Africa.

4.3 Methods

4.3.1 Study participants

Study participants were all women, 18-23 years old identified with acute HIV infection through twice weekly HIV RNA testing of sexually active women not living with HIV. Five study participants were untreated with ART during acute HIV infection but subsequently went on treatment when South African national treatment guidelines changed, this group we referred to as the late treated group (Figure 4.1). Additionally, 5 participants who were treated during hyperacute infection (early treated) were included. Immune cells from these participants were sorted and the proviral DNA landscape was characterized using IPDA.

4.3.2 Flow cytometry and DNA extraction

Cells were sorted using a FACS ARIA II flow cytometer (BD Biosciences) with a purity range of 90–100% (Figure 3.2). The gating strategy involved selecting singlet PBMCs, followed by the exclusion of dead cells (Aqua-, Invitrogen, Massachusetts, USA). CD3+CD4^{+}+ lymphocytes were identified based on size and granularity.

Within the CD4+ population, subpopulations were further sorted based on the expression of phenotypic markers: naïve CD4+ T cells (N; CD45RO-CCR7+CD27+), central memory T cells (CM; CD45RO+CCR7+CD27+), transitional memory T cells (TM; CD45RO+CD27+CCR7-), and effector memory T cells (EM; CD45RO+CD27-CCR7-) as previously described in (Kwon et al., 2020). Additionally, within the CD3-population, myeloid cells were identified and sorted as CD3-CD14+ cells (BD Biosciences). Using these cell-defining markers to identify the target cell populations sorting was performed. A ‘4-way purity’ sort option was used to collect pure cell populations, and a representative post-sort analysis was done to ensure no

contamination. Thereafter DNA was extracted according to the manufacturer's instructions (Qiagen, Hilden, Germany).

4.3.3 Characterization of the proviral DNA landscape using intact proviral DNA assay (IPDA)

Proviral DNA was quantified using a multiplex ddPCR, targeting parts of the HIV Ψ (*psi*) and *env* regions, using the primer sets shown in Table 2.9. The *RPP30* host gene was used to measure cellular input. DNA integrity was assessed by analysis of the DNA shearing index (DSI), used to indicate DNA fragmentation. DNA from PBMCs of HIV-negative donors was used as a DNA template control, J-Lat full-length clone 15.4 cells (NIH AIDS Reagent Program) as an HIV-positive control, and PCR grade water as a no template control. All cell subsets were assessed in duplicate (Buchholtz et al., 2024).

Thereafter, ddPCR mastermixes were made for both *psi/env* and *RPP30*. DNA was added to mastermix containing ddPCR supermix (Bio-Rad, California, USA), restriction enzyme Xho1 (Inqaba Biotec, Nairobi, Kenya), and a cocktail of specific primers and probes. For the RPP30 reaction, DNA was diluted based on the concentration of DNA after the extraction to make a predilution mix. Thereafter the predilution was added to the mastermix containing ddPCR supermix (Bio-Rad, California, USA), restriction enzyme Xho1 (Inqaba Biotec, Nairobi, Kenya), and a cocktail of specific primers and probes.

Thereafter, droplets were generated using the automated droplet generator QX200 AutoDG (Bio-Rad, California, USA). The following cycling conditions were followed: cycle conditions were performed according to the manufacturer’s protocol (Bio-Rad, California, USA) 95 °C for 10 min, 45 cycles of 94 °C for 30 seconds and 58 °C for

1min, 72°C for 1min. The QX Manager software (Bio-Rad, California, USA) was used to analyze the results. Positive and negative droplets were discriminated by manual threshold gating using the 2-D plot function on QX Manager software (Bio-Rad, California, USA) (Buchholtz et al., 2024). Results were exported and analyzed using GraphPad Prism version 9.5.1 (GraphPad, Massachusetts, USA).

4.3.4 Quantifying msRNA using Specific Quantification of inducible HIV-1 reservoir by LAMP (SQuHIVLa)

4.3.4.1 Isolation of CD4+ T cells from leukapheresis samples

Leukapheresis samples were thawed and resuspended in culture RPMI -1640 media (Gibco, ThermoFisher Scientific, California, USA) supplemented with 10% FBS and 100ug/ul penicillin-streptomycin. We started with approximately 40 – 60 million cells The supernatant was then decanted and resuspended in a buffer, consisting of phosphate-buffered saline (PBS) (ThermoFisher Scientific, Massachusetts, USA), bovine serum albumin (BSA) (Promega, Wisconsin, USA), and ethylenediaminetetraacetic acid (EDTA) (Merck, Massachusetts, USA), supplemented with DNase (New England Biolabs, Massachusetts, USA). Cells were counted and viability was determined using the TC20 automated cell counter (Bio-Rad, California, USA). Thereafter, the protocol for isolating CD4+ T cells that was described by Miltenyi Biotec (Miltenyi biotech, North Rhine-Westphalia, Germany) was followed.

4.3.4.2 Specific Quantification of inducible HIV-1 reservoir by LAMP (SQuHIVLa)

Once CD4+ T cells were isolated and viability was determined, the cells were then plated out and rested for five hours at 37˚ C in a humidified, 5% CO_2 incubator. CD4+ T cells were then stimulated with 100 ng/mL of PMA (Sigma-Aldrich, Missouri, USA)

and 1 ug/mL ionomycin (Sigma-Aldrich, Missouri, USA) for approximately 12- 14 hours (Hossain et al., 2023).

After the stimulation, the cells appeared aggregated and clumped. The activated CD4+ T cells were then counted and washed using PBS (ThermoFisher Scientific, Massachusetts, USA). Dilutions were made accordingly: 20,000 cells, 5,000 cells, 1,250 cells, and 313 cells. 5 µl of each of these cell dilutions were added to 15 µl of mastermix containing $MgSO_4$ (Inqaba Biotech, Nairobi, Kenya), dNTPs (Life Technologies, California, USA) specific primers and probes, Bst 2.0 Warmstart DNA polymerase, Warmstart RxT Reverse Transcriptase (New England Biolabs, Massachusetts, USA), RNasin RNase Inhibitor (New England Biolabs, Massachusetts, USA), 10X Isothermal Amplification buffer (New England Biolabs, Massachusetts, USA), Titron X 4% (Sigma-Alrich, Missouri, USA).

For the RT-LAMP reaction the following cycling conditions were used, incubation at 45˚C for 60 minutes, continuous 65˚C with flourescence reads every 30 seconds for 180 cycles. After the RT-LAMP reaction, the positive wells at each dilution were scored, and the maximum likelihood method was used to determine the frequency of cells expressing *tat/rev* msRNA using the IUPMStats v1.0 online software (Rosenbloom et al., 2015). Infectious units per million cells (IUPM) were calculated using the IUPMStats Infection Frequency Calculator (Siliciano and Siliciano, 2021).

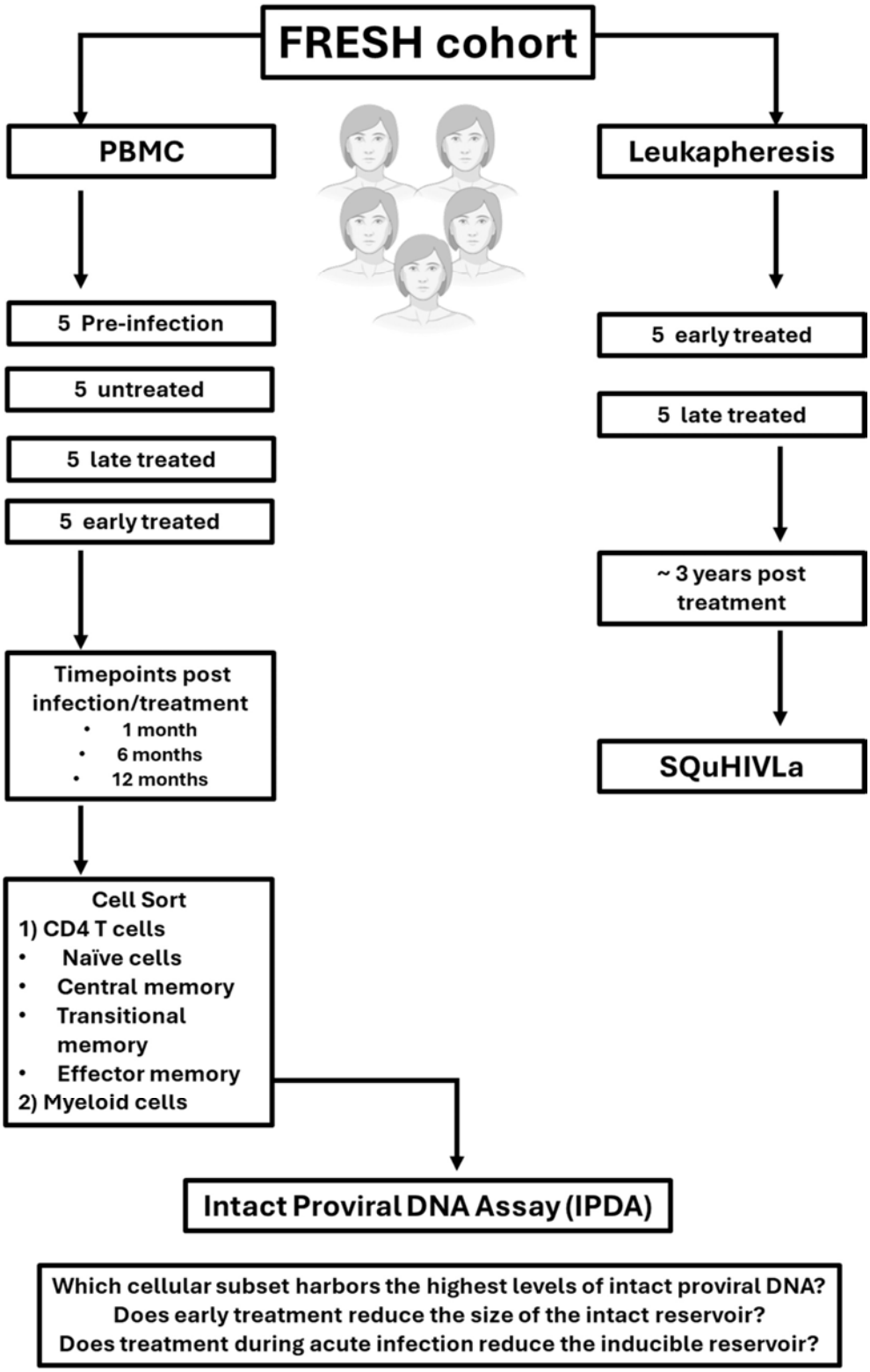

Figure 4.1 Schematic illustration of Chapter 4 outline.

4.4 Results

4.4.1 Characterization of the HIV-1 proviral reservoir landscape within immune cells.

Inferred genome intactness or defectiveness was measured at 1 month, 6 months, and 12 months post-infection during untreated infection (Figure 4.2). During untreated infection, at 12 months post-infection, quantification of 3′ deleted/hypermutated proviral DNA measured ~763 average DNA copies/million cells (range: 325.2 – 983.2 average DNA copies/million cells) and 5′ deleted proviral DNA measured ~236 average DNA copies/million cells (range: 39.2 – 348.2 average DNA copies/million cells) in CM CD4+ T cells (Figure 4.2A). We observed there was no significant decrease from 1 month to 12 months post-infection in defective proviral DNA levels in all cell types (Figure 4.2A). Additionally, we observed no change in the frequency of intact DNA from one month post-infection (189.2 average DNA copies/million cells) to 12 months post-infection (163 average DNA copies/million cells) (Figure 4.2A) in CM CD4+ T cells. In EM ($p = 0.062$) (Figure 4.2B), TM ($p = 0.62$) (Figure 4.2C), N ($p = 0.25$) (Figure 4.2D), and M ($p = >0.99$) (Figure 4.2E) there was no reduction in the frequency of intact DNA from 1 month to 12 months post-infection. Moreover, there was no reduction in the levels of defective proviral DNA in both 3′deleted/hypermutated and 5′deleted proviral DNA in each cell subset (Figure 4.2).

Next, we determined the effects of treatment on the frequency of intact and defective genomes in study participants who were treated during chronic and acute infection (Figure 4.3 and Figure 4.4). First, we assessed the levels of intact and defective proviral DNA in chronically treated individuals. We observed that CM ($p = 0.0146$) (Figure 4.3A) and EM ($p = 0.0079$) (Figure 4.3B) CD4+ T cells displayed a significant

reduction in the frequency of intact proviral DNA from 1 month to 12 months post-treatment. There was no significant decrease in the levels of intact DNA in TM ($p = 0.071$) and N ($p = 0.72$) CD4+ T cells from 1 month to 12 months post-treatment (Figure 4.3C and Figure 4.3D respectively). Intact proviral DNA was detected in myeloid cells but at a lower frequency than in memory CD4+ T cells (16.5 fold less). At 1 month post-treatment, the number of intact copies of DNA in myeloid cells decreased from an average of 198 DNA copies/million cells to 12 DNA copies/million cells at 12 months post-treatment in one study participant (Figure 4.3E). Although the levels of intact proviral DNA decreased with one year of treatment in selected cell subsets, mostly in CD4+ T cells, there was no change in the levels of defective (3´ defective and 5´ defective) proviral DNA in each of the cell subsets (Figure 4.3).

Next, we determined the effects of treatment during hyperacute infection (Figure 4.4). In all cell subsets examined, we observed a decrease in the levels of defective proviral DNA, however, there was only a significant decrease in EM CD4+ cells for 5´ deleted proviral DNA from 1 month to 12 months post-treatment ($p = 0.0092$) (Figure 4.4B). Interestingly, in CM ($p = 0.020$) (Figure 4.4A) and EM ($p = 0.0079$) (Figure 4.4B) CD4+ T cells there was a significant decrease in the frequency of intact genomes from 1 month to 12 months post-treatment. Early treatment resulted in a steady decrease in the frequency of defective and intact proviral DNA in all cell subsets.

Moreover, we assessed the impact of treatment from baseline (untreated) to 12 months post-treatment in study participants who were late treated, we observed a decrease in the frequency of intact proviral DNA in memory CD4+ T cells (CM $p = 0.0079$, EM $p = 0.079$, TM $p = 0.0185$) (Figure 4.5 A-C respectively). Naïve CD4+ T cells ($p = >0.99$) (Figure 4.5D) and myeloid cells ($p = 0.5$) (Figure 4.5E) didn't show a significant decrease in the levels of intact proviral DNA. This indicated that after one

year of treatment, intact proviral DNA decreased in all cell subsets, however more so in memory CD4+ T cells than myeloid cells (Figure 4.5). There was no change in the levels of 3´deleted/hypermutated or 5´deleted proviral DNA in each of the cell subsets (Figure 4.5).

Furthermore, we compared the frequencies of intact proviral DNA levels at baseline to determine which cell subset is preferentially seeded upon infection (Figure 4.6). We compared 1 month post-infection in those that were untreated and the 1 month post-treatment timepoint in those that were treated during hyperacute infection (Figure 4.6). We observed that at 1 month during untreated infection intact DNA levels were CM (average 189 DNA copies/million cells), EM (2,729 DNA copies/million cells), TM (17.9 DNA copies/million cells), N (2 DNA copies/million cells), M (2 DNA copies/million cells).

At 1 month during hyperacute treatment, the average intact proviral DNA quantities were as follows in the different cell subsets: CM (5 DNA copies/million cells), EM (892 DNA copies/million cells), TM (2 DNA copies/million cells), N (2 DNA copies/million cells), M (2 DNA copies/million cells). Overall, we observed that treatment during hyperacute infection resulted in lower quantities of intact proviral DNA compared to untreated infection at baseline. However, although those that were treated during hyperacute infection had lower levels of intact proviral DNA compared to untreated infection we detected a high frequency of intact proviral DNA within CM ($p = 0.0096$) and EM ($p = 0.0135$) CD4+ T cells regardless of whether the study participants were untreated or early treated (Figure 4.6).

Additionally, we examined differences in intact proviral DNA levels between those participants who were treated in chronic and those who initiated treatment in acute

infection to determine the impact of the timing of ART initiation on the frequencies of intact proviral DNA (Figure 4.7). After 12 months post-treatment we observed that participants who initiated ART during chronic infection had higher average quantities of intact proviral DNA in all subsets (CM = 14.2 copies/million cells, EM = 56.03 average copies/million cells, TM = 3.9 copies/million cells, N = 0.76 copies/million cells, M = 2.4 copies/million cells) compared to participants who initiated treatment in acute infection (CM = 0 copies/million cells, EM = 2.4 copies/million cells, TM = 0 copies/million cells, N = 0 copies/million cells, M= 0 copies/million cells) (Figure 4.7). Interestingly, we noted that intact proviral DNA was still detectable in effector memory CD4+ T cells in one study participant after a year of treatment (12 copies/million cells) (Figure 4.7).

Furthermore, since we observed the greatest frequency of intact proviral DNA with central and effector memory CD4+ T cells, we compared the frequency of proviral DNA between the two cell subsets. When comparing total HIV proviral DNA in central and effector CD4+ T cells, there was no statistically significant difference in the levels of proviral DNA (Figure 4.8A). However, when comparing the levels of intact proviral DNA we observed that there were significant differences between central memory and effector memory CD4+ T cells (Figure 4.8B). Statistically significant differences were noted both at one month post-infection ($p= 0.0079$) and at one year post-treatment ($p= 0.0317$) in those participants who initiated treatment during chronic infection (Figure 4.8B).

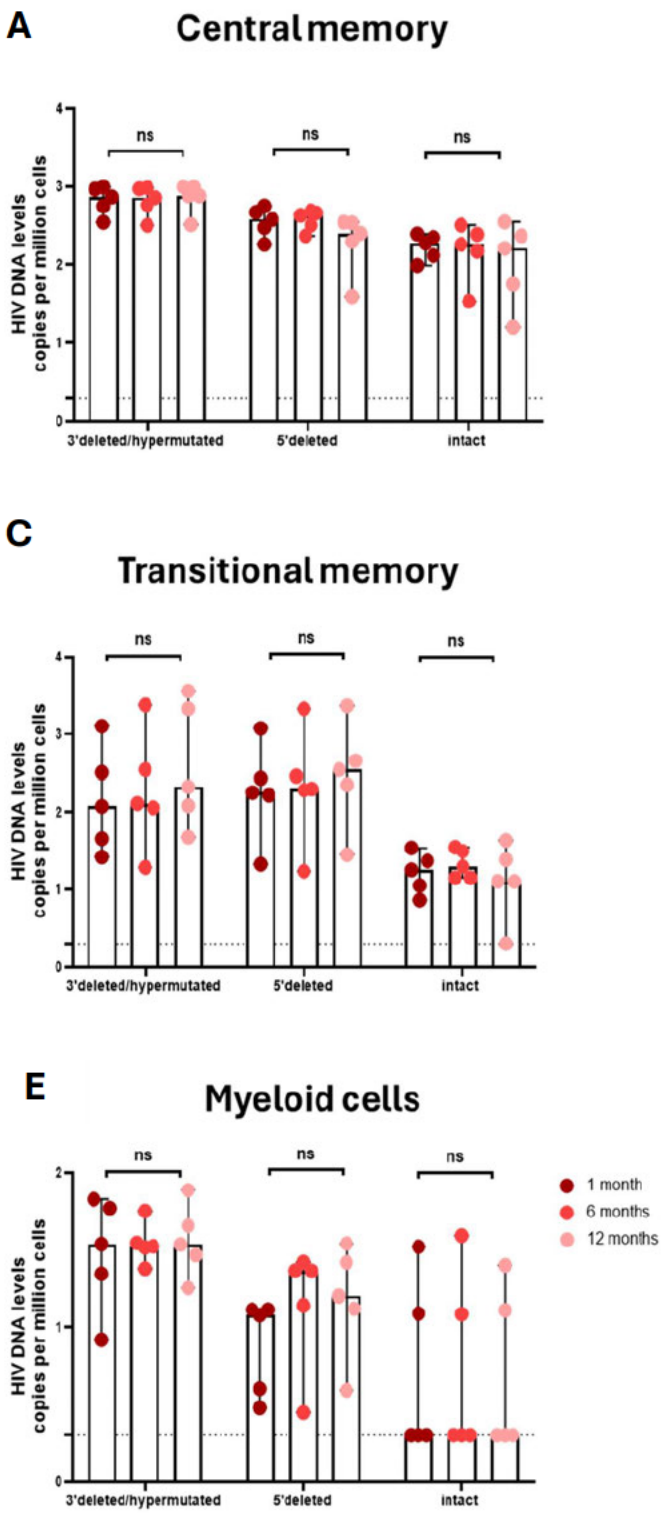
A
Central memory
B
Effector memory
C
Transitional memory
D
Naïve cells
E
Myeloid cells
HIV DNA levels
copies per million cells
ns
3'deleted/hypermutated
5'deleted
intact
1 month
6 months
12 months

Figure 4.2 **Characterizing the proviral landscape within immune cells during untreated infection.** No decrease in defective or intact genomes during untreated infection in all cellular subsets that were assessed (A-E). 1 month (dark red), 6 months (medium red), and 12 months (light red) post-infection timepoints are represented. ns= non-significant. 3´ deleted/hypermutated, 5´ deleted, and intact proviral DNA levels are shown.

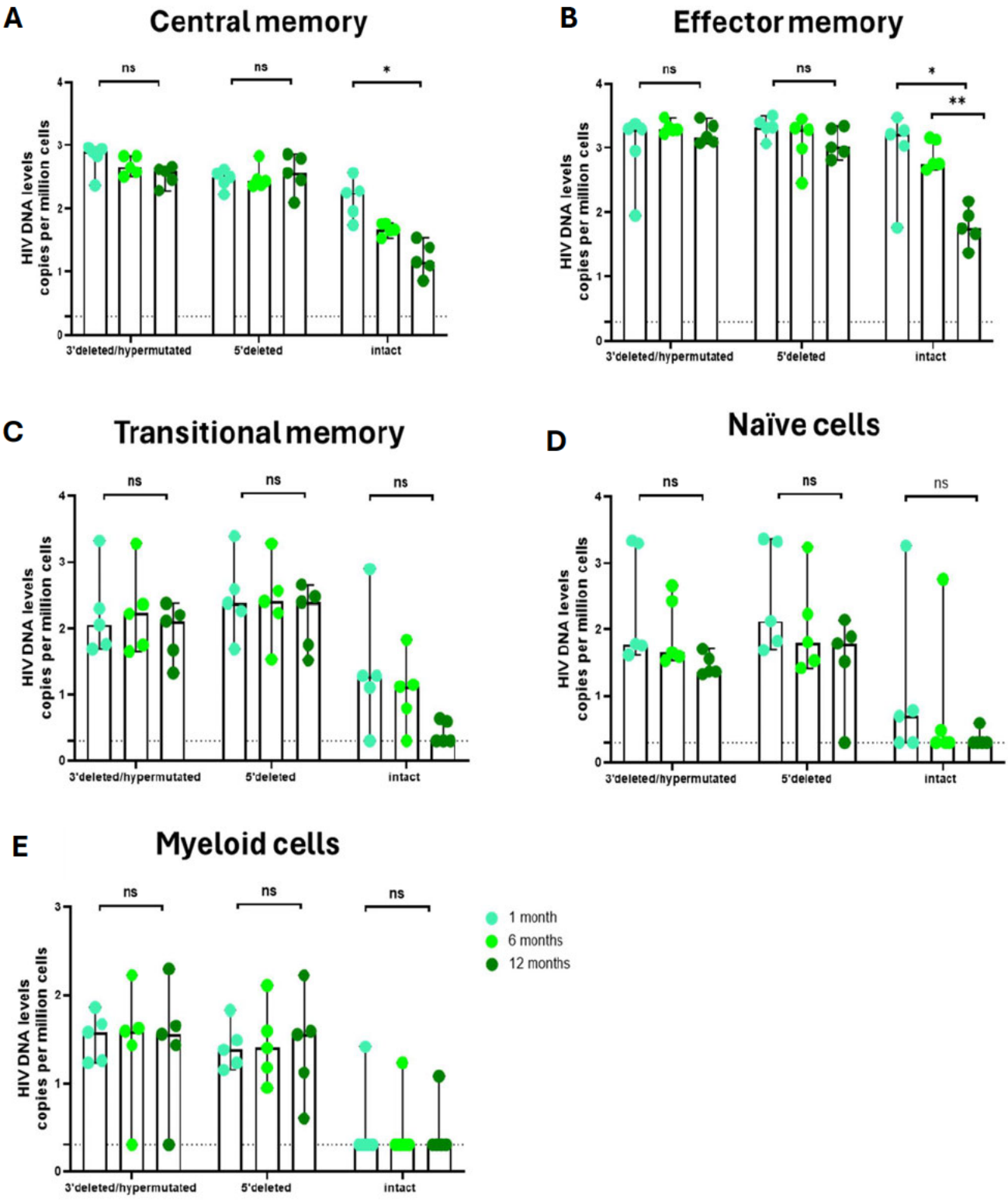
A
Central memory
B
Effector memory
C
Transitional memory
D
Naïve cells
E
Myeloid cells
HIV DNA levels
copies per million cells
ns
*
**
3'deleted/hypermutated
5'deleted
intact
1 month
6 months
12 months

Figure 4.3 Characterizing the proviral landscape within immune cells from individuals that have been treated during chronic infection (late treated). Treatment during chronic infection decreases the frequency of intact genomes in memory CD4+ T cells (A-C) but not naïve CD4+ T cells and myeloid cells (D-E). 1 month (light green), 6 months (medium green), and 12 months (dark green) post-infection timepoints are represented. ns= non-significant. */** p= <0.05, 3´ deleted/hypermutated, 5´ deleted, and intact proviral DNA levels are shown.

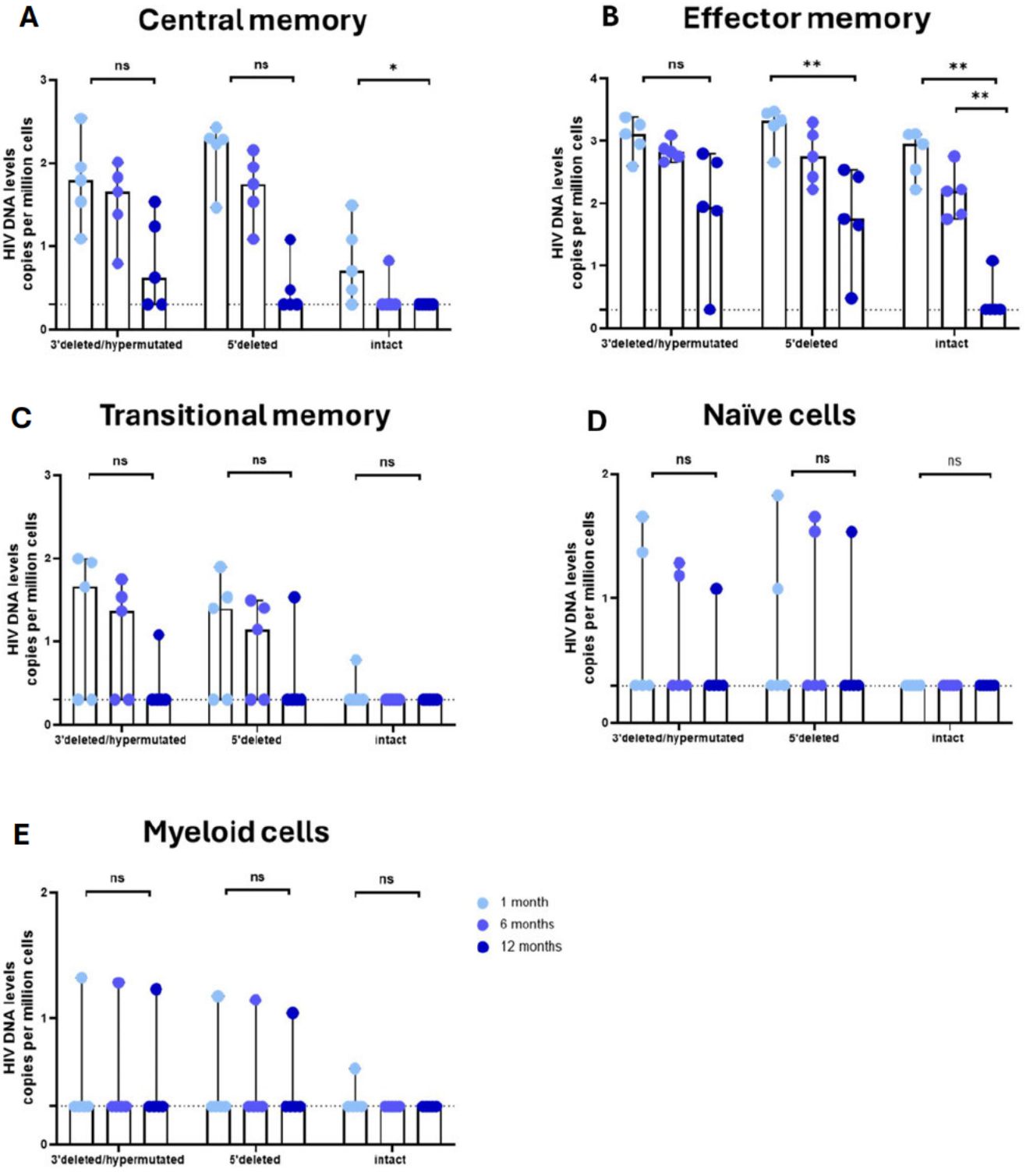
A
Central memory
B
Effector memory
C
Transitional memory
D
Naïve cells
E
Myeloid cells
HIV DNA levels
copies per million cells
ns
*
**
3'deleted/hypermutated
5'deleted
intact
1 month
6 months
12 months

Figure 4.4 **Characterizing the proviral landscape within immune cells from individuals that have been treated during acute infection (early treated).** Treatment during hyperacute infection rapidly declines defective and intact genomes. Different cell subsets are represented in the panels from A-E. 1 month (light blue), 6 months (medium blue) and 12 months (dark blue) post-infection timepoints are represented. ns= non-significant. */** p= <0.05, 3´ deleted/hypermutated, 5´ deleted, and intact proviral DNA levels are shown.

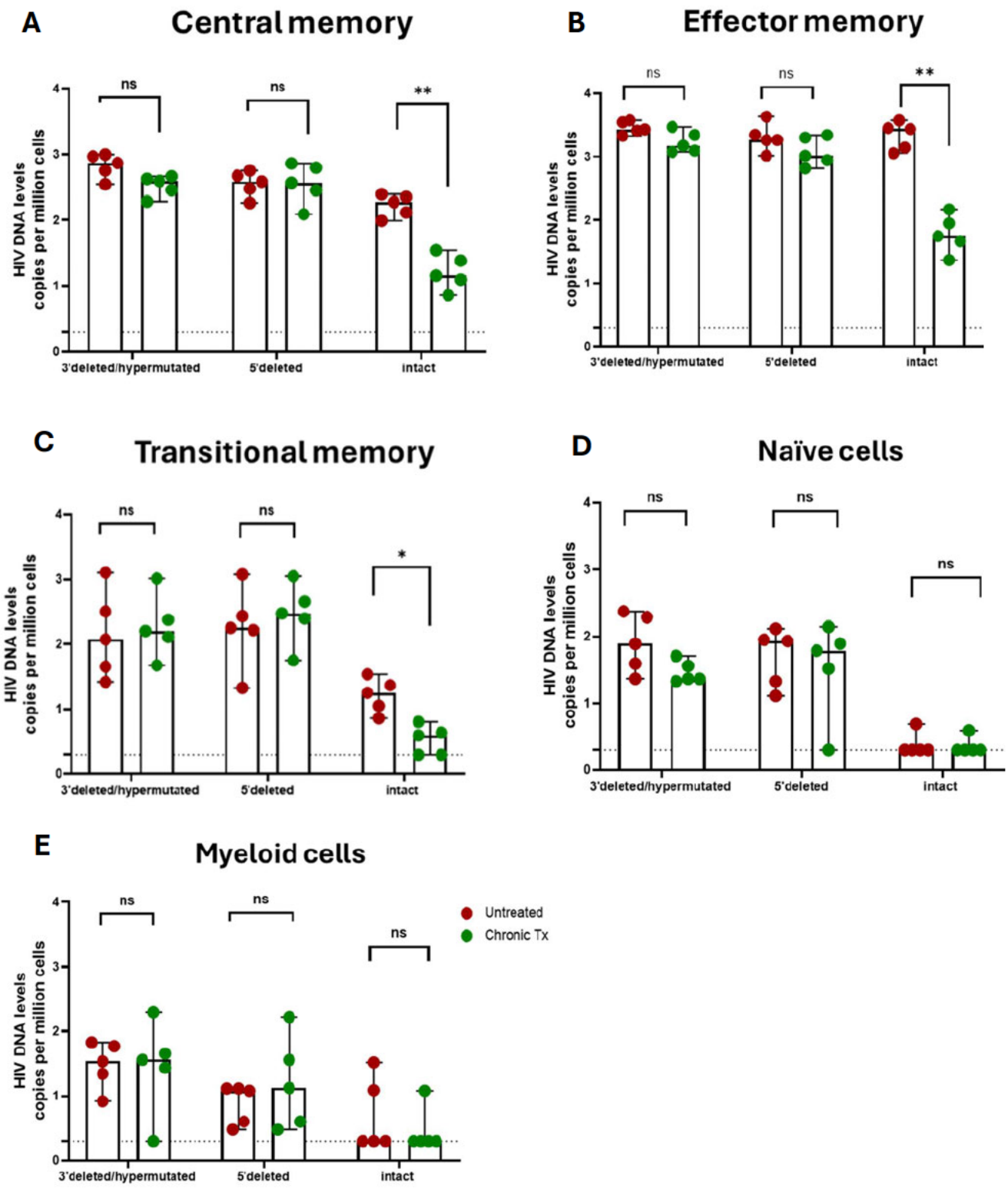
A
Central memory
B
Effector memory
C
Transitional memory
D
Naïve cells
E
Myeloid cells
HIV DNA levels
copies per million cells
ns
**
*
3'deleted/hypermutated
5'deleted
intact
Untreated
Chronic Tx

Figure 4.5 Intact proviral DNA decreases significantly after a year of treatment in memory CD4+ T cell subsets. Central memory (A), Effector memory (B), Transitional memory (C), Naïve cells (D), and Myeloid cells (E) are shown. 1 month post-infection is shown in red and one year post-treatment is shown in green. ns= non-significant. */** p= <0.05, intact proviral DNA levels are shown.

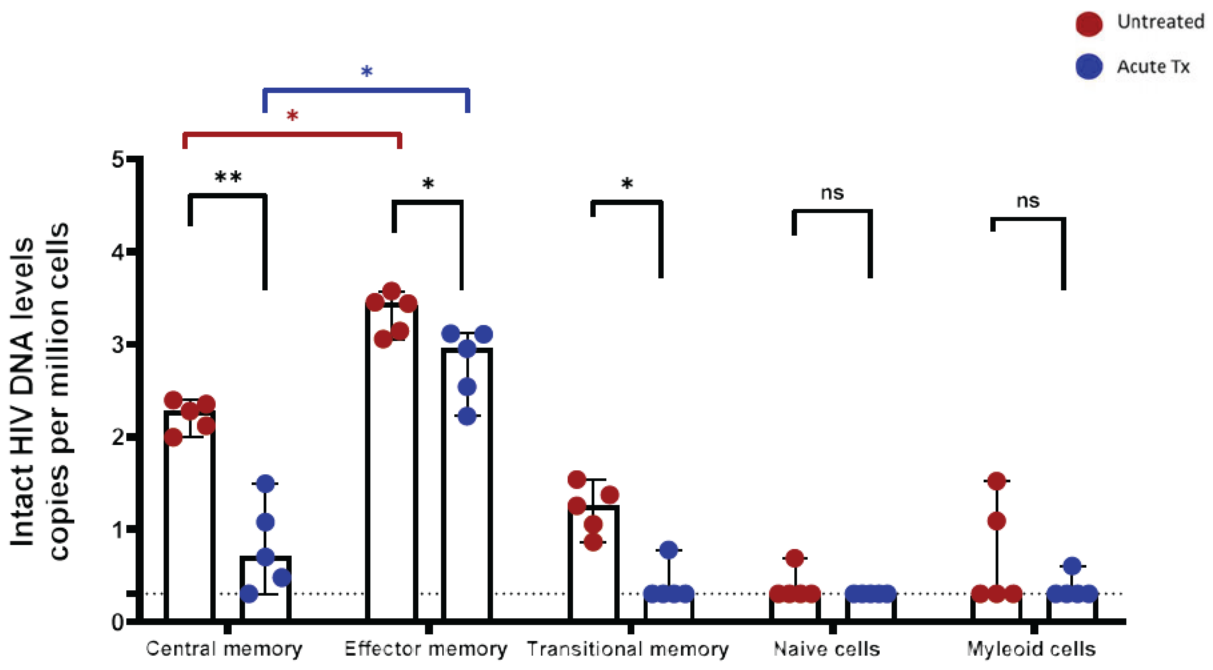

Figure 4.6 Higher levels of intact HIV DNA within effector and central memory CD4+ T cells at baseline. 1 month post-infection for those that were untreated is shown in red. 1-month post-infection for those who were treated during hyperacute infection is shown in blue (acute treated). Log intact HIV DNA levels (copies/million cells are measured. ns= non-significant. */** p= <0.05, intact proviral DNA levels are shown.

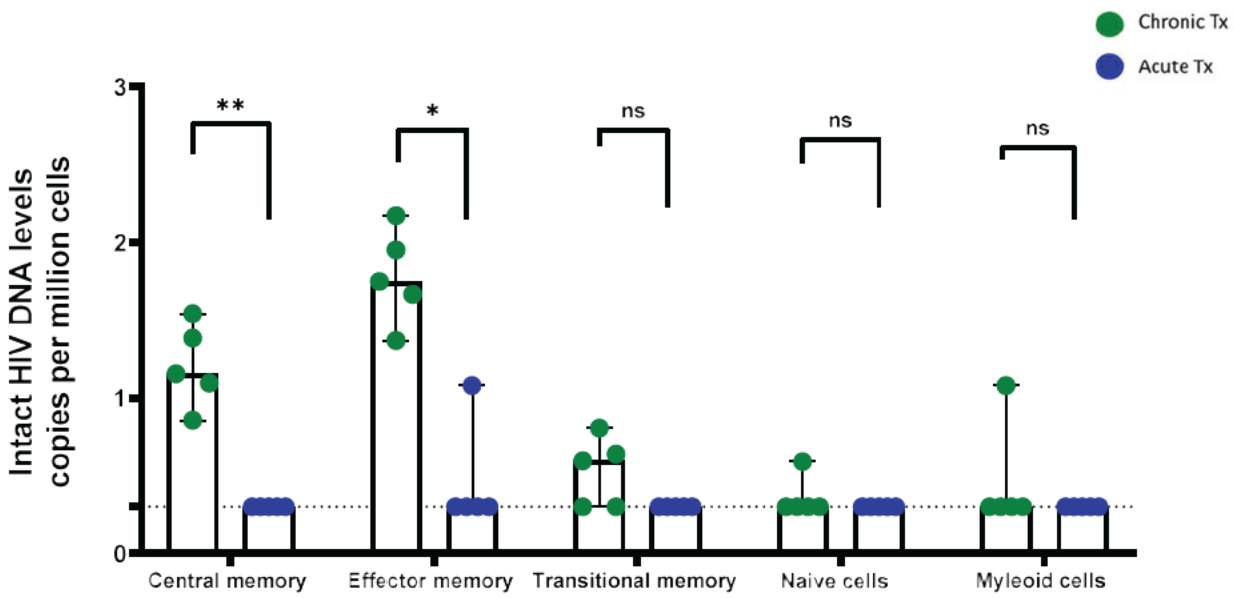

Figure 4.7 Early treatment significantly reduces intact proviral DNA after one year of treatment. Those who were treated during chronic infection are shown in green and those who were treated during hyperacute infection are shown in blue. ns= non-significant. */** p= <0.05, intact proviral DNA levels are shown.

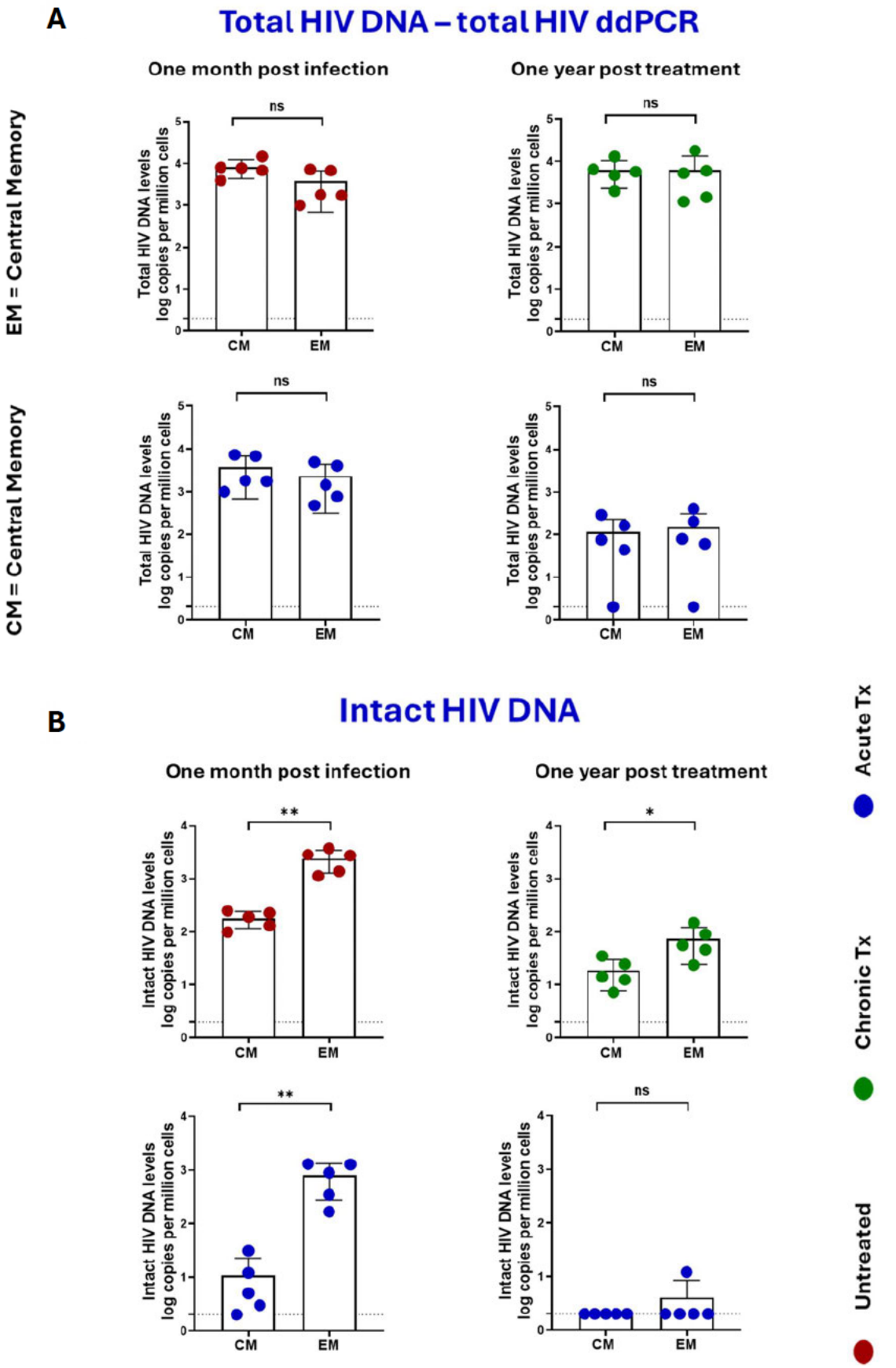
A
Total HIV DNA – total HIV ddPCR
One month post infection
One year post treatment
EM = Central Memory
CM = Central Memory
Total HIV DNA levels log copies per million cells
ns
CM
EM
B
Intact HIV DNA
Intact HIV DNA levels log copies per million cells
**
*
Acute Tx
Chronic Tx
Untreated

Figure 4.8 No difference in total HIV DNA levels after one year of treatment in central and effector memory CD4+ T cells. However, there was a decrease in the frequency of intact HIV DNA detected in central compared to effector memory CD4+ T cells. A) Total HIV DNA level one month post-detection from individuals who were untreated (red) in central (CM) and effector (EM) memory CD4+ T cells. One year post-treatment is shown in green. Blue depicts those treated during acute infection. B) Intact HIV DNA was measured at one month post-infection (red= untreated, blue= acute treated) and one year post-treatment (green= chronically treated, blue = acutely treated). ns= non-significant. */** p= <0.05, intact proviral DNA levels are shown.

4.4.2 Measuring the inducible reservoir using SQuHIVLa in participants commencing ART in chronic versus acute infection.

The IPDA infers genome intactness and defectiveness and provides an estimation of the frequency of intact proviral DNA that can be reactivated if stimulated. Emerging work has shown that measuring Tat/Rev multiply spliced (msRNA) is a reliable predictor of the inducible reservoir after stimulation (Zerbato et al., 2021, Hossain et al., 2024). It has been reported that upon latency reversal Tat/Rev may be a relevant and promising indicator of the inducible, replication competent viral reservoir (Hossain et al., 2024). Strong correlations were observed between supernatant HIV-1 RNA and msRNA (Zerbato et al., 2021).

Here, we used SQuHIVLa to quantify the inducible reservoir after 3 years of treatment in 10 study participants, comparing five chronically treated versus 5 that initiated treatment in the acute phase (Hossain et al., 2024). SQuHIVLa measures Tat/Rev msRNA using RT-LAMP by real-time PCR. Chronically treated participants' infectious units per million cells ranged from 33.54 and 82.40 IUPM. Acutely treated participants had a range of infectious units per million cells between 3.91 and 9.97 IUPM.

Figure 4.9 depicts an example of a chronically treated participant. This participant initiated therapy 427 DPOPV. This participant had infectious units per million cells of 67.10 IUPM. Figure 4.10 highlights a participant who was treated during the hyperacute stage of infection. This participant initiated therapy 1 DPOPV. PID 879 had infectious units per million cells of 4.74 IUPM. Post-stimulation of total PBMCs it was observed that chronically treated participants had significantly higher inducible reservoir levels compared to acutely treated participants ($p = 0.0038$). This indicates that those treated during hyperacute infection have a smaller inducible reservoir than those who are treated during chronic infection (Figure 4.11).

Participant characteristics:
PID 208
Sex: Female
Age at infection: 23 years
Date of first positive sample: 24 January 2014
Initiated therapy: 27 March 2015
Chronically treated on day 427 post detection

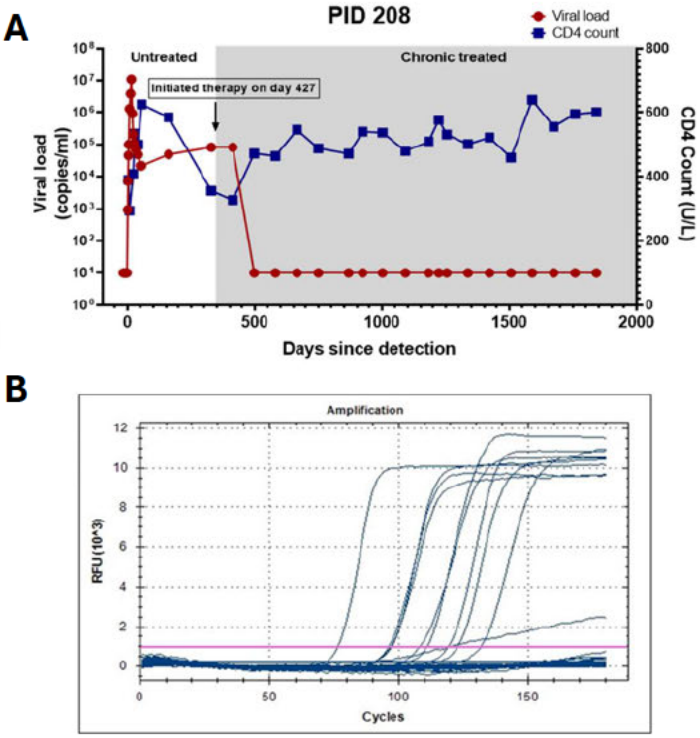

Figure 4.9 Chronically treated participant PID 208. A 23-year-old female whose date of first positive sample was recorded on 24 January 2014. This participant initiated therapy on day 427 post-infection. A) Viral load and CD4 count trajectories for PID 208. Also highlights the day treatment was initiated. B) Real-time PCR results using SQuHIVLa to determine infectious units per million cells. Peaks above the threshold (pink) indicate amplification of Tat/Rev msRNA.

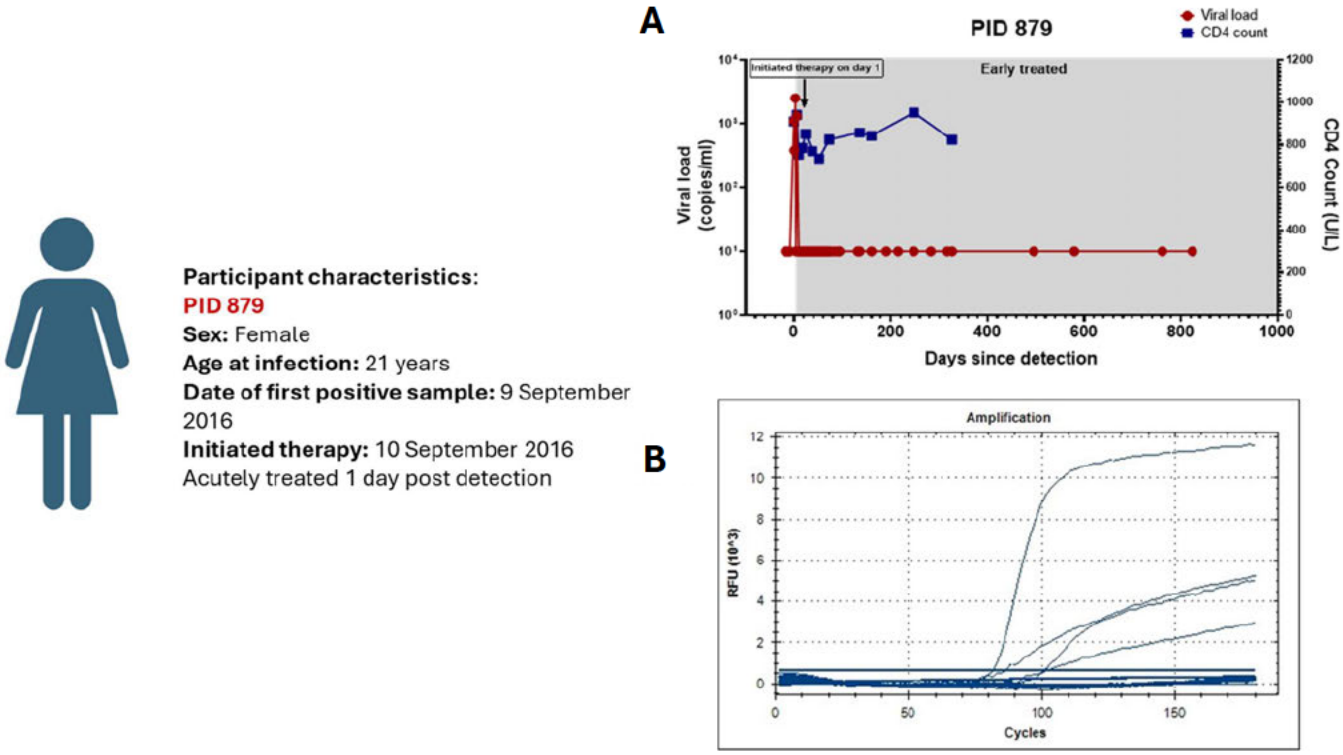

Figure 4.10 Acutely treated participants PID 879. A 21-year-old female whose date of first positive sample was on 9th September 2016. This participant initiated therapy 1 day post-detection. A) Viral load (red) and CD4 count (blue) trajectories for PID 879 B) Real-time PCR results using SQuHIVLa to determine infectious units per million cells. Peaks above the threshold indicate amplification of Tat/Rev msRNA.

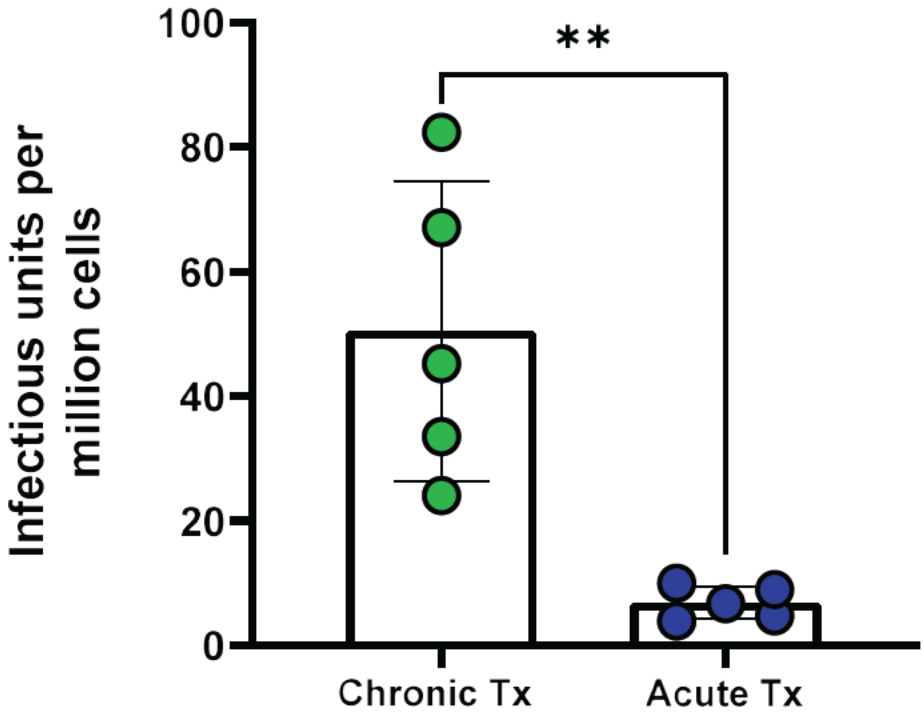

Figure 4.11 Late treated participants (green) versus early treated participants (blue). Infectious units per million cells are measured showing Tat/Rev msRNA measurements. Medians with SD are represented. Chronically treated participants had significantly higher levels of Tat/Rev msRNA than those individuals who were treated during hyperacute infection. ** p =<0.05.

4.5 Discussion

In this chapter, we utilized two novel assays to explore the proviral landscape within immune cells and to identify the key differences in the HIV reservoir between individuals treated during chronic infection versus those treated in the hyperacute stage of infection. This allowed us to refine our understanding of how HIV persists within the body and how the timing of ART impacts the viral reservoir over time. Specifically, we utilized the IPDA, a novel tool recently adapted for the analysis of HIV subtype C samples, to assess which immune cell subset harboured the highest frequency of intact proviral DNA (Buchholtz et al., 2024). Based on findings from the previous chapter which showed that central and effector memory CD4+ T cells harboured high levels of total HIV proviral DNA, we hypothesized that central memory and effector memory CD4+ T cells would mirror this finding and show high frequencies of intact proviral DNA.

Our results revealed that, while both CM and EM subsets contained high levels of total proviral DNA that were comparable with no statistical differences on average as highlighted in the previous chapter, there was a notably elevated presence of intact proviral DNA within the effector memory CD4+ T cells. This discovery was significant, as it underscored the unique role of these cells in maintaining the viral reservoir despite ART. Effector memory CD4+ T cells, which are crucial for the body's immune response, seem to serve as a primary reservoir for intact proviral DNA, making them a focal point in understanding HIV persistence and potential therapeutic interventions and further mechanistic studies are needed to fully understand characteristics of effector memory CD4+ T cells and the unique cellular transcriptional and phenotypic profiles that enable them to harbour high frequencies of intact proviral DNA.

When investigating the impact of treatment on intact proviral DNA levels, we hypothesized that ART would significantly reduce both intact and defective proviral DNA, regardless of when treatment was initiated. Our data revealed that during untreated infection, there was no statistically significant difference in the frequency of intact or defective proviral DNA between participants one month post-infection compared to that one year post-infection. Moreover, when ART was initiated late—during chronic infection—there was no reduction in the frequency of defective proviral DNA following 12 months of ART. We also observed that one year post-treatment, both central and effector memory CD4+ T cells exhibited a marked reduction in the levels of intact proviral DNA.

In individuals who initiated ART during hyperacute infection, the findings were even more striking. One year after starting treatment, we observed a significant drop in intact proviral DNA levels within memory CD4+ T cells. Intact proviral DNA was undetectable across all the cell subsets of interest, including CD4+ T cells and myeloid cells, in nearly all participants, except for one individual who still showed detectable levels of intact proviral DNA after one year of treatment in effector memory CD4+ T cells. This outlier case underscores either the variability in the characteristics of the infecting virus or host differences in response to early ART and highlights the importance of further studies to better understand the mechanisms that underlie differential viral persistence following ART initiation.

Next, we turned our attention to measuring the levels of the inducible reservoir in participants who were either late or early treated using SQuHIVLa. Traditionally, the quantitative viral outgrowth assay (QVOA) has been the gold standard for assessing the inducible reservoir. However, recent advancements have shown that measuring multiple spliced RNA (msRNA) can also serve as a reliable predictor (Zerbato et al.,

2021, Hossain et al., 2024). Here, we utilized the SQuHIVLa assay, a recently developed tool that we and others designed to measure *Tat/Rev* msRNA, as a proxy for the inducible reservoir (Hossain et al., 2024). We used cryopreserved leukapheresis samples of participants who were treated late (chronic infection) and early (acute infection). Our results revealed that individuals treated during chronic infection had a significantly higher inducible reservoir compared to those treated during acute infection. This finding emphasizes the profound impact of early ART in limiting the size of the inducible viral reservoir. Furthermore, this significant size difference could potentially reduce the time to viral rebound once therapy is stopped and therefore this evidence could help explain why those treated early have better viral control once therapy is stopped. However, further mechanistic studies are needed to confirm this finding.

In conclusion, the data presented in this chapter highlight the critical benefits of early ART initiation. We demonstrated that central and effector memory CD4+ T cells are key targets for the HIV proviral DNA reservoir. Notably, although intact proviral DNA levels decline with ART, we also discovered that intact HIV DNA can persist in myeloid cells. Importantly, our findings suggest that early ART effectively restricts the viral reservoir to CD4+ T cells, and that intact proviral DNA preferentially resides within effector memory CD4+ T cells compared to central memory cells. Moreover, our results suggest that early ART reduces the reservoir size and cellular complexity over time, making future therapeutic interventions more likely to succeed in targeting and potentially eradicating the HIV reservoir.

5 Chapter 5: The role of APOBEC3G/-F in shaping reservoir landscapes in individuals who initiated antiretroviral treatment in acute or chronic infection

5.1 Abstract

Introduction: Achieving a functional cure for HIV-1, where viral replication is controlled without continuous antiretroviral therapy (ART), is a critical goal in HIV research. This requires maintaining undetectable or low viral loads despite persistent reservoirs of integrated proviral DNA. The APOBEC3 (A3) family of cytidine deaminases, particularly A3G and A3F, are anti-viral host proteins with the ability to induce cytosine-to-uracil mutations in viral DNA during reverse transcription, rendering the virus defective, and may therefore potentially be harnessed in therapies targeting the HIV-1 reservoir. This study assessed the impact of A3G and -3F proteins on the viral reservoir landscape.

Methods: Samples from ten women from Durban, South Africa, were analysed pre- and post-HIV-1 infection and ART treatment. Five initiated ART during hyperacute infection (median of 1 day post-positive viral load (DPOPV)), while the other 5 began ART in chronic infection (median of 774 DPOPV). A3G and A3F mRNA levels and defective proviral DNA were measured in various cell subsets (central memory (CM), effector memory (EM), transitional memory (TM), naïve CD4+ T cells (N), and myeloid cells (M)) by ddPCR. Viral genome sequences generated by FLIP-seq were analysed for APOBEC induced hypermutations.

Results: Before infection, A3G expression was consistently higher than A3F (~ 1.5 fold higher), across all cell populations. In untreated HIV-1 infection, both A3G and A3F were downregulated, with a greater reduction in A3G, across all cell subsets. ART

partially restored their expression in late treated participants. Treatment initiation during acute infection limited the downregulation of APOBEC proteins,

Participants initiating ART during chronic infection had higher levels of defective DNA compared to early-treated individuals in all subsets except naïve CD4+ T cells (CM $p = 0.0001$, EM $p = 0.0001$, TM $p = 0.0032$, N $p = 0.104$, and M $p = 0.025$). In late-treated individuals, A3G expression correlated with larger defective reservoirs in transitional memory CD4+ T cells ($p = 0.003$, $r = 0.97$). Furthermore, proviral DNA sequencing revealed that A3G-induced hypermutation was more frequent than A3F ($p = 0.0006$). Hypermutation patterns showed a bimodal distribution, with higher frequency at the 3′ and 5′ ends of the HIV genome, regions susceptible to prolonged single-stranded states during reverse transcription. Total A3G expression levels during pre-infection ($p = 0.027$, $r = 0.91$) and 12 months post-treatment ($p = 0.032$, $r = 0.90$) correlated positively with the percentage of hypermutation.

Conclusion: Early ART initiation preserves A3 activity by maintaining a key component of innate immune function, creating a conducive environment for targeting proviral DNA. The results indicate that A3G activity may influence the genetic composition of the reservoir. These findings advance our knowledge of how timing of ART initiation influences innate immune functions and how these functions shape the HIV reservoir landscape. Overall, these results underscore the therapeutic potential of enhancing A3G-mediated hypermutation to disrupt HIV reservoirs. Future strategies should focus on transcriptional profiling to understand cell-specific A3 regulation and develop methods to enhance A3 activity.

5.2 Introduction

Efforts to eliminate HIV-1 have been ongoing and have been mainly focused on the size and activity of latent viral reservoirs within the body (Lambrechts et al., 2020). Studies have shown that the majority of proviral DNA present in these reservoirs are replication-defective and cannot cause viral rebound once cART is discontinued (Ndung'u et al., 2019, Dybul et al., 2021). This is a promising insight for the development of an HIV-1 cure (Ndung'u et al., 2019, Dybul et al., 2021, Pace and Frater, 2014).

Ideally, the ultimate goal would be to eradicate the virus from the body completely (Dybul et al., 2021, Ndung'u et al., 2019, Matsuda and Maeda, 2024). However, since over 90% of the latent reservoirs are made up of defective viruses, a more realistic initial goal would be a functional cure (Ikeda et al., 2021, Xu et al., 2017). This would allow people living with HIV to live without combination antiretroviral therapy (cART) while maintaining detectable levels of proviral DNA and undetectable or very low levels of the virus in their blood, controlled by innate and adaptive immune mechanisms (Davenport et al., 2019, Ikeda et al., 2021).

Elite controllers and long-term non-progressors, who make up less than 1% of the global population of people living with HIV (Gonzalo-Gil et al., 2017, Promer and Karris, 2018, Woldemeskel et al., 2020) are natural models for a functional HIV-1 cure because their immune systems can control the virus without medication (Gonzalo-Gil et al., 2017, Promer and Karris, 2018, Woldemeskel et al., 2020, Cuevas et al., 2015). However, the mechanisms behind this natural viral control remain largely unknown, and further research into these patients could unlock crucial knowledge about post-treatment control.

One intriguing component of the human immune response to HIV-1 is the anti-viral mechanism of the cytidine deaminase APOBEC3 (A3) family of proteins (Ikeda et al., 2021). These proteins, encoded by seven genes on chromosome 22, play a key role in the body's innate immune defence against viruses (Koito and Ikeda, 2012). In particular, five A3 proteins (A3C-Ile188, A3D, A3F, A3G, and A3H) are expressed in and can restrict HIV-1 replication in CD4+ T cells (Desimmie et al., 2014, Ooms et al., 2013, Hultquist et al., 2011, Refsland et al., 2014, Anderson et al., 2018, Refsland et al., 2010). However, the effect of APOBEC expression within diverse immune cells on HIV infection clinical outcomes and persistence following ART initiation is largely unknown particularly in African settings as most studies have been conducted in the global north (Stopak et al., 2003). Genetic and environmental factors such as coinfections could have an impact on their expression and activity. A3 proteins are incorporated into newly formed viral particles, where they induce the deamination of cytosine to uracil in viral DNA (Sheehy et al., 2003, Harris and Dudley, 2015). This process leads to the accumulation of G-to-A mutations, that inactivate viral replication by introducing stop codons in viral proteins (Sheehy et al., 2003, Takaori-Kondo, 2006).

HIV-1 has evolved a defence mechanism to counteract A3 proteins (Harris and Dudley, 2015, Binka et al., 2012). The viral infectivity factor (Vif) hijacks a cellular protein complex to degrade the A3 proteins through a proteasome-mediated pathway, neutralizing their antiviral effects (Binka et al., 2012, Harris and Dudley, 2015, Salamango and Harris, 2020). Despite this, proviral DNA and viral reservoirs still show high levels of G-to-A mutations caused by A3 activity, indicating the potency and ongoing activity of these proteins (Takaori-Kondo, 2006, Malim and Bieniasz, 2012, Harris and Dudley, 2015, Cuevas et al., 2015). Interestingly, these mutations are

reportedly linked to slower disease progression in HIV-1-infected individuals, including elite controllers and long-term non-progressors (Biasin et al., 2007). For example, studies have shown that CD4+ T cells from individuals with higher levels of A3G expression are less susceptible to HIV-1 infection compared to cells from those with lower levels of A3G (Biasin et al., 2007, Refsland et al., 2010, De Pasquale et al., 2013). Furthermore, a study by De Pasquale et al., 2013 showed that in viraemic controllers with lower proviral DNA levels in resting memory CD4+ T cells, there was an association with higher expression of A3G (De Pasquale et al., 2013). Thus, the antiviral activity of A3 proteins may be an attractive target to induce a functional cure (De Pasquale et al., 2013, Ikeda et al., 2021, Ikeda et al., 2023).

However, what remains unknown is the ability of a single A3 protein to have a greater mutagenic inhibitory effect on the proviral reservoir landscape. Data on hypermutation profiling in non-subtype B viruses in Africa are limited and require further investigation. Here, we aimed to assess A3G and A3F expression levels in CD4+ T and myeloid cells. Additionally, we correlated A3G and A3F expression levels with the average defective reservoir levels measured by IPDA. Furthermore, we determined hypermutation profiles in late-treated individuals using sequences generated from peripheral blood mononuclear cells (PBMCs).

5.3 Methods

5.3.1 Study participants and cell sorting

We isolated cell subsets from 5 pre-infection (uninfected), 5 untreated, 5 late treated, and 5 early treated individuals (Figure 5.1). We measured A3G and A3F expression in central memory (CM), effector memory (EM), transitional memory (TM), naïve CD4+ T cells (N), and myeloid cells (M) isolated by cell sorting using the following panel:- Cells were sorted on a FACS ARIA II flow cytometer (BD Biosciences) with purity ranging from 90-100%, as follows: from singlets PBMC, live (Aqua-) (Invitrogen, Massachusetts, USA) CD3+CD4+ lymphocytes were selected based on size and granularity criteria.

We then sorted the following subpopulations from the CD4+ population according to their expression of phenotypic markers CD4+ naïve cells (N, CD45RO-CCR7+CD27+), CM (CD45RO+CCR7+CD27+), TM (CD45RO+CD27+CCR7-) and EM (CD45RO+CD27-CCR7-). Furthermore, from the CD3- population, myeloid cells were defined and sorted as (CD3-CD14+) (Kwon et al., 2020) (BD Biosciences).

5.3.2 Measurement of A3G and A3F expression in vitro

To test A3G and A3F expression levels *in vitro* using ddPCR we transfected HEK 293 T cells with A3G and A3F expression cloned into expression plasmid. Additionally, we included a negative control of untransfected cells Supplementary Figure 4 shows the expression of A3G (Supplementary Figure 4A) and A3F (Supplementary Figure 4B) using ddPCR. This was subsequently used as a positive control in each experiment when assessing A3G and A3F expression levels in cell subsets.

5.3.3 cDNA synthesis

RNA from the sorted cells was converted into cDNA using the iScriptTM cDNA synthesis kit according to manufacturer instructions (Bio-Rad, California, USA). Cycling conditions were as follows: priming for 5 minutes at 25˚C, reverse transcription at 20 minutes at 46˚C, and RT inactivation for 1 minute at 95˚C.

5.3.4 APOBEC3G/-F mRNA expression using ddPCR

A3G/F gene expression patterns in these cell subsets were determined by digital droplet PCR (ddPCR) (Bio-Rad, California, USA) using predesigned TaqMan gene expression assays containing specific primers and probes labelled with the FAM fluorescent dye (ThermoFisher Scientific, Waltham, USA). The following kits were purchased: Predesigned TaqMan assay was used to measure GAPDH mRNA expression (Hs02786624_g1) (ThermoFisher Scientific, Waltham, USA). To measure A3G mRNA expression the following predesigned kit was used Hs00222415_m1 (ThermoFisher Scientific, Waltham, USA). Further, to measure A3F mRNA expression Hs01665324_m1 was used (ThermoFisher, Waltham, USA). The housekeeping gene GAPDH was used as the housekeeping/reference gene (ThermoFisher Scientific, Waltham, USA).

cDNA was diluted and added to the A3G and A3F PCR mix. cDNA was added to the reaction measuring GAPDH expression. ddPCR was performed using the following cycling conditions: 95 °C for 10 min, 45 cycles of 94 °C for 30 s and 60 °C for 1 min, 72 °C for 1 min. A3G and A3F mRNA expression levels were measured in cell subsets at different time points, including pre-infection, post-infection, and post-ART initiation. Samples were run in triplicate and average values were used to compute A3G, A3F,

and GAPDH copy numbers. mRNA expressed by 293T cells transfected with A3G and 3F plasmids was used as the positive control.

Relative expression levels of A3G or A3F to GAPDH in each sample were determined by dividing the concentration of the target gene (A3G or A3F) by the concentration of the housekeeping gene (GAPDH). The resulting target/reference ratio expressed the amount of A3G or A3F normalized to the level of GAPDH.

5.3.5 Full-length individual proviral sequencing (FLIP-seq) assay

Near full-length proviral sequences generated by FLIP-seq were previously described (Reddy et al., 2024, Lee et al., 2019b, Lee et al., 2017). Five late treated participants were longitudinally assessed. Total HIV-DNA copy number was determined by ddPCR and was used to calculate the DNA sample dilution to achieve one PCR-positive reaction in every three reactions.

This method of limiting dilution gives a Poisson probability of 85.7% that each PCR amplicon originated from a single HIV-DNA template (Lee, 2021). A nested PCR approach was used to amplify the near-full genome using one unit of Platinum™ Taq DNA Polymerase High Fidelity (Invitrogen, Waltham, USA) with the following primers first round PCR: forward primer 5′- AAATCTCTAGCAGTGGCGCCCGAACAG-3′, reverse primer 5′- TGAGGGATCTCTAGTTACCAGAGTC-3′; second round PCR: forward primer 5′- GCGCCCGAACAGGGACYTGAAARCGAAAG-3′, reverse primer 5′-GCACTCAAGGCAAGCTTTATTGAGGCTTA-3′ (HXB2 coordinates 638-9632, 8994 bp). Each 20 µL reaction mix contained 1× reaction buffer, 2 mM $MgSO_4$, 0.2 mM dNTP, 0.4 µM each of forward and reverse primers (Lee et al., 2019b, Reddy et al., 2024). The thermal cycling conditions were 2 min at 92 °C, 10 cycles 10 s at 92

°C, 30 s at 60 °C, 10 min at 68°C, 20 cycles 10 s at 92 °C, 30 s at 55 °C, 10 min at 68 °C, 10 min at 68 °C, 4 °C infinite hold.

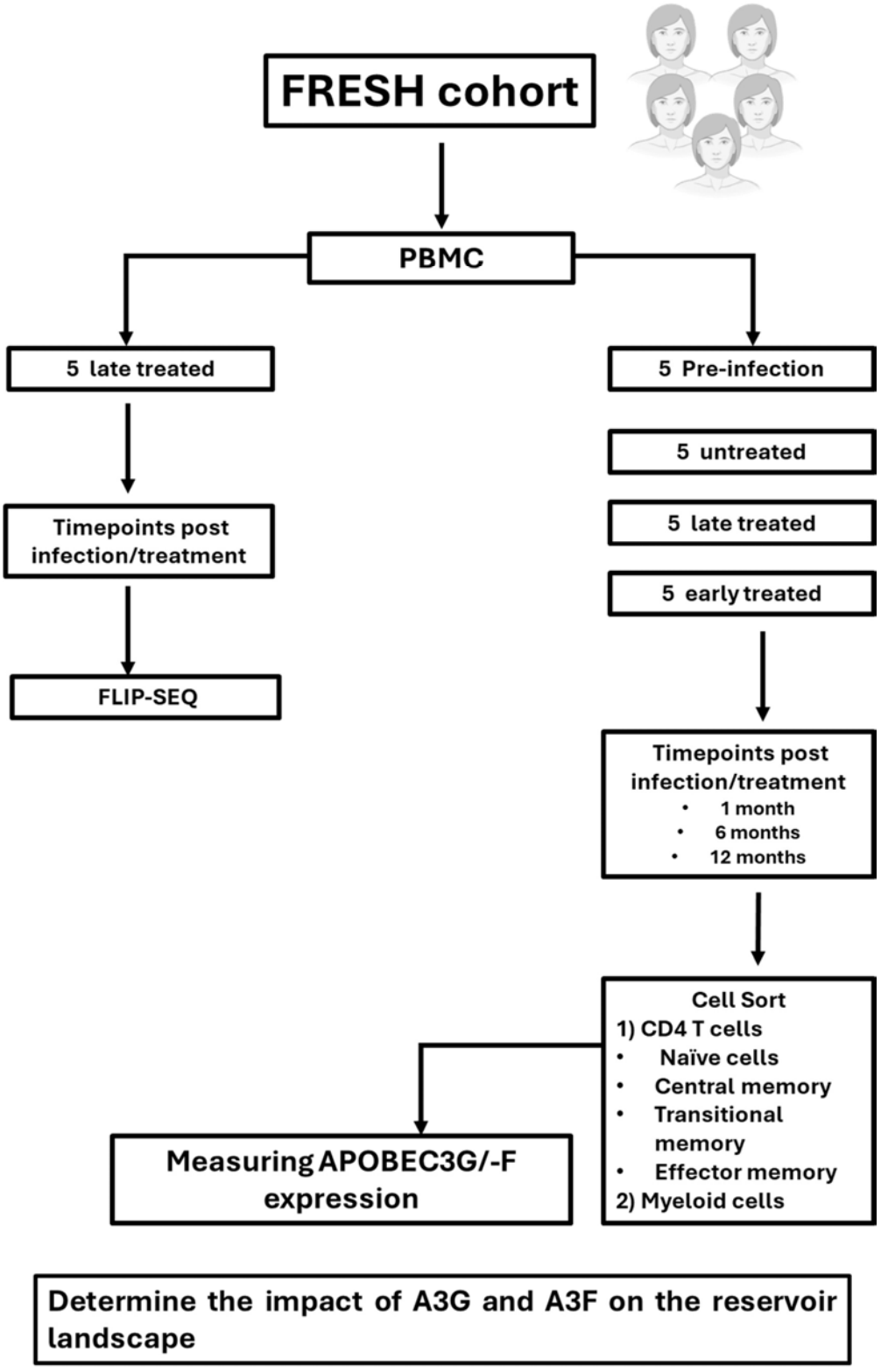

Figure 5.1 Schematic diagram of the pipeline of Chapter 5.

5.4 Results

5.4.1 Longitudinal measurement of A3G and A3F mRNA expression in cell subsets.

We observed that before infection there are high levels of A3G and A3F relative to GAPDH. The average A3G mRNA expression levels in cellular subsets were in CM = 0.50 RNA copies, EM = 0.65 RNA copies, TM = 0.85 RNA copies, N = 0.78 RNA copies, and M = 0.73 RNA copies (Figure 5.2A). The average A3F mRNA expression levels in cellular subsets were in CM = 0.47 RNA copies, EM = 0.37 RNA copies, TM = 0.45 RNA copies, N = 0.57 RNA copies, and M = 0.63 RNA copies (Figure 5.2B). A3G was expressed at approximately 1.5 fold higher than A3F in all subsets (Figure 5.2).

Next, we measured A3G and A3F mRNA during untreated HIV infection. Figure 5.3 highlights all immune cell subsets from a single representative study participant (PID 102). This participant initiated ART treatment during chronic infection at 808 DPOPV (Supplementary Figure 1). Before infection, there were high levels of A3G (CM = 0.88 RNA copies, EM = 0.56 RNA copies, TM = 0.36 RNA copies, N = 0.64 RNA copies, M = 0.45 RNA copies) and A3F (CM = 0.56 RNA copies, EM = 0.35 RNA copies, TM = 0.56 RNA copies, N = 0.47 RNA copies, M = 0.32 RNA copies) relative to GAPDH (Figure 5.3).

Following HIV infection, we observed a decline in A3G and A3F mRNA expression. At one month post-infection A3G expression levels decreased to CM = 0.027 RNA copies, EM = 0.28 RNA copies, TM = 0.11 RNA copies, N = 0.22 RNA copies, and M = 0.30 RNA copies. On the other hand, A3F mRNA decreased to 0.46 RNA copies in CM, EM = 0.11 RNA copies, TM = 0.44 RNA copies, N = 0.34 RNA copies, and M =

0.27 RNA copies. There was a steady decrease in A3G and A3F mRNA expression over time in cell subsets during untreated infection (Figure 5.3).

At 12 months post-treatment there was a steady recovery of A3G (CM = 0.12 RNA copies, EM = 0.12 RNA copies, TM = 0.13 RNA copies, N = 0.11 RNA copies, M = 0.11 RNA copies) and A3F (0.37 RNA copies in CM, EM = 0.38, TM = 0.39 RNA copies, N = 0.28 RNA copies M = 0.34 RNA copies) expression relative to GAPDH (Figure 5.3). Similar patterns of A3 expression were seen in all immune cell subsets analysed in all participants.

From pre-infection to 12 months post-infection the fold reduction in A3G mRNA expression in CM = 85-fold, EM = 61-fold, TM = 85-fold, N = 73-fold, and M = 52-fold for PID 102 (Figure 5.3). Although A3F mRNA expression decreased from pre-infection to 12 months post-infection (fold reduction in CM = 1-fold, EM = 3-fold, TM = 3-fold, N = 2-fold, and M = 1-fold), there was a greater decrease in A3G mRNA expression in PID 102 (Figure 5.3).

Upon initiation of ART, there was an increase in A3G and A3F mRNA expression (Figure 5.3) in all cellular subsets (A3G fold increase in CM = 0.23-fold, EM = 0.25-fold, TM = 2.3-fold, N = 1.6-fold, and M = 0.13-fold) (A3F fold increase in CM = 0.79-fold, EM = 0.26-fold, TM = 0.70-fold, N = 0.4-fold, and M = 0.37-fold (Figure 5.3).

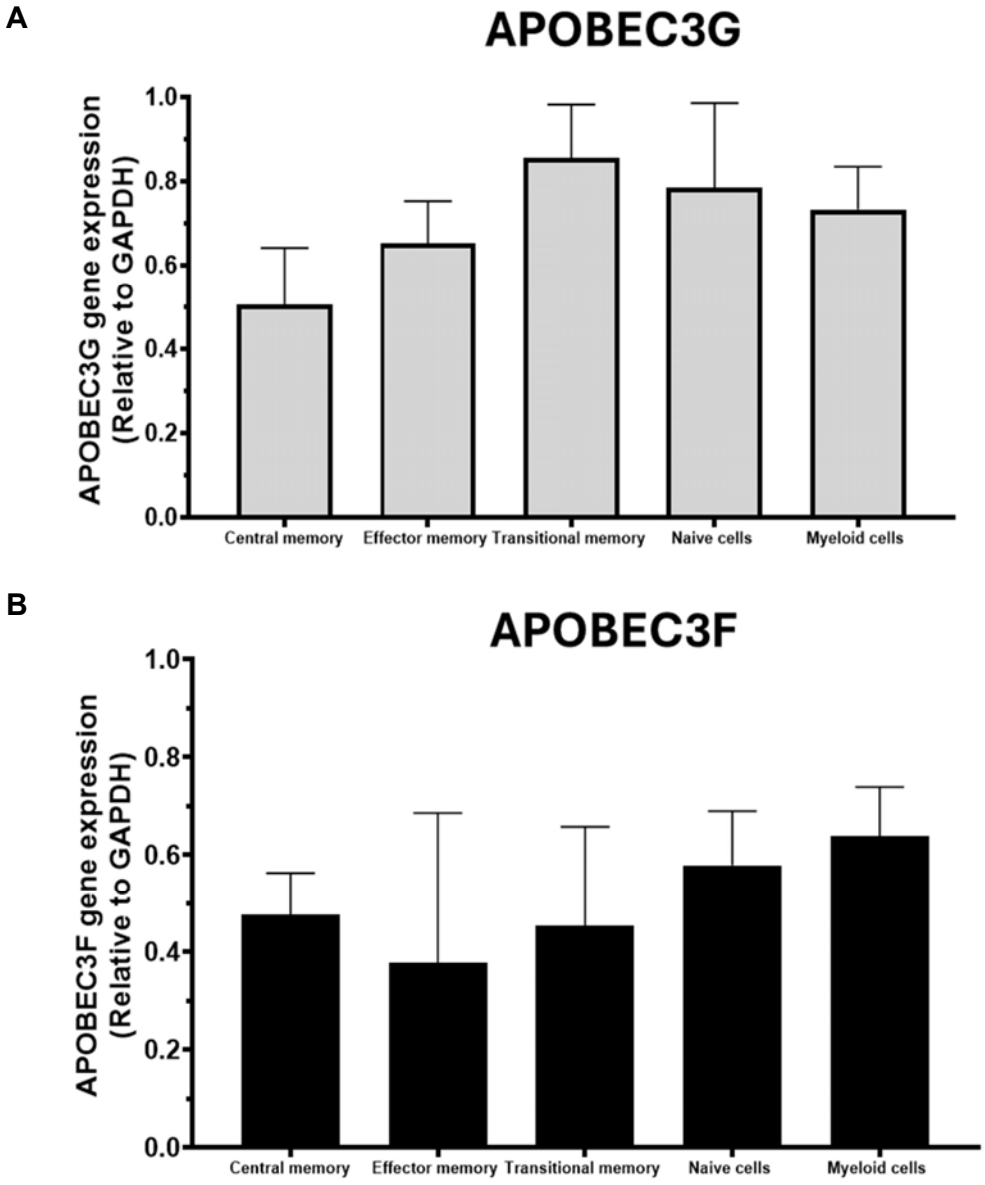

Figure 5.2 Expression of A3G (A) and A3F (B) in memory CD4+ T cells and myeloid cells during pre-infection. A3F is expressed approximately 1.5-fold lower than A3G.

Additionally, we assessed A3G and A3F mRNA expression in five participants who initiated treatment during acute HIV infection. Figure 5.4 shows a representative participant (PID 879) who initiated treatment in acute infection at 1 DPOPV.

A3G expression levels before infection, after 1 month of infection, and after 1 year of treatment were CM = 0.94, 0.78, and 0.76 RNA copies, EM = 0.95, 0.79, and 0.72 RNA copies, TM = 0.87, 0.63, and 0.72 RNA copies, N = 0.99, 0.72, and 0.83 RNA copies, M = 0.98, 0.76, and 0.73 RNA copies respectively. A3F expression levels before infection, after 1 month of infection, and after 1 year of treatment were as follows:- CM = 0.78, 0.76, and 0.68 RNA copies, EM = 0.83, 0.82, and 0.56 RNA copies, TM = 0.75, 0.52, and 0.62 RNA copies, N = 0.76, 0.56, and 0.67 RNA copies, M = 0.73, 0.73, and 0.85 RNA copies respectively.

From pre-infection to 12 months post-treatment the fold reduction in A3G expression was in CM = 1.2-fold, EM = 1.2-fold, TM = 1.3-fold, naïve cells = 1.3-fold, and myeloid cells = 1.2-fold in PID 879. Additionally, the fold reduction in A3F mRNA expression in CM = 1.0-fold, EM = 1.0-fold, TM = 1.4-fold, N = 1.3-fold, and M = 1.1-fold respectively in PID 879 (Figure 5.4).

Before infection, 12 months post-infection and 12 months post-treatment average A3G mRNA expression levels were as follows for those who were untreated and late treated participants:- CM = 0.79, 0.012, and 0.11 RNA copies, EM = 0.67, 0.021, and 0.27 RNA copies, TM = 0.65, 0.17 and 0.21 RNA copies, N = 0.82, 0.1, and 0.25 RNA copies, M = 0.64, 0.05, and 0.30 RNA copies respectively (Figure 5.5A).

Furthermore, the average A3F mRNA expression in each of the cell subsets before infection, at 12 months post-infection, and 12 months post-treatment were as follows:- CM = 0.56, 0.15, and 0.38 RNA copies, EM = 0.51, 0.13 and RNA copies, TM = 0.54,

0.13, and 0.35 RNA copies, N = 0.52, 0.15 and 0.35 RNA copies, and M = 0.48, 0.25, 0.30 RNA copies respectively (Figure 5.5A).

Before infection in those who were early treated, average A3G mRNA expression was as follows:- CM = 0.95 RNA copies, EM = 0.95 RNA copies, TM = 0.86 RNA copies, N = 0.93 RNA copies, and M = 0.94 RNA copies. Average A3F mRNA expression was as follows:- CM = 0.77 RNA copies, EM = 0.82 RNA copies, TM = 0.77 RNA copies, N = 0.74 RNA copies, and M = 0.82 RNA copies (Figure 5.5B).

At 1 month post-treatment there was a transient decrease in A3G and A3F mRNA expression. Average A3G mRNA expression in each cell subsets was as follows:- CM = 0.71 RNA copies, EM = 0.76 RNA copies, TM = 0.63 RNA copies, N = 0.73 RNA copies, and M = 0.75 RNA copies. Average A3F mRNA expression in each of the cell subsets was as follows:- CM = 0.76 RNA copies, EM = 0.84 RNA copies, TM = 0.63 RNA copies, N = 0.61 RNA copies, and M = 0.72 RNA copies (Figure 5.5B).

At 12 months post-treatment in early treated participants, average A3G mRNA expression was as follows: CM = 0.77 RNA copies, EM = 0.92 RNA copies, TM = 0.77 RNA copies, N = 0.83 RNA copies, and M = 0.77 RNA copies. Average A3F mRNA expression in each cell subset was as follows: CM = 0.67, EM = 0.81 RNA copies, TM = 0.68 RNA copies, N = 0.7 RNA copies, and M = 0.84 RNA copies (Figure 5.5B).

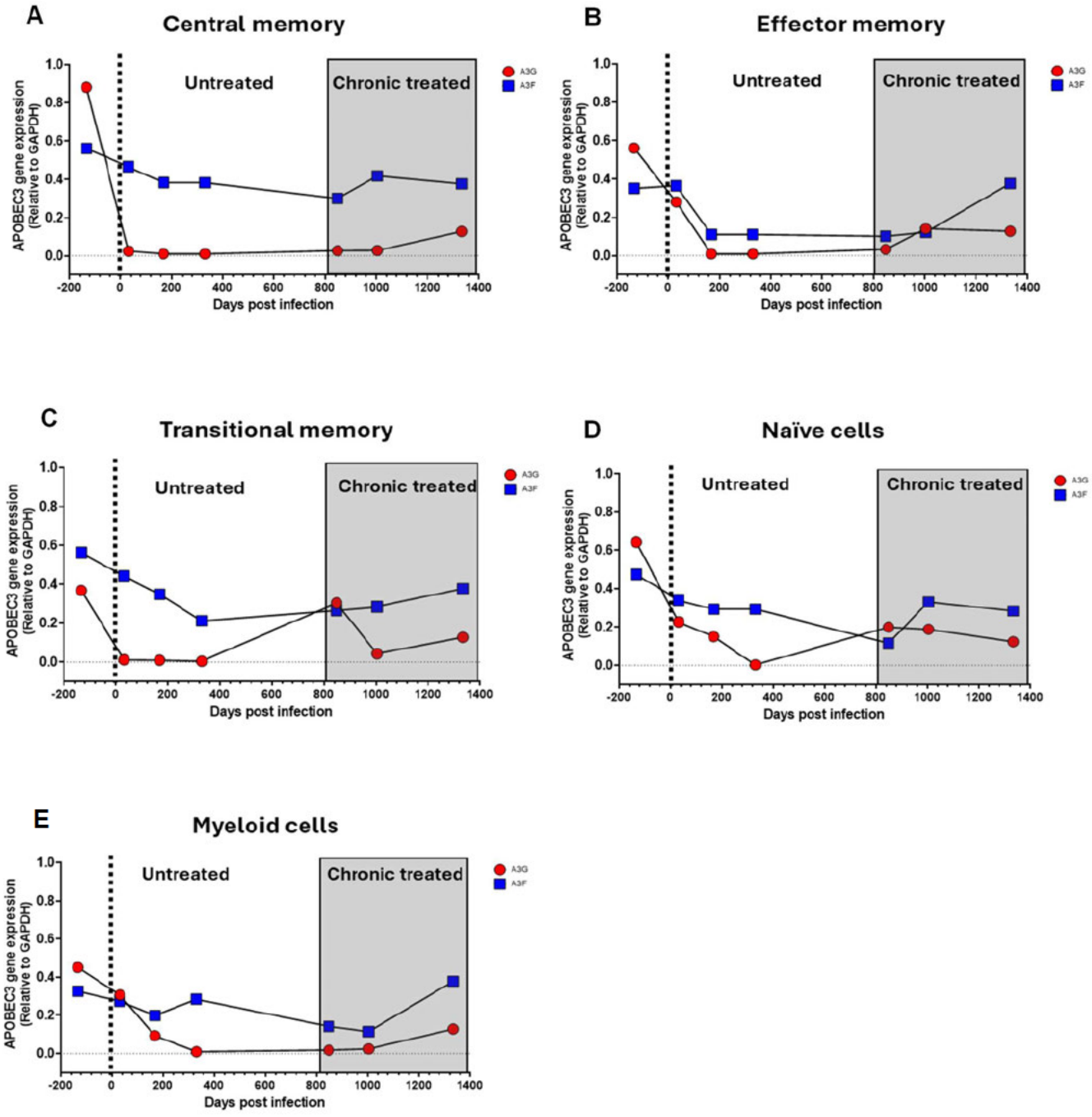

Figure 5.3 A3 mRNA cellular expression profile of PID 102. This participant initiated ART treatment during chronic infection (808 DPOPV). The red squares show the A3G expression, and the blue squares show the A3F expression. Panels A-E show changes in expression levels in the different cell subsets. (A) central memory, (B)

effector memory, (C) transitional memory, (D) naïve cells, (E) myeloid cells. The dotted black indicates the time of first detection of plasma viremia. The white area shows untreated infection, and the grey shaded area shows when the participant was under ART treatment.

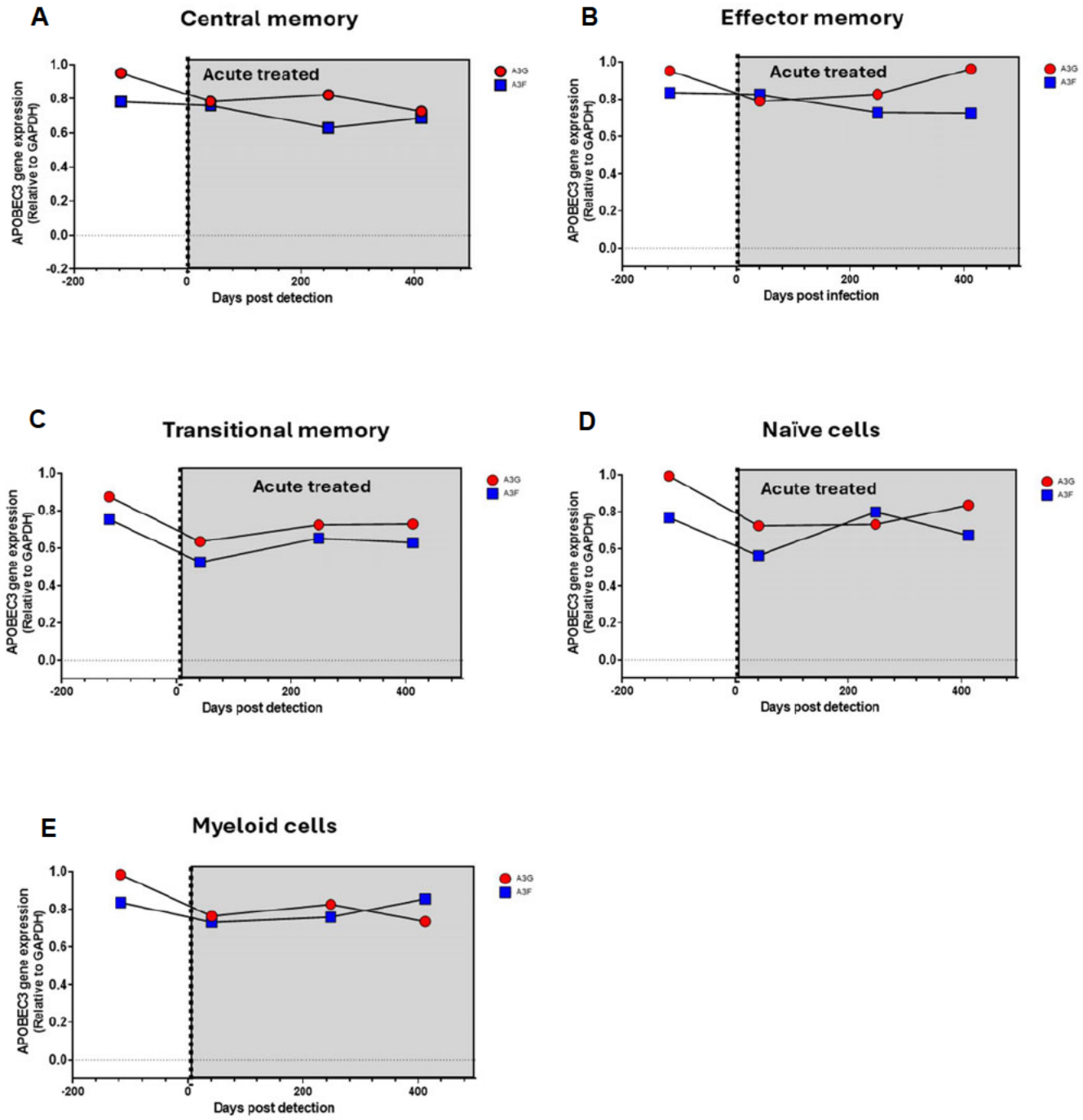

Figure 5.4 A3 mRNA cellular expression profile of PID 879. This participant initiated ART treatment during acute HIV infection (1 DPOPV). The red squares show the A3G expression, and the blue squares show the A3F expression. The dotted line indicates the time of first detection of plasma viremia. The grey area represents treated infection.

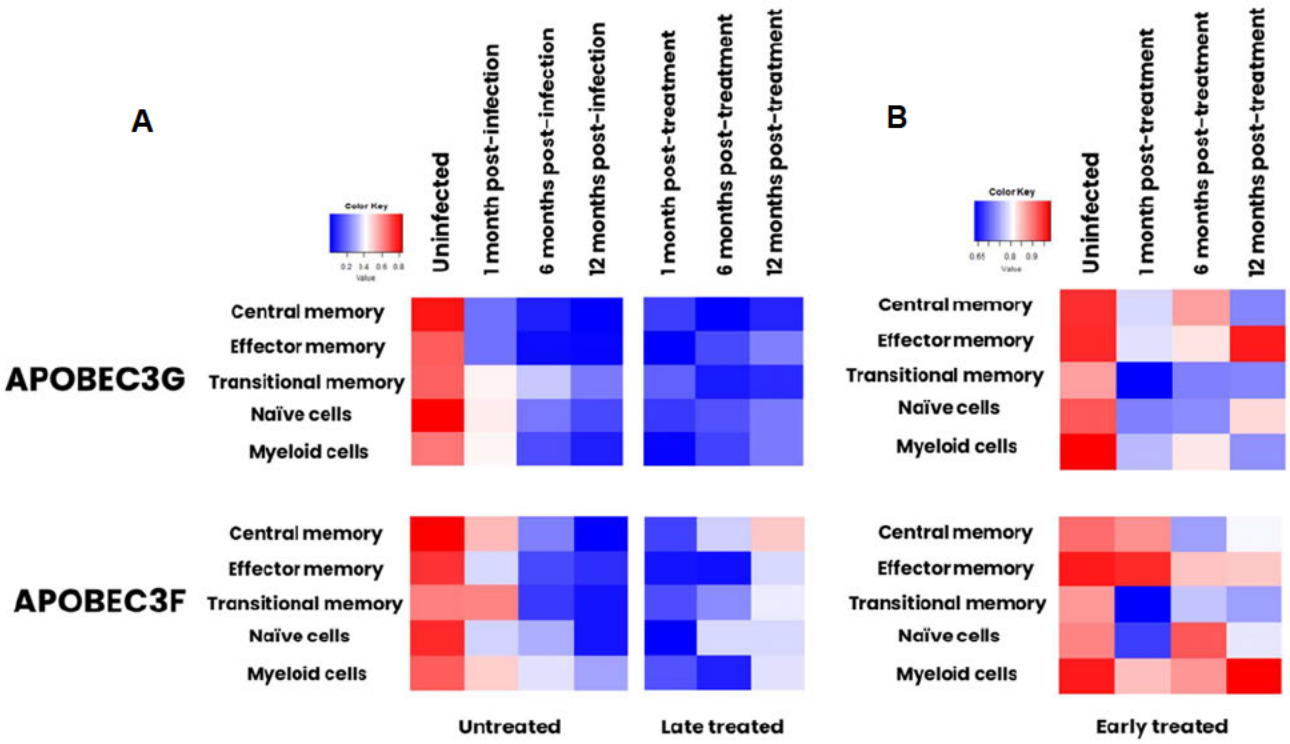

Figure 5.5 APOBEC3G and APOBEC3F expression. A) 5 untreated and late treated participants and B) 5 early treated study participants.

5.4.2 Correlation of A3G and A3F mRNA expression levels with the defective reservoir measured by IPDA from immune cells.

Here, we wanted to determine the impact of A3G and A3F mRNA expression on the levels of 3´ deleted/hypermutated and 5´ deleted proviral DNA measured by IPDA within each cell subset. First, we determined the levels of average defective HIV DNA within each of the cell subsets at 12 months post-treatment in participants who were late treated (green) and early treated (blue) (Figure 5.6). We chose this time point because it is the best representation of the stable reservoir since participants had been on treatment for 12 months.

Participants who were late treated had significantly higher levels of average defective proviral DNA detected within each cellular compartment compared to early treated participants except for naïve CD4+ T cells (CM p = 0.0001, EM p = 0.0001, TM p = 0.0032, N p = 0.104, M p = 0.025) (Figure 5.6).

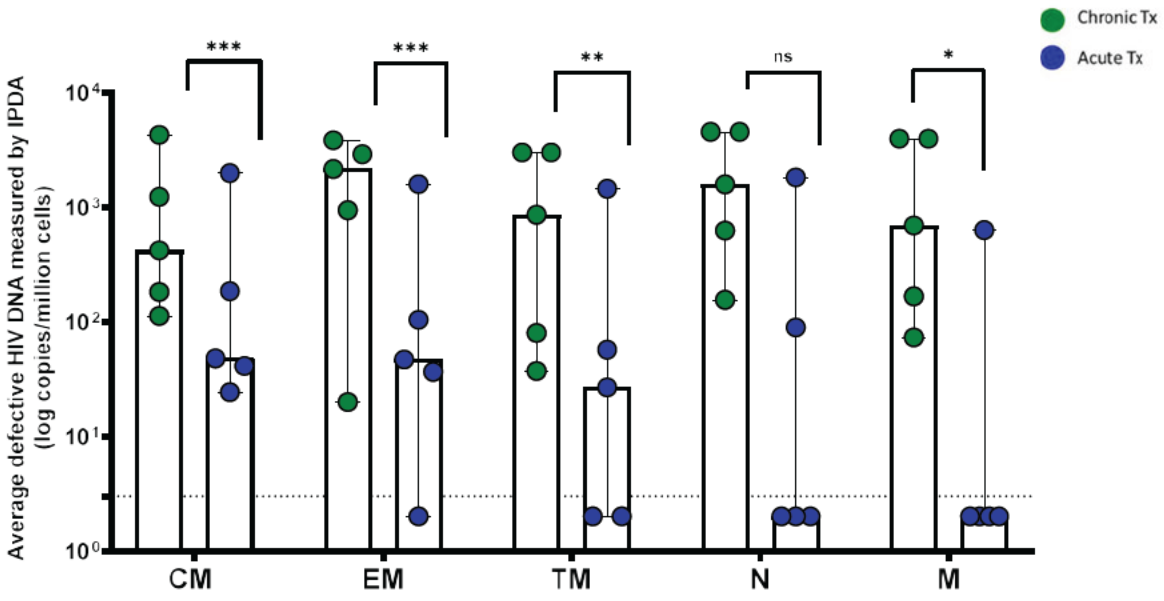

Figure 5.6 Measurement of average defective HIV DNA at 12 months post-treatment by IPDA. Green shows late treatment and blue shows early treatment.

Average defective proviral DNA in late vs early treated participants in each cell subset was (CM = 421.0, 47,97; EM = 2160.4, 47.05; TM = 862.4, 26.79, N = 1588.5, 2, M = 695.5, 2 copies/million cells) respectively (Figure 5.6).

Next, we correlated the average defective proviral DNA levels at 12 months post-treatment within each cell subset with the levels of A3G and A3F mRNA expression from each subset measured during pre-infection, 1 month post-infection, and 12 months post-treatment.

Before infection and 1 month of infection, there was no correlation between A3G or A3F mRNA expression levels and average defective proviral DNA (Supplementary Figures 7 and 8). However, when we compared A3G and A3F expression at 12 months post-treatment and average defective HIV DNA, we observed that there was a strong significant positive correlation in transition memory CD4+ T cells ($r = 0.97$, $p = 0.003$) when comparing A3G mRNA expression and average defective HIV DNA levels (Figure 5.7C). No other cell subset showed any association with A3G or A3F and average defective HIV DNA levels (Supplementary Figure 9).

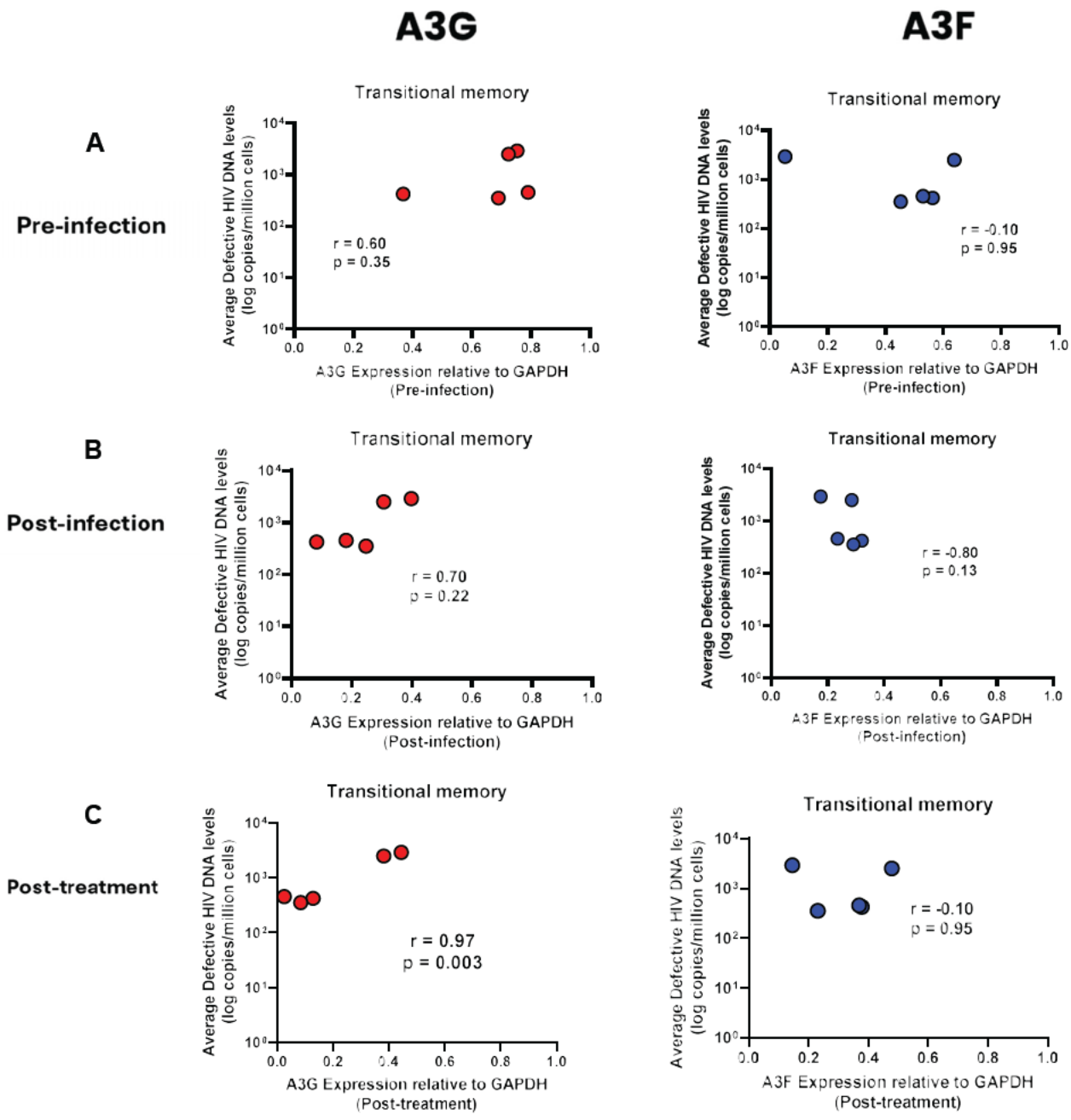

Figure 5.7 Correlation of A3G and A3F versus average defective HIV DNA. Correlation analysis showing average defective HIV DNA at 12 months post-treatment in transitional memory CD4+ T cells versus A) A3G (left) and A3F (right) expression levels during pre-infection. B) A3G (left) and A3F (right) expression at 1 month post-infection. C) A3G (left) and A3F (right) expression levels at 12 months post-treatment.

5.4.3 Patterns of A3G and A3F hypermutation on the HIV proviral genome

Sequences were generated from total PBMCs using the FLIPS assay from 5 late treated individuals, and the frequency and distribution of A3G and A3F induced hypermutation on the HIV proviral genome was determined. First, we quantified each participant's total A3G and A3F mRNA expression (Figure 5.8). Before infection, average A3G mRNA expression ranged between 0.58 to 0.81 RNA copies (Figure 5.8A). Average A3F mRNA expression ranged between 0.43 to 0.66 RNA copies (Figure 5.8A).

At 12 months post-infection, levels of A3G (range = 0.05 - 0.4 RNA copies) and A3F (range = 0.05 - 0.4 RNA copies) mRNA decreased (Figure 5.8B). At 12 months post-treatment there was an increase in A3G (range = 0.01 - 0.26 RNA copies) and A3F (range = 0.25 - 0.34 RNA copies) mRNA expression (Figure 5.8C). Next, we quantified the frequency of A3G and A3F induced hypermutation across each proviral sequence from different participants (Figure 5.9). The frequency of A3G-induced hypermutation (57.9 - 69.2%) was higher than the frequency of A3F induced hypermutation (21.2 - 30.7%) ($p=0.0006$) (Figure 5.9A).

Additionally, we determined the distribution of A3G and A3F hypermutation across the HIV genome. A3 induced hypermutation was quantified for each participant and Figure 5.10A shows a highlighter plot displaying the hypermutation profile for PID 198. Approximately 70% of the hypermutation in this participant (PID 198) was driven by A3G and ~20% of the hypermutation was induced by A3F (Figure 5.10B). The distribution of hypermutation across the HIV genome from this participant, was bimodal (Figure 5.10C), with a higher frequency of hypermutation present at the 5´end and the 3´ end of the HIV genome (Figure 5.10C). All 5 participants had the same

distribution of A3G and A3F induced hypermutation across the HIV genome (Supplementary Figure 10).

Furthermore, we correlated total A3G and A3F mRNA expression levels during pre-infection, 12 months post-infection, and 12 months post-treatment with the frequency of hypermutation (Figure 5.11). Before infection, we observed that A3G mRNA expression levels correlated positively with the frequency of A3G induced hypermutation ($p = 0.027$, $r = 0.91$) (Figure 5.11Ai). There was no correlation between pre-infection A3F mRNA expression and frequency hypermutation induced by A3F ($p = 0.30$, $r = -0.58$) (Figure 5.11Aii).

At 1 month post-infection there was no correlation between A3G mRNA expression and frequency of A3G hypermutation ($p = 0.87$, $r = 0.098$) (Figure 5.11Bi). Additionally, there was no correlation between A3F mRNA expression and frequency of A3F hypermutation at 12 months post-infection ($p = 0.48$, $r = 0.41$) (Figure 5.11Bii).

Interestingly, at 12 months post-treatment, a positive correlation was observed between A3G mRNA expression and the percentage of A3G driven hypermutation ($p = 0.032$, $r = 0.90$) (Figure 5.12Ci). Additionally, it was observed that there was no correlation between the percentage of A3F driven hypermutation and A3F mRNA expression ($p = 0.24$, $r = 0.63$) (Figure 5.11Cii).

A

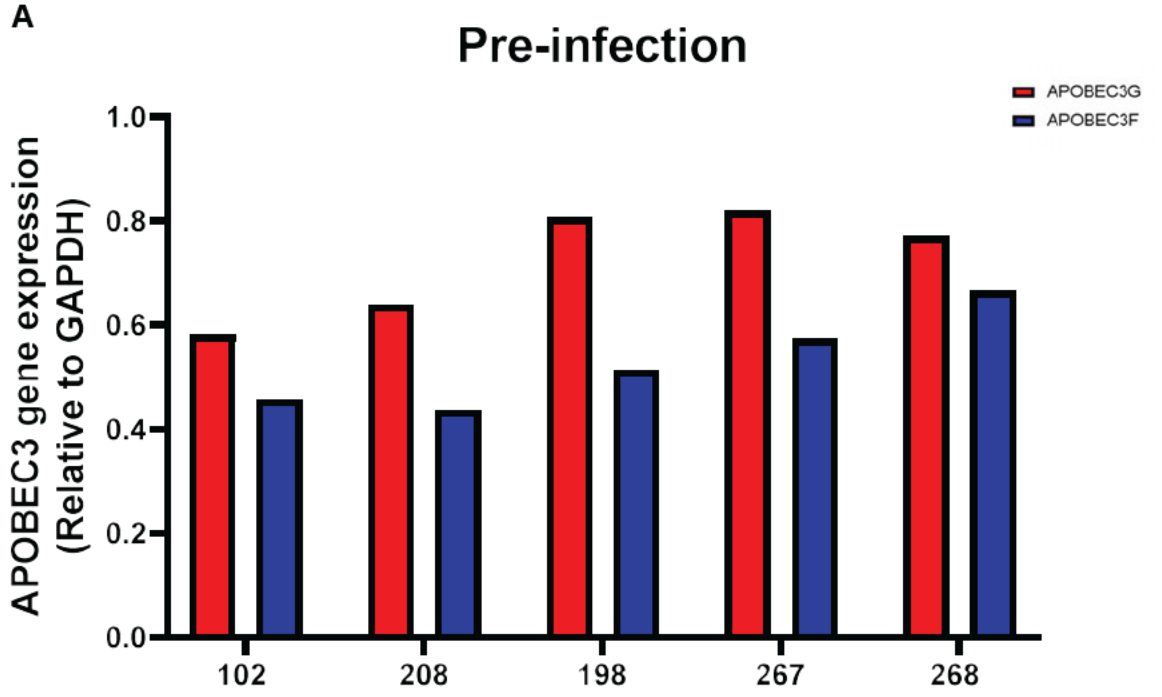
Pre-infection
APOBEC3G
APOBEC3F
APOBEC3 gene expression
(Relative to GAPDH)
1.0
0.8
0.6
0.4
0.2
0.0
102
208
198
267
268

B

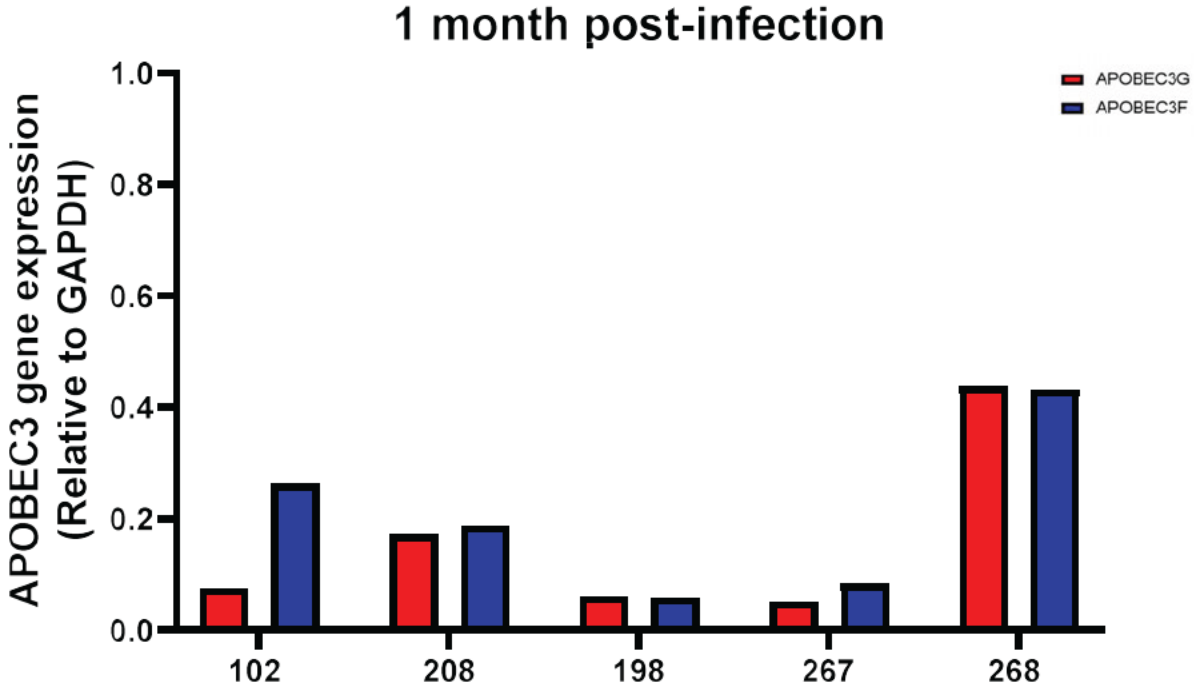
1 month post-infection
APOBEC3G
APOBEC3F
APOBEC3 gene expression
(Relative to GAPDH)
1.0
0.8
0.6
0.4
0.2
0.0
102
208
198
267
268

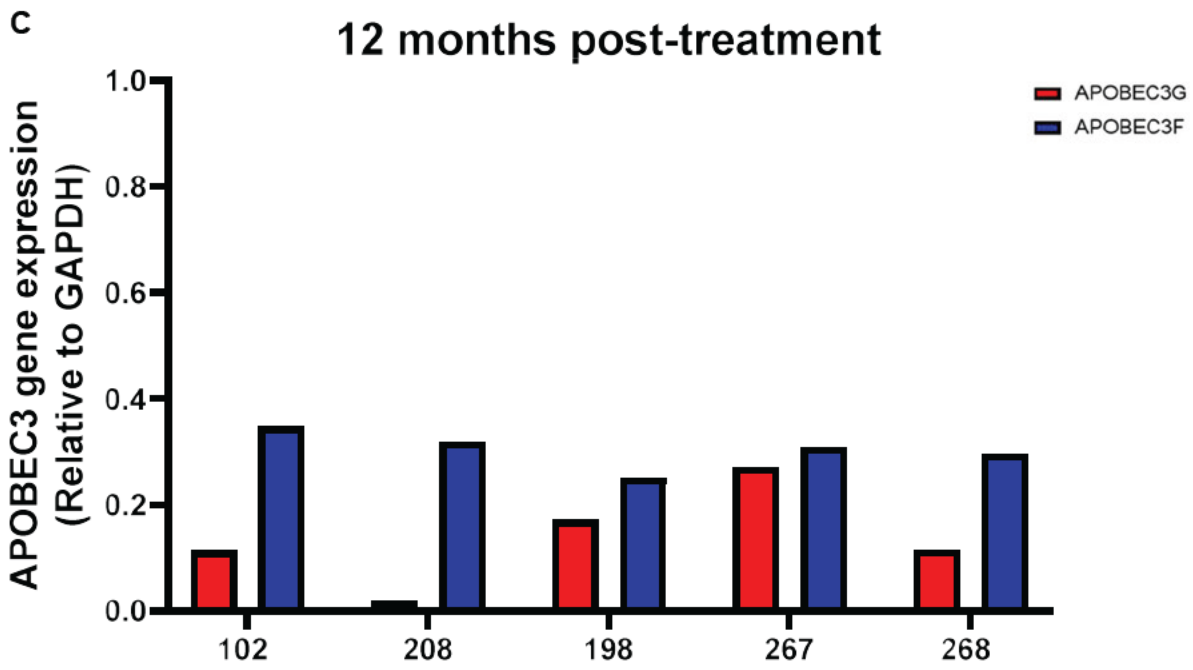

Figure 5.8 APOBEC3G/-F mRNA expression in 5 late treated study participants. A) Pre-infection timepoint B) 12 months post-infection timepoint C) 12 months post-treatment. Red bars show A3G mRNA expression relative to GAPDH. Blue bars show A3F mRNA expression relative to GAPDH.

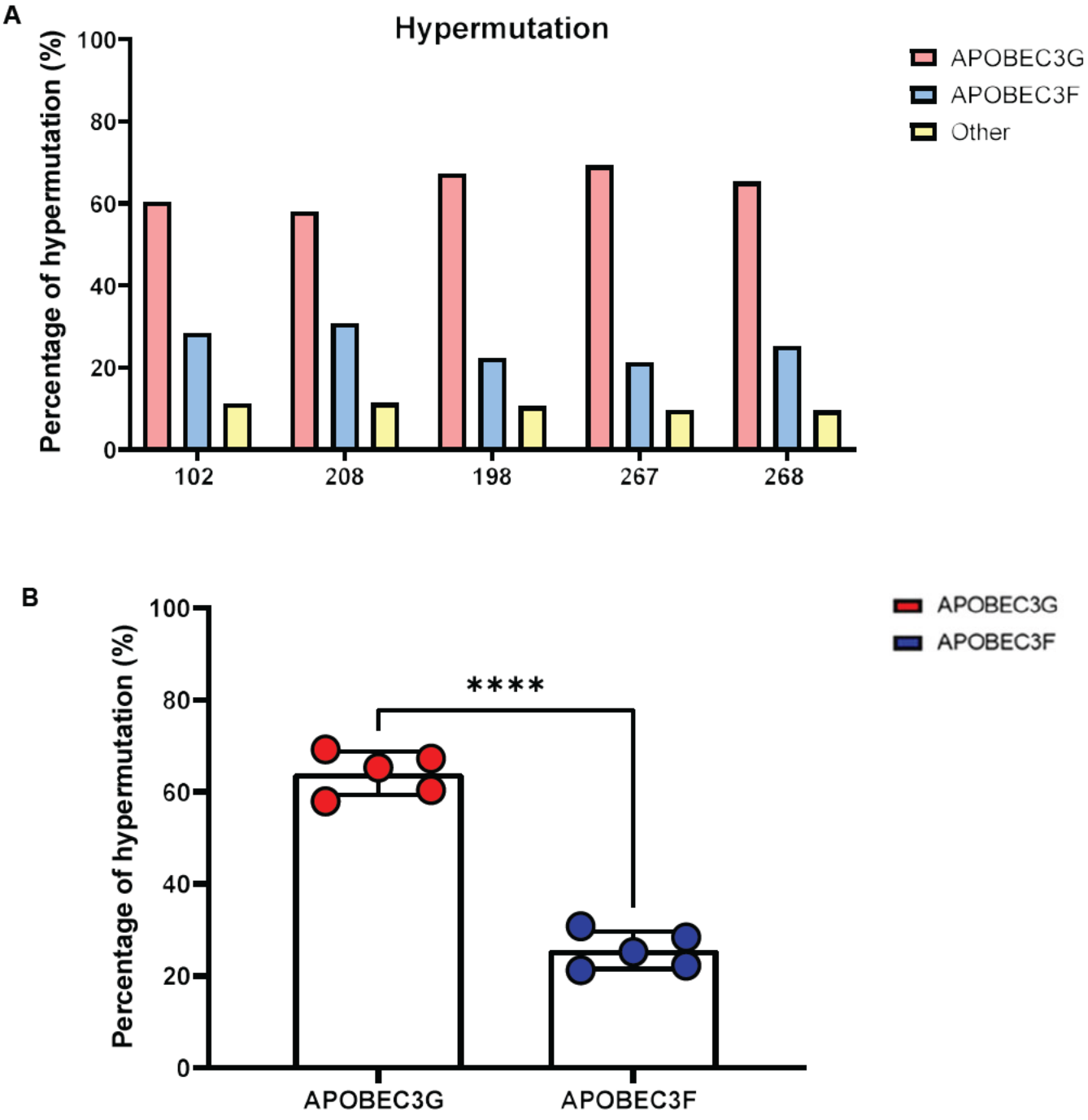

Figure 5.9 Frequency of A3G and A3F hypermutation. A) Percentage of hypermutation for 5 study participants. B) Difference between percentage hypermutation driven by A3G and A3F. Red represents A3G, and blue represents A3F *p=<0.05

A

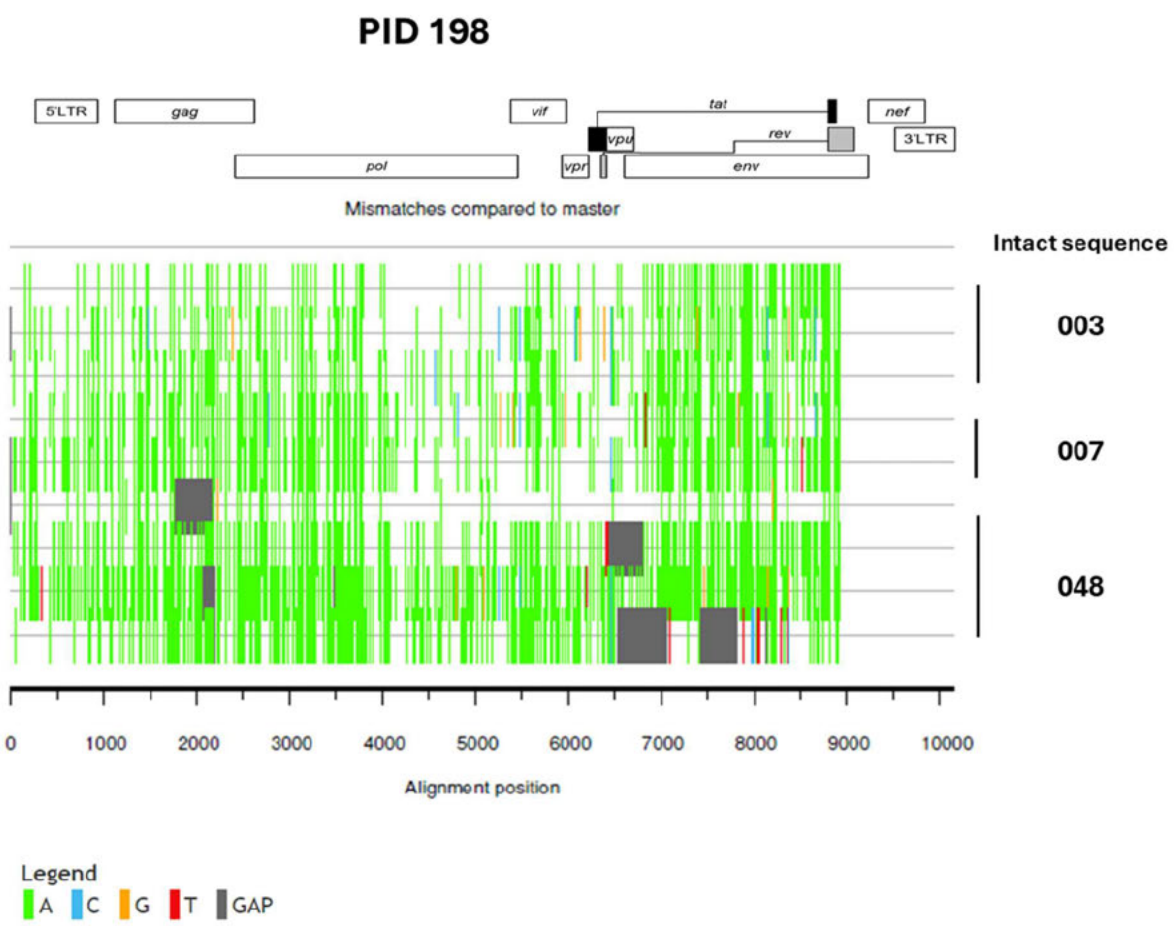
PID 198
5'LTR
gag
pol
vif
vpr
tat
vpu
rev
env
nef
3'LTR
Mismatches compared to master
Intact sequence
003
007
048
0
1000
2000
3000
4000
5000
6000
7000
8000
9000
10000
Alignment position
Legend
A
C
G
T
GAP

B

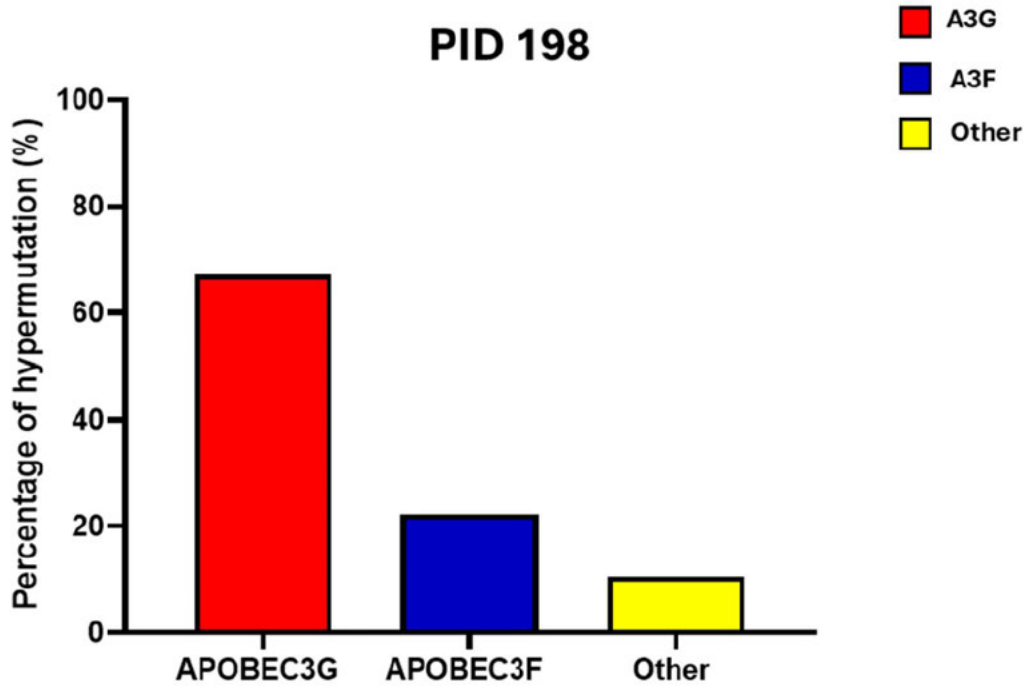
PID 198
A3G
A3F
Other
Percentage of hypermutation (%)
100
80
60
40
20
0
APOBEC3G
APOBEC3F
Other

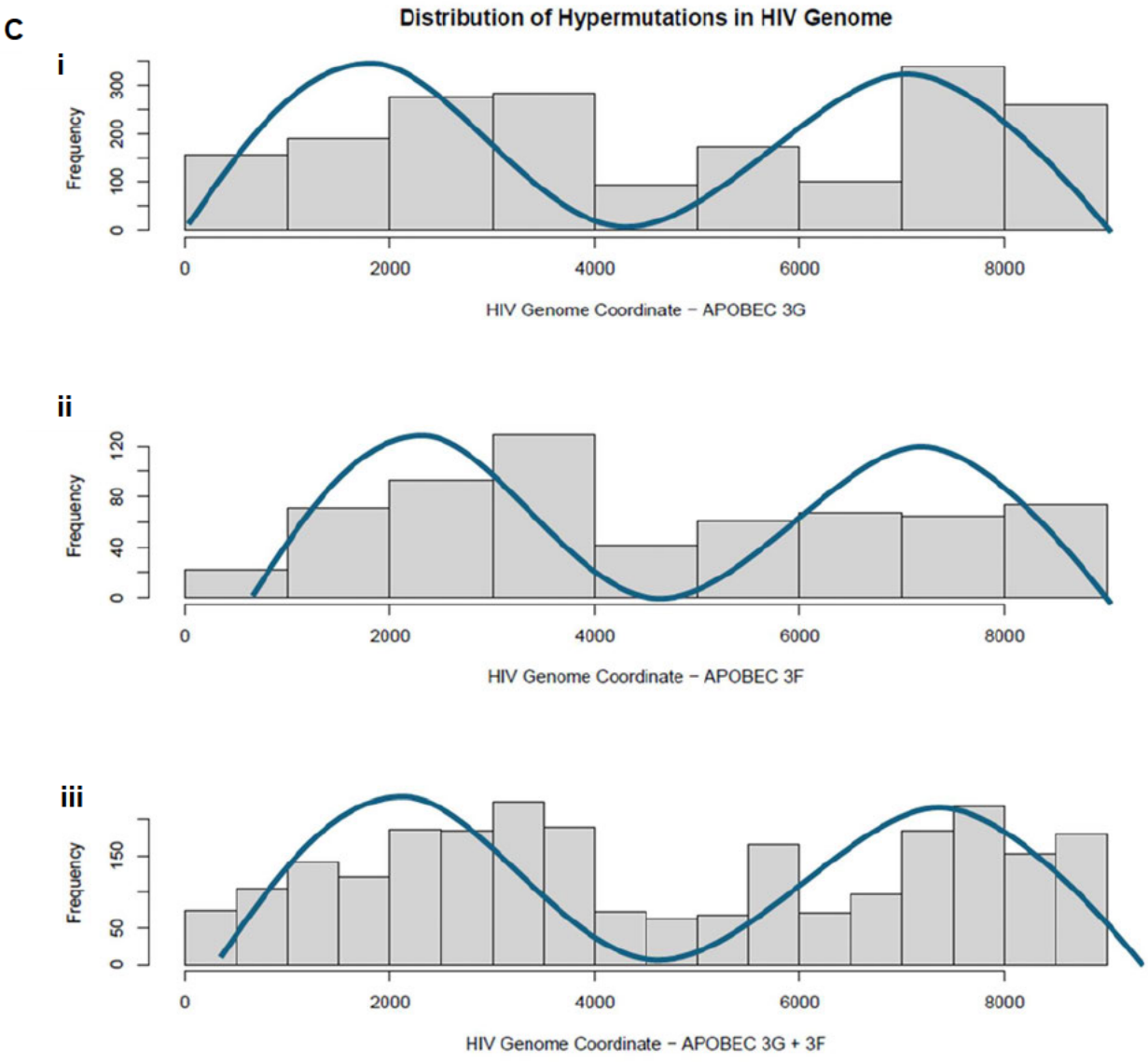

Figure 5.10 Frequency and distribution of A3G and A3F induced hypermutation in PID 198. A) Highlighter plot showing A3G and A3F hypermutation across the HIV genome. Green lines represent G-A induced hypermutation. All sequences were aligned to an intact reference sequence from the same participant. B) Quantification of A3G and A3F hypermutation. C) Distribution of hypermutation across the HIV genome. (i) distribution of A3G induced hypermutation (ii) distribution of A3F induced hypermutation (iii) distribution of A3G + A3F induced hypermutation.

A

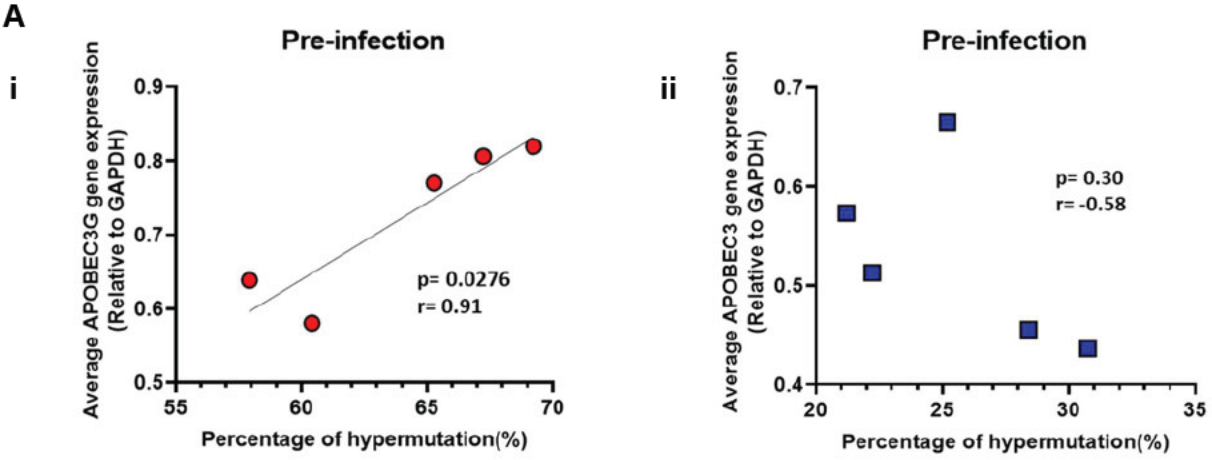

B

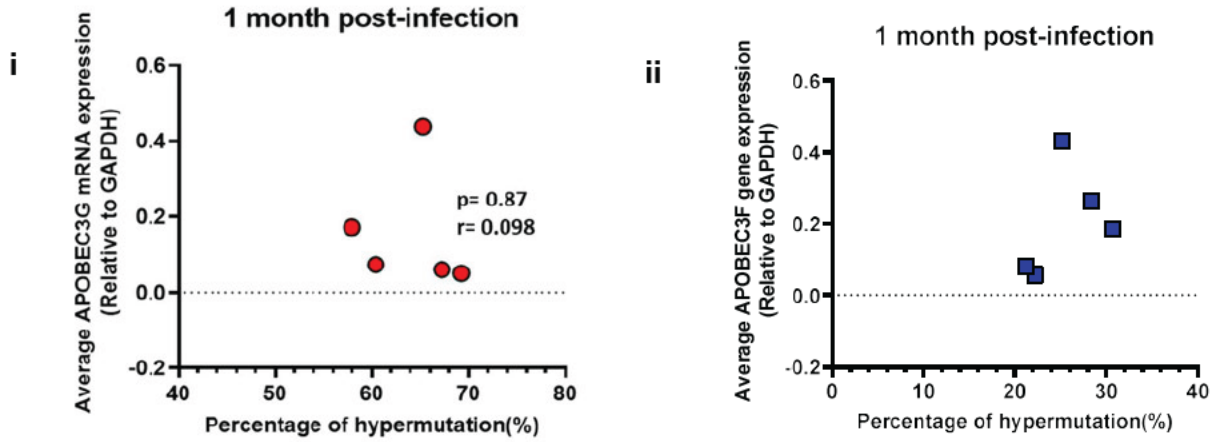

C

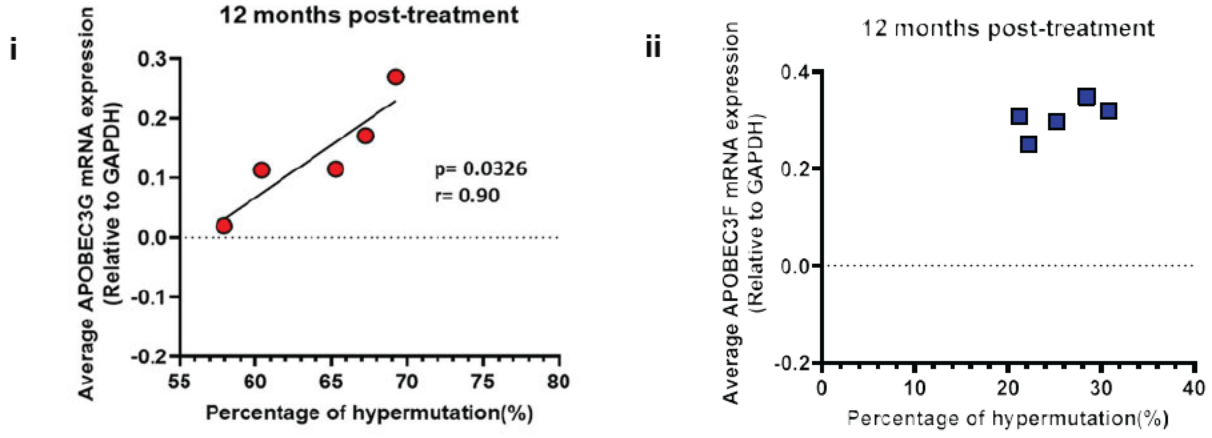

APOBEC3G
APOBEC3F

Figure 5.11 Correlation between A3 mRNA expression and percentage of hypermutation in 5 late treated participants. Red circles represent A3G, and blue squares represent A3F. A) (i) Pre-infection A3G mRNA expression levels and the percentage of A3G induced hypermutation. (ii) Pre-infection A3F mRNA expression levels and the percentage of A3F induced hypermutation. B) (i) 12 months post-infection A3G mRNA expression levels and the percentage of A3G induced hypermutation. (ii) 12 months post-infection A3F mRNA expression levels and percentage of A3F induced hypermutation. C) (i) 12 months post-treatment A3G mRNA expression levels and the percentage of A3G induced hypermutation. (ii) 12 months post-treatment A3F mRNA expression levels and the percentage of A3F induced hypermutation. *p= <0.05.

5.5 Discussion

Achieving a functional cure for HIV-1, where viral replication is controlled without the need for continuous antiretroviral therapy (ART), remains a central challenge in HIV research (Ikeda et al., 2021). Functional cure strategies aim to maintain undetectable or low viral loads through the host's immune system, even in the presence of latent reservoirs of integrated proviral DNA (Rodríguez-Muñoz and Moreno, 2019). These reservoirs represent one of the most significant barriers to achieving sustained virologic remission (Rodríguez-Muñoz and Moreno, 2019).

Insights into natural mechanisms of viral control, as seen in elite controllers and long-term non-progressors—individuals capable of suppressing HIV-1 replication without ART—are invaluable (Mastrangelo et al., 2022, Matsuda and Maeda, 2024, Ndung'u et al., 2018, Li and Blankson, 2021). Despite substantial research, the mechanisms driving this natural suppression remain only partially understood and require more intense, robust interrogation. Another model of functional cure is post-treatment viral control whereby an individual who interrupts ART treatment is able to durably control viral rebound. However, the duration of post-treatment control (PTC) is variable and the mechanisms underlying PTC are unknown. However, studies show that initiation of treatment during acute HIV infection may result in higher likelihood of PTC. Therefore, studies of antiviral mechanisms following ART in acute versus chronic treatment may provide mechanistic insights that may be harnessed to achieve a functional cure.

One emerging focus is the A3 family of cytosine deaminases particularly A3G and A3F, the two restriction factors known to have robust anti-HIV activity and their role in establishing a functional cure for HIV (Ikeda et al., 2021). Studies have shown that

elite controllers and long-term non-progressors have elevated expression levels of A3 proteins which is one of the contributing factors that may lead to sustained virological control (Kourteva et al., 2012, Gonzalo-Gil et al., 2017, Rodríguez-Muñoz and Moreno, 2019). Cytidine deaminase host restriction factors limit HIV-1 replication by causing hypermutation, but Vif counters this by degrading A3 proteins, ensuring viral survival (Sheehy et al., 2003, Takaori-Kondo, 2006, Simon et al., 2005). Despite this, elevated A3-mediated mutagenesis in proviral DNA reservoirs has been associated with delayed disease progression in elite and viremic controllers, highlighting their potential as therapeutic targets (Gonzalo-Gil et al., 2017).

To investigate the role of A3G and A3F in shaping the proviral landscape in HIV-1 infection, we first measured A3G and A3F mRNA expression in CD4+ T cells and myeloid cells. Secondly, we correlated A3G and A3F expression with the size and quality of the defective reservoir found in cells targeted by HIV measured by IPDA. Thirdly, we characterized the A3 induced hypermutation profile of proviral DNA sequences from PBMCs from individuals initiating treatment in chronic infection.

Our initial *in vitro* experiments demonstrated robust expression of A3G and A3F mRNA in HEK 293T cells, confirming their utility as positive controls in expression experiments. When assessing A3G and A3F expression levels in CD4+ T cells and myeloid cells we observed no significant differences in A3G or A3F mRNA expression across the cell populations analysed. However, A3G expression was consistently higher than A3F by approximately 1.5-fold, aligning with findings by Koning et al. 2009 that highlighted elevated A3G levels in hematopoietic cells from HIV-negative individuals (Koning et al., 2009).

In the context of untreated HIV-1 infection, both A3G and A3F expression were downregulated across all cell subsets, with A3G showing a greater relative decrease across all cell populations. ART initiated during chronic infection partially restored A3G and A3F mRNA expression over time, but the expression of these innate immune proteins was not restored to pre-infection levels. Conversely, ART initiation during acute infection effectively preserved A3G and A3F expression, as only a transient decrease was observed, suggesting that these proteins may be capable of more potent innate immune responses in this context if viral replication was reignited. A study by Reddy et al.,2010 also showed downregulation of A3G expression in total PBMCs (Reddy et al., 2010). Studies have also confirmed that besides Vif-dependant mechanisms of reducing the levels of A3 proteins, there are also Vif-independent mechanisms where transcription is affected (Stupfler et al., 2021).

Using the IPDA, we quantified levels of average defective proviral DNA in memory CD4+ T cells and myeloid cells at 12 months post-treatment. Participants who initiated ART during chronic infection exhibited significantly higher levels of defective DNA compared to those treated early. Notably, early treated participants displayed a skewed distribution of defective DNA, predominantly localized to memory CD4+ T cells, whereas late-treated participants exhibited defective DNA in both CD4+ T cells and myeloid cells. This suggests that early treatment potentially prevents seeding and establishment of the reservoir within the myeloid compartment within the blood, thus focusing efforts on cure strategies

While correlations between A3G/A3F expression and defective reservoir size were generally non-significant, a notable exception was observed in TM CD4+ T cells of late-treated individuals, where higher A3G expression correlated with larger defective reservoirs. This finding suggests that A3G activity may contribute to shaping the

defective proviral landscape in specific cellular contexts. The relationship between A3 proteins and HIV-1 progression suggests that boosting the mutagenic activity of A3 proteins could be a potential strategy for a functional cure. If we can manipulate A3-mediated mutations to reach lethal levels, it could provide a powerful method to combat HIV-1 (Imamichi et al., 2020, Ikeda et al., 2021, Matsuda and Maeda, 2024). This exciting prospect opens the door to new therapeutic approaches that could one day make a functional HIV-1 cure a reality.

Next, we analysed proviral archived genomic sequences, which were recently published (Reddy et al., 2024). The sequences were generated using the FLIP-seq assay from five late-treated participants to assess the extent of A3-induced hypermutation (Reddy et al., 2024). A3G-mediated hypermutation footprints were significantly more frequent than those of A3F, even though A3G expression exhibited greater downregulation. This underscores the dominant role of A3G in mutagenesis across the proviral genome. If interventional efforts are focused on preserving A3G innate immune responses, then this would potentially drive the reservoir into a more defective, hypermutated state, thus leading to a functional cure.

We were interested in investigating the locations of hypermutation across the HIV genome. Hypermutation patterns across the HIV genome exhibited a bimodal distribution, with clusters at the 3′ and 5′ ends of the HIV genome. These regions, enriched in purines and susceptible to prolonged single-stranded states during reverse transcription, are "hot spots" for A3 activity, as described by (Armitage et al., 2014).

However, some limitations of the study were noted, such as the small sample size. Additionally, FLIP-Seq was done on whole PBMCs instead of individual cell subsets. Furthermore, the complexity of the HIV lifecycle, where APOBEC induces mutation in

the targets rather than where it is expressed, could potentially play a role in the activity of A3 proteins. Because of these limitations, these results need to be interpreted with caution, and in vitro mechanistic studies could provide further insights. Furthermore, A limitation of this study is the use of GAPDH as a reference gene, as its expression is not universally stable across cell types, metabolic states, or populations, which may influence normalization and interpretation of gene expression results. This will be considered for future experiments.

Our findings highlight the therapeutic potential of leveraging A3-mediated hypermutation to disrupt HIV reservoirs. However, these results are preliminary and should be treated as hypothesis-generating instead of conclusive. Early ART initiation preserves A3G and A3F expression, reduces defective reservoir size, and maintains innate immune function, creating a favourable environment for interventions targeting proviral DNA mutagenesis. Future research should explore transcriptional profiling of immune subsets to elucidate cell-specific A3 regulation and develop strategies to enhance A3 activity while mitigating HIV-induced downregulation.

This study provides critical insights into the interplay between APOBEC3 proteins and the HIV-1 reservoir. Early ART significantly reduces reservoir size and preserves innate immune responses, positioning it as a cornerstone in functional cure strategies. By enhancing A3-mediated mutagenesis and counteracting Vif-mediated degradation, novel therapeutic approaches could drive HIV-1 reservoirs toward irreversible inactivation, advancing the quest for a functional cure.

6 Chapter 6: Discussion

ART has transformed HIV into a manageable chronic condition by suppressing viral replication. However, it fails to eradicate the virus due to latent reservoirs in immune cells, necessitating lifelong treatment and posing challenges such as drug toxicity and financial burdens, particularly in resource-limited settings (Matsuda and Maeda, 2024).

Early ART initiation reduces viral transmission and reservoir size but does not fully restore life expectancy or prevent age-related complications (Dong et al., 2018, Ndung'u et al., 2018). The persistence of replication-competent HIV in resting memory CD4+ T cells and other immune subsets complicates eradication. Identifying these reservoirs is critical for cure strategies, yet research remains disproportionately focused on subtype B in men, with limited data on subtype C and women despite well-known sex-based differences in immune responses (Ndung'u et al., 2019). Additionally, host restriction factors like A3G and A3F induce HIV hypermutation, but their role in defective provirus formation is not well understood and further investigations into understanding the A3 footprint on the HIV genome may lead to novel therapeutic targets to restrict replication-competent HIV and advance cure research (Ikeda et al., 2021, Ikeda et al., 2023).

This study investigated the HIV reservoir in the context of subtype C in African women. Utilizing the FRESH cohort which involved followed up of participants before infection and after initiation of ART therefore enabled a unique analysis of reservoir dynamics within immune cells, enhancing the study's significance. Precisely documented infection timing facilitated investigations into reservoir establishment and seeding.

Additionally, well-defined ART initiation allowed for the examination of multiple study groups, including individuals treated during acute and chronic infection, offering valuable data on reservoir persistence across different treatment timelines and immune cell subsets.

This study aimed to provide a comprehensive longitudinal analysis of the HIV-1 subtype C reservoir within immune cells from the blood of PLWH and establish the impact of A3 proteins on the viral reservoir in a cohort of young women from Durban, South Africa. The study focused on hyperacute infection which is a critical period for understanding the establishment of the viral reservoir and followed participants longitudinal allowing further investigation of the dynamics of the viral reservoir.

To do this we identified immune cell subsets harbouring the highest levels of total HIV-DNA. Additionally, we evaluated the effects of early and late ART initiation on reservoir size within both CD4+ T cells and myeloid cells. Furthermore, we measured intact and replication-competent proviruses using advanced techniques such as the IPDA and SQuHIVLa (Buchholtz et al., 2024, Hossain et al., 2024). Moreover, we analysed A3G and A3F mRNA expression in immune cells and their contributions to the defective hypermutated pool of viral genomes. Also, we performed a comprehensive analysis of viral genome sequences from study participants who were late treated to establish the patterns of hypermutation driven by A3G and A3F within archived reservoir viruses.

6.1 The highest total HIV DNA levels are found within the central and effector memory CD4+ T cell compartments

Total HIV DNA is a key marker for assessing reservoirs as it is simple, standardized, and clinically relevant, reflecting infection history and treatment efficacy (Belmonti et

al., 2021, Rouzioux and Avettand-Fenoël, 2018, Avettand-Fènoël et al., 2016). While it does not distinguish between defective and intact viral forms, total HIV DNA predicts disease progression and provides insights into HIV pathogenesis. Reservoirs primarily exist in latently infected memory CD4+ T cells but also in myeloid cells, complicating eradication efforts (Avettand-Fènoël et al., 2016). Early cART initiation reduces reservoir size, limiting viral rebound and preserving immune function (De Clercq et al., 2022). Studies on subtype C HIV-1 in South Africa analysed proviral DNA levels in total PBMCs, revealing that treatment timing influences reservoir size and distribution (Reddy et al., 2024).

In Chapter 3 we investigated the contribution of immune cell subsets to maintaining the total HIV-1 reservoir. We found that central and effector memory CD4+ T cell compartments harbour the highest levels of total HIV-DNA. Previous studies have shown that central, effector and transitional memory CD4+ T cells play critical roles in maintaining a large portion of the total HIV reservoir (Hiener et al., 2017, Gupta et al., 2017, Duette et al., 2022, Hiener et al., 2018). Our findings revealed significant heterogeneity in the cellular reservoir, varying among participants. We observed that the total proviral DNA levels within immune cells were dynamic and changed over time in participants who were late and early treated. This underscores the complexity and diversity of the HIV reservoir within immune cells, indicating that the reservoir cannot be fully understood by focusing on a single cell type. Despite this heterogeneity and dynamism, CM and EM CD4+ T cells consistently harboured the highest levels of total HIV proviral DNA. This was seen in participants who were treated early or late. This aligns with their long lifespan and ability to remain resting (Song et al., 2020, Borghans and Ribeiro, 2017), which enables them to evade immune surveillance and ART. This

characteristic supports their role as stable reservoirs capable of potentially reigniting viral replication upon treatment interruption (Song et al., 2020).

Furthermore, it can be noted that the observation on distribution and frequency of HIV-infected cells may not solely reflect the initial seeding of the viral reservoir but could also be shaped by antigen-driven or homeostatic proliferation of infected CD4+ T cells. Antigenic proliferation occurs when T cells recognising cognate antigens expand in response to infection or vaccination, whereas homeostatic proliferation maintains T cell numbers in the absence of antigen through cytokine-driven signals such as IL-7 and IL-15 (Chomont et al., 2009; Cohn et al., 2015). Both mechanisms can lead to clonal expansion of latently infected cells, effectively increasing the proportion of certain infected subsets over time. This may explain why participants treated during chronic infection displayed more heterogeneous or unexpectedly high levels of proviral DNA in central and effector memory T cell compartments. Clonal expansion could also obscure the original distribution of the reservoir, complicating the interpretation of reservoir dynamics in the context of suppressive ART. Incorporating these considerations is important for understanding the persistence and stability of HIV reservoirs in individuals initiating therapy later in infection.

6.2 Total HIV DNA was detected in the myeloid cell population

While CD4+ T cells are traditionally considered the primary HIV reservoirs, studies have suggested that myeloid cells, including monocytes and macrophages, may also contribute to viral persistence and potential rebound (Sonza et al., 2001, Honeycutt et al., 2016, Baxter et al., 2014, Andrade et al., 2020). In Chapter 3, we also explored myeloid cells as a potential source of the HIV reservoir. A previous study showed that myeloid cells only (no lymphocytes) isolated from humanized mice contained HIV

DNA. This was in the presence of ART (Honeycutt et al., 2016). Another study by Andrade et al., 2020 showed that macrophages can sustain latent infection and produce virions (Andrade et al., 2020). The presence of proviral DNA in these cells highlights the need for inclusive strategies targeting all potential reservoirs.

We found that in addition to CD4+ T cells, proviral DNA was also detectable within the myeloid cell compartment, albeit at levels approximately 10-fold lower than those in CD4+ T cells at one year post-treatment. Interestingly we also observed that 4/5 late treated participants had HIV proviral DNA detected within their myeloid compartment which contrasted with participants treated early. We observed that only 1/5 early treated participants had detectable HIV proviral DNA in their myeloid compartment at one year post-treatment.

Debates persist regarding the mechanisms underlying proviral detection in myeloid cells, particularly whether it reflects productive infection or phagocytosis of latently infected CD4+ T (Baxter et al., 2014, Kandathil et al., 2016, Sattentau and Stevenson, 2016). We quantified TREC, a marker of newly produced CD4 T cells, to exclude the presence of T cells from the myeloid cell population. TREC was undetectable, thereby eliminating the possibility of engulfment of CD4+ T cells by phagocytosis by myeloid cells.

6.3 Treatment during acute but not chronic infection significantly reduced total HIV-DNA in all immune cell subsets

Moreover, in Chapter 3 we further investigated the impact of ART on total proviral DNA levels across immune cell subsets in individuals who initiated therapy during either chronic or hyperacute phases of infection. A previous showed that ART initiated within

6 months of HIV infection resulted in lower T cell activation and a smaller reservoir size (Jain et al., 2013). Our results revealed that ART initiation during chronic infection did not significantly reduce proviral DNA levels, even after one year of treatment. This suggests that once reservoirs are established, particularly within memory CD4+ T cells, they become highly resistant to reduction through ART alone and thereafter ART together with other novel interventions are needed.

In contrast, early ART initiation during the hyperacute phase led to a rapid and substantial reduction in proviral DNA levels across all cell subsets. However, early ART did not entirely prevent reservoir seeding, as proviral DNA was detectable at baseline (1 month post-infection) even in early treated individuals. Nonetheless, early treatment resulted in significantly lower proviral DNA levels after one year compared to late-treated individuals. Furthermore, we hypothesized that early treatment would shift the reservoir towards the myeloid population given that there is monocyte expansion during acute infection with no CD4+ T cell activation when ART is initiated in hyperacute infection (Muema et al., 2020, Naidoo et al., 2024). Here, we observed that early treatment prevented the establishment of the proviral reservoir within myeloid cells and the reservoir was maintained within CD4+ T cells. Late treatment, however, allowed for persistence and maintenance within myeloid cells post-treatment.

6.4 Intact proviral DNA predominately found within effector memory CD4+ T cells

We utilized the IPDA, a recently developed and validated technique now adapted for analyzing HIV subtype C samples, to identify the immune cell subsets harbouring the highest frequencies of intact and defective proviral DNA (Buchholtz et al., 2024, Bruner

et al., 2019). This method offers a precise and quantitative approach to distinguish between intact and defective proviruses within infected cells. The presence of intact proviral DNA poses a great obstacle as this is the driver of viral recrudescence upon ART cessation (Pinkevych et al., 2019).

Building on the findings from the previous chapter, which identified central memory (CM) and effector memory (EM) CD4+ T cells as the principal reservoirs for total HIV proviral DNA, we hypothesized that the distribution of intact proviral genomes would parallel that of total proviral DNA across CD4+ T cell subsets. Specifically, we postulated that intact and defective genomes would be evenly distributed among CD4+ T cells, with the relative distribution of intact genomes reflecting the overall proportions of total proviral DNA in different immune subsets.

Our results supported this hypothesis, confirming that CM and EM CD4+ T cells contained substantial levels of total proviral DNA. However, a key finding was the significant enrichment of intact proviral DNA within the EM CD4+ T cell subset. This observation underscores the pivotal role of EM CD4+ T cells in maintaining the viral reservoir, even under suppressive ART. Given their essential role in adaptive immune responses, the propensity of EM CD4+ T cells to harbour intact proviruses identifies them as critical targets for future therapeutic strategies aimed at reservoir reduction or elimination. Considering the presumed high turnover of EM compared to CM CD4 T cells (as “effector” cells), it is unclear why they continue to harbour high levels of intact proviral genomes even after prolonged ART. This will require further investigation.

Further investigation is needed to elucidate the transcriptional and phenotypic features that enable EM CD4+ T cells to serve as preferential reservoirs for intact proviral DNA. Prior studies have shown that in peripheral blood, cells harbouring genome-intact

proviruses and large clones of infected cells often express a distinct set of surface markers that confer resistance to immune-mediated killing. These markers include those that inhibit recognition and elimination by cytotoxic T lymphocytes (CTLs) and natural killer (NK) cells. Additionally, these reservoir-enriched cells frequently exhibit elevated expression of immune checkpoint molecules, such as PD-1, HLA-DR and CD127 (Sun et al., 2023, Horsburgh et al., 2020, Lee et al., 2019a) . These checkpoint markers are associated with reduced transcriptional activity of proviral genes, potentially limiting the exposure of reservoir cells to immune surveillance and phagocytosis by host immune responses (Sun et al., 2023).

Additionally, it was shown that the few cells harbouring genetically intact and inducible viral genomes express higher levels of integrin VLA-4 compared to uninfected cells or harbouring defective proviral DNA (Dufour et al., 2023). Furthermore, single-cell multi-omics profiling of T cells harbouring HIV RNA showed that ongoing TNF response is the major immune dysfunction in delayed versus immediate ART, shapes the transcriptional program of HIV RNA+ cells, and is an upstream regulator shaping T cell clonal expansion (Collora et al., 2022). They also showed that cytotoxic CD4+ T lymphocytes, particularly those expressing GZMK (granzyme K) and GZMB (granzyme B), harbour HIV RNA+ cells and T cell clones harbouring them (Collora et al., 2022).

While the aforementioned findings provide valuable insights, they are primarily derived from studies conducted in populations from the Global North, where different HIV subtypes, immune responses, and treatment paradigms predominate. There is a pressing need for more comprehensive investigations into the immunological and phenotypic characteristics of EM CD4+ T cells in settings where subtype C HIV-1 infections are prevalent, such as sub-Saharan Africa. Subtype-specific differences in

immune responses, as well as contextual factors such as earlier ART initiation and coinfections, could significantly influence the behaviour of EM CD4+ T cells as reservoirs for intact proviral DNA.

These findings emphasize the importance of subtype-specific research to uncover potential therapeutic vulnerabilities within EM CD4+ T cells. Such research may guide the development of targeted strategies, including immune-based therapies and latency-reversing agents, tailored to the unique virological and immunological landscapes of populations disproportionately affected by subtype C HIV-1 infections.

6.5 ART reduces the levels of intact proviral DNA in chronic and acute treated individuals

Further in Chapter 4, we next explored the impact of ART initiation timing on the levels of intact and defective proviral DNA. Here, we hypothesize that participants treated during chronic infection would have higher levels of intact and defective reservoirs compared to those individuals treated during acute infection.

Our data indicated that during untreated infection, there was no statistically significant difference in the frequency of intact or defective proviral DNA between individuals assessed one month post-infection versus one year post-infection. However, ART initiation during chronic infection failed to reduce defective proviral DNA frequencies. Interestingly, one year after treatment, both CM and EM CD4+ T cells demonstrated a marked significant reduction in intact proviral DNA levels.

In individuals initiating ART during hyperacute infection, the effects were even more pronounced. Within one year of treatment, intact proviral DNA levels in memory CD4+ T cells were significantly reduced, becoming undetectable across all cell subsets,

including CD4+ T cells and myeloid cells, in nearly all participants. An exception was observed in one individual, where intact proviral DNA persisted in EM CD4+ T cells. This outlier underscores the variability in individual responses to early ART, emphasizing the importance of personalized treatment strategies in HIV management. Furthermore, we observed a marked reduction in defective proviral DNA present within EM CD4+ T cells, in participants who were treated early.

6.6 Chronic treated individuals have a higher inducible reservoir than those treated during acute HIV infection

In Chapter 4, we evaluated the impact of ART on the inducible HIV reservoir using the SQuHIVLa assay, a new technique designed to measure Tat/Rev msRNA as a biomarker for the inducible reservoir. While the QVOA has traditionally been the gold standard for assessing replication-competent HIV reservoirs, recent advances have established msRNA quantification as a reliable, efficient, and scalable surrogate marker for reservoir size (Zhang and Chen, 2023, Gupta et al., 2017, Zerbato et al., 2021, Hossain et al., 2024, Siliciano and Siliciano, 2018, Lungu et al., 2021). These advances are particularly important for resource-constrained settings, as measuring Tat/Rev msRNA provides an accessible, affordable, and scalable alternative suitable for implementation in low- and middle-income regions, including sub-Saharan Africa (Hossain et al., 2024, Zhang and Chen, 2023, Siliciano and Siliciano, 2018, Lungu and Procopio, 2022).

To assess the inducible reservoir, we used cryopreserved peripheral blood mononuclear cell samples obtained by leukapheresis from the FRESH cohort participants treated during chronic and hyperacute stages of HIV infection. We hypothesized that participants who initiated ART during chronic infection would exhibit

higher levels of the inducible reservoir compared to those treated during acute infection. Our findings supported this hypothesis, demonstrating that individuals treated during chronic infection displayed significantly higher levels of inducible reservoir activity, as evidenced by elevated Tat/Rev msRNA expression.

These results highlight the profound influence of early ART initiation in limiting the size of the inducible reservoir. Importantly, the reduced reservoir size observed in early treated individuals may correlate with an extended time to viral rebound following treatment cessation, offering potential clinical implications for HIV remission strategies. These findings provide a compelling rationale for prioritizing early ART initiation to optimize long-term therapeutic outcomes and warrant further mechanistic investigations to validate these observations.

Building on these insights developing novel strategies to limit the inducible reservoir is essential. In Chapter 5 we explored the role of innate immune host restriction factors, specifically A3G and A3F, in shaping the reservoir landscape. These restriction factors, known for their capacity to induce hypermutation and impair viral replication, may provide critical insights into the mechanisms that govern reservoir dynamics and persistence (Lee et al., 2019b, Hiener et al., 2018, Hiener et al., 2017). Understanding the interplay between A3-mediated antiviral activity and reservoir formation could pave the way for novel therapeutic approaches aimed at reservoir reduction and achieving a functional cure for HIV (Ikeda et al., 2021).

6.7 Greater downregulation of A3G than A3F in chronic and acute treated individuals

Achieving a functional cure for HIV-1, defined as the sustained suppression of viral replication in the absence of continuous ART, remains a central goal in HIV research

(Ikeda et al., 2021). Functional cure strategies aim to harness and augment the host immune system to maintain undetectable viral loads while addressing the persistent challenge of latent HIV reservoirs (Ikeda et al., 2021, Imamichi et al., 2020). These reservoirs consist of transcriptionally silent, integrated proviral DNA, predominantly localized in resting memory CD4+ T cells, and represent a significant obstacle to achieving long-term remission (Lecossier et al., 2003, Ikeda et al., 2021) .

Insights into the natural mechanisms of viral control come from studying elite controllers and long-term non-progressors (Mastrangelo et al., 2022). These rare individuals are capable of suppressing HIV-1 replication without ART, likely due to a combination of unique host genetic factors, potent immune responses, and efficient viral restriction mechanisms. However, the precise biological pathways underlying their ability to achieve durable virological control remain incompletely understood. Among the mechanisms of interest are host restriction factors, such as the A3 family of cytosine deaminases, which play pivotal roles in innate antiviral defence. Notably, A3G and A3F have demonstrated significant anti-HIV activity, and their contribution to the potential for a functional cure warrants detailed investigation. Post-treatment controllers, who go into remission when ART is stopped are another model of a functional cure. Post-treatment control is more common in people living with HIV who initiate treatment in acute or primary infection, and it is therefore important to understand the underlying mechanisms which could potentially include preserved robust innate immune responses.

A3 proteins act during the reverse transcription of HIV-1, where they catalyse cytosine-to-uracil deamination on the negative-strand viral DNA (Sheehy et al., 2003). This enzymatic activity results in guanine-to-adenine (G-to-A) hypermutations in the proviral DNA, leading to the generation of defective proviruses incapable of producing

infectious virions (Lecossier et al., 2003). This mutagenic mechanism effectively impairs viral replication and contributes to reducing the fitness of the viral reservoir (Sheehy et al., 2003, Lecossier et al., 2003). However, HIV-1 has evolved sophisticated countermeasures, most notably the Vif (virion infectivity factor) protein, which targets A3 proteins for ubiquitination and subsequent proteasomal degradation. Despite these viral adaptations, elevated A3-mediated hypermutation has been associated with delayed disease progression in elite controllers, underscoring the potential therapeutic significance of enhancing A3 activity in broader HIV-infected populations.

To elucidate the role of A3G and A3F in shaping the HIV reservoir and their potential to aid in functional cure strategies, we conducted a series of experimental investigations detailed in Chapter 5. We began by measuring the expression of A3G and A3F mRNA across various cellular subsets, including CD4+ T cells and myeloid cells, hypothesizing that A3G expression would exceed A3F levels in all subsets. Consistent with prior findings, our results demonstrated that A3G expression was significantly higher than A3F in hematopoietic cells (Koning et al., 2009).

In untreated HIV-1 infection, both A3G and A3F expression were markedly downregulated, with A3G exhibiting a more pronounced decrease. This suppression likely reflects a combination of viral strategies to evade innate immunity, and the progressive immune dysfunction associated with chronic infection. ART initiated during chronic infection partially restored A3 expression levels, but early ART initiation was notably more effective. Early ART preserved A3G and A3F expression to a greater extent, helping to maintain the innate immune system's antiviral capabilities and mitigating the severe immune dysregulation observed in late-treated individuals.

These findings underscore the critical importance of early ART in preserving innate immune responses, particularly those mediated by A3 proteins. Furthermore, they highlight the therapeutic potential of targeting A3G and A3F to augment antiviral defences and impair the formation and maintenance of the latent HIV reservoir. Future studies should explore strategies to enhance A3 activity while overcoming Vif-mediated antagonism, as well as further delineating the mechanisms by which A3 proteins contribute to reservoir dynamics and immune control. These efforts could pave the way toward the development of novel interventions aimed at achieving a durable functional cure for HIV-1.

6.8 Defective HIV reservoir levels correlate positively with A3G mRNA expression in transitional memory CD4+ T cells

To investigate the relationship between defective proviral DNA levels and A3G and A3F expression, we performed a correlation analysis. We hypothesized that elevated A3G and A3F expression levels would be positively associated with increased levels of defective proviral DNA, given the known role of A3 proteins in inducing hypermutation in HIV proviruses. Quantitative analyses of the defective proviral reservoir across cellular subsets using IPDA revealed notable differences between early-treated and late-treated participants. Early treated individuals exhibited significantly smaller defective proviral reservoirs, which were predominantly localized within memory CD4+ T cells. Conversely, in late-treated participants, the defective reservoirs were larger and distributed across both CD4+ T cell subsets and myeloid cell populations.

Interestingly, within TM CD4+ T cells, higher A3G expression levels were found to correlate with increased amounts of defective proviral DNA. This observation suggests

that A3G-mediated hypermutation may play a key role in shaping the reservoir landscape within this specific cell type. However, further studies are required to validate and strengthen this finding. Specifically, more robust and longitudinal investigations are necessary to confirm the causal relationship between A3G activity and the generation of defective proviruses within TM CD4+ T cells.

To gain a deeper understanding of the underlying mechanisms, transcriptomic profiling of memory CD4+ T cells is also warranted, specifically TM CD4+ T cells. This approach would help determine whether the upregulation of interferon-alpha (IFN-α)-mediated responses occurs in this subset following HIV infection. IFN-α is a critical cytokine in the innate immune response and has been associated with enhanced APOBEC3 activity (Wang et al., 2008, Altfeld and Gale, 2015). Elevated IFN-α levels could contribute to increased activity of A3 proteins and could potentially increase the levels of hypermutation and thus contribute to the accumulation of defective proviruses. These findings could provide valuable insights into the interplay between the host immune response and the formation of the defective proviral reservoir, ultimately aiding in the development of targeted therapeutic strategies for reservoir reduction.

6.9 A3G has a higher hypermutation footprint on the proviral reservoir landscape

In the next phase of our investigation, we quantified the hypermutation profiles of proviral sequences derived from five study participants who initiated antiretroviral therapy during advanced stages of infection. This analysis aimed to explore the extent and genomic distribution of hypermutations induced by A3G and A3F.

To achieve this, we analysed previously published full-length proviral DNA sequences, which provided a detailed and comprehensive view of the genomic landscape and the extent of hypermutation induced by A3G and A3F (Reddy et al., 2024, Lee et al., 2019b). These sequences, derived from PBMCs, were utilized as an alternative to sequencing from sorted cell populations. Amplification of proviral genomes from sorted cells proved unsuccessful, likely due to the limited number of cells available and the potential introduction of PCR inhibitors during the cell sorting process, which reduced the likelihood of obtaining reliable sequences from specific cell subsets.

We hypothesized that A3G, a more potent antiviral factor characterized by a higher cytidine deamination rate and stronger substrate specificity, would exert a more pronounced effect on the proviral reservoir compared to A3F by inducing a greater frequency of APOBEC3-mediated hypermutations. This hypothesis is consistent with prior studies demonstrating that A3G exhibits superior catalytic efficiency and targets a broader range of single-stranded DNA regions during the reverse transcription process compared to A3F.

Our analysis of the proviral genome sequences revealed a bimodal distribution of hypermutation, with distinct clusters localized at the 3′ and 5′ ends of the HIV-1 genome. These regions are rich in purines, particularly guanine, which are preferentially targeted by A3 enzymes. Moreover, the extended single-stranded DNA states that occur during reverse transcription in these genomic regions increase their susceptibility to cytidine deamination. Such structural and compositional vulnerabilities explain the observed clustering of hypermutation activity.

Among the APOBEC3 enzymes analysed, A3G-mediated hypermutation footprints were markedly more frequent and prominent than those of A3F. This finding

underscores the dominant role of A3G in shaping the proviral landscape, even though HIV-1 employs mechanisms such as the viral protein Vif (virion infectivity factor) to degrade A3G and thereby mitigate its antiviral effects. The relative abundance and resilience of A3G activity in the face of viral countermeasures highlight its critical contribution to the intrinsic immune defence against HIV-1.

6.10 Study Limitations and Future Directions

6.10.1 Limitations

The study's small sample size, comprising only five untreated, five late-treated, and five early treated female participants significantly constrains its statistical power and limits the generalizability of its findings to the broader HIV-1 population. This limitation hinders the ability to draw robust conclusions or apply findings universally across diverse demographic and clinical profiles, particularly when considering variations in age, sex, comorbidities, and treatment history. Expanding the cohort size in future studies would improve statistical rigour, enable subgroup analyses, and enhance confidence in the applicability of the results to the global HIV-1 population. Despite this limitation, we were able to comprehensively and longitudinally characterize the reservoir and an important component of the innate immune response in immune cell subsets that are targeted by HIV, and this data has important implications for HIV cure strategies. Additionally, sampling depth, meaning the number of cells that were sampled, is a limiting factor, particularly for those that were treated during acute HIV infection.

A limitation of this study is that a proportion of the HIV DNA detected during untreated infection and shortly after ART initiation may represent unintegrated viral forms or virion-associated DNA rather than true integrated provirus. As 2-LTR circle assays and

methods to exclude virion-bound DNA were not applied, caution is warranted when interpreting these results as reflective of the intact proviral reservoir. The use of innovative assays, including the IPDA and SQuHIVLa, provides novel insights into viral reservoirs. However, these methodologies are relatively new and require broader validation. Mechanistic insights into the role of A3G and A3F in reservoir dynamics remain incomplete. For instance, it is unclear how fluctuations in A3 activity over time or across different cell types influence the establishment and maintenance of defective reservoirs. Addressing these gaps requires robust, longitudinal studies incorporating single-cell analyses, transcriptomics, and advanced molecular imaging to delineate the temporal and spatial aspects of A3-mediated viral restriction.

Although correlations between A3 expression and defective reservoirs were observed in the study, causal relationships remain speculative. Establishing causality necessitates functional studies that manipulate A3 expression experimentally to observe its effects on reservoir dynamics directly. Such studies could include knockdown or overexpression models in vitro and in vivo, combined with advanced genomic tools to analyse resultant changes in proviral composition and reservoir size. Understanding these dynamics could provide valuable insights into potential therapeutic strategies targeting reservoir eradication or reduction.

Lastly, the study focused on reservoirs in peripheral blood, potentially overlooking critical tissue reservoirs in lymph nodes, the gastrointestinal tract, and other anatomical compartments. Tissue reservoirs harbour a substantial portion of latent HIV and differ in their cellular composition, microenvironment, and exposure to antiretroviral drugs. These factors influence reservoir establishment, persistence, and reactivation potential. Comprehensive analyses incorporating tissue biopsies and imaging studies are essential to capture the full complexity of HIV reservoirs and their

interactions with the host immune system. This broader approach would provide a more holistic understanding of reservoir biology and HIV persistence, informing more effective strategies for cure research. In summary, addressing these limitations through larger cohorts, enhanced assay validation, mechanistic studies, and inclusion of tissue reservoirs is vital for advancing the understanding of HIV reservoir dynamics and persistence.

6.10.2 Future Directions

Future research into HIV reservoirs within immune cell subsets can significantly enhance our understanding of persistent infection and inform eradication strategies. A key area is the diversity of HIV reservoirs across different immune cells. Studies show that proviral DNA content varies between cell types, indicating that a universal approach may not be effective. Exploring the dynamic changes in reservoir composition, particularly in individuals with different treatment histories, could reveal how treatment timing influences the persistence of proviral DNA and guide targeted interventions.

Focusing on effector memory (EM) CD4+ T cells, which harbour substantial intact proviral DNA, could provide crucial insights into HIV integration sites. Employing advanced technologies, such as CRISPR-based gene editing and next-generation sequencing, could map HIV integration across cell types. Understanding whether the HIV genome integrates into transcriptionally active or inactive regions can help identify areas that prevent viral reactivation and inform strategies to reduce the inducible reservoir.

Another focus should be on the transcriptional and phenotypic properties that make EM CD4+ T cells resilient to immune responses and ART. Investigating specific gene

expression profiles, immune pathways, and surface markers like PD-1, LAG-3, and TIGIT could reveal how these cells evade immune detection. These markers are associated with reduced proviral transcription, minimizing immune recognition and aiding in the persistence of the viral reservoir. Research could also explore whether targeting these checkpoint molecules might enhance immune responses and reduce the EM CD4+ T cell reservoir.

In summary, expanding research on the heterogeneity of HIV reservoirs, their integration sites, and the phenotypic traits that sustain EM CD4+ T cell reservoirs can lead to more precise, effective therapies for HIV eradication.

6.11 Conclusions

This study underscores the intricate dynamics of HIV reservoirs across immune cell subsets and emphasizes the impact of early ART initiation on reservoir characteristics. CM and EM CD4+ T cells consistently emerged as key reservoirs for both total and intact HIV proviral DNA, highlighting their critical role in viral persistence. Despite the heterogeneity observed in reservoir size and distribution among individuals, EM CD4+ T cells were uniquely enriched with intact proviruses, positioning them as pivotal targets for therapeutic strategies.

Our findings also revealed the presence of proviral DNA within myeloid cells, albeit at lower levels compared to CD4+ T-cells. The detection of HIV reservoirs in myeloid cells, even in the absence of T-cell contamination, emphasizes the need for comprehensive eradication strategies addressing diverse cellular compartments, not only focusing on the T-cell compartment.

The timing of ART initiation significantly influenced reservoir size and composition. Early ART reduced both intact and defective proviral DNA levels more effectively than

late ART, limiting reservoir seeding and preserving innate immune function. This supports prioritizing early ART initiation to optimize long-term therapeutic outcomes. Additionally, the study revealed that early ART effectively curtailed the establishment of myeloid reservoirs, further underscoring its benefits.

Investigation into the role of A3 proteins, particularly A3G and A3F, shed light on their contribution to shaping the defective proviral reservoir through hypermutation. Elevated A3 expression correlated with increased defective proviruses in TM CD4+ T cells, highlighting their potential as targets for enhancing reservoir reduction strategies. However, the persistence of intact proviruses, particularly within EM CD4+ T cells, despite ART and A3 activity, underscores the resilience of these reservoirs.

The study also demonstrated the value of novel techniques such as IPDA and Tat/Rev msRNA quantification using SQuHIVLa for distinguishing between intact and defective reservoirs and assessing the inducible reservoir. These methodologies provide scalable alternatives for resource-constrained settings and advance our understanding of HIV persistence.

Finally, our analysis emphasized the need for subtype-specific research, particularly in settings with a high prevalence of subtype C HIV-1, to uncover unique therapeutic vulnerabilities and develop tailored interventions. Future efforts should focus on exploring the phenotypic and transcriptional features of EM CD4+ T cells, enhancing A3 activity while mitigating Vif antagonism, and identifying and enhancing immune-based strategies to achieve a functional cure for HIV.

This comprehensive investigation paves the way for innovative therapeutic approaches aimed at reducing the HIV reservoir and advancing the goal of achieving durable remission.

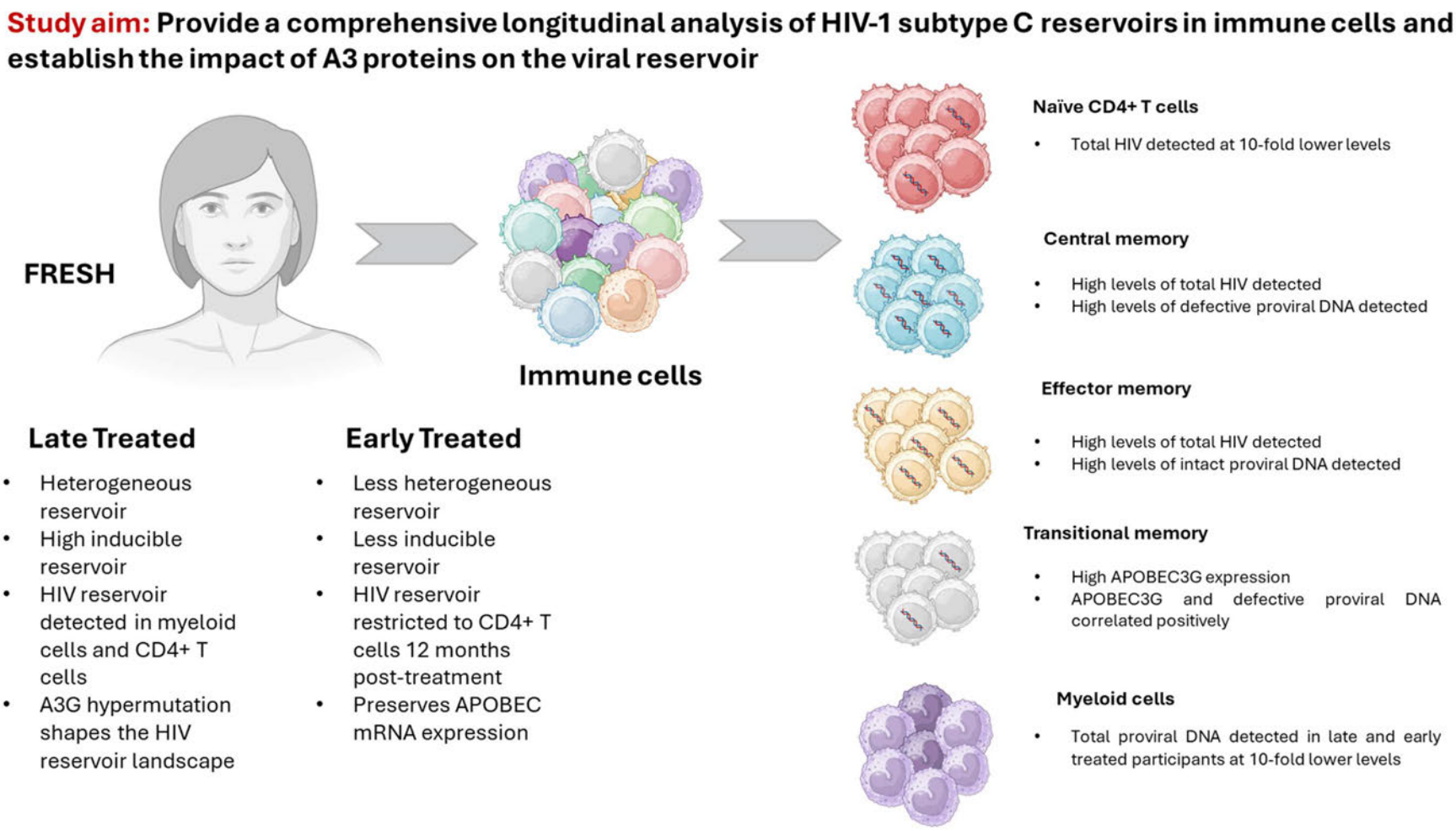

Figure 6.1 Study summary and main findings

7 References

2023 UNAIDS Global Aids Update. 2023 UNAIDS Global Aids Update.

Bijkerk H. 1981. Kaposi's sarcoma and Pneumocystis pneumonia among homosexual men--New York City and California. *MMWR Morb Mortal Wkly Rep,* 30**,** 305-8.

ALTFELD, M. & GALE, M., JR. 2015. Innate immunity against HIV-1 infection. *Nat Immunol,* 16**,** 554-62.

AMOÊDO, N. D., AFONSO, A. O., CUNHA, S. M., OLIVEIRA, R. H., MACHADO, E. S. & SOARES, M. A. 2011. Expression of APOBEC3G/3F and G-to-A hypermutation levels in HIV-1-infected children with different profiles of disease progression. *PLoS One,* 6**,** e24118.

ANANWORANICH, J., CHOMONT, N., ELLER, L. A., KROON, E., TOVANABUTRA, S., BOSE, M., NAU, M., FLETCHER, J. L. K., TIPSUK, S., VANDERGEETEN, C., O'CONNELL, R. J., PINYAKORN, S., MICHAEL, N., PHANUPHAK, N. & ROBB, M. L. 2016. HIV DNA Set Point is Rapidly Established in Acute HIV Infection and Dramatically Reduced by Early ART. *EBioMedicine,* 11**,** 68-72.

ANDERSON, B. D. & HARRIS, R. S. 2015. Transcriptional regulation of APOBEC3 antiviral immunity through the CBF-β/RUNX axis. *Science Advances,* 1**,** e1500296.

ANDERSON, B. D., IKEDA, T., MOGHADASI, S. A., MARTIN, A. S., BROWN, W. L. & HARRIS, R. S. 2018. Natural APOBEC3C variants can elicit differential HIV-1 restriction activity. *Retrovirology,* 15**,** 78.

ANDRADE, V. M., MAVIAN, C., BABIC, D., CORDEIRO, T., SHARKEY, M., BARRIOS, L., BRANDER, C., MARTINEZ-PICADO, J., DALMAU, J., LLANO, A., LI, J. Z., JACOBSON, J., LAVINE, C. L., SEAMAN, M. S., SALEMI, M. & STEVENSON, M. 2020. A minor population of macrophage-tropic HIV-1 variants is identified in recrudescing viremia following analytic treatment interruption. *Proc Natl Acad Sci U S A,* 117**,** 9981-9990.

ANGLEMYER, A., RUTHERFORD, G. W., EASTERBROOK, P. J., HORVATH, T., VITÓRIA, M., JAN, M. & DOHERTY, M. C. 2014. Early initiation of antiretroviral therapy in HIV-infected adults and adolescents: a systematic review. *AIDS,* 28**,** S105-S118.

ARMITAGE, A. E., DEFORCHE, K., WELCH, J. J., VAN LAETHEM, K., CAMACHO, R., RAMBAUT, A. & IVERSEN, A. K. 2014. Possible footprints of APOBEC3F and/or other APOBEC3 deaminases, but not APOBEC3G, on HIV-1 from patients with acute/early and chronic infections. *J Virol,* 88**,** 12882-94.

ARTHUR, L. O., BESS, J. W., JR., SOWDER, R. C., 2ND, BENVENISTE, R. E., MANN, D. L., CHERMANN, J. C. & HENDERSON, L. E. 1992. Cellular proteins bound to immunodeficiency viruses: implications for pathogenesis and vaccines. *Science,* 258**,** 1935-8.

ARTS, E. J. & HAZUDA, D. J. 2012. HIV-1 antiretroviral drug therapy. *Cold Spring Harb Perspect Med,* 2**,** a007161.

AVETTAND-FÈNOËL, V., CHAIX, M. L., BLANCHE, S., BURGARD, M., FLOCH, C., TOURE, K., ALLEMON, M. C., WARSZAWSKI, J. & ROUZIOUX, C. 2009. LTR real-time PCR for HIV-1 DNA quantitation in blood cells for early diagnosis in infants born to seropositive mothers treated in HAART area (ANRS CO 01). *J Med Virol,* 81**,** 217-23.

AVETTAND-FÈNOËL, V., HOCQUELOUX, L., GHOSN, J., CHERET, A., FRANGE, P., MELARD, A., VIARD, J. P. & ROUZIOUX, C. 2016. Total HIV-1 DNA, a Marker of Viral Reservoir Dynamics with Clinical Implications. *Clin Microbiol Rev,* 29**,** 859-80.

BAILEY, J. R., SEDAGHAT, A. R., KIEFFER, T., BRENNAN, T., LEE, P. K., WIND-ROTOLO, M., HAGGERTY, C. M., KAMIREDDI, A. R., LIU, Y., LEE, J., PERSAUD, D., GALLANT, J. E., COFRANCESCO, J., JR., QUINN, T. C., WILKE, C. O., RAY, S. C., SILICIANO, J. D., NETTLES, R. E. & SILICIANO, R. F. 2006. Residual human immunodeficiency virus type 1

viremia in some patients on antiretroviral therapy is dominated by a small number of invariant clones rarely found in circulating CD4+ T cells. *J Virol,* 80**,** 6441-57.

BAIYEGUNHI, O. O., MANN, J., KHABA, T., NKOSI, T., MBATHA, A., OGUNSHOLA, F., CHASARA, C., ISMAIL, N., NGUBANE, T., JAJBHAY, I., PANSEGROUW, J., DONG, K. L., WALKER, B. D., NDUNG'U, T. & NDHLOVU, Z. M. 2022. CD8 lymphocytes mitigate HIV-1 persistence in lymph node follicular helper T cells during hyperacute-treated infection. *Nat Commun,* 13**,** 4041.

BARRÉ-SINOUSSI, F., CHERMANN, J. C., REY, F., NUGEYRE, M. T., CHAMARET, S., GRUEST, J., DAUGUET, C., AXLER-BLIN, C., VÉZINET-BRUN, F., ROUZIOUX, C., ROZENBAUM, W. & MONTAGNIER, L. 1983. Isolation of a T-lymphotropic retrovirus from a patient at risk for acquired immune deficiency syndrome (AIDS). *Science,* 220**,** 868-71.

BAXTER, A. E., RUSSELL, R. A., DUNCAN, C. J., MOORE, M. D., WILLBERG, C. B., PABLOS, J. L., FINZI, A., KAUFMANN, D. E., OCHSENBAUER, C., KAPPES, J. C., GROOT, F. & SATTENTAU, Q. J. 2014. Macrophage infection via selective capture of HIV-1-infected CD4+ T cells. *Cell Host Microbe,* 16**,** 711-21.

BECK, S. E. & BLANKSON, J. N. 2020. Replacing cART with CAR-T Cells: Using Immunotherapy to Cure HIV. *Mol Ther,* 28**,** 1561-1562.

BELMONTI, S., DI GIAMBENEDETTO, S. & LOMBARDI, F. 2021. Quantification of Total HIV DNA as a Marker to Measure Viral Reservoir: Methods and Potential Implications for Clinical Practice. *Diagnostics (Basel),* 12.

BIASIN, M., PIACENTINI, L., LO CAPUTO, S., KANARI, Y., MAGRI, G., TRABATTONI, D., NADDEO, V., LOPALCO, L., CLIVIO, A., CESANA, E., FASANO, F., BERGAMASCHI, C., MAZZOTTA, F., MIYAZAWA, M. & CLERICI, M. 2007. Apolipoprotein B mRNA-editing enzyme, catalytic polypeptide-like 3G: a possible role in the resistance to HIV of HIV-exposed seronegative individuals. *J Infect Dis,* 195**,** 960-4.

BINKA, M., OOMS, M., STEWARD, M. & SIMON, V. 2012. The activity spectrum of Vif from multiple HIV-1 subtypes against APOBEC3G, APOBEC3F, and APOBEC3H. *J Virol,* 86**,** 49-59.

BORGHANS, J. & RIBEIRO, R. M. 2017. The maths of memory. *eLife,* 6**,** e26754.

BOUTAYEB, A. 2009. The impact of HIV/AIDS on human development in African countries. *BMC Public Health,* 9**,** S3.

BRUNER, K. M., MURRAY, A. J., POLLACK, R. A., SOLIMAN, M. G., LASKEY, S. B., CAPOFERRI, A. A., LAI, J., STRAIN, M. C., LADA, S. M., HOH, R., HO, Y. C., RICHMAN, D. D., DEEKS, S. G., SILICIANO, J. D. & SILICIANO, R. F. 2016. Defective proviruses rapidly accumulate during acute HIV-1 infection. *Nat Med,* 22**,** 1043-9.

BRUNER, K. M., WANG, Z., SIMONETTI, F. R., BENDER, A. M., KWON, K. J., SENGUPTA, S., FRAY, E. J., BEG, S. A., ANTAR, A. A. R., JENIKE, K. M., BERTAGNOLLI, L. N., CAPOFERRI, A. A., KUFERA, J. T., TIMMONS, A., NOBLES, C., GREGG, J., WADA, N., HO, Y. C., ZHANG, H., MARGOLICK, J. B., BLANKSON, J. N., DEEKS, S. G., BUSHMAN, F. D., SILICIANO, J. D., LAIRD, G. M. & SILICIANO, R. F. 2019. A quantitative approach for measuring the reservoir of latent HIV-1 proviruses. *Nature,* 566**,** 120-125.

BUCHHOLTZ, N., NÜHN, M. M., DE JONG, T. C. M., STIENSTRA, T. A. T., REDDY, K., NDUNG'U, T., NDHLOVU, Z. M., FISHER, K., PALMER, S., WENSING, A. M. J., SYMONS, J. & NIJHUIS, M. 2024. Development of a highly sensitive and specific intact proviral DNA assay for HIV-1 subtype B and C. *Virol J,* 21**,** 36.

BURNIE, J. & GUZZO, C. 2019. The Incorporation of Host Proteins into the External HIV-1 Envelope. *Viruses,* 11**,** 85.

BUSHMAN, F. D. 2002. Integration site selection by lentiviruses: biology and possible control. *Curr Top Microbiol Immunol,* 261**,** 165-77.

CHANG, J. J., WOODS, M., LINDSAY, R. J., DOYLE, E. H., GRIESBECK, M., CHAN, E. S., ROBBINS, G. K., BOSCH, R. J. & ALTFELD, M. 2013. Higher expression of several interferon-

stimulated genes in HIV-1-infected females after adjusting for the level of viral replication. *J Infect Dis,* 208**,** 830-8.

CHAWLA, A., WANG, C., PATTON, C., MURRAY, M., PUNEKAR, Y., DE RUITER, A. & STEINHART, C. 2018. A Review of Long-Term Toxicity of Antiretroviral Treatment Regimens and Implications for an Aging Population. *Infect Dis Ther,* 7**,** 183-195.

CHIU, Y. L. & GREENE, W. C. 2006. Multifaceted antiviral actions of APOBEC3 cytidine deaminases. *Trends Immunol,* 27**,** 291-7.

CHOMONT, N., DAFONSECA, S., VANDERGEETEN, C., ANCUTA, P. & SÉKALY, R. P. 2011. Maintenance of CD4+ T-cell memory and HIV persistence: keeping memory, keeping HIV. *Curr Opin HIV AIDS,* 6**,** 30-6.

CHOMONT, N., EL-FAR, M., ANCUTA, P., TRAUTMANN, L., PROCOPIO, F. A., YASSINE-DIAB, B., BOUCHER, G., BOULASSEL, M. R., GHATTAS, G., BRENCHLEY, J. M., SCHACKER, T. W., HILL, B. J., DOUEK, D. C., ROUTY, J. P., HADDAD, E. K. & SÉKALY, R. P. 2009. HIV reservoir size and persistence are driven by T cell survival and homeostatic proliferation. *Nat Med,* 15**,** 893-900.

CHOU, T. C., MAGGIRWAR, N. S. & MARSDEN, M. D. 2024. HIV Persistence, Latency, and Cure Approaches: Where Are We Now? *Viruses,* 16**,** 1163.

CHUN, T. W., JUSTEMENT, J. S., MURRAY, D., HALLAHAN, C. W., MAENZA, J., COLLIER, A. C., SHETH, P. M., KAUL, R., OSTROWSKI, M., MOIR, S., KOVACS, C. & FAUCI, A. S. 2010. Rebound of plasma viremia following cessation of antiretroviral therapy despite profoundly low levels of HIV reservoir: implications for eradication. *Aids,* 24**,** 2803-8.

CHUN, T. W., STUYVER, L., MIZELL, S. B., EHLER, L. A., MICAN, J. A., BASELER, M., LLOYD, A. L., NOWAK, M. A. & FAUCI, A. S. 1997. Presence of an inducible HIV-1 latent reservoir during highly active antiretroviral therapy. *Proc Natl Acad Sci U S A,* 94**,** 13193-7.

CHURCHILL, M. J., DEEKS, S. G., MARGOLIS, D. M., SILICIANO, R. F. & SWANSTROM, R. 2016. HIV reservoirs: what, where and how to target them. *Nat Rev Microbiol,* 14**,** 55-60.

COHEN, M. S., GAY, C. L., BUSCH, M. P. & HECHT, F. M. 2010. The detection of acute HIV infection. *J Infect Dis,* 202 Suppl 2**,** S270-7.

COHEN, M. S., SHAW, G. M., MCMICHAEL, A. J. & HAYNES, B. F. 2011. Acute HIV-1 Infection. *N Engl J Med,* 364**,** 1943-54.

COHN, L. B., CHOMONT, N. & DEEKS, S. G. 2020. The Biology of the HIV-1 Latent Reservoir and Implications for Cure Strategies. *Cell Host Microbe,* 27**,** 519-530.

COLLORA, J. A., LIU, R., PINTO-SANTINI, D., RAVINDRA, N., GANOZA, C., LAMA, J. R., ALFARO, R., CHIARELLA, J., SPUDICH, S., MOUNZER, K., TEBAS, P., MONTANER, L. J., VAN DIJK, D., DUERR, A. & HO, Y. C. 2022. Single-cell multiomics reveals persistence of HIV-1 in expanded cytotoxic T cell clones. *Immunity,* 55**,** 1013-1031.e7.

CUEVAS, J. M., GELLER, R., GARIJO, R., LÓPEZ-ALDEGUER, J. & SANJUÁN, R. 2015. Extremely High Mutation Rate of HIV-1 In Vivo. *PLoS Biol,* 13**,** e1002251.

DALGLEISH, A. G., BEVERLEY, P. C., CLAPHAM, P. R., CRAWFORD, D. H., GREAVES, M. F. & WEISS, R. A. 1984. The CD4 (T4) antigen is an essential component of the receptor for the AIDS retrovirus. *Nature,* 312**,** 763-7.

DAVENPORT, M. P., KHOURY, D. S., CROMER, D., LEWIN, S. R., KELLEHER, A. D. & KENT, S. J. 2019. Functional cure of HIV: the scale of the challenge. *Nature Reviews Immunology,* 19**,** 45-54.

DE CLERCQ, J., RUTSAERT, S., DE SCHEERDER, M. A., VERHOFSTEDE, C., CALLENS, S. & VANDEKERCKHOVE, L. 2022. Benefits of antiretroviral therapy initiation during acute HIV infection. *Acta Clin Belg,* 77**,** 168-176.

DE COCK, K. M., JAFFE, H. W. & CURRAN, J. W. 2021. Reflections on 40 Years of AIDS. *Emerg Infect Dis,* 27**,** 1553-1560.

DE PASQUALE, M., KOURTEVA, Y., ALLOS, T. & D'AQUILA, R. T. 2013. Lower HIV provirus levels are associated with more APOBEC3G protein in blood resting memory CD4+ T lymphocytes of controllers in vivo. *PLoS One,* 8**,** e76002.

DEEKS, S. G., ARCHIN, N., CANNON, P., COLLINS, S., JONES, R. B., DE JONG, M., LAMBOTTE, O., LAMPLOUGH, R., NDUNG'U, T., SUGARMAN, J., TIEMESSEN, C. T., VANDEKERCKHOVE, L. & LEWIN, S. R. 2021. Research priorities for an HIV cure: International AIDS Society Global Scientific Strategy 2021. *Nat Med,* 27**,** 2085-2098.

DEEKS, S. G., OVERBAUGH, J., PHILLIPS, A. & BUCHBINDER, S. 2015. HIV infection. *Nature Reviews Disease Primers,* 1**,** 15035.

DESIMMIE, B. A., DELVIKS-FRANKENBERRRY, K. A., BURDICK, R. C., QI, D., IZUMI, T. & PATHAK, V. K. 2014. Multiple APOBEC3 restriction factors for HIV-1 and one Vif to rule them all. *J Mol Biol,* 426**,** 1220-45.

DONG, K. L., MOODLEY, A., KWON, D. S., GHEBREMICHAEL, M. S., DONG, M., ISMAIL, N., NDHLOVU, Z. M., MABUKA, J. M., MUEMA, D. M., PRETORIUS, K., LIN, N., WALKER, B. D. & NDUNG'U, T. 2018. Detection and treatment of Fiebig stage I HIV-1 infection in young at-risk women in South Africa: a prospective cohort study. *Lancet HIV,* 5**,** e35-e44.

DUETTE, G., HIENER, B., MORGAN, H., MAZUR, F. G., MATHIVANAN, V., HORSBURGH, B. A., FISHER, K., TONG, O., LEE, E., AHN, H., SHAIK, A., FROMENTIN, R., HOH, R., BACCHUS-SOUFFAN, C., NASR, N., CUNNINGHAM, A. L., HUNT, P. W., CHOMONT, N., TURVILLE, S. G., DEEKS, S. G., KELLEHER, A. D., SCHLUB, T. E. & PALMER, S. 2022. The HIV-1 proviral landscape reveals that Nef contributes to HIV-1 persistence in effector memory CD4+ T cells. *J Clin Invest,* 132.

DUFOUR, C., RICHARD, C., PARDONS, M., MASSANELLA, M., ACKAOUI, A., MURRELL, B., ROUTY, B., THOMAS, R., ROUTY, J.-P., FROMENTIN, R. & CHOMONT, N. 2023. Phenotypic characterization of single CD4+ T cells harboring genetically intact and inducible HIV genomes. *Nature Communications,* 14**,** 1115.

DYBUL, M., ATTOYE, T., BAPTISTE, S., CHERUTICH, P., DABIS, F., DEEKS, S. G., DIEFFENBACH, C., DOEHLE, B., GOODENOW, M. M., JIANG, A., KEMPS, D., LEWIN, S. R., LUMPKIN, M. M., MATHAE, L., MCCUNE, J. M., NDUNG'U, T., NSUBUGA, M., PEAY, H. L., POTTAGE, J., WARREN, M. & SIKAZWE, I. 2021. The case for an HIV cure and how to get there. *The Lancet HIV,* 8**,** e51-e58.

EINKAUF, K. B., OSBORN, M. R., GAO, C., SUN, W., SUN, X., LIAN, X., PARSONS, E. M., GLADKOV, G. T., SEIGER, K. W., BLACKMER, J. E., JIANG, C., YUKL, S. A., ROSENBERG, E. S., YU, X. G. & LICHTERFELD, M. 2022. Parallel analysis of transcription, integration, and sequence of single HIV-1 proviruses. *Cell,* 185**,** 266-282.e15.

ELLERY, P. J., TIPPETT, E., CHIU, Y. L., PAUKOVICS, G., CAMERON, P. U., SOLOMON, A., LEWIN, S. R., GORRY, P. R., JAWOROWSKI, A., GREENE, W. C., SONZA, S. & CROWE, S. M. 2007. The CD16+ monocyte subset is more permissive to infection and preferentially harbors HIV-1 in vivo. *J Immunol,* 178**,** 6581-9.

ENGELMAN, A. & CHEREPANOV, P. 2012. The structural biology of HIV-1: mechanistic and therapeutic insights. *Nat Rev Microbiol,* 10**,** 279-90.

ERIKSSON, S., GRAF, E. H., DAHL, V., STRAIN, M. C., YUKL, S. A., LYSENKO, E. S., BOSCH, R. J., LAI, J., CHIOMA, S., EMAD, F., ABDEL-MOHSEN, M., HOH, R., HECHT, F., HUNT, P., SOMSOUK, M., WONG, J., JOHNSTON, R., SILICIANO, R. F., RICHMAN, D. D., O'DOHERTY, U., PALMER, S., DEEKS, S. G. & SILICIANO, J. D. 2013. Comparative analysis of measures of viral reservoirs in HIV-1 eradication studies. *PLoS Pathog,* 9**,** e1003174.

FARROW, M. A. & SHEEHY, A. M. 2008. Vif and Apobec3G in the innate immune response to HIV: a tale of two proteins. *Future Microbiol,* 3**,** 145-54.

FENWICK, C., JOO, V., JACQUIER, P., NOTO, A., BANGA, R., PERREAU, M. & PANTALEO, G. 2019. T-cell exhaustion in HIV infection. *Immunol Rev,* 292**,** 149-163.

FEOLA, D. J., THORNTON, A. C. & GARVY, B. A. 2006. Effects of antiretroviral therapy on immunity in patients infected with HIV. *Curr Pharm Des,* 12**,** 1015-22.

FIEBIG, E. W., WRIGHT, D. J., RAWAL, B. D., GARRETT, P. E., SCHUMACHER, R. T., PEDDADA, L., HELDEBRANT, C., SMITH, R., CONRAD, A., KLEINMAN, S. H. & BUSCH, M. P. 2003. Dynamics of HIV viremia and antibody seroconversion in plasma donors: implications for diagnosis and staging of primary HIV infection. *Aids,* 17**,** 1871-9.

FINZI, D., BLANKSON, J., SILICIANO, J. D., MARGOLICK, J. B., CHADWICK, K., PIERSON, T., SMITH, K., LISZIEWICZ, J., LORI, F., FLEXNER, C., QUINN, T. C., CHAISSON, R. E., ROSENBERG, E., WALKER, B., GANGE, S., GALLANT, J. & SILICIANO, R. F. 1999. Latent infection of CD4+ T cells provides a mechanism for lifelong persistence of HIV-1, even in patients on effective combination therapy. *Nat Med,* 5**,** 512-7.

FINZI, D., HERMANKOVA, M., PIERSON, T., CARRUTH, L. M., BUCK, C., CHAISSON, R. E., QUINN, T. C., CHADWICK, K., MARGOLICK, J., BROOKMEYER, R., GALLANT, J., MARKOWITZ, M., HO, D. D., RICHMAN, D. D. & SILICIANO, R. F. 1997. Identification of a reservoir for HIV-1 in patients on highly active antiretroviral therapy. *Science,* 278**,** 1295-300.

FOLKS, T. M., POWELL, D., LIGHTFOOTE, M., KOENIG, S., FAUCI, A. S., BENN, S., RABSON, A., DAUGHERTY, D., GENDELMAN, H. E., HOGGAN, M. D. & ET AL. 1986. Biological and biochemical characterization of a cloned Leu-3- cell surviving infection with the acquired immune deficiency syndrome retrovirus. *J Exp Med,* 164**,** 280-90.

FRANK, I., ACHARYA, A., ROUTHU, N. K., ARAVANTINOU, M., HARPER, J. L., MALDONADO, S., SOLE CIGOLI, M., SEMOVA, S., MAZEL, S., PAIARDINI, M., DERBY, N., BYRAREDDY, S. N. & MARTINELLI, E. 2019. A Tat/Rev Induced Limiting Dilution Assay to Measure Viral Reservoirs in Non-Human Primate Models of HIV Infection. *Sci Rep,* 9**,** 12078.

GALLO, R. C., SALAHUDDIN, S. Z., POPOVIC, M., SHEARER, G. M., KAPLAN, M., HAYNES, B. F., PALKER, T. J., REDFIELD, R., OLESKE, J., SAFAI, B. & ET AL. 1984. Frequent detection and isolation of cytopathic retroviruses (HTLV-III) from patients with AIDS and at risk for AIDS. *Science,* 224**,** 500-3.

GANDHI, R. T., CYKTOR, J. C., BOSCH, R. J., MAR, H., LAIRD, G. M., MARTIN, A., COLLIER, A. C., RIDDLER, S. A., MACATANGAY, B. J., RINALDO, C. R., ERON, J. J., SILICIANO, J. D., MCMAHON, D. K. & MELLORS, J. W. 2021. Selective Decay of Intact HIV-1 Proviral DNA on Antiretroviral Therapy. *J Infect Dis,* 223**,** 225-233.

GANOR, Y., REAL, F., SENNEPIN, A., DUTERTRE, C. A., PREVEDEL, L., XU, L., TUDOR, D., CHARMETEAU, B., COUEDEL-COURTEILLE, A., MARION, S., ZENAK, A. R., JOURDAIN, J. P., ZHOU, Z., SCHMITT, A., CAPRON, C., EUGENIN, E. A., CHEYNIER, R., REVOL, M., CRISTOFARI, S., HOSMALIN, A. & BOMSEL, M. 2019. HIV-1 reservoirs in urethral macrophages of patients under suppressive antiretroviral therapy. *Nat Microbiol,* 4**,** 633-644.

GAO, F., BAILES, E., ROBERTSON, D. L., CHEN, Y., RODENBURG, C. M., MICHAEL, S. F., CUMMINS, L. B., ARTHUR, L. O., PEETERS, M., SHAW, G. M., SHARP, P. M. & HAHN, B. H. 1999. Origin of HIV-1 in the chimpanzee Pan troglodytes troglodytes. *Nature,* 397**,** 436-41.

GARTNER, M. J., ROCHE, M., CHURCHILL, M. J., GORRY, P. R. & FLYNN, J. K. 2020. Understanding the mechanisms driving the spread of subtype C HIV-1. *EBioMedicine,* 53**,** 102682.

GONZALO-GIL, E., IKEDIOBI, U. & SUTTON, R. E. 2017. Mechanisms of Virologic Control and Clinical Characteristics of HIV+ Elite/Viremic Controllers. *Yale J Biol Med,* 90**,** 245-259.

GOSMANN, C., ANAHTAR, M. N., HANDLEY, S. A., FARCASANU, M., ABU-ALI, G., BOWMAN, B. A., PADAVATTAN, N., DESAI, C., DROIT, L., MOODLEY, A., DONG, M., CHEN, Y., ISMAIL, N., NDUNG'U, T., GHEBREMICHAEL, M. S., WESEMANN, D. R., MITCHELL, C., DONG, K. L., HUTTENHOWER, C., WALKER, B. D., VIRGIN, H. W. & KWON, D. S. 2017. Lactobacillus-Deficient Cervicovaginal Bacterial Communities Are Associated with Increased HIV Acquisition in Young South African Women. *Immunity,* 46**,** 29-37.

GOTTLIEB, M. S. 1996. From the Centers for Disease Control and Prevention. Pneumocystis pneumonia--Los Angeles, 1981. *Jama,* 276**,** 1020-2.

GOTTLIEB, M. S., SCHROFF, R., SCHANKER, H. M., WEISMAN, J. D., FAN, P. T., WOLF, R. A. & SAXON, A. 1981. Pneumocystis carinii pneumonia and mucosal candidiasis in previously healthy homosexual men: evidence of a new acquired cellular immunodeficiency. *N Engl J Med,* 305**,** 1425-31.

GULICK, R. M., MELLORS, J. W., HAVLIR, D., ERON, J. J., GONZALEZ, C., MCMAHON, D., RICHMAN, D. D., VALENTINE, F. T., JONAS, L., MEIBOHM, A., EMINI, E. A. & CHODAKEWITZ, J. A. 1997. Treatment with indinavir, zidovudine, and lamivudine in adults with human immunodeficiency virus infection and prior antiretroviral therapy. *N Engl J Med,* 337**,** 734-9.

GUPTA, P., SANYAL, A. & MAILLIARD, R. B. 2017. TZA: a novel assay for measuring the latent HIV-1 reservoir. *Expert Rev Mol Diagn,* 17**,** 1033-1035.

HAMMER, S. M., SQUIRES, K. E., HUGHES, M. D., GRIMES, J. M., DEMETER, L. M., CURRIER, J. S., ERON, J. J., JR., FEINBERG, J. E., BALFOUR, H. H., JR., DEYTON, L. R., CHODAKEWITZ, J. A. & FISCHL, M. A. 1997. A controlled trial of two nucleoside analogues plus indinavir in persons with human immunodeficiency virus infection and CD4 cell counts of 200 per cubic millimeter or less. AIDS Clinical Trials Group 320 Study Team. *N Engl J Med,* 337**,** 725-33.

HARRICH, D. & HOOKER, B. 2002. Mechanistic aspects of HIV-1 reverse transcription initiation. *Rev Med Virol,* 12**,** 31-45.

HARRIS, R. S., BISHOP, K. N., SHEEHY, A. M., CRAIG, H. M., PETERSEN-MAHRT, S. K., WATT, I. N., NEUBERGER, M. S. & MALIM, M. H. 2003. DNA deamination mediates innate immunity to retroviral infection. *Cell,* 113**,** 803-9.

HARRIS, R. S. & DUDLEY, J. P. 2015. APOBECs and virus restriction. *Virology,* 479-480**,** 131-45.

HEMELAAR, J., ELANGOVAN, R., YUN, J., DICKSON-TETTEH, L., FLEMINGER, I., KIRTLEY, S., WILLIAMS, B., GOUWS-WILLIAMS, E. & GHYS, P. D. 2019. Global and regional molecular epidemiology of HIV-1, 1990-2015: a systematic review, global survey, and trend analysis. *Lancet Infect Dis,* 19**,** 143-155.

HIENER, B., EDEN, J. S., HORSBURGH, B. A. & PALMER, S. 2018. Amplification of Near Full-length HIV-1 Proviruses for Next-Generation Sequencing. *J Vis Exp*.

HIENER, B., HORSBURGH, B. A., EDEN, J. S., BARTON, K., SCHLUB, T. E., LEE, E., VON STOCKENSTROM, S., ODEVALL, L., MILUSH, J. M., LIEGLER, T., SINCLAIR, E., HOH, R., BORITZ, E. A., DOUEK, D., FROMENTIN, R., CHOMONT, N., DEEKS, S. G., HECHT, F. M. & PALMER, S. 2017. Identification of Genetically Intact HIV-1 Proviruses in Specific CD4(+) T Cells from Effectively Treated Participants. *Cell Rep,* 21**,** 813-822.

HITCHCOCK, A. M., KUFEL, W. D., DWYER, K. A. M. & SIDMAN, E. F. 2024. Lenacapavir: A novel injectable HIV-1 capsid inhibitor. *Int J Antimicrob Agents,* 63**,** 107009.

HO, Y. C., SHAN, L., HOSMANE, N. N., WANG, J., LASKEY, S. B., ROSENBLOOM, D. I., LAI, J., BLANKSON, J. N., SILICIANO, J. D. & SILICIANO, R. F. 2013. Replication-competent noninduced proviruses in the latent reservoir increase barrier to HIV-1 cure. *Cell,* 155**,** 540-51.

HONEYCUTT, J. B., WAHL, A., BAKER, C., SPAGNUOLO, R. A., FOSTER, J., ZAKHAROVA, O., WIETGREFE, S., CARO-VEGAS, C., MADDEN, V., SHARPE, G., HAASE, A. T., ERON, J. J. & GARCIA, J. V. 2016. Macrophages sustain HIV replication in vivo independently of T cells. *J Clin Invest,* 126**,** 1353-66.

HORSBURGH, B. A., LEE, E., HIENER, B., EDEN, J. S., SCHLUB, T. E., VON STOCKENSTROM, S., ODEVALL, L., MILUSH, J. M., LIEGLER, T., SINCLAIR, E., HOH, R., BORITZ, E. A., DOUEK, D. C., FROMENTIN, R., CHOMONT, N., DEEKS, S. G., HECHT, F. M. & PALMER, S. 2020. High levels of genetically intact HIV in HLA-DR+ memory T cells indicates their value for reservoir studies. *Aids,* 34**,** 659-668.

HOSSAIN, T., LUNGU, C., DE SCHRIJVER, S., KUALI, M., CRESPO, R., REDDY, N., NGUBANE, A., KAN, T. W., REDDY, K., RAO, S., PALSTRA, R. J., MADLALA, P., NDUNG'U, T. & MAHMOUDI, T. 2024. Specific quantification of inducible HIV-1 reservoir by RT-LAMP. *Commun Med (Lond),* 4**,** 123.

HOSSAIN, T., LUNGU, C., SCHRIJVER, S. D., KUALI, M., RAO, S., NGUBANE, A., KAN, T. W., PALSTRA, R.-J., MADLALA, P., NDUNG'U, T. & MAHMOUDI, T. 2023. SQuHIVLa: A novel assay for Specific Quantification of inducible HIV-1 reservoir by LAMP. *bioRxiv***,** 2023.07.14.548928.

HU, Z., LUO, Z., WAN, Z., WU, H., LI, W., ZHANG, T. & JIANG, W. 2015. HIV-associated memory B cell perturbations. *Vaccine,* 33**,** 2524-9.

HULTQUIST, J. F., LENGYEL, J. A., REFSLAND, E. W., LARUE, R. S., LACKEY, L., BROWN, W. L. & HARRIS, R. S. 2011. Human and rhesus APOBEC3D, APOBEC3F, APOBEC3G, and APOBEC3H demonstrate a conserved capacity to restrict Vif-deficient HIV-1. *J Virol,* 85**,** 11220-34.

HÜTTER, G., NOWAK, D., MOSSNER, M., GANEPOLA, S., MÜSSIG, A., ALLERS, K., SCHNEIDER, T., HOFMANN, J., KÜCHERER, C., BLAU, O., BLAU, I. W., HOFMANN, W. K. & THIEL, E. 2009. Long-term control of HIV by CCR5 Delta32/Delta32 stem-cell transplantation. *N Engl J Med,* 360**,** 692-8.

IKEDA, T., SHIMIZU, R., NASSER, H., CARPENTER, M. A., CHENG, A. Z., BROWN, W. L., SAUTER, D. & HARRIS, R. S. 2023. APOBEC3 degradation is the primary function of HIV-1 Vif determining virion infectivity in the myeloid cell line THP-1. *mBio,* 14**,** e0078223.

IKEDA, T., YUE, Y., SHIMIZU, R. & NASSER, H. 2021. Potential Utilization of APOBEC3-Mediated Mutagenesis for an HIV-1 Functional Cure. *Front Microbiol,* 12**,** 686357.

IMAMICHI, H., SMITH, M., ADELSBERGER, J. W., IZUMI, T., SCRIMIERI, F., SHERMAN, B. T., REHM, C. A., IMAMICHI, T., PAU, A., CATALFAMO, M., FAUCI, A. S. & LANE, H. C. 2020. Defective HIV-1 proviruses produce viral proteins. *Proc Natl Acad Sci U S A,* 117**,** 3704-3710.

JAIN, V., HARTOGENSIS, W., BACCHETTI, P., HUNT, P. W., HATANO, H., SINCLAIR, E., EPLING, L., LEE, T. H., BUSCH, M. P., MCCUNE, J. M., PILCHER, C. D., HECHT, F. M. & DEEKS, S. G. 2013. Antiretroviral therapy initiated within 6 months of HIV infection is associated with lower T-cell activation and smaller HIV reservoir size. *J Infect Dis,* 208**,** 1202-11.

JESUDASON, T. 2023. Global progress reported for AIDS. *The Lancet Infectious Diseases,* 23**,** e342.

JONES, B. R., MILLER, R. L., KINLOCH, N. N., TSAI, O., RIGSBY, H., SUDDERUDDIN, H., SHAHID, A., GANASE, B., BRUMME, C. J., HARRIS, M., POON, A. F. Y., BROCKMAN, M. A., FROMENTIN, R., CHOMONT, N., JOY, J. B. & BRUMME, Z. L. 2020. Genetic Diversity, Compartmentalization, and Age of HIV Proviruses Persisting in CD4(+) T Cell Subsets during Long-Term Combination Antiretroviral Therapy. *J Virol,* 94.

JONES, R. B. & WALKER, B. D. 2016. HIV-specific $CD8^+$ T cells and HIV eradication. *J Clin Invest,* 126**,** 455-63.

KANDATHIL, A. J., SUGAWARA, S. & BALAGOPAL, A. 2016. Are T cells the only HIV-1 reservoir? *Retrovirology,* 13**,** 86.

KAZER, S. W., WALKER, B. D. & SHALEK, A. K. 2020. Evolution and Diversity of Immune Responses during Acute HIV Infection. *Immunity,* 53**,** 908-924.

KEARNEY, M. F., WIEGAND, A., SHAO, W., MCMANUS, W. R., BALE, M. J., LUKE, B., MALDARELLI, F., MELLORS, J. W. & COFFIN, J. M. 2017. Ongoing HIV Replication During ART Reconsidered. *Open Forum Infect Dis,* 4**,** ofx173.

KOITO, A. & IKEDA, T. 2012. Apolipoprotein B mRNA-editing, catalytic polypeptide cytidine deaminases and retroviral restriction. *Wiley Interdiscip Rev RNA,* 3**,** 529-41.

KONING, F. A., NEWMAN, E. N., KIM, E. Y., KUNSTMAN, K. J., WOLINSKY, S. M. & MALIM, M. H. 2009. Defining APOBEC3 expression patterns in human tissues and hematopoietic cell subsets. *J Virol,* 83**,** 9474-85.

KOURTEVA, Y., DE PASQUALE, M., ALLOS, T., MCMUNN, C. & D'AQUILA, R. T. 2012. APOBEC3G expression and hypermutation are inversely associated with human immunodeficiency virus type 1 (HIV-1) burden in vivo. *Virology,* 430**,** 1-9.

KUNIHOLM, J., COOTE, C. & HENDERSON, A. J. 2022. Defective HIV-1 genomes and their potential impact on HIV pathogenesis. *Retrovirology,* 19**,** 13.

KWOK, J. S. Y., CHEUNG, S. K. F., HO, J. C. Y., TANG, I. W. H., CHU, P. W. K., LEUNG, E. Y. S., LEE, P. P. W., CHEUK, D. K. L., LEE, V., IP, P. & LAU, Y. L. 2020. Establishing Simultaneous T Cell Receptor Excision Circles (TREC) and K-Deleting Recombination Excision Circles (KREC) Quantification Assays and Laboratory Reference Intervals in Healthy Individuals of Different Age Groups in Hong Kong. *Front Immunol,* 11**,** 1411.

KWON, K. J., TIMMONS, A. E., SENGUPTA, S., SIMONETTI, F. R., ZHANG, H., HOH, R., DEEKS, S. G., SILICIANO, J. D. & SILICIANO, R. F. 2020. Different human resting memory CD4(+) T cell subsets show similar low inducibility of latent HIV-1 proviruses. *Sci Transl Med,* 12.

LAIRD, G. M., ROSENBLOOM, D. I., LAI, J., SILICIANO, R. F. & SILICIANO, J. D. 2016. Measuring the Frequency of Latent HIV-1 in Resting $CD4^+$ T Cells Using a Limiting Dilution Coculture Assay. *Methods Mol Biol,* 1354**,** 239-53.

LAMBRECHTS, L., COLE, B., RUTSAERT, S., TRYPSTEEN, W. & VANDEKERCKHOVE, L. 2020. Emerging PCR-Based Techniques to Study HIV-1 Reservoir Persistence. *Viruses,* 12.

LECOSSIER, D., BOUCHONNET, F., CLAVEL, F. & HANCE, A. J. 2003. Hypermutation of HIV-1 DNA in the absence of the Vif protein. *Science,* 300**,** 1112.

LEE, E., BACCHETTI, P., MILUSH, J., SHAO, W., BORITZ, E., DOUEK, D., FROMENTIN, R., LIEGLER, T., HOH, R., DEEKS, S. G., HECHT, F. M., CHOMONT, N. & PALMER, S. 2019a. Memory CD4 + T-Cells Expressing HLA-DR Contribute to HIV Persistence During Prolonged Antiretroviral Therapy. *Front Microbiol,* 10**,** 2214.

LEE, G. Q. 2021. Chemistry and Bioinformatics Considerations in Using Next-Generation Sequencing Technologies to Inferring HIV Proviral DNA Genome-Intactness. *Viruses,* 13.

LEE, G. Q. & LICHTERFELD, M. 2016. Diversity of HIV-1 reservoirs in CD4+ T-cell subpopulations. *Curr Opin HIV AIDS,* 11**,** 383-7.

LEE, G. Q., ORLOVA-FINK, N., EINKAUF, K., CHOWDHURY, F. Z., SUN, X., HARRINGTON, S., KUO, H. H., HUA, S., CHEN, H. R., OUYANG, Z., REDDY, K., DONG, K., NDUNG'U, T., WALKER, B. D., ROSENBERG, E. S., YU, X. G. & LICHTERFELD, M. 2017. Clonal expansion of genome-intact HIV-1 in functionally polarized Th1 CD4+ T cells. *J Clin Invest,* 127**,** 2689-2696.

LEE, G. Q., REDDY, K., EINKAUF, K. B., GOUNDER, K., CHEVALIER, J. M., DONG, K. L., WALKER, B. D., YU, X. G., NDUNG'U, T. & LICHTERFELD, M. 2019b. HIV-1 DNA sequence diversity and evolution during acute subtype C infection. *Nat Commun,* 10**,** 2737.

LEE, S. K., SONDGEROTH, A., XU, Y., WARREN, J., ZHOU, S., GILLEECE, M., HAUSER, B. M., GAY, C. L., KURUC, J. D., ARCHIN, N. M., ERON, J. J., MARGOLIS, D. M., GOONETILLEKE, N. & SWANSTROM, R. 2024. Sequence Analysis of Inducible, Replication-Competent Virus Reveals No Evidence of HIV-1 Evolution During Suppressive Antiviral Therapy, Indicating a Lack of Ongoing Viral Replication. *Open Forum Infect Dis,* 11**,** ofae212.

LEWIN, S. R. & ROUZIOUX, C. 2011. HIV cure and eradication: how will we get from the laboratory to effective clinical trials? *Aids,* 25**,** 885-97.

LI, G., PIAMPONGSANT, S., FARIA, N. R., VOET, A., PINEDA-PEÑA, A.-C., KHOURI, R., LEMEY, P., VANDAMME, A.-M. & THEYS, K. 2015. An integrated map of HIV genome-wide variation from a population perspective. *Retrovirology,* 12**,** 18.

LI, J. Z. & BLANKSON, J. N. 2021. How elite controllers and posttreatment controllers inform our search for an HIV-1 cure. *J Clin Invest,* 131.

LI, X., SINGH, N. K., COLLINS, D. R., NG, R., ZHANG, A., LAMOTHE-MOLINA, P. A., SHAHINIAN, P., XU, S., TAN, K., PIECHOCKA-TROCHA, A., URBACH, J. M., WEBER, J. K., GAIHA, G. D., TAKOU MBAH, O. C., HUYNH, T., CHEEVER, S., CHEN, J., BIRNBAUM, M., ZHOU, R.,

WALKER, B. D. & WANG, J. H. 2023. Molecular basis of differential HLA class I-restricted T cell recognition of a highly networked HIV peptide. *Nat Commun,* 14**,** 2929.

LIU, R., PAXTON, W. A., CHOE, S., CERADINI, D., MARTIN, S. R., HORUK, R., MACDONALD, M. E., STUHLMANN, H., KOUP, R. A. & LANDAU, N. R. 1996. Homozygous defect in HIV-1 coreceptor accounts for resistance of some multiply-exposed individuals to HIV-1 infection. *Cell,* 86**,** 367-77.

LORENZO-REDONDO, R., FRYER, H. R., BEDFORD, T., KIM, E. Y., ARCHER, J., POND, S. L. K., CHUNG, Y. S., PENUGONDA, S., CHIPMAN, J., FLETCHER, C. V., SCHACKER, T. W., MALIM, M. H., RAMBAUT, A., HAASE, A. T., MCLEAN, A. R. & WOLINSKY, S. M. 2016. Persistent HIV-1 replication maintains the tissue reservoir during therapy. *Nature,* 530**,** 51-56.

LUNGU, C., BANGA, R., GRUTERS, R. A. & PROCOPIO, F. A. 2021. Inducible HIV-1 Reservoir Quantification: Clinical Relevance, Applications and Advancements of TILDA. *Front Microbiol,* 12**,** 686690.

LUNGU, C. & PROCOPIO, F. A. 2022. TILDA: Tat/Rev Induced Limiting Dilution Assay. *Methods Mol Biol,* 2407**,** 365-372.

LYNCH, H. E. & SEMPOWSKI, G. D. 2013. Molecular measurement of T cell receptor excision circles. *Methods Mol Biol,* 979**,** 147-59.

MALIM, M. H. & BIENIASZ, P. D. 2012. HIV Restriction Factors and Mechanisms of Evasion. *Cold Spring Harb Perspect Med,* 2**,** a006940.

MASSANELLA, M., IGNACIO, R. A. B., LAMA, J. R., PAGLIUZZA, A., DASGUPTA, S., ALFARO, R., RIOS, J., GANOZA, C., PINTO-SANTINI, D., GILADA, T., DUERR, A. & CHOMONT, N. 2021. Long-term effects of early antiretroviral initiation on HIV reservoir markers: a longitudinal analysis of the MERLIN clinical study. *Lancet Microbe,* 2**,** e198-e209.

MASTRANGELO, A., BANGA, R. & PERREAU, M. 2022. Elite and posttreatment controllers, two facets of HIV control. *Curr Opin HIV AIDS,* 17**,** 325-332.

MATSUDA, K. & MAEDA, K. 2024. HIV Reservoirs and Treatment Strategies toward Curing HIV Infection. *International Journal of Molecular Sciences,* 25**,** 2621.

MENÉNDEZ-ARIAS, L. & DELGADO, R. 2022. Update and latest advances in antiretroviral therapy. *Trends Pharmacol Sci,* 43**,** 16-29.

MIKHAEL, N. L. & ELSORADY, M. 2019. Clinical significance of T cell receptor excision circle (TREC) quantitation after allogenic HSCT. *Blood Res,* 54**,** 274-281.

MOHAMMADI, A., ETEMAD, B., ZHANG, X., LI, Y., BEDWELL, G. J., SHARAF, R., KITTILSON, A., MELBERG, M., WONG, C., FAJNZYLBER, J., WORRALL, D. P., ROSENTHAL, A., JORDAN, H., JILG, N., KASEKE, C., GIGUEL, F., LIAN, X., DEO, R., GILLESPIE, E., CHISHTI, R., ABRHA, S., ADAMS, T., SIAGIAN, A., ANDERSON, P. L., DEEKS, S. G., LEDERMAN, M. M., YAWETZ, S., KURITZKES, D. R., LICHTERFELD, M. D., TSIBRIS, A., CARRINGTON, M., BRUMME, Z. L., CASTILLO-MANCILLA, J. R., ENGELMAN, A. N., GAIHA, G. D. & LI, J. Z. 2023. Viral and Host Mediators of Non-Suppressible HIV-1 Viremia. *medRxiv*.

MOIR, S. & FAUCI, A. S. 2017. B-cell responses to HIV infection. *Immunol Rev,* 275**,** 33-48.

MUEMA, D. M., AKILIMALI, N. A., NDUMNEGO, O. C., RASEHLO, S. S., DURGIAH, R., OJWACH, D. B. A., ISMAIL, N., DONG, M., MOODLEY, A., DONG, K. L., NDHLOVU, Z. M., MABUKA, J. M., WALKER, B. D., MANN, J. K. & NDUNG'U, T. 2020. Association between the cytokine storm, immune cell dynamics, and viral replicative capacity in hyperacute HIV infection. *BMC Med,* 18**,** 81.

MUSSIL, B., SAUERMANN, U., MOTZKUS, D., STAHL-HENNIG, C. & SOPPER, S. 2011. Increased APOBEC3G and APOBEC3F expression is associated with low viral load and prolonged survival in simian immunodeficiency virus infected rhesus monkeys. *Retrovirology,* 8**,** 77.

NACHEGA, J. B., MUSOKE, P., KILMARX, P. H., GANDHI, M., GRINSZTEJN, B., POZNIAK, A., RAWAT, A., WILSON, L., MILLS, E. J., ALTICE, F. L., MELLORS, J. W. & QUINN, T. C. 2023. Global HIV control: is the glass half empty or half full? *The Lancet HIV,* 10**,** e617-e622.

NAIDOO, K. K., HIGHTON, A. J., BAIYEGUNHI, O. O., BHENGU, S. P., DONG, K. L., BUNDERS, M. J., ALTFELD, M. & NDUNG'U, T. 2024. Early Initiation of Antiretroviral Therapy Preserves the Metabolic Function of CD4+ T Cells in Subtype C Human Immunodeficiency Virus 1 Infection. *J Infect Dis,* 229**,** 753-762.

NAIDOO, K. K., NDUMNEGO, O. C., ISMAIL, N., DONG, K. L. & NDUNG'U, T. 2021. Antigen Presenting Cells Contribute to Persistent Immune Activation Despite Antiretroviral Therapy Initiation During Hyperacute HIV-1 Infection. *Front Immunol,* 12**,** 738743.

NAIF, H. M. 2013. Pathogenesis of HIV Infection. *Infect Dis Rep,* 5**,** e6.

NDHLOVU, Z. M., KAMYA, P., MEWALAL, N., KLØVERPRIS, H. N., NKOSI, T., PRETORIUS, K., LAHER, F., OGUNSHOLA, F., CHOPERA, D., SHEKHAR, K., GHEBREMICHAEL, M., ISMAIL, N., MOODLEY, A., MALIK, A., LESLIE, A., GOULDER, P. J., BUUS, S., CHAKRABORTY, A., DONG, K., NDUNG'U, T. & WALKER, B. D. 2015. Magnitude and Kinetics of CD8+ T Cell Activation during Hyperacute HIV Infection Impact Viral Set Point. *Immunity,* 43**,** 591-604.

NDUNG'U, T., DONG, K. L., KWON, D. S. & WALKER, B. D. 2018. A FRESH approach: Combining basic science and social good. *Sci Immunol,* 3.

NDUNG'U, T., MCCUNE, J. M. & DEEKS, S. G. 2019. Why and where an HIV cure is needed and how it might be achieved. *Nature,* 576**,** 397-405.

NG, C. T., SNELL, L. M., BROOKS, D. G. & OLDSTONE, M. B. 2013. Networking at the level of host immunity: immune cell interactions during persistent viral infections. *Cell Host Microbe,* 13**,** 652-64.

OGBENNA, A. A., MELONI, S., INZAULE, S., HAMERS, R. L., SIGALOFF, K., OSIBOGUN, A., ADEYEMO, T. A., OKONKWO, P., SAMUELS, J. O., KANKI, P. J., RINKE DE WIT, T. F. & AKANMU, A. S. 2020. The impact of HIV-1 subtypes on virologic and immunologic treatment outcomes at the Lagos University Teaching Hospital: A longitudinal evaluation. *PLoS One,* 15**,** e0238027.

OOMS, M., BRAYTON, B., LETKO, M., MAIO, S. M., PILCHER, C. D., HECHT, F. M., BARBOUR, J. D. & SIMON, V. 2013. HIV-1 Vif adaptation to human APOBEC3H haplotypes. *Cell Host Microbe,* 14**,** 411-21.

PACE, M. & FRATER, J. 2014. A cure for HIV: is it in sight? *Expert Rev Anti Infect Ther,* 12**,** 783-91.

PACE, M. & FRATER, J. 2019. Curing HIV by 'kick and kill': from theory to practice? *Expert Review of Anti-infective Therapy,* 17**,** 383-386.

PATEL, P., BORKOWF, C. B., BROOKS, J. T., LASRY, A., LANSKY, A. & MERMIN, J. 2014. Estimating per-act HIV transmission risk: a systematic review. *Aids,* 28**,** 1509-19.

PERELSON, A. S., ESSUNGER, P., CAO, Y., VESANEN, M., HURLEY, A., SAKSELA, K., MARKOWITZ, M. & HO, D. D. 1997. Decay characteristics of HIV-1-infected compartments during combination therapy. *Nature,* 387**,** 188-91.

PERSAUD, D., SIBERRY, G. K., AHONKHAI, A., KAJDAS, J., MONIE, D., HUTTON, N., WATSON, D. C., QUINN, T. C., RAY, S. C. & SILICIANO, R. F. 2004. Continued production of drug-sensitive human immunodeficiency virus type 1 in children on combination antiretroviral therapy who have undetectable viral loads. *J Virol,* 78**,** 968-79.

PINKEVYCH, M., FENNESSEY, C. M., CROMER, D., REID, C., TRUBEY, C. M., LIFSON, J. D., KEELE, B. F. & DAVENPORT, M. P. 2019. Predictors of SIV recrudescence following antiretroviral treatment interruption. *Elife,* 8**,** e49022.

POHLMEYER, C. W., BUCKHEIT, R. W., 3RD, SILICIANO, R. F. & BLANKSON, J. N. 2013. CD8+ T cells from HLA-B*57 elite suppressors effectively suppress replication of HIV-1 escape mutants. *Retrovirology,* 10**,** 152.

POLLACK, R. A., JONES, R. B., PERTEA, M., BRUNER, K. M., MARTIN, A. R., THOMAS, A. S., CAPOFERRI, A. A., BEG, S. A., HUANG, S. H., KARANDISH, S., HAO, H., HALPER-STROMBERG, E., YONG, P. C., KOVACS, C., BENKO, E., SILICIANO, R. F. & HO, Y. C. 2017. Defective HIV-1 Proviruses Are Expressed and Can Be Recognized by Cytotoxic T Lymphocytes, which Shape the Proviral Landscape. *Cell Host Microbe,* 21**,** 494-506.e4.

PROMER, K. & KARRIS, M. Y. 2018. Current Treatment Options for HIV Elite Controllers: a Review. *Curr Treat Options Infect Dis,* 10**,** 302-309.

PURCELL, D. F. & MARTIN, M. A. 1993. Alternative splicing of human immunodeficiency virus type 1 mRNA modulates viral protein expression, replication, and infectivity. *J Virol,* 67**,** 6365-78.

RAMJEE, G., WAND, H., WHITAKER, C., MCCORMACK, S., PADIAN, N., KELLY, C. & NUNN, A. 2012. HIV incidence among non-pregnant women living in selected rural, semi-rural and urban areas in KwaZulu-Natal, South Africa. *AIDS Behav,* 16**,** 2062-71.

RASHID, F., ZAONGO, S. D., IQBAL, H., HARYPURSAT, V., SONG, F. & CHEN, Y. 2024. Interactions between HIV proteins and host restriction factors: implications for potential therapeutic intervention in HIV infection. *Front Immunol,* 15**,** 1390650.

REDDY, K., LEE, G. Q., REDDY, N., CHIKOWORE, T. J. B., BAISLEY, K., DONG, K. L., WALKER, B. D., YU, X. G., LICHTERFELD, M. & NDUNG'U, T. 2024. Differences in HIV-1 reservoir size, landscape characteristics and decay dynamics in acute and chronic treated HIV-1 Clade C infection. *medRxiv***,** 2024.02.16.24302713.

REDDY, K., OOMS, M., LETKO, M., GARRETT, N., SIMON, V. & NDUNG'U, T. 2016. Functional characterization of Vif proteins from HIV-1 infected patients with different APOBEC3G haplotypes. *Aids,* 30**,** 1723-9.

REDDY, K., WINKLER, C. A., WERNER, L., MLISANA, K., ABDOOL KARIM, S. S. & NDUNG'U, T. 2010. APOBEC3G expression is dysregulated in primary HIV-1 infection and polymorphic variants influence CD4+ T-cell counts and plasma viral load. *Aids,* 24**,** 195-204.

REEVES, D. B., BACCHUS-SOUFFAN, C., FITCH, M., ABDEL-MOHSEN, M., HOH, R., AHN, H., STONE, M., HECHT, F., MARTIN, J., DEEKS, S. G., HELLERSTEIN, M. K., MCCUNE, J. M., SCHIFFER, J. T. & HUNT, P. W. 2023. Estimating the contribution of CD4 T cell subset proliferation and differentiation to HIV persistence. *Nat Commun,* 14**,** 6145.

REFSLAND, E. W., HULTQUIST, J. F., LUENGAS, E. M., IKEDA, T., SHABAN, N. M., LAW, E. K., BROWN, W. L., REILLY, C., EMERMAN, M. & HARRIS, R. S. 2014. Natural polymorphisms in human APOBEC3H and HIV-1 Vif combine in primary T lymphocytes to affect viral G-to-A mutation levels and infectivity. *PLoS Genet,* 10**,** e1004761.

REFSLAND, E. W., STENGLEIN, M. D., SHINDO, K., ALBIN, J. S., BROWN, W. L. & HARRIS, R. S. 2010. Quantitative profiling of the full APOBEC3 mRNA repertoire in lymphocytes and tissues: implications for HIV-1 restriction. *Nucleic Acids Res,* 38**,** 4274-84.

RICHMAN, D. D., MARGOLIS, D. M., DELANEY, M., GREENE, W. C., HAZUDA, D. & POMERANTZ, R. J. 2009. The challenge of finding a cure for HIV infection. *Science,* 323**,** 1304-7.

RODRÍGUEZ-MUÑOZ, J. & MORENO, S. 2019. Strategies for the cure of HIV infection. *Enfermedades Infecciosas y Microbiología Clínica (English Edition),* 37**,** 265-273.

ROSENBLOOM, D. I., ELLIOTT, O., HILL, A. L., HENRICH, T. J., SILICIANO, J. M. & SILICIANO, R. F. 2015. Designing and Interpreting Limiting Dilution Assays: General Principles and Applications to the Latent Reservoir for Human Immunodeficiency Virus-1. *Open Forum Infect Dis,* 2**,** ofv123.

ROSSI, E., MEUSER, M. E., CUNANAN, C. J. & COCKLIN, S. 2021. Structure, Function, and Interactions of the HIV-1 Capsid Protein. *Life (Basel),* 11.

ROUZIOUX, C. & AVETTAND-FENOËL, V. 2018. Total HIV DNA: a global marker of HIV persistence. *Retrovirology,* 15**,** 30.

SALAMANGO, D. J. & HARRIS, R. S. 2020. Dual Functionality of HIV-1 Vif in APOBEC3 Counteraction and Cell Cycle Arrest. *Front Microbiol,* 11**,** 622012.

SANDEFUR, S., SMITH, R. M., VARTHAKAVI, V. & SPEARMAN, P. 2000. Mapping and characterization of the N-terminal I domain of human immunodeficiency virus type 1 Pr55(Gag). *J Virol,* 74**,** 7238-49.

SANYAL, A., RANGACHAR, V. S. & GUPTA, P. 2019. TZA, a Sensitive Reporter Cell-based Assay to Accurately and Rapidly Quantify Inducible, Replication-competent Latent HIV-1 from Resting CD4(+) T Cells. *Bio Protoc,* 9.

SATTENTAU, QUENTIN J. & STEVENSON, M. 2016. Macrophages and HIV-1: An Unhealthy Constellation. *Cell Host & Microbe,* 19**,** 304-310.

SELHORST, P., COMBRINCK, C., NDABAMBI, N., ISMAIL, S. D., ABRAHAMS, M. R., LACERDA, M., SAMSUNDER, N., GARRETT, N., ABDOOL KARIM, Q., ABDOOL KARIM, S. S. & WILLIAMSON, C. 2017. Replication Capacity of Viruses from Acute Infection Drives HIV-1 Disease Progression. *J Virol,* 91.

SHARP, P. M. & HAHN, B. H. 2011. Origins of HIV and the AIDS pandemic. *Cold Spring Harb Perspect Med,* 1**,** a006841.

SHEEHY, A. M., GADDIS, N. C. & MALIM, M. H. 2003. The antiretroviral enzyme APOBEC3G is degraded by the proteasome in response to HIV-1 Vif. *Nat Med,* 9**,** 1404-7.

SHELTON, E. M., REEVES, D. B. & BENDER IGNACIO, R. A. 2020. Initiation of Antiretroviral Therapy during Primary HIV Infection: Effects on the Latent HIV Reservoir, Including on Analytic Treatment Interruptions. *AIDS Rev,* 23**,** 28-39.

SHEN, L. & SILICIANO, R. F. 2008. Viral reservoirs, residual viremia, and the potential of highly active antiretroviral therapy to eradicate HIV infection. *J Allergy Clin Immunol,* 122**,** 22-8.

SILICIANO, J. D., KAJDAS, J., FINZI, D., QUINN, T. C., CHADWICK, K., MARGOLICK, J. B., KOVACS, C., GANGE, S. J. & SILICIANO, R. F. 2003. Long-term follow-up studies confirm the stability of the latent reservoir for HIV-1 in resting CD4+ T cells. *Nat Med,* 9**,** 727-8.

SILICIANO, J. D. & SILICIANO, R. F. 2018. Assays to Measure Latency, Reservoirs, and Reactivation. *Curr Top Microbiol Immunol,* 417**,** 23-41.

SILICIANO, J. D. & SILICIANO, R. F. 2021. Low Inducibility of Latent Human Immunodeficiency Virus Type 1 Proviruses as a Major Barrier to Cure. *J Infect Dis,* 223**,** 13-21.

SILICIANO, R. F. & GREENE, W. C. 2011. HIV latency. *Cold Spring Harb Perspect Med,* 1**,** a007096.

SIMON, V., HO, D. D. & ABDOOL KARIM, Q. 2006. HIV/AIDS epidemiology, pathogenesis, prevention, and treatment. *Lancet,* 368**,** 489-504.

SIMON, V., ZENNOU, V., MURRAY, D., HUANG, Y., HO, D. D. & BIENIASZ, P. D. 2005. Natural variation in Vif: differential impact on APOBEC3G/3F and a potential role in HIV-1 diversification. *PLoS Pathog,* 1**,** e6.

SIMONETTI, F. R., WHITE, J. A., TUMIOTTO, C., RITTER, K. D., CAI, M., GANDHI, R. T., DEEKS, S. G., HOWELL, B. J., MONTANER, L. J., BLANKSON, J. N., MARTIN, A., LAIRD, G. M., SILICIANO, R. F., MELLORS, J. W. & SILICIANO, J. D. 2020. Intact proviral DNA assay analysis of large cohorts of people with HIV provides a benchmark for the frequency and composition of persistent proviral DNA. *Proc Natl Acad Sci U S A,* 117**,** 18692-18700.

SONG, C.-B., ZHANG, L.-L., WU, X., FU, Y.-J., JIANG, Y.-J., SHANG, H. & ZHANG, Z.-N. 2020. CD4+CD38+ central memory T cells contribute to HIV persistence in HIV-infected individuals on long-term ART. *Journal of Translational Medicine,* 18**,** 95.

SONZA, S., MUTIMER, H. P., OELRICHS, R., JARDINE, D., HARVEY, K., DUNNE, A., PURCELL, D. F., BIRCH, C. & CROWE, S. M. 2001. Monocytes harbour replication-competent, non-latent HIV-1 in patients on highly active antiretroviral therapy. *Aids,* 15**,** 17-22.

STERLING, T. R., VLAHOV, D., ASTEMBORSKI, J., HOOVER, D. R., MARGOLICK, J. B. & QUINN, T. C. 2001. Initial plasma HIV-1 RNA levels and progression to AIDS in women and men. *N Engl J Med,* 344**,** 720-5.

STOPAK, K., DE NORONHA, C., YONEMOTO, W. & GREENE, W. C. 2003. HIV-1 Vif blocks the antiviral activity of APOBEC3G by impairing both its translation and intracellular stability. *Mol Cell,* 12**,** 591-601.

STUPFLER, B., VERRIEZ, C., GALLOIS-MONTBRUN, S., MARQUET, R. & PAILLART, J. C. 2021. Degradation-Independent Inhibition of APOBEC3G by the HIV-1 Vif Protein. *Viruses,* 13.

SUN, W., GAO, C., HARTANA, C. A., OSBORN, M. R., EINKAUF, K. B., LIAN, X., BONE, B., BONHEUR, N., CHUN, T.-W., ROSENBERG, E. S., WALKER, B. D., YU, X. G. & LICHTERFELD, M. 2023. Phenotypic signatures of immune selection in HIV-1 reservoir cells. *Nature,* 614**,** 309-317.

TAKAORI-KONDO, A. 2006. APOBEC family proteins: novel antiviral innate immunity. *Int J Hematol,* 83**,** 213-6.

TANG, Y., CHAILLON, A., GIANELLA, S., WONG, L. M., LI, D., SIMERMEYER, T. L., PORRACHIA, M., IGNACIO, C., WOODWORTH, B., ZHONG, D., DU, J., DE LA PARRA POLINA, E., KIRCHHERR, J., ALLARD, B., CLOHOSEY, M. L., MOESER, M., SONDGEROTH, A. L., WHITEHILL, G. D., SINGH, V., DASHTI, A., SMITH, D. M., ERON, J. J., BAR, K. J., CHAHROUDI, A., JOSEPH, S. B., ARCHIN, N. M., MARGOLIS, D. M. & JIANG, G. 2023. Brain microglia serve as a persistent HIV reservoir despite durable antiretroviral therapy. *J Clin Invest,* 133.

THOMPSON, A. E. 2015. The Immune System. *JAMA,* 313**,** 1686-1686.

TURNER, B. G. & SUMMERS, M. F. 1999. Structural biology of HIV. *J Mol Biol,* 285**,** 1-32.

VAN ZYL, G., BALE, M. J. & KEARNEY, M. F. 2018. HIV evolution and diversity in ART-treated patients. *Retrovirology,* 15**,** 14.

VEENHUIS, R. T., ABREU, C. M., COSTA, P. A. G., FERREIRA, E. A., RATLIFF, J., POHLENZ, L., SHIRK, E. N., RUBIN, L. H., BLANKSON, J. N., GAMA, L. & CLEMENTS, J. E. 2023. Monocyte-derived macrophages contain persistent latent HIV reservoirs. *Nat Microbiol,* 8**,** 833-844.

VEMPARALA, B., CHOWDHURY, S., GUEDJ, J. & DIXIT, N. M. 2024. Modelling HIV-1 control and remission. *npj Systems Biology and Applications,* 10**,** 84.

VIDAL-FOLCH, N., MILOSEVIC, D., MAJUMDAR, R., GAVRILOV, D., MATERN, D., RAYMOND, K., RINALDO, P., TORTORELLI, S., ABRAHAM, R. S. & OGLESBEE, D. 2017. A Droplet Digital PCR Method for Severe Combined Immunodeficiency Newborn Screening. *J Mol Diagn,* 19**,** 755-765.

VIRGILIO, M. C. & COLLINS, K. L. 2020. The Impact of Cellular Proliferation on the HIV-1 Reservoir. *Viruses,* 12.

VOLBERDING, P. A. & DEEKS, S. G. 2010. Antiretroviral therapy and management of HIV infection. *Lancet,* 376**,** 49-62.

VOLMINK, J. & MARAIS, B. 2008. HIV: mother-to-child transmission. *BMJ Clin Evid,* 2008.

WANG, F. X., HUANG, J., ZHANG, H., MA, X. & ZHANG, H. 2008. APOBEC3G upregulation by alpha interferon restricts human immunodeficiency virus type 1 infection in human peripheral plasmacytoid dendritic cells. *J Gen Virol,* 89**,** 722-730.

WANG, Z., SIMONETTI, F. R., SILICIANO, R. F. & LAIRD, G. M. 2018. Measuring replication competent HIV-1: advances and challenges in defining the latent reservoir. *Retrovirology,* 15**,** 21.

WEISS, C. D., LEVY, J. A. & WHITE, J. M. 1990. Oligomeric organization of gp120 on infectious human immunodeficiency virus type 1 particles. *J Virol,* 64**,** 5674-7.

WERTHEIM, J. O. & WOROBEY, M. 2009. Dating the age of the SIV lineages that gave rise to HIV-1 and HIV-2. *PLoS Comput Biol,* 5**,** e1000377.

WILLIAMS, D. W., FLORES, B. R., XU, Y., WANG, Y., YU, D., PETERS, B. A., ADEDIMEJI, A., WILSON, T. E., MERENSTEIN, D., TIEN, P. C., COHEN, M. H., WEBER, K. M., ADIMORA, A. A., OFOTOKUN, I., FISCHL, M., TURAN, J., TURAN, B., LAUMET, G., LANDAY, A. L., DASTGHEYB, R. M., GANGE, S. J., WEISER, S. D. & RUBIN, L. H. 2022. T-cell activation state differentially contributes to neuropsychiatric complications in women with HIV. *Brain Behav Immun Health,* 25**,** 100498.

WOLDEMESKEL, B. A., KWAA, A. K. & BLANKSON, J. N. 2020. Viral reservoirs in elite controllers of HIV-1 infection: Implications for HIV cure strategies. *EBioMedicine,* 62**,** 103118.

WONG, E. B., OLIVIER, S., GUNDA, R., KOOLE, O., SURUJDEEN, A., GARETA, D., MUNATSI, D., MODISE, T. H., DREYER, J., NXUMALO, S., SMIT, T. K., ORDING-JESPERSEN, G., MPOFANA, I. B., KHAN, K., SIKHOSANA, Z. E. L., MOODLEY, S., SHEN, Y. J., KHOZA, T., MHLONGO, N., BUCIBO, S., NYAMANDE, K., BAISLEY, K. J., CUADROS, D., TANSER, F., GRANT, A. D., HERBST, K., SEELEY, J., HANEKOM, W. A., NDUNG'U, T., SIEDNER, M. J. & PILLAY, D. 2021. Convergence of infectious and non-communicable disease epidemics in rural South Africa: a cross-sectional, population-based multimorbidity study. *Lancet Glob Health,* 9**,** e967-e976.

XU, W., LI, H., WANG, Q., HUA, C., ZHANG, H., LI, W., JIANG, S. & LU, L. 2017. Advancements in Developing Strategies for Sterilizing and Functional HIV Cures. *Biomed Res Int,* 2017**,** 6096134.

YANG, O. O., SARKIS, P. T., ALI, A., HARLOW, J. D., BRANDER, C., KALAMS, S. A. & WALKER, B. D. 2003. Determinant of HIV-1 mutational escape from cytotoxic T lymphocytes. *J Exp Med,* 197**,** 1365-75.

ZERBATO, J. M., KHOURY, G., ZHAO, W., GARTNER, M. J., PASCOE, R. D., RHODES, A., DANTANARAYANA, A., GOOEY, M., ANDERSON, J., BACCHETTI, P., DEEKS, S. G., MCMAHON, J., ROCHE, M., RASMUSSEN, T. A., PURCELL, D. F. & LEWIN, S. R. 2021. Multiply spliced HIV RNA is a predictive measure of virus production ex vivo and in vivo following reversal of HIV latency. *EBioMedicine,* 65**,** 103241.

ZHANG, L., RAMRATNAM, B., TENNER-RACZ, K., HE, Y., VESANEN, M., LEWIN, S., TALAL, A., RACZ, P., PERELSON, A. S., KORBER, B. T., MARKOWITZ, M. & HO, D. D. 1999. Quantifying residual HIV-1 replication in patients receiving combination antiretroviral therapy. *N Engl J Med,* 340**,** 1605-13.

ZHANG, X. & CHEN, J. 2023. HIV Reservoir: How to Measure It? *Curr HIV/AIDS Rep,* 20**,** 29-41.

ZHAO, J. C. & DENG, K. 2020. Heterogeneity of HIV-1 latent reservoirs. *Chin Med J (Engl),* 133**,** 2867-2873.

ZHOU, C., WU, Y., ZHANG, Y., WANG, Y., WU, H., ZHANG, T., CHEN, G. & HUANG, X. 2023. Factors associated with post-treatment control of viral load in HIV-infected patients: a systematic review and meta-analysis. *Int J Infect Dis,* 129**,** 216-227.

ZILA, V., MARGIOTTA, E., TUROŇOVÁ, B., MÜLLER, T. G., ZIMMERLI, C. E., MATTEI, S., ALLEGRETTI, M., BÖRNER, K., RADA, J., MÜLLER, B., LUSIC, M., KRÄUSSLICH, H. G. & BECK, M. 2021. Cone-shaped HIV-1 capsids are transported through intact nuclear pores. *Cell,* 184**,** 1032-1046.e18.

8 Appendices

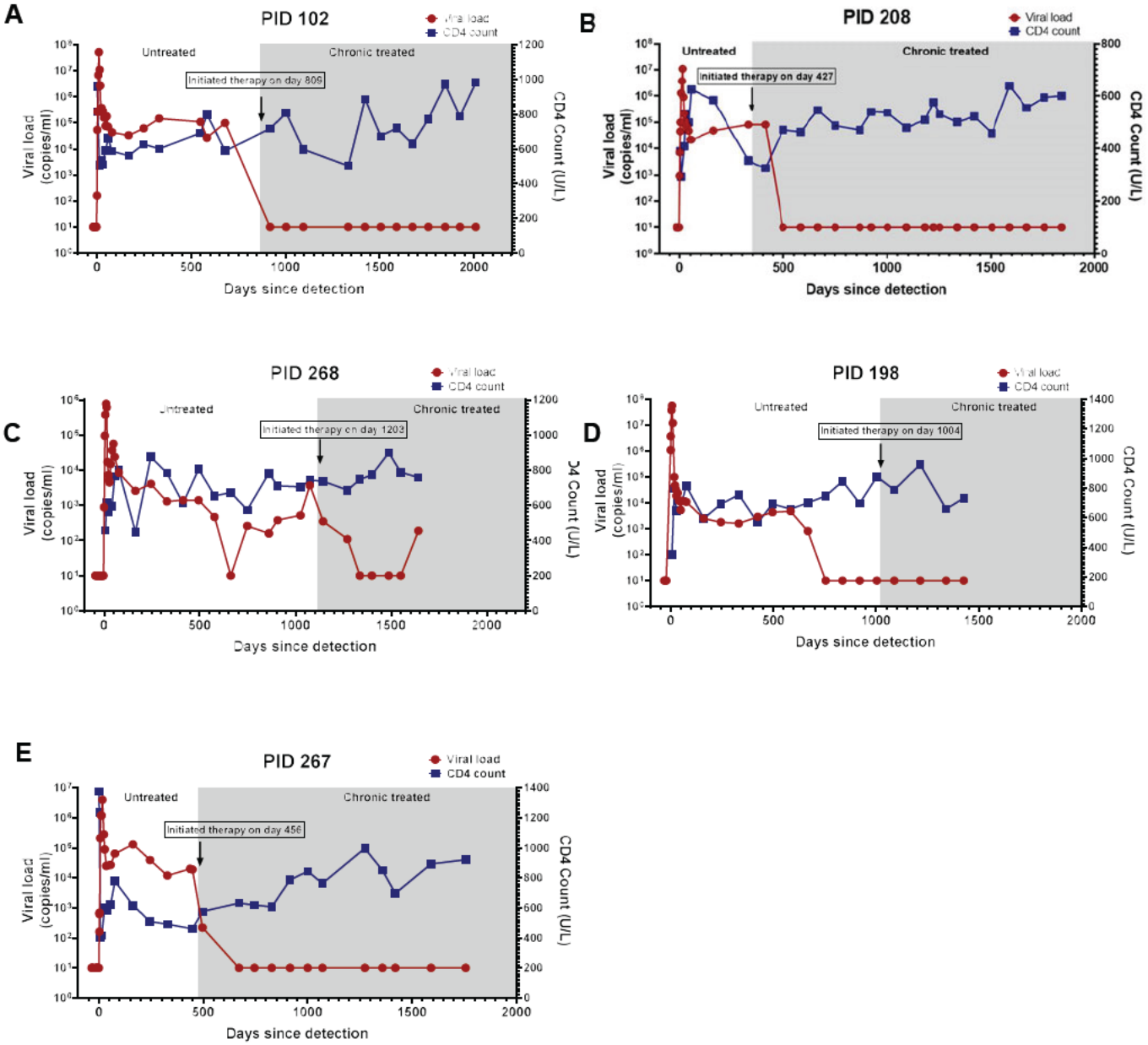

Supplementary Figure 1. Viral load (Red) and CD4 count (Blue) of five chronically treated individuals. The white area shows untreated infection, and the grey area displays treated infection. These graphs also highlight the day of treatment initiation. Participants initiated therapy at a median of 779 days post-detection.

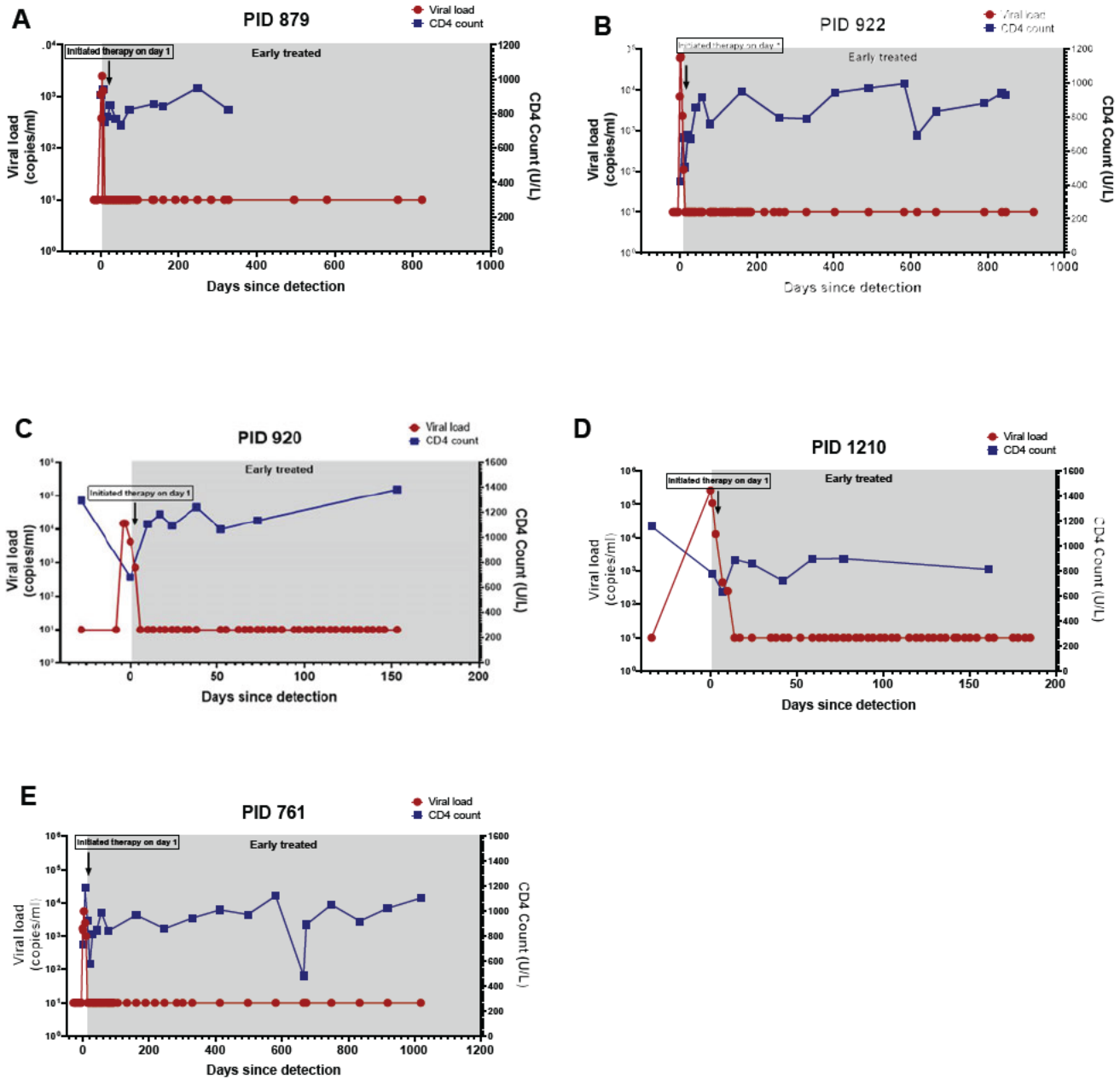

Supplementary Figure 2. Five acutely treated participants. The grey area shows treated infection. Viral load is shown in red and CD4 count is shown in blue. Participants were treated at a median of 1 day post-detection.

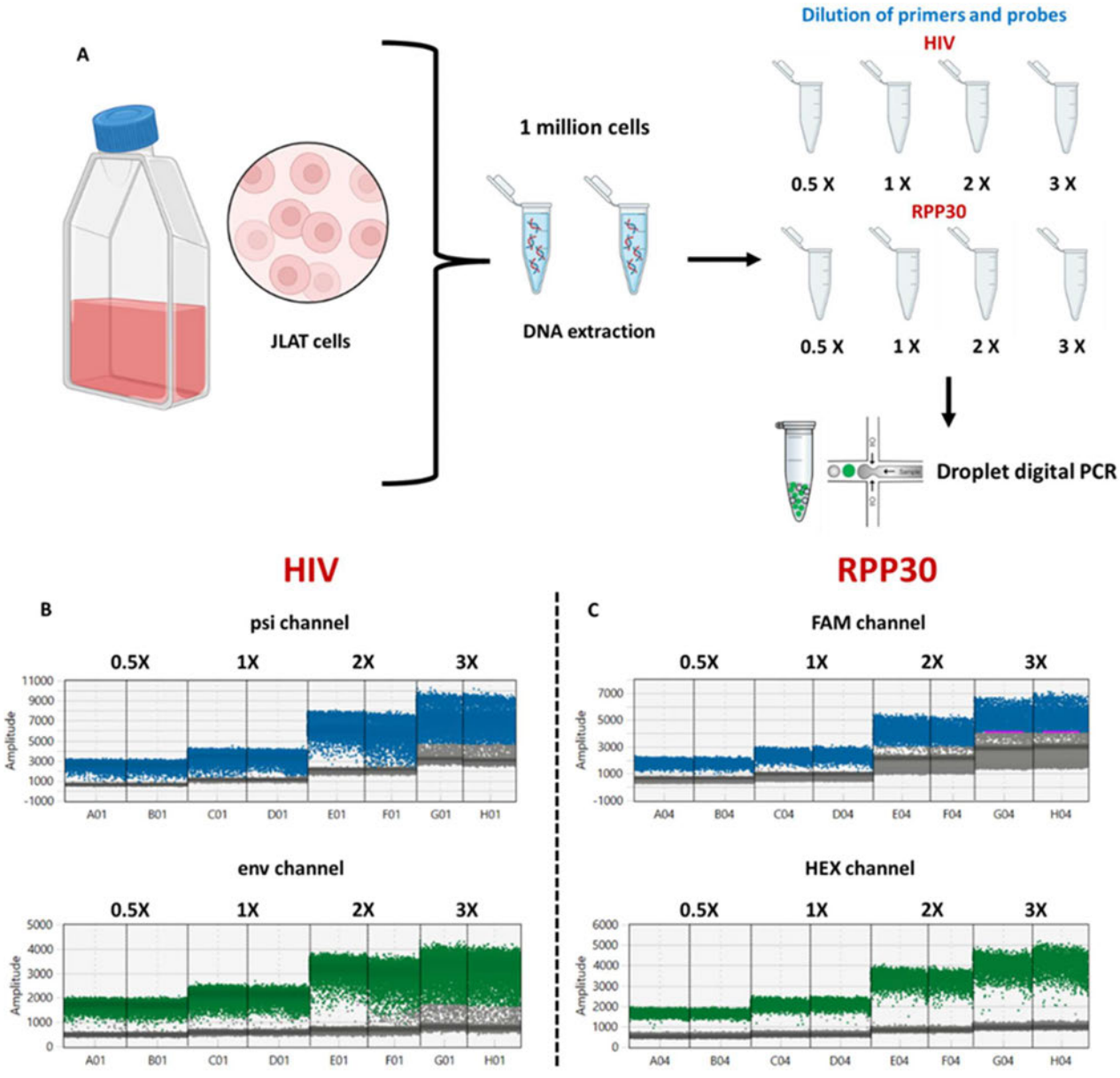

Supplementary Figure 3. Titration of IPDA primers and probes A) Experimental design of titration experiment for IPDA primers and probes. Dilutions with varying amounts of primer and probe were titrated to produce an amplitude of 5000 units. B) HIV panel showing the *psi* and *env* results from this it was determined that the 1X cocktail of primers and probes. Additionally, it was observed that with increasing volumes of primer and probe, there was increasing fluorescence noted. C) RPP30

panel shows that the 1X cocktail of primers and probes also gave optimal fluorescence of 3000 units for both the FAM and HEX channels. Furthermore, it was observed that with increasing volumes of the primer and probe, there is also increasing flourescence.

Table 8.1 Number of cells sampled for each assay

Cell Type	Average Total number of sorted	Average number of cells used to measure total HIV DNA	Average number of cells used for IPDA
Central memory	249 621 (130 267-378 318)	34 915 (22 353 – 46 364)	205 689(54 679-215 162)
Effector memory	124 367 (106 000-189 276)	28 255 (13 099-38 813)	89 617(61 467 – 116 749)
Transitional memory	132 763 (102 319-192 371)	18 923 (8616 – 27 166)	113 840 (67 627 – 126 767)
Naïve cells	287 378 (213 263-389 126)	35 450 (11 272 – 48 035)	117 671 (96 727-226 891)
Myeloid cells	214 376 (156 267-298 172)	31 900 (16 356 – 42 234)	177 626 (105 678 – 205 913)
CD8 T cells	218 279 (178 279-270 283)	38 459 (21 671 -56 281)	102 387 (98 243 - 218 273)

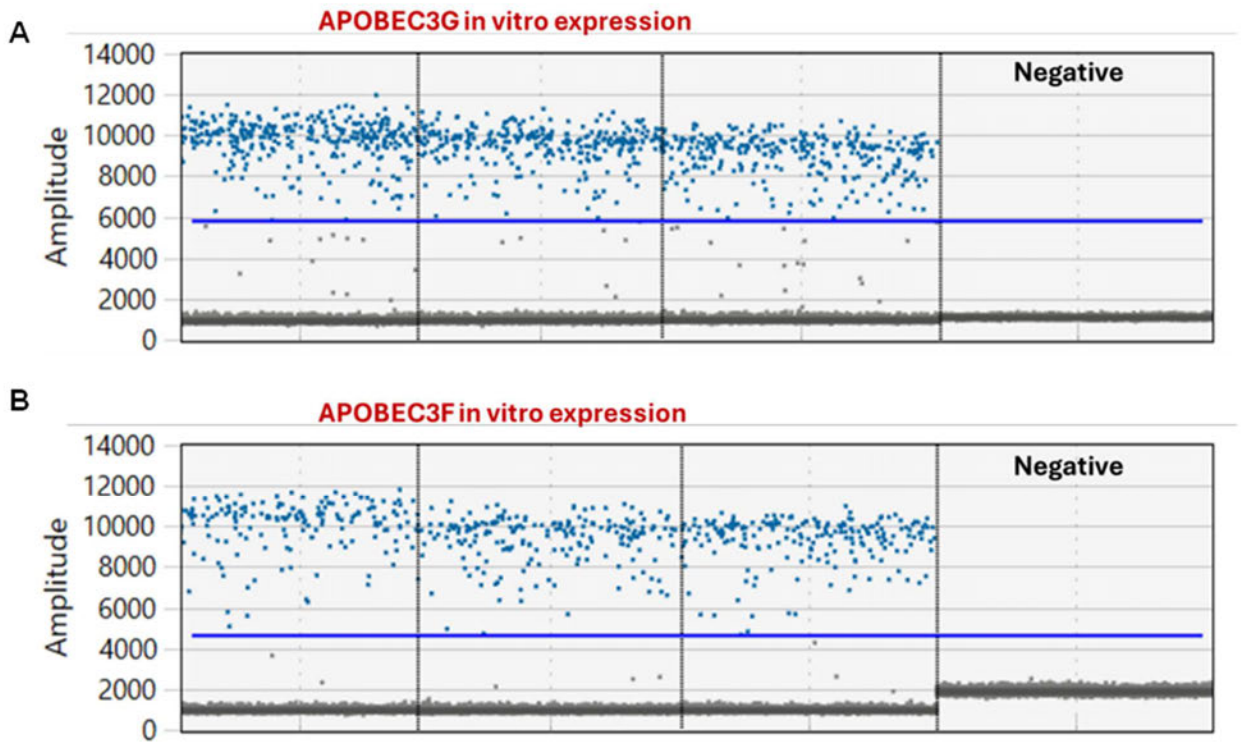

Figure 4. *In vitro* expression of (A) A3G and (B) A3F. The blue dots indicate positive amplification. Negative sample shows HEK 293 T cells with no A3 plasmid transfected.

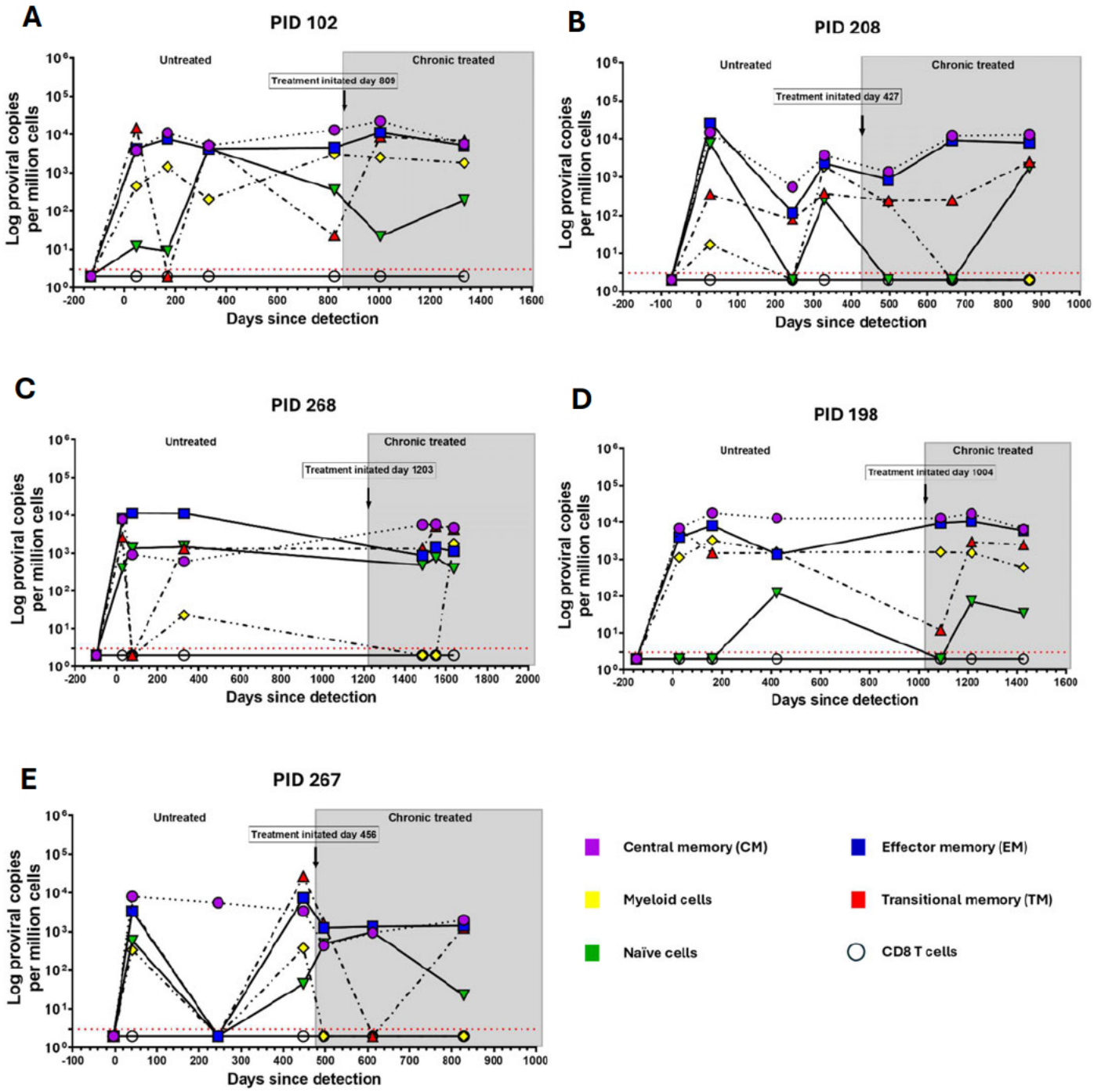

Supplementary Figure 5. Total proviral DNA levels for 5 late treated participants. Different shapes indicate different cellular subsets. The white area indicates untreated infection, and the grey area indicates treated infection. Day treatment was initiated is also indicated on the graph.

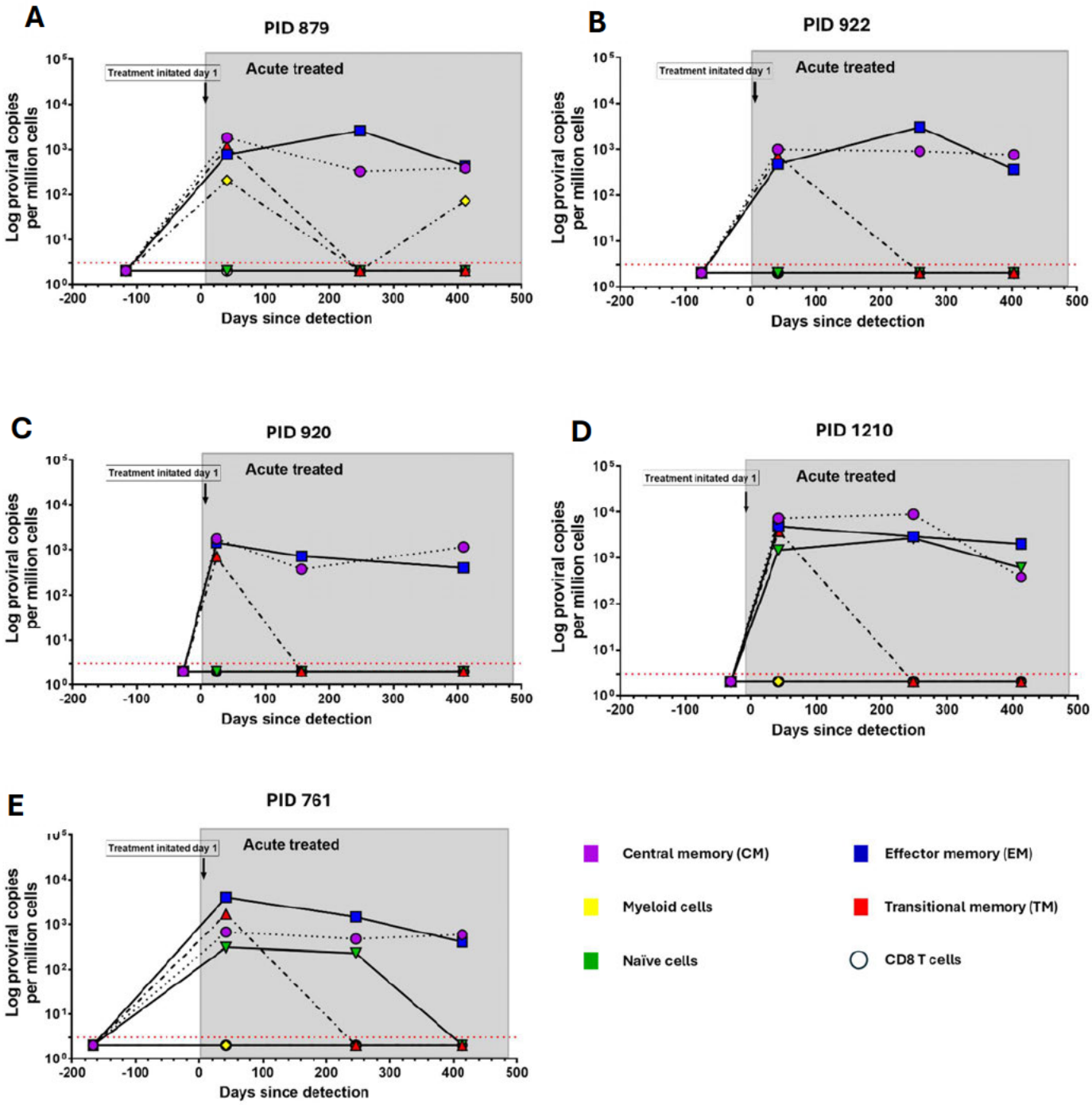

Supplementary Figure 6. Total proviral DNA levels for 5 early treated participants. Different shapes indicate different cellular subsets. The white area indicates untreated infection, and the grey area indicates treated infection. Day treatment was initiated is also indicated on the graph.

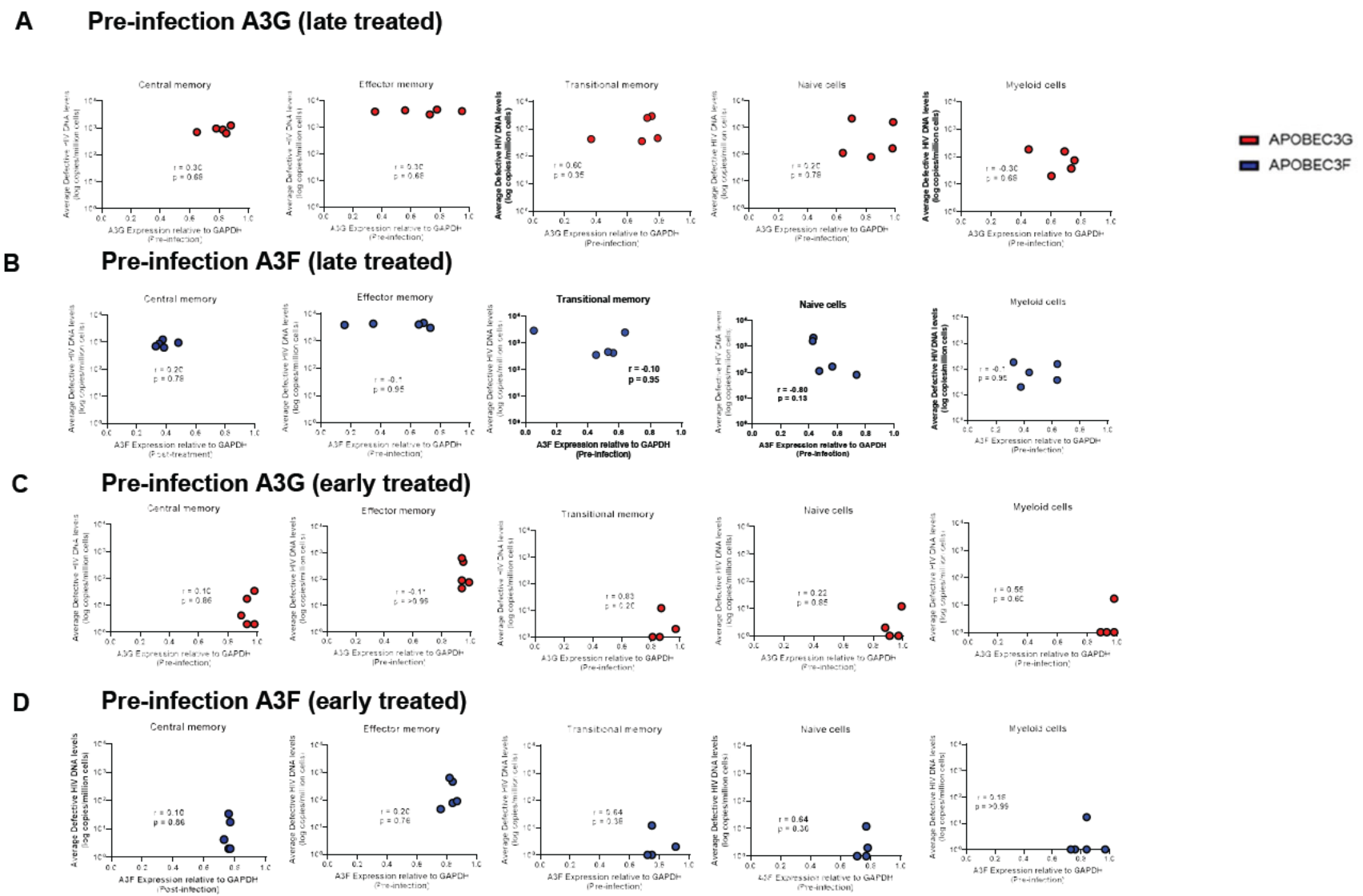

Supplementary Figure 7. Pre-infection APOBEC3G/-F expression levels versus average defective HIV DNA measured 12 months post-treatment.

A **1 month post-infection A3G (late treated)**

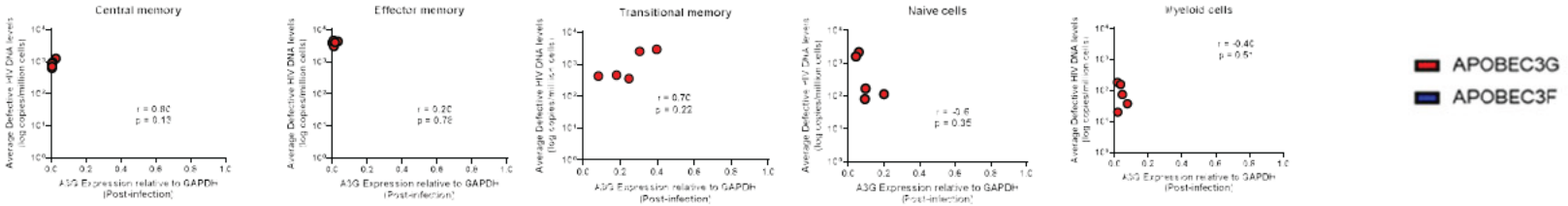

B **1 month post-infection A3F (late treated)**

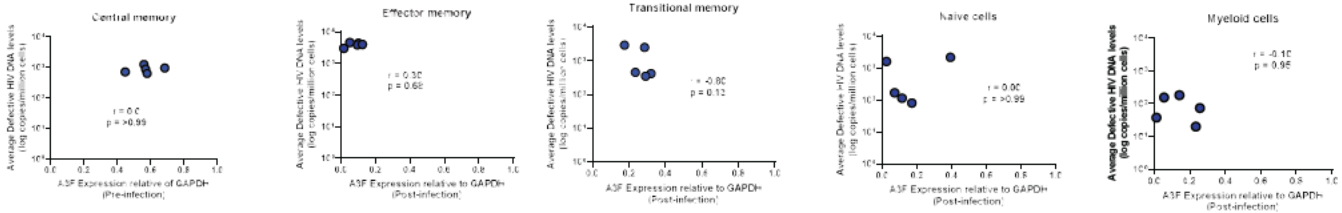

C **1 month post-infection A3G (early treated)**

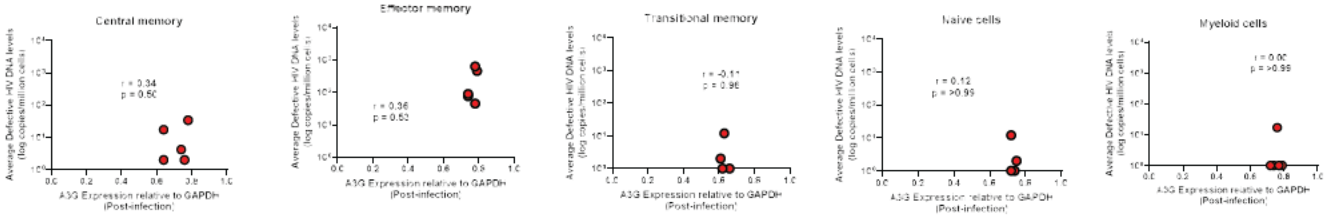

D **1 month post-infection A3F (early treated)**

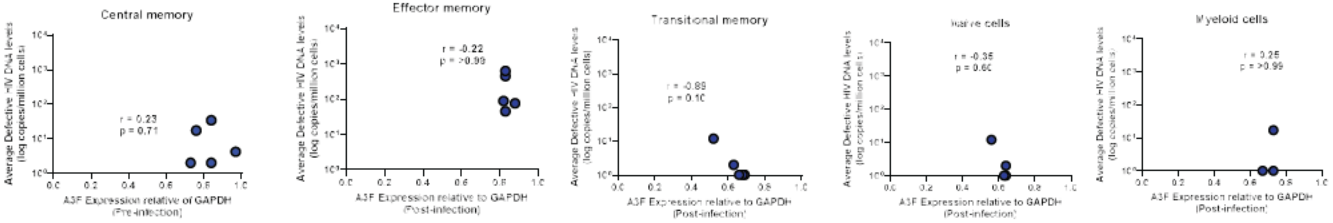

Supplementary Figure 8. APOBEC3G/-F expression levels were measured at one month post-infection versus average defective HIV DNA measured at 12 months post-treatment.

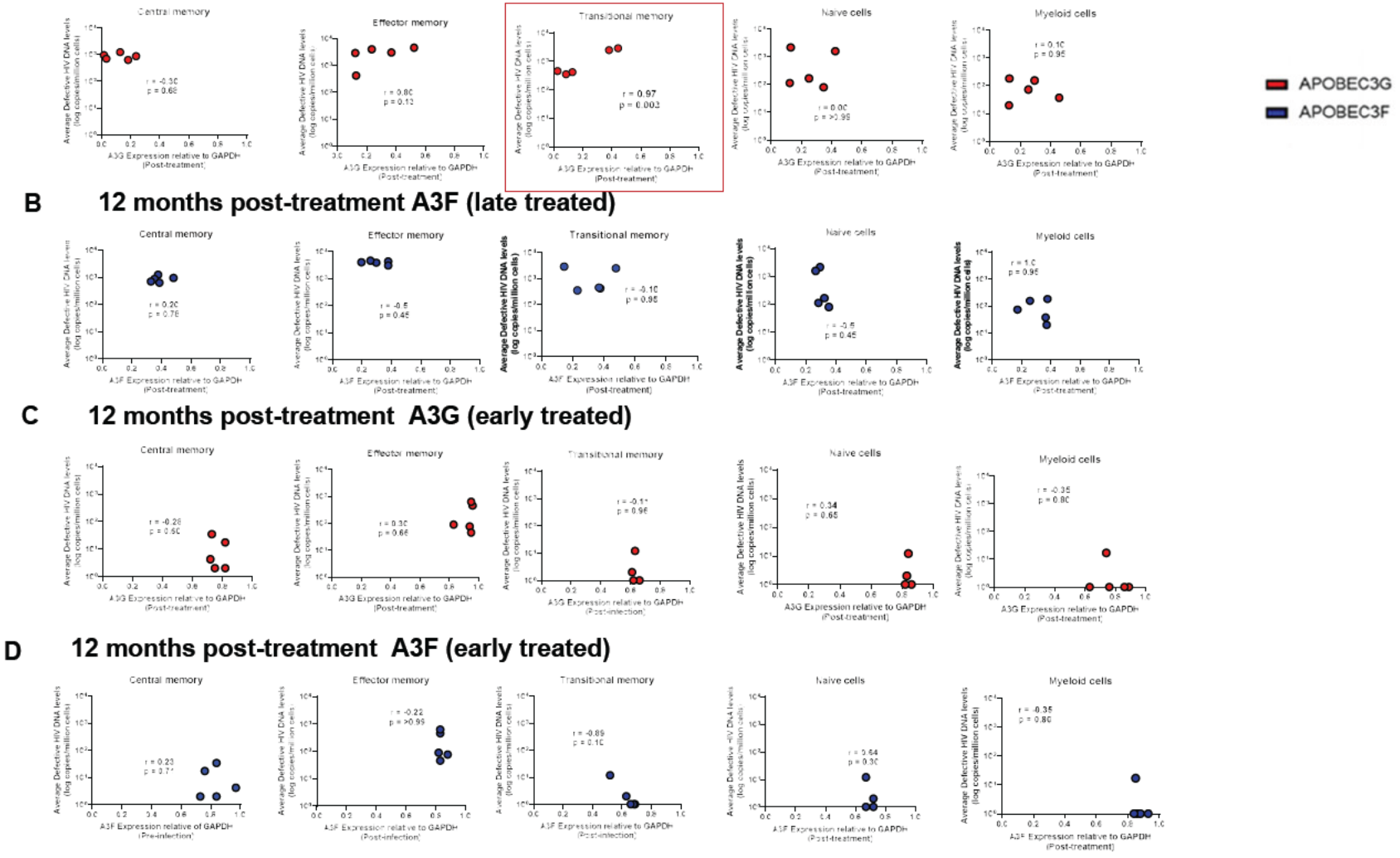

Supplementary Figure 9. A3G and A3F expression were measured at 12 months post-treatment versus average defective HIV DNA measured at 12 months post-treatment. Red box indicates the cell subset with positive correlation.

A

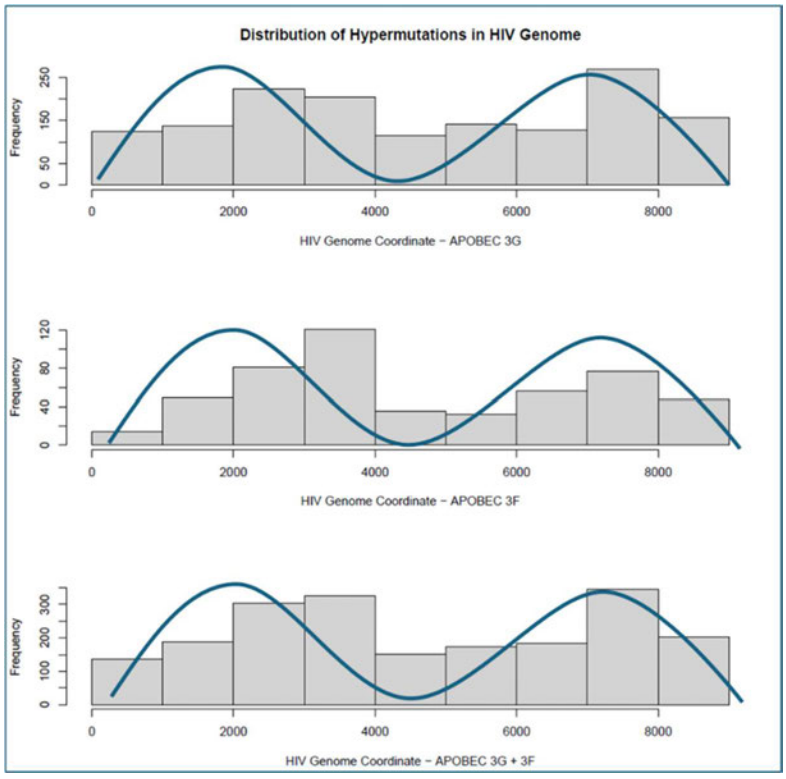
Distribution of Hypermutations in HIV Genome
Frequency
0
50
150
250
0
2000
4000
6000
8000
HIV Genome Coordinate – APOBEC 3G
Frequency
0
40
80
120
0
2000
4000
6000
8000
HIV Genome Coordinate – APOBEC 3F
Frequency
0
100
200
300
0
2000
4000
6000
8000
HIV Genome Coordinate – APOBEC 3G + 3F

B

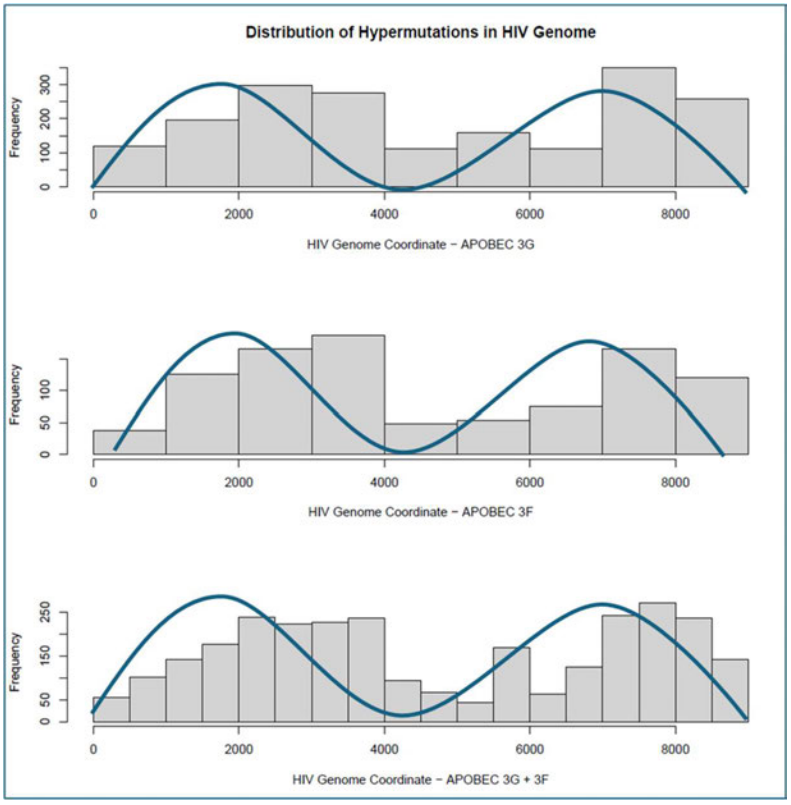
Distribution of Hypermutations in HIV Genome
Frequency
0
100
200
300
0
2000
4000
6000
8000
HIV Genome Coordinate – APOBEC 3G
Frequency
0
50
100
0
2000
4000
6000
8000
HIV Genome Coordinate – APOBEC 3F
Frequency
0
50
150
250
0
2000
4000
6000
8000
HIV Genome Coordinate – APOBEC 3G + 3F

C

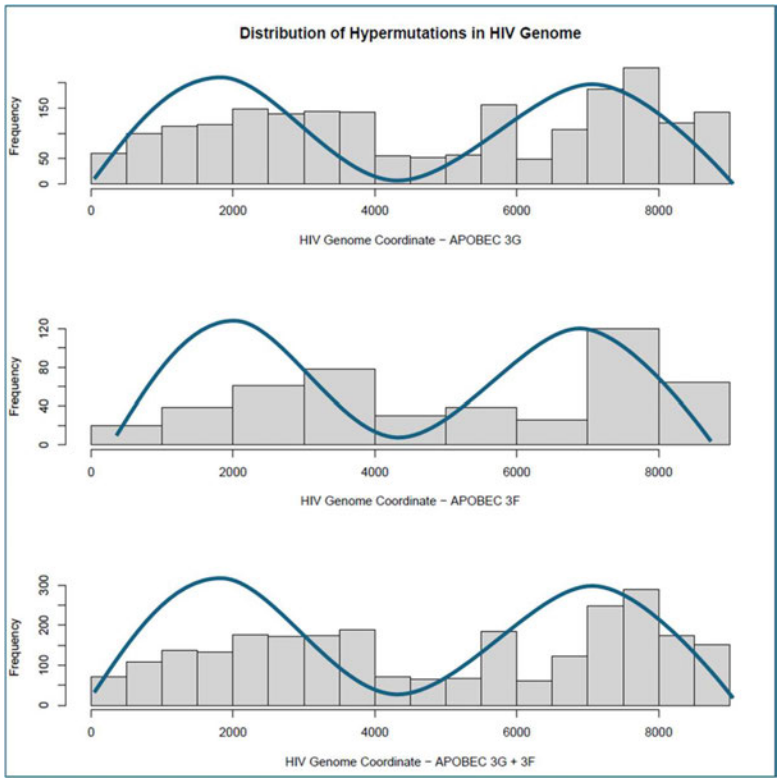
Distribution of Hypermutations in HIV Genome
Frequency
0
50
150
0
2000
4000
6000
8000
HIV Genome Coordinate – APOBEC 3G
Frequency
0
40
80
120
0
2000
4000
6000
8000
HIV Genome Coordinate – APOBEC 3F
Frequency
0
100
200
300
0
2000
4000
6000
8000
HIV Genome Coordinate – APOBEC 3G + 3F

D

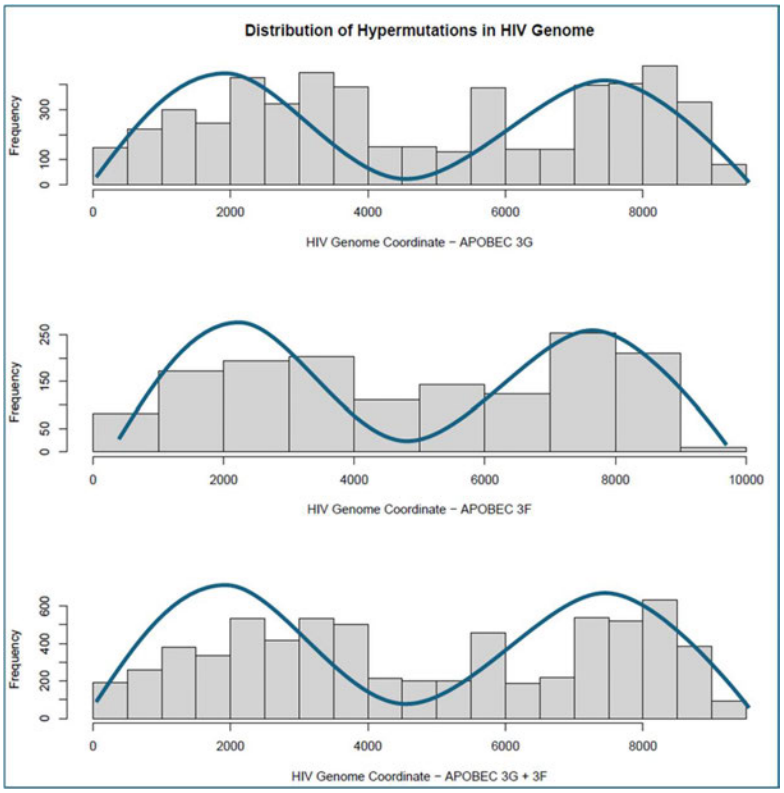
Distribution of Hypermutations in HIV Genome
Frequency
0
100
300
0
2000
4000
6000
8000
HIV Genome Coordinate – APOBEC 3G
Frequency
0
50
150
250
0
2000
4000
6000
8000
10000
HIV Genome Coordinate – APOBEC 3F
Frequency
0
200
400
600
0
2000
4000
6000
8000
HIV Genome Coordinate – APOBEC 3G + 3F

Supplementary Figure 10. The distribution of hypermutation across the HIV genome in the study participants. A) PID 102 B) PID 267 C) 268 D) 208. The blue line highlights the increase and decrease of hypermutation across the HIV genome.